Faculty of Science and Engineering
Department of Petroleum Engineering

True Triaxial Testing of Sandstones and Shales

Vida Minaeian

This thesis is presented for the Degree of
Doctor of Philosophy
of
Curtin University

August 2014

Declaration

To the best of my knowledge and belief this thesis contains no material previously published by any other person except where due acknowledgment has been made. This thesis contains no material which has been accepted for the award of any other degree or diploma in any university.

Name: Vida Minaeian
Signature: 
Date: 8 August 2014

Copyright

I warrant that I have obtained, where necessary, permission from the copyright owners to use any third-party copyright material reproduced in the thesis (e.g. questionnaires, artwork, unpublished letters), or to use any of my own published work (e.g. journal articles) in which the copyright is held by another party (e.g. publisher, co–author).

Name: Vida Minaeian
Signature: 
Date: 8 August 2014

Abstract

Failure and deformational characteristics of geomaterials are commonly evaluated through conventional triaxial tests under axisymmetric conditions ($\sigma_1>\sigma_2=\sigma_3$). However, field measurements reveal that such simple axisymmetric conditions are rarely encountered in-situ and fully anisotropic stress states ($\sigma_1\neq\sigma_2\neq\sigma_3$) are often existent. This suggests that conventional triaxial tests, in which only the maximum and minimum principal stresses are taken into account, cannot completely account for the failure behaviour of rocks under real in-situ conditions. Previous true triaxial experiments along with theoretical investigations have revealed that the intermediate principal stress (σ_2) can significantly affect the rock mechanical response and hence should not be overlooked.

Sandstones and shales are among the most common sedimentary rocks and their mechanical and deformational response to the changes in the in-situ stress conditions is of importance in wellbore stability analysis, sand production, seal integrity analysis, waste storage and hydraulic fracturing in gas shale reservoirs. However, our knowledge of failure properties of these rock types under realistic true triaxial crustal stress conditions is limited. This research aims to investigate the dependence of failure characteristics of a set of synthetic sandstones and two sets of shales (Carynginia Shale and Pierre Shale) on true triaxial principal stresses, with particular emphasis on the influence of σ_2. The results showed that increasing σ_2 at a constant σ_3, induced significant increases in failure strength, stiffness and the timing of the onset of dilatancy in both sandstones and shales. Changing the intermediate stress magnitude from an axisymmetric stress state ($\sigma_1>\sigma_2=\sigma_3$) to a true triaxial stress state ($\sigma_1>\sigma_2>\sigma_3$) also markedly affected the Poisson's ratios, inelastic deformation and volumetric changes, stress-induced fractures and failure mode in the specimens. The findings suggest that the impact of σ_2 on rock behaviour can be as significant as that of the minimum principal stress, a fact that is overlooked in conventional triaxial tests. The mechanical response of the sandstones, Carynginia Shale and Pierre Shale to similar true triaxial stress states has also been compared and some correlations have been found between the mechanical behaviour of these rocks and their physical properties.

The second objective of this study was to investigate the effect of saturation on the deformational behaviour of shales under true triaxial loading. Shales are very sensitive to water saturation state, mainly due to their small pore size and appreciable amounts of clay minerals. However, the effect of changing water saturation has rarely been studied in the gas shale context even under ambient, uniaxial or conventional triaxial conditions. In the present study, preserved samples of Pierre Shale were subjected to different water saturation levels and their mechanical parameters were measured under true triaxial conditions. The results revealed a general increase in the true triaxial strength and elastic modulus and decrease in the Poisson's ratios as water saturation decreased. These findings confirmed the impact of water saturation on rock properties and also highlighted the importance of good preservation for clay-bearing shales.

Finally, multistage true triaxial testing was used to evaluate the σ_2 impact on rock mechanical properties and the suitability of such a method was examined in this thesis. Multistage true triaxial tests were considered as they could be beneficial in the present study firstly to avoid the effect of sample variability on obtained data, and secondly to acquire more information from the limited number of available shale samples. Over the course of each multistage true triaxial test, a sample was loaded to several levels of intermediate principal stress, while the minimum stress was held constant. Comparing the results of the multistage true triaxial tests on the synthetic sandstones with the equivalent single-stage true triaxial measurements revealed noticeable differences between the resultant rock strengths and elastic properties. The findings of these tests are discussed and the potential mechanisms responsible for the observed disagreements are explained in this thesis.

Acknowledgements

I wish to express my sincere thanks to my supervisor, Professor Vamegh Rasouli, for his guidance, understanding and ongoing support in my research path and daily life. I greatly appreciate his responsiveness and encouragement through the process of this study and also the freedom and flexibility he has given me in my research.

I would like to express my deep gratitude to my associate supervisor, Dr David Dewhurst from CSIRO Earth Science and Resource Engineering. His inputs and guidance has been invaluable for completion of this research. I have greatly benefitted from his ideas and insights.

I wish to extend my thanks to Dr Joel Sarout from CSIRO, and Dr Ali Saeedi from Curtin University, for their advices during my studies. Appreciations are also due to Sam Battah, Bruce Maney, Leigh Kiewiet, Calaudio Delle Piane, Lionel Esteban, Shane Kager, Stephen Firns and Ian Penny from CSIRO for their valuable helps and suggestions. I would like to offer my thanks to my friends and colleagues at the Department of Petroleum Engineering who made my PhD journey joyful and memorable.

I gratefully acknowledge the financial support of the Minerals and Energy Research Institute of WA (MERIWA) and Curtin University for my research scholarship.

I would like to express my heartfelt thanks to my parents and my sisters for their everlasting support and care. Similarly, my sincere thanks are due to my in-laws for their understanding and care.

Finally and most importantly, I would like to thank my husband for his endless and unconditional support, patience and love. Much credit goes to him for his help in completion of the experimental work in my thesis. Without his support and encouragement this thesis would have not been possible.

To my beloved husband, Ramin, my partner in everything.

Contents

List of Figures

List of Tables

Nomenclature

C_0	Uniaxial compressive strength (UCS)
E	Young's modulus
LVDT	linear variable differential transducer
RH	relative humidity
S_0	internal cohesion
S_w	water saturation
SG	strain gauge
TI	transversely isotropic
TTSC	true triaxial stress cell
UCS	uniaxial compressive strength
ε_1	principal strain along σ_1 axis
ε_2	principal strain along σ_2 axis
ε_3	principal strain along σ_3 axis
ε_v	volumetric strain
ϕ	internal friction angle
ϕ	porosity
μ_i	coefficient of internal friction
ν	Poisson's ratio
ν_{12}	Poisson's ratio along σ_2 axis
ν_{13}	Poisson's ratio along σ_3 axis
σ_1	maximum principal stress
σ_2	intermediate principal stress
σ_3	minimum principal stress
σ_c	confining pressure
σ_f	maximum differential stress at failure (σ_1-σ_3)
σ_f^C	strength obtained at σ_2=σ_3
σ_f^T	highest true triaxial strength
$\sigma_{m,2}$	mean normal stress acting on the shear failure planes

σ_n	normal stress on a plane
σ_{oct}	octahedral normal stress (mean normal stress)
τ	shear stress along a plane
τ_{oct}	octahedral shear stress

1 Introduction

1.1 Overview and motivation

One of the major aims of experimental rock mechanics studies is to estimate strength and deformation characteristics of rocks under stress states simulating in-situ stress conditions (Haimson and Chang 2000). The common method for characterizing mechanical properties of rocks in laboratory is to conduct conventional triaxial compression tests on cylindrical core samples. In these types of tests the rock sample is subjected to a uniform confining pressure ($\sigma_c=\sigma_2=\sigma_3$) and an axial stress ($\sigma_1$). Applying equal intermediate stress (σ_2) and minimum stress (σ_3) in such techniques (called axisymmetric stress conditions) is a major practical limitation, as in real in-situ conditions the rock is generally subjected to three independent principal stresses. Growing number of field measurements have revealed anisotropic stress states, i.e. $\sigma_1\neq\sigma_2\neq\sigma_3$, at shallow to intermediate crustal depths in many cases (e.g. Haimson 1978, McGarr and Gay 1978, Brace and Kohlstedt 1980, Vernik and Zoback 1992). Therefore, the data extracted from conventional triaxial tests ($\sigma_1>\sigma_2=\sigma_3$) does not provide an adequate understanding of the rock behaviour under realistic true triaxial crustal stress conditions ($\sigma_1>\sigma_2>\sigma_3$).

Mogi (1971) was the first one to investigate the mechanical behaviour of rocks when subjected to three independent principal stresses. He designed a true triaxial cell for testing rectangular prismatic rock specimens and developed true triaxial failure criteria based on the experimental results of different rock types. After Mogi (1971), different laboratories worldwide developed polyaxial machines and true triaxial experiments were conducted on different rock types (e.g. Takahashi and Koide 1989, Smart 1995, Wawersik et al. 1997, Haimson and Chang 2000, Tiwari and Rao 2004, Popp and Salzer 2007, Young et al. 2012, Fuenkajorn et al. 2012). The outcome of the true triaxial studies on various rock types such as granite, marble, dolomite, limestone, trachyte, salt, clay and siltstone, confirmed that the

intermediate stress (σ_2) can significantly affect the rock strength and failure characteristics.

Sandstones are one of the most widespread rocks in the earth's crust, and they are of interest in different engineering cases such as oil/gas reservoirs, carbon dioxide sequestration and waste storage (Wawersik et al. 2001). Thus having a good understanding of their mechanical response to general stress states is necessary, as changes in the in-situ stress conditions can cause deformation and failure of the host formations. However, only limited true triaxial experimental investigations have been conducted on sandstones (Takahashi and Koide 1989, Wawersik et al. 1997, Ingraham 2012, Ma 2014). In addition, among the true triaxial studies on rocks, very few investigated their elastic properties: examples include the study of Tiwari and Rao (2004) on sand-lime brick, Oku et al. (2007) on siltstone and Sriapai et al. (2013) on salt. Therefore, the first motivation of the present study was to elucidate the impact of true triaxial stress conditions on strength, failure, elastic and inelastic properties of sandstones. For this purpose, several synthetic sandstone samples were manufactured which could be assumed as isotropic and homogenous rocks.

Shales constitute the major rock type in sedimentary basins. They could be the source rock or cap rock for conventional reservoirs and also most of the layers above the reservoir to the surface are shale or mudstone (Horsrud et al. 1998). Moreover, gas shale reservoirs are becoming an increasingly important and interesting source of energy in the hydrocarbon supply system. In gas shales, the shale composes both the source and the reservoir (Boyer et al. 2006). Therefore, understanding mechanical properties of shales is important and required in many geomechanical, drilling and production engineering problems. Such applications include hydraulic fracturing design and identifying the target zones, which requires a good knowledge of the rock mechanical characteristics under in-situ stresses. Also for drilling effectively, in terms of safety and costs, rock strength and elastic properties are required to analyse wellbore stability and to determine safe mud weight windows (Mese 1995). Mechanical behaviour of shales has been studied to some extent in the past under uniaxial or standard triaxial conditions (Mese 1995, Niandou et al. 1997, Horsrud 2001, Gautam 2005, Dewhurst et al. 2011). However, to date only few experimental studies investigated behaviour of shales when subjected to true triaxial stress states (Takahashi and Koide 1989, Popp and Salzer 2007, Naumann et al. 2007). Consequently, our understanding of the mechanical response of shales under a

general stress state is still inadequate. In this study the impact of changing true triaxial stress state on strength, elastic and inelastic properties of Carynginia Shale, a gas shale formation from the North Perth Basin in Western Australia, and Pierre-1 Shale from the United States is investigated.

Moreover, saturation is an important parameter that influences the physical and mechanical properties of shales. Conventional shales and many gas shales are composed of considerable amount of clay (Dewhurst et al. 2012). Thus the mechanical characteristics of shales change significantly with saturation and interactions between their clay minerals and pore fluid (Mese 1995). For instance previous experimental works have shown that desaturation could cause an increase in strength and stiffness of shales (e.g. Valès et al. 2004, Dewhurst et al. 2012). Most of the findings on saturation impact on clayey rocks (including clays, claystone, shales, mudstones) are based on ambient, uniaxial or triaxial stress conditions (Mese 1995, Horsrud et al. 1998, Blumling et al. 2002, Valès et al. 2004, Zhang and Rothfuchs 2004, Ramos da Silva et al. 2008, Tsang et al. 2012). However, there is a lack of experimental work to determine the effect of saturation on behaviour of shales under true triaxial stress conditions. Therefore, in the present study, preserved samples of Pierre-1 Shale from the United States were used to examine the impact of changing water saturation on true triaxial mechanical properties of shales. The Pierre-1 Shale is referred to as Pierre Shale in this work, for simplicity.

For extracting strength, elastic moduli, deformational and failure characteristics of rocks, normally compressive failure tests are conducted. The conventional method of performing compressive failure tests under triaxial conditions, is to load the rock sample to a predefined level of confining pressure (σ_c), then increasing the maximum stress (σ_1) until the specimen undergoes failure. Such an approach is called a single-stage test, in which only one strength data point can be extracted from each tested rock sample (Kim and Ko 1979). In order to derive more measurements from a single core plug, scientists suggested a new method of testing, called multistage technique (Kim and Ko 1979, Kovari et al. 1983, Crawford and Wylie 1987, Kovari and Tisa 1975). The fundamental idea for multistage testing is that a specific level of σ_c is applied on the sample, then σ_1 is increased up to a level just before the sample actually breaks. Afterwards, σ_c is increased to a higher level and the procedure in the first stage is repeated for several levels of confining pressure. This way the strength data corresponding to several confining pressure levels can be derived from a single

sample, while the undesired influence of heterogeneity among different samples on produced results is eliminated. Many researchers have investigated mechanical behaviour of shales and sandstones using multistage technique under triaxial stress conditions (e.g. Holt and Fjær 1991, Pagoulatos 2004, Gräsle 2011, Amann et al. 2012). However, multistage testing method has been rarely employed under true triaxial stress states in the past. Macari and Hoyos (2001) used multistage technique under true triaxial conditions on an unsaturated soil. They applied triaxial compression ($\sigma_2=\sigma_3$), simple shear ($[\sigma_2-\sigma_3]/[\sigma_1-\sigma_3]=0.5$) or triaxial extension ($\sigma_2=\sigma_1$) stress states on the sample through multiple stages. The objective of their studies was to investigate the impact of matric suction on strength and stress-strain behaviour of the soil. However, employing true triaxial multistage tests to examine the influence of σ_2 on rock deformational characteristics is a novel idea, which has been evaluated in the present work. In this method, a constant σ_3 was applied on a single rock sample, while σ_2 was changed to different levels. This approach has been examined in this study on the synthetic sandstone samples and the results has been compared to the results of single-stage true triaxial tests conducted at identical stress conditions on similar specimens.

In order to investigate rocks deformational behaviour under a general stress state in this work, a True Triaxial Stress Cell (TTSC) developed at the Department of Petroleum Engineering of Curtin University was used (Rasouli and Evans 2010). While this apparatus has been used for simulations such as sanding analysis and hydraulic fracturing, it has not been employed for conducting compressive failure tests and measuring rock elastic and inelastic deformational response in the past. Thus as a part of the present study, some modifications were applied to the cell and a new experimental setup was established for conducting true triaxial failure tests.

1.2 Research objectives

Based on the brief overview of the problem addressed in the previous section, the objectives of this thesis are summarized as below:

- Present a comprehensive literature review of the past and latest developments in true triaxial testing and the impact of the intermediate stress on the behaviour of rocks, with particular focus on sandstones and shales.

- State the shortcomings in understanding the failure characteristics and elastic properties of shales and sandstones under a general stress state.
- Design and preparation of an experimental setup to conduct compressive failure tests in the TTSC.
- Manufacture synthetic sandstone samples to study the influence of true triaxial stress conditions on failure characteristics. Also as the synthetic sandstones are reproducible, they were used in investigating properness of the experimental setup.
- Carry out tests using the multistage true triaxial testing technique for investigating the influence of σ_2 on rock deformational properties. Examine reliability of this method through comparing results of multistage and single-stage true triaxial tests on the synthetic sandstones.
- Evaluate deformational properties of the Carynginia Shale samples when subjected to three independent stresses.
- Investigate the influence of stress conditions and variable water saturation on mechanical behaviour of the Pierre Shale.
- Comparison of the results of true triaxial tests on these sandstones and shales.

1.3 Research significance

In this thesis, the influence of intermediate stress as well as the minimum stress on strength and deformability of sandstone, shale and gas shale specimens has been studied based on true triaxial lab testing. The originality and significance of this research compared to previous investigations are highlighted below:

- A laboratory procedure has been established for performing true triaxial failure tests on 50 mm cubes of rock in the True Triaxial Stress Cell (TTSC). The TTSC setup has been modified to conduct compressive failure tests for the first time.
- The new idea of using multistage true triaxial testing technique to evaluating σ_2 impact on rock mechanical behaviour has been examined. The reliability of the produced data and properness of the technique has been evaluated and discussed through comparing the obtained results against the equivalent single-stage true triaxial tests results. To the best of our knowledge, this approach has

not been examined in the past for evaluating σ_2-effect on rock deformational properties.

- For the tested rocks, the impact of σ_2 has been studied comprehensively on their deformational characteristics including failure strength, elastic parameters, inelastic deformation, dilatancy, failure mode and fractures patterns. Only few of the existing experimental studies have presented such complete analysis of rock deformational behaviour under true triaxial stress conditions.
- In this research the influence of changing true triaxial stress conditions on the Young's moduli and Poisson's ratios of the sandstones and shales has been examined. There have been very few previous experimental investigations on the elastic properties of rocks under true triaxial stress states. Particularly, there is a lack of studies carried out on the impact of the intermediate stress on elastic parameters of sandstones and shales.
- The experimental results of the three groups of tested rocks have been used to fit 3D failure envelopes to the laboratory data corresponding to the synthetic sandstones, the Carynginia Shale and the Pierre Shale.
- The influence of changes in water saturation has been investigated on strength and deformational behaviour of the Pierre Shale in the presence of three independent stresses. This research direction has been poorly studied in the past and hence is novel in both its origin and applications.

1.4 Thesis structure

In this Chapter an overview of true triaxial testing of rocks was presented and the need for further experimental investigations in sandstones and shales was discussed. Moreover, the objectives and significance of this study were outlined. Based on the objectives of this work, the thesis is arranged in seven Chapters. Figure 1.1 presents the thesis structure and the highlights of each chapter. The layout of the thesis is briefly reviewed below.

Chapter 2 covers a brief review of the history of true triaxial experiments and the developed poly-axial testing machines. The effect of intermediate stress on behaviour of shales and sandstones is also discussed. Previous findings on the influence of

saturation on shales deformational properties are investigated. Then the concept and most important aspects of multistage tests are explained.

In Chapter 3 the experimental methodology used in this research is detailed. In this Chapter the sample preparation procedure and the testing machine and instrumentation are explained. Also the experimental procedure for conducting the single-stage and multistage true triaxial tests are presented.

In Chapter 4 the laboratory data obtained from testing the synthetic sandstones are elaborated. The impact of stress magnitude and anisotropy on mechanical properties of these samples are discussed. Besides, the challenges of conducting the multistage true triaxial tests are discussed and the obtained results are presented. Then the properness of this technique in evaluating the impact of σ_2 on rock behaviour is discussed.

Chapter 5 presents the laboratory measurements for shales. The deformational characteristics of the Carynginia Shale and the Pierre Shale under true triaxial stress conditions is analysed. Also the influence of changing water saturation from 100% to 40% on behaviour of the preserved Pierre Shale specimens is discussed.

In Chapter 6 the deformational characteristics of the synthetic sandstones, the Carynginia Shale and the Pierre Shale, obtained under similar stress states, are compared and the underlying mechanisms responsible for the observed results are discussed.

Finally in Chapter 7 the main concluding remarks of this research are summarized and some recommendations for further research are proposed.

Chapter 1 Introduction

- An overview of true triaxial testing of rocks and stating motivations for this research
- The objectives and significance of this study
- The layout and structure of the thesis

Chapter 2 Effect of the intermediate stress on mechanical behaviour of rocks

- Review of previous true triaxial investigations
- Discussing the impact of the intermediate principal stress on failure and deformational parameters of rocks
- Explaining the influence of water saturation on shales mechanical properties and expressing the importance of preservation for shales
- Presenting basic concept, benefits and challenges of multistage technique

Chapter 3 Experimental methodology

- Presenting the methods of sample preparation
- Describing the testing apparatus and the measuring devices
- Explaining the established experimental setup and procedure

Chapter 4 Deformational properties of sandstones under true triaxial testing

- Presenting the results of single-stage and multi-stage true triaxial tests on the sandstones
- Discussing the impact of stresses on failure properties of the sandstones
- Examining the validation of the multistage tests against the single-stage tests

Chapter 5 Deformational properties of shales under true triaxial stresses and variable water saturation

- Presenting the experimental results of true triaxial tests on Carynginia Shale and Pierre Shale
- Elucidating the impact of stresses on the failure characteristics of these shales
- Investigating the influence of changing water saturation on behaviour of shales

Chapter 6 Experimental results: Comparison and discussion

- Comparison between the mechanical response of the tested sandstones and shales under similar stress states
- Discussion on the underlying mechanisms for the observed results

Chapter 7 Conclusions and recommendations

References

Figure 1.1 Thesis structure

2 Effect of the intermediate stress on mechanical behaviour of rocks

2.1 Introduction

In this Chapter, the history of true triaxial testing of rocks is briefly reviewed and some of the most important 2D and 3D failure theories are presented. Also, previous experimental studies in the literature on the impact of intermediate stress on behaviour of sandstones and shales are reviewed. Then, the importance of sample preservation in case of shales is explained and previous findings on the impact of saturation on deformational properties of these rocks are discussed. The principles and various methods of conducting multistage tests are briefly reviewed. At the end, the pitfalls of previous investigations are described.

2.2 Experimental studies on the impact of intermediate stress

One of the earliest experimental studies that showed the potential impact of intermediate principal stress (σ_2) on rock strength was the work of Böker (1915). Böker (1915) implemented triaxial extension tests ($\sigma_1=\sigma_2\geq\sigma_3$) on Carrara marble, which was previously studied by von Karman (1911) under triaxial compression conditions ($\sigma_1\geq\sigma_2=\sigma_3$). He obtained different strength values from von Karman results, under the same σ_3 levels. Murrell (1963) compared the results of the compression and extension tests of von Karman and Böker and plotted the σ_1 value at failure against σ_3. He pointed out that the rock was generally stronger when $\sigma_2=\sigma_1$ than in case of $\sigma_2=\sigma_3$. From this comparison he then concluded that the intermediate stress had an obvious effect on rock strength and hence cannot be neglected. Later, Handin et al. (1967) conducted similar comparison between the results of conventional compression and extension tests on limestone, dolomite and glass. Their studies confirmed that the failure strength was greater in extension tests ($\sigma_2=\sigma_1$)

than in conventional triaxial tests ($\sigma_2=\sigma_3$). Based on their observations in testing various materials with widely different mechanical properties, they concluded that the cause of the difference in absolute strength magnitudes for the two kinds of tests was the effect of σ_2. The studies of Handin et al. (1967) also revealed that the angle between the failure plane and the maximum stress, decreased from compression to extension tests, due to the σ_2 effect.

Mogi (1971) was the first one to examine the effect of σ_2 on rock behaviour through 3D experiments. He designed a true triaxial cell to apply three independent stresses on rectangular prismatic rock specimens via two sets of pistons and a pressure vessel. His experiments on several carbonate and silicate rocks, including dolomite, limestone, trachyte and marble, indicated that the intermediate stress can significantly affect the rock strength. Mogi plotted the obtained failure data of different rock types in the σ_1-σ_2 domain. He found that at any constant level of σ_3, rock strength generally increased with increasing σ_2 until it reached a plateau and then as σ_2 approached σ_1 the strength decreased to some extent. Generally for each set of tests with constant σ_3, the experimental data fitted a downward concave curve in σ_1-σ_2 domain, which could be predicted by some theoretical failure models such as the criterion proposed by Wiebols and Cook (1968). These failure theories will be reviewed in section 2.3.

After Mogi (1971), different laboratories worldwide developed polyaxial machines and true triaxial experiments were conducted on different earth materials (e.g. Michelis 1985, Takahashi and Koide 1989, Smart 1995, Wawersik et al. 1997, Haimson and Chang 2000, Popp and Salzer 2007, Young et al. 2011, Fuenkajorn et al. 2012). Table 2.1 lists some of the true triaxial apparatus along with the specimen details, loading mechanism and capacity and related references.

Studies of the above mentioned researchers on various rock types such as granite, amphibolite, salt, siltstone, sandstone, shale and limestone, confirmed earlier findings of Mogi (1971). Therefore, they generally proved that the intermediate principal stress affects the strength, deformational properties, dilatancy and failure-plane angles of rocks and this should be taken into account when investigating the rock mechanical behaviour (see Haimson 2006, Mogi 2007). A more detailed review of the previous experimental findings on the influence of σ_2 on deformational properties of sandstones and shales will be discussed later in section 2.4.

Table 2.1 Some of the worldwide true triaxial cells along with their loading system configuration and samples details.

Apparatus / Location	Researcher/ Reference	Specimen		Loading mechanism	Load capacity
		Shape	Size (mm)		
University of Tokyo	Mogi (1971)	Prismatic	15×15×30	σ_1 & σ_2: Hydraulic pistons σ_3: confining fluid	σ_1: 70 ton jack σ_2: 30 ton jack σ_3: 800 MPa
National Technical University of Athens	Michelis (1985)	Prismatic	50×50×100	σ_1: Rigid piston σ_2 & σ_3: Fluid cushions	Axial: 1500 MPa Lateral differential: 300 MPa
Geological Survey of Japan	Takahashi and Koide (1989)	Prismatic	35×35×70	σ_1 & σ_2: Rigid pistons σ_3: confining fluid	Not stated
Heriot-Watt University	Smart (1995), Crawford et al. (1995)	Cylindrical	D=30 mm L/D=2.25:1	σ_1: Hydraulic piston σ_2 & σ_3: Hydraulic fluid (trapped tubes)	Axial: 1000 kN Lateral differential: 14 MPa
Sandia National Laboratories	Wawersik et al. (1997) Ingraham (2012)	Prismatic	57×57×25 76×76×178	σ_1 & σ_2: Hydraulic rams σ_3: confining fluid	σ_1: 4.9 MN σ_2: 2000 MPa σ_3: 400 MPa
University of Mons	Tshibangu (1997)	Quasi-cubical	31×30×30	Rigid pistons	500 MPa
University of Wisconsin	Haimson and Chang (2000)	Prismatic	19×19×38	σ_1 & σ_2: Hydraulic pistons σ_3: confining fluid	σ_1 & σ_2: 1600 MPa σ_3: 400 MPa
University of Toronto	Young et al. (2011)	Cubic	80×80×80 40×40×40	Hydraulic rams	Axial: 6800 kN Lateral: 3400 kN
Indian Institute of Technology Delhi	Rao and Tiwari (2002)	Cubic	150×150×150	Hydraulic rams	σ_1: 1000 kN σ_2 & σ_3: 300 kN
University of Kiel	Popp and Salzer (2007)	Cubic	43×43×43	Hydraulic rams	2000 kN
Laboratorie 3SR (Grenoble)	Bésuelle and Hall (2011)	Prismatic	50×30×25 50×30×50	σ_1 & σ_2: Hydraulic pistons σ_3: confining fluid	σ_1: 500 kN σ_2: 700 kN σ_3: 100 MPa
Suranaree University of Technology	Fuenkajorn et al. (2012)	Prismatic	up to: 100×100×200	Axial: Hydraulic load cell Lateral: Cantilever beams	Axial: 1000 kN Lateral: 100 kN

2.3 Theoretical studies on rock failure and impact of σ_2

Coulomb failure theory is perhaps the simplest and the most commonly used failure criterion for rocks and soils (Jaeger et al. 2007). Coulomb postulated that failure in the rock/soil occurs along a plane as a result of the acting shear stress (τ) along it

exceeding the frictional resistance. The resisting frictional force is proportional to the normal stress (σ_n) acting on the plane and the internal cohesion (S_0) which is considered as the inherent shear strength of the material. The Coulomb criterion is expressed as:

$$|\tau| = S_0 + \mu_i \, \sigma_n , \tag{2.1}$$

or:

$$\sigma_1 = C_0 + \sigma_3 \left(\sqrt{\mu_i^2 + 1} + \mu_i \right)^2 , \tag{2.2}$$

in which μ_i is the coefficient of internal friction and it is a material constant. C_0 is the uniaxial compressive strength (UCS). Both of these parameters can be determined through conventional laboratory experiments (Jaeger et al. 2007).

The Coulomb criterion neglects the impact of intermediate principal stress on failure of material. Similar to the Coulomb theory, numerous failure criteria have been developed for brittle rocks which have the general form of (Haimson 2006):

$$\sigma_1 = F_1(\sigma_3) \quad or \quad F_2(\sigma_1, \sigma_3) = 0 , \tag{2.3}$$

in which F_1 and F_2 are functions that depend on the properties of material.

Examples of such failure criteria are Mohr, Griffith and McClintock and Walsh (Jaeger et al. 2007), which disregard the effect of σ_2 on failure. In the last century various efforts including theoretical studies and experimental investigations have been devoted to include the effect of all three principal stresses on rock failure response (Haimson 2006). Significant progress has been made in this regard which proved that describing rock deformation and failure properties while ignoring the effect of the intermediate stress, cannot reflect the rock behaviour under general stress states (see Haimson 2006, Mogi 2007). Over the years, several failure criteria have been proposed to formulate the influence of all principal stresses on rock failure (Nádai 1950, Drucker and Prager 1952, Wiebols and Cook 1968, Lade and Duncan 1975, Zhou 1994, Ewy 1998, You 2009). Here some of the most important developed true triaxial failure theories are briefly reviewed.

Perhaps one of the most well-known and simplest 3D failure theories is the von Mises theory (Nádai 1950), which was initially proposed to estimate yielding of ductile materials (such as metals). This criterion assumes that failure happens if the

distortional strain energy, which is represented by the octahedral shear stress (τ_{oct}), reaches a constant limit value that depends on the material properties:

$$\tau_{oct} \equiv \frac{1}{3}\sqrt{(\sigma_1-\sigma_2)^2+(\sigma_2-\sigma_3)^2+(\sigma_1-\sigma_3)^2} = constant\,. \qquad (2.4)$$

However, this criterion was found to be inappropriate for brittle materials such as rocks (Jaeger et al. 2007), as the failure stress (strength) typically increases with increasing confining stress. Nádai (1950) modified the von Mises yield criterion to describe the pressure dependent behaviour of polycrystalline materials such as rocks. He proposed describing the octahedral shear stress as a monotonically increasing function (f_N) of octahedral normal stress (σ_{oct}):

$$\tau_{oct} = f_N(\sigma_{oct}), \qquad (2.5)$$

in which:

$$\sigma_{oct} = \frac{1}{3}(\sigma_1+\sigma_2+\sigma_3)\,. \qquad (2.6)$$

This equation explains that the shear stress generally increases with mean normal stress up to the brittle failure point. Freudenthal (1951), Drucker and Prager (1952) and Bresler and Pister (1957) developed different forms of this criterion for concrete and soil based on a linear relationship between τ_{oct} and σ_{oct} (Haimson 2006).

Later Wiebols and Cook (1968) proposed a true triaxial failure criterion based on strain energy. They postulated rock as an elastic material that contains numerous evenly-distributed, randomly-oriented closed microcracks (Haimson 2006). Applying three principal compressive stresses on rock induces shear stress (τ) and normal stress (σ_n) on crack surfaces. Frictional sliding along the surfaces of the closed cracks causes storing of strain energy in rock. Failure occurs when the amount of effective strain energy in the rock reaches a certain critical value, which is a function of both applied stresses and the material properties. The numerically-derived Wiebols and Cook criterion predicts that at a constant σ_3, the value of σ_1 at failure (strength) is always larger under triaxial extension conditions ($\sigma_1=\sigma_2>\sigma_3$) than triaxial compression condition ($\sigma_1>\sigma_2=\sigma_3$). For both of these stress states, strength increases linearly with increasing the confining pressure (σ_3). Under true triaxial stress states

($\sigma_1>\sigma_2>\sigma_3$) at a constant level of σ_3, the strength increases with raising σ_2 until it reaches a maximum value and then declines at higher σ_2. An example of the failure envelopes numerically calculated based on the Wiebols and Cook criterion is shown in Figure 2.1. One of the limitations of the Wiebols and Cook criterion is that it requires knowledge of the coefficient of sliding friction between the surfaces of cracks (μ_s), for which there are no laboratory techniques capable of such a measurement (Haimson 2006). However, comparing a large number of experimental results with the estimated curves of this criterion indicated a reasonable agreement (Mogi 1971, Haimson 2006) and hence confirmed the capability of this theory in predicting variations of strength under true triaxial stress conditions (Haimson 2006).

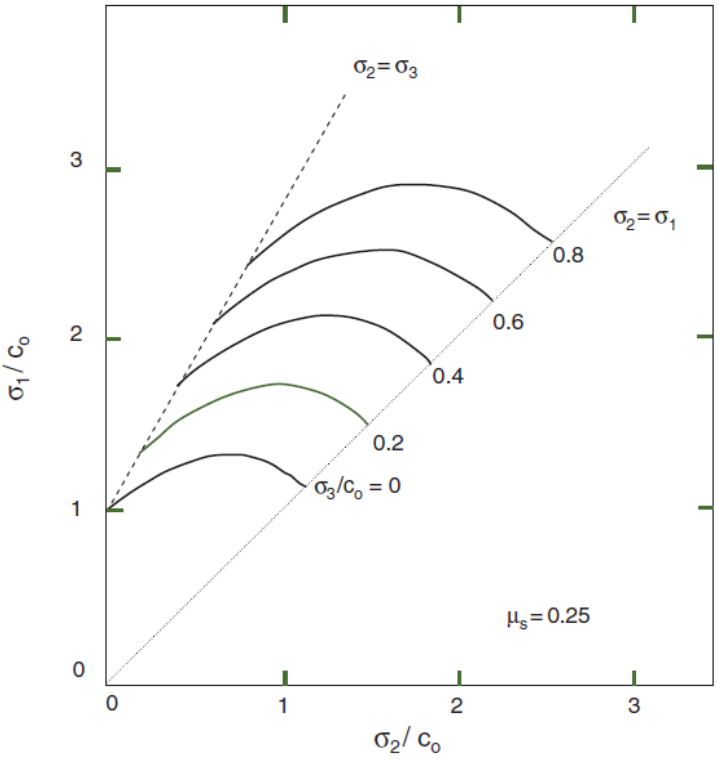

Figure 2.1 Typical variations of rock true triaxial strength (σ_1) as a function of σ_2, as predicted by the Wiebols and Cook criterion. The stresses are normalized by the uniaxial compressive strength (C_0). The coefficient of sliding friction (μ_s) is assumed to be 0.25 (Haimson 2006).

Zhou (1994) proposed a modified von Mises criterion with similar features to the Wiebols and Cook criterion. This criterion is referred to as the modified Wiebols and Cook criterion (Colmenares and Zoback 2002). It expresses the rock failure as:

$$J_2^{1/2} = A + BJ_1 + CJ_1^2, \tag{2.7}$$

where,

$$J_1 = \frac{1}{3} \times (\sigma_1 + \sigma_2 + \sigma_3), \tag{2.8}$$

$$J_2^{1/2} = \sqrt{\frac{1}{6}\left((\sigma_1 - \sigma_2)^2 + (\sigma_1 - \sigma_3)^2 + (\sigma_2 - \sigma_3)^2\right)}. \tag{2.9}$$

The parameters *A*, *B* and *C* are constants that depend on rock properties and are defined as:

$$C = \frac{\sqrt{27}}{2C_1 + (q-1)\sigma_3 - C_0} \times \left(\frac{C_1 + (q-1)\sigma_3 - C_0}{2C_1 + (2q+1)\sigma_3 - C_0} - \frac{q-1}{q+2} \right), \tag{2.10}$$

$$B = \frac{\sqrt{3}(q-1)}{q+2} - \frac{C}{3}\left(2C_0 + (q+2)\sigma_3\right), \tag{2.11}$$

$$A = \frac{C_0}{\sqrt{3}} - \frac{C_0}{3} B - \frac{C_0^2}{9} C, \tag{2.12}$$

in which C_0 is the uniaxial compressive strength of the rock, μ_i is the coefficient of internal friction ($\mu_i = \tan \phi$), and q and C_1 are defined as follows:

$$q = \left[\left(\mu_i^2 + 1\right)^{1/2} + \mu_i\right] = \tan^2\left(\frac{\pi}{4} + \frac{\phi}{2}\right), \tag{2.13}$$

$$C_1 = (1 + 0.6\mu_i) C_0. \tag{2.14}$$

Colmenares and Zoback (2002) compared laboratory data of five different rock types (dolomite, limestone, amphibolite, sandstone and shale) with a number of failure criteria. Based on the associated misfits of these criteria with the experimental data, they suggested that using the modified Wiebols and Cook criterion does clearly describe failure in many rock types.

As previously explained in section 2.2, Mogi (1971) conducted true triaxial tests on various rock types such as dolomite, trachyte and marble. He observed that in σ_1-σ_2 domain the data fitted a downward concave curve at any constant σ_3, which was in a convincing agreement with Wiebols and Cook (1968) predicted model. Mogi (1971) also attempted to obtain an empirical failure criterion using his experimental data. He found that plotting the data for Dunham dolomite and Mizuho trachyte in octahedral stress (τ_{oct}-σ_{oct}) domain (following Nádai (1950)) does not generate a

uniform criterion. He also showed that brittle failure in true triaxial tests happens in form of shearing along planes striking parallel to σ_2. Therefore, it was more realistic to assume that the critical distortional strain energy which leads to failure, as a monotonically increasing function of the mean normal stress acting on these planes ($\sigma_{m,2}$) rather than the octahedral normal stress (σ_{oct}):

$$\tau_{oct} = f(\sigma_{m,2}). \tag{2.15}$$

Therefore, Mogi (1971) showed that plotting the experimental data in a τ_{oct}-$\sigma_{m,2}$ diagram produced a single curve for each of the tested brittle rocks, expressed in form of power functions. Mogi's suggested criterion has been widely used by many other researchers (e.g. Chang and Haimson 2000, Oku et al. 2007, Lee and Haimson 2011).

2.4 Effect of σ_2 on behaviour of sandstones and shales

2.4.1 Sandstones

Although some previous true triaxial research has been done on sandstones (Wawersik et al. 1997, Young et al. 2011, Ingraham 2012, Ma and Haimson 2013), only limited number of these studies particularly targeted the impact of changing σ_2 on failure characteristics and elastic and inelastic properties of these rock types (Takahashi and Koide 1989, Crawford et al. 1995, Kwaśniewski et al. 2003, Ma 2014). Some of the earlier findings on the relation of mechanical behaviour of sandstones with the intermediate principal stress are reviewed below.

Takahashi and Koide (1989) conducted true triaxial tests on three different sandstones. Their experimental results showed that increasing σ_2 had a strengthening effect on the tested sandstones, which generally confirmed the earlier findings by Mogi (1971) on other rock types. The obtained failure strength data were in good agreement with their proposed form of the Wiebols and Cook (1968) criterion. Generally they observed that the impact of increasing σ_2 on strength was more pronounced under higher levels of minimum stress. In addition, they found that increasing σ_2 enhanced the difference between the strains along the minimum and intermediate stress axes and caused the dilatant strain to mainly occur along σ_3.

Crawford et al. (1995) used a specially designed true triaxial cell (Smart 1995) which applied anisotropic lateral stresses ($\sigma_2>\sigma_3$) on cylindrical core specimens. They presented tests results on two different sandstones, which indicated significant increase in the fracture strength, as well as the residual strength of tested rocks due to increasing the intermediate principal stress. Microseismic data (acoustic emissions) acquistion and macroscopic observation of failed samples, showed that the microcracks strike along the σ_2 direction and opened in the σ_3 direction under true triaxial stress states.

Ingraham et al. (2013) conducted true triaxial tests on Castlegate sandstones. The nature and purpose of their investigations was different from the present study. Their aim was to examine the dependence of failure on the third invariant of deviatoric stress by applying different magnitudes of constant mean stress during testing. They found that the mean stress influenced the strength, shear band angle and failure mode of the tested rock.

Ma (2014) studied two high porosity sandstones which underwent compaction deformation, Coconino Sandstone and Bentheim Sandstone, to understand the effect of σ_2 on their failure strength, failure plane angle and failure mode. For both sandstones, σ_2 was raised from $\sigma_2=\sigma_3$ to $\sigma_2=\sigma_1$ at a specific level of σ_3. At a constant σ_3, strength increased with increasing intermediate stress up to a maximum level and then it declined, in a manner consistent with previous tests noted and also the Wiebols and Cook criterion (Figure 2.1). He observed up to 15% increase in strength with raising σ_2 over σ_3. Also increasing σ_2 at a constant σ_3 caused an increase in the angle between the maximum principal stress direction and the normal to the failure plane (called failure-plane angle). In addition, his microstructural investigations indicated that when σ_2 was higher than the $\sigma_2=\sigma_3$ level in different tests, the microcracks were preferentially aligned close to the intermediate stress axis.

2.4.2 Shales

Shales belong to a class of fine-grained clastic sedimentary rocks known as mudrocks which include claystone, siltstone, argillite and shales (Tucker 2001, Blatt et al. 2006). The preferential alignment of clay minerals, thin laminations and bedding in shale can result in significant anisotropy of rock properties (i.e. directional dependence). In the past, some experimental studies have been devoted to shales to characterize their deformation and failure properties and to understand the

influence of stress conditions on them (Lin and Heuze 1987, Mese 1995, Niandou et al. 1997, Valès et al. 2004, Gautam 2005, Corkum and Martin 2007, Popp et al. 2008, Delle Piane et al. 2011, Dewhurst et al. 2011, Amann et al. 2012). However, the information gathered by these investigations was obtained under uniaxial or triaxial conditions, and do not always simulate the real in-situ stress states. Few true triaxial investigations have been conducted on mudrocks to date, such as studies by Oku et al. (2007) on siltstone and studies by Bésuelle and Hall (2011) on argillite. Very limited true triaxial investigations have been performed in shales, and none on preserved material and these are shortly reviewed below.

Takahashi and Koide (1989) were perhaps the first who investigated shale failure characteristics under a 3D anisotropic stress state. They performed true triaxial tests on Yuubari shale and found that increasing σ_2 caused growth in the fracture strength of these shales and this strength growth was more distinct at higher σ_3 levels. The shales failed in brittle mode under the applied stress range and investigating the post-failure samples indicated that the macroscopic fault planes had propagated parallel to the σ_2 direction. Residual strength was found to be almost unaffected by the intermediate stress in these specimens.

Popp and Salzer (2007) tested Opalinus Clay in a true triaxial cell. They reported that the specimens were cut from the shaly facies and indicated well-developed bedding planes. The samples were loaded in a way to apply the maximum stress normal, parallel and 45° to the bedding. During each test the minimum and intermediate stress were equal ($\sigma_2=\sigma_3$) and were kept constant while σ_1 was increased until failure. The results showed that increasing the lateral stress ($\sigma_2=\sigma_3$) generally increased the failure strength. However, the study mainly focused on investigating dilatancy in the tested specimens rather than the impact of σ_2. Popp and Salzer monitored the evolution of ultrasonic wave velocities in different directions during loading to study the velocity anisotropy of the samples. Also they used it for detection of dilatancy onset and to monitor the changes in dilatancy with the applied stress state. They found that when σ_1 was normal to bedding, volumetric strains were dominated by the effect of compaction perpendicular to bedding and hence were not useful for determining of the onset of dilatancy. This was due to closure of bedding parallel cracks and background porosity being more volumetrically significant than the opening and propagation of axially oriented microcracks forming parallel to σ_1

and σ_2, induced by axial loading. As an alternative, they suggested using changes in wave velocities as an indicator of microcrack initiation in the samples.

Naumann et al. (2007) also studied deformational behaviour of Opalinus Clay in the laboratory. They conducted true triaxial tests on samples with different bedding orientation with respect to the maximum principal stress axis. Similar to the study by Popp and Salzer (2007), Naumann et al. applied $\sigma_2=\sigma_3$ in their true triaxial experiments. However, they kept the mean stress constant during each test, by maintaining σ_2 and σ_3 equal and reducing simultaneously while increasing σ_1. Thus, as σ_2 was not kept constant during each test, its influence on mechanical response of the tested rock was not directly investigated. Their results indicated that the samples cut parallel to bedding were generally stronger than the samples cut perpendicular to bedding. They also found that the bedding plane orientation affected the degree of anisotropy in strength, dilatancy and creep behaviour of the clay samples.

2.5 Importance of saturation and preservation in shales

When a core is transferred from the bottom-hole to the atmospheric conditions, it may undergo stress release, pore pressure release, temperature alteration or chemical effects (when in contact with drilling mud) (Fjær et al. 2008). In low-permeability rocks such as shales (with permeability in the range of nanoDarcies or lower), pore pressure equilibrium is not achieved promptly after core-retrieval from bottom-hole, which probably causes microscopic or macroscopic tensile failure in the core. This phenomenon along with the volumetric expansion of cores due to stress release after retrieval, results in incompletely saturated shale cores. Consequently, exposure to wetting fluids, such as water, after retrieval may induce large capillary pressure in shale cores due to their partially-saturated state and presence of gas/air in their pores. The cause of the capillary pressure is to counterbalance the surface tension created at the contact of the wetting fluid (water) and non-wetting fluid (gas). Depending on the pore size, the generated capillary pressure inside a shale core might be so large that it exceeds the tensile strength of the rock and hence result in rupture and disintegration of the sample. Therefore, shales are very sensitive to exposure to wetting fluids or loss of their pore fluid, which may cause sample disintegration or mechanical strengthening in shales, depending on their microstructure and composition. This shows the importance of sample preservation in shales and need for extra care in

handling shale cores to avoid significant changes to their natural water content (Fjær et al. 2008).

In general, changes in saturation state can significantly alter the mechanical behaviour of shales. As in shales and other rocks with small pore size (such as chalk), partial fluid saturation (e.g. water/gas) can lead to high capillary suction forces between their grains (Papamichos et al. 1997). Capillary forces occur due to a property of fluids called surface tension, which in case of rocks/soils is generated at the interface of water, as the wetting phase, and mineral grains, gas or air, as the non-wetting phase. At low water saturation degrees, water forms capillary menisci in small pores or narrow paths between grains. The surface tension at the contact of water and air in neighbouring pores causes a frictional force which acts as cohesion and pulls grains together. On the other hand, at high water saturations, the pores are filled with water and hence the surface tension is reduced. Consequently, the capillary suction between the grains which acted as cohesion, disappears. Figure 2.2 displays the changes in capillary suction with saturation degree in a shale in comparison to sandstones with significantly larger pore size. Suction is noticeably greater in shale than in sandstones and it is eventually reduced by increasing saturation degree. For the sandstones suction forces quickly vanished due to an even slight increase in saturation as their smallest pores were readily filled with water. Hence, as a result of capillarity, saturation state plays an important role in defining shale rock properties (Schmitt et al. 1994, Papamichos et al. 1997, Horsrud et al. 1998). Therefore, the extent of impact of saturation on shales behaviour basically depends on the capillary effects, which itself is controlled by the pore size in shale and thus their clay fraction and mineralogy (Schmitt et al. 1994).

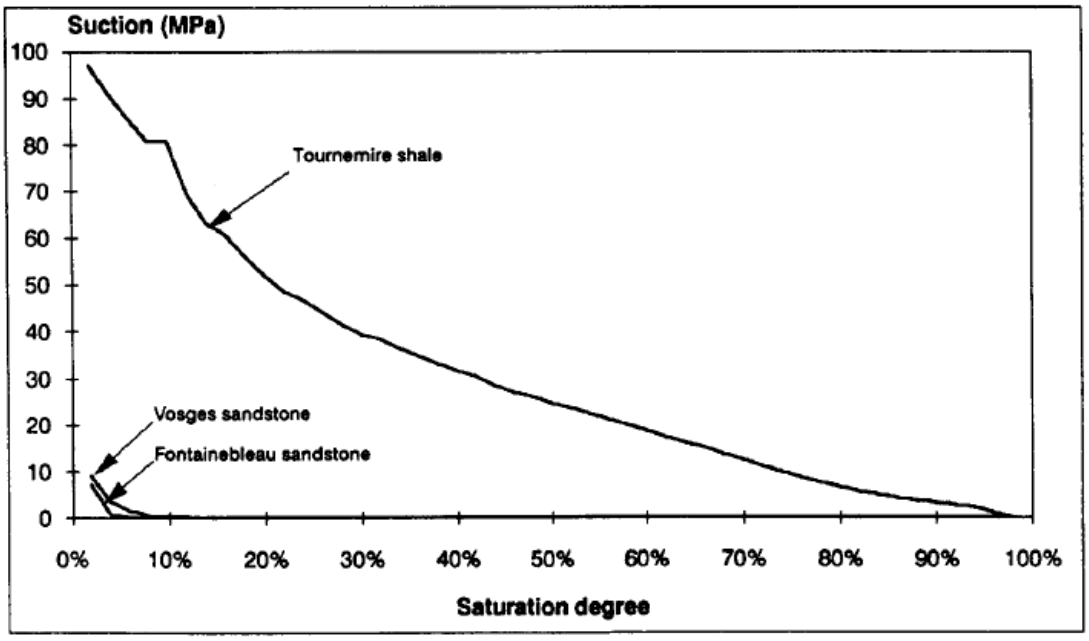

Figure 2.2 Evolution of capillary suction with saturation. Capillary forces are larger in shale than in sandstones, due to their smaller pore size. As water saturation increased in shales, suction slowly decreased (Schmitt et al. 1994).

Previous experimental investigations has confirmed the saturation impact on shales and clayey rocks (Schmitt et al. 1994, Mese 1995, Horsrud et al. 1998, Blumling et al. 2002, Valès et al. 2004, Zhang and Rothfuchs 2004, Corkum and Martin 2007, Ghorbani et al. 2009, Dewhurst et al. 2012, Tsang et al. 2012). Mese (1995) performed triaxial tests on Barnett Shale and found that reduction in saturation caused an increase in static and dynamic Young's modulus as well as the compressive strength of these shales. Blumling et al. (2002) studied Opalinus Clay and observed similar results. Decreasing water content increased the rock peak strength. They further found that the rock failure mode was tranferred from ductile to brittle mode by reducing its water content. Valès et al. (2004) conducted a comprehensive study on the influence of water saturation on Tournemire Shale. They evaluated the correlation of mechanical properties (such as elastic moduli and failure data) with a decreasing degree of water saturation, taking into consideration the influence of bedding planes orientation with respect to the applied stresses. Generally, the results indicated that deceasing saturation caused increase in strength, stiffness and cohesion and reduction in the Poisson's ratio of the tested shales. Recently, Dewhurst et al. (2012) studied the physical and mechanical behaviour of old, stiff, low porosity shales from the Officer Basin in Australia. Reducing saturation, caused noticeable increases in static and dynamic Young's and shear

moduli and significant decreases in Poisson's ratio and Bulk modulus. However, their results indicated the rock strength to be unaffected when saturation was changed from fully-saturated to partially-saturated state. They suggested that the low clay content (~30%) of these shales and heterogeneity between tested samples as possible reasons for this contradictory observation with respect to previous findings in the literature. Further tests on more clay rich shales (Opalinus, Pierre) did find both strength and static elastic property increases with decreasing water saturation (Dewhurst et al. 2013).

These findings with regard to the impact of saturation on shales have been acquired under ambient, uniaxial or triaxial stress conditions. However, no studies have been performed to determine the effect of saturation on shale deformational behaviour under true triaxial loading to date.

2.6 Multistage tests

In conventional triaxial tests (known as single-stage tests), at a specific level of confining pressure, axial load (σ_1) is increased on the rock specimen until its peak strength is obtained and sometimes beyond until residual strength is achieved post failure (Kim and Ko 1979). Hence, at each confining pressure, only one point on the failure envelope can be extracted. In order to determine the entire failure envelope using only one specimen, two approaches were proposed initially by Kovari and Tisa (1975) and later in the ISRM suggested methods by Kovari et al. (1983). The first approach is called a "multiple failure state test" (commonly referred to as "multistage" test) and the second one is the "continuous failure state test". In the first method, an initial level of confining pressure is applied on the rock and axial stress is then increased to a point close to failure (imminent failure point) but loading is stopped before the sample breaks. After termination of loading, the sample is subjected to a new level of confining pressure in the next stage and the same process as previous stage is repeated. Only at the last stage is the rock sample brought to failure. Hence, this way the rock failure stress is defined at several levels of confining stress. A continuous failure state test is generally similar to the multistage test, but in this case both confining and axial stress are increased simultaneously to directly produce a continuous failure envelope.

Kim and Ko (1979) validated multistage tests by comparing their results to several single-stage tests data. Validity of the results was confirmed for ductile and somewhat brittle rocks. However, they reported that the robustness of this method was much lower for very brittle hard rocks at low confining pressures, as for such rocks, due to their sharp peak, detection of the peak strength before significant damage being induced in the sample was difficult. As Holt and Fjær (1991) also compared the failure envelopes of a sandstone obtained in multistage and single-stage tests and found satisfactory agreement between the results. They suggested using acoustic measurements during the multistage triaxial tests to monitor changes in the microcracks pattern inside the specimen. Based on their observations, Holt and Fjær (1991) explained that if a sample was significantly damaged during one of the initial stages of the test, the strength would be underestimated in the subsequent stages. Therefore, loading should be terminated before substantial damage occurs in the sample (Youn and Tonon 2010). Different criteria have been suggested to determine the termination point of each loading stage.

Kovari and Tisa (1975), Kim and Ko (1979) and some other researchers used the point where the stress-axial strain curve deviates from linear elastic behaviour and approaches a plateau, as the imminent failure point. Crawford and Wylie (1987) described the stress level at which the volumetric strain reached zero as the indicator of failure to terminate loading in each cycle. Pagoulatos (2004) suggested using the inflection point of volumetric strain curve where the derivative of the volumetric strain becomes zero. Youn and Tonon (2010) proposed a method in which loading was controlled by the rate of radial strain so that failure was approached more slowly. Loading was terminated as the stress-radial strain curve reached a plateau.

The multistage technique has been widely used in the past to investigate the influence of stresses on strength and failure behaviour of rocks under triaxial stress conditions (Crawford and Wylie 1987, Kim and Ko 1979, Zhang and Rothfuchs 2004, Dewhurst et al. 2011, Gräsle 2011, Amann et al. 2012). However, conducting multistage tests under true triaxial stress states has been uncommon (Macari and Hoyos 2001). The feasibility of this technique in evaluating the σ_2 impact on rock mechanical properties was examined in this thesis. Multistage true triaxial tests were considered here as they could be beneficial in the present study firstly to avoid the effect of sample variability on obtained data, and secondly to acquire more information from the limited number of available shale samples.

2.7 Summary

The review of the literature performed in this Chapter showed that our understanding of the failure characteristics and deformational properties of sandstones and shales under true triaxial stress states is limited. Hence experimental studies are required to further investigate the influence of intermediate stress on the mechanical behaviour of these rocks. Also, the impact of water saturation on the mechanical response of shales is poorly understood, and no studies have been performed to determine this effect under true triaxial loading. In this thesis, mechanical properties of sandstones and shales have been evaluated in the laboratory to shed more light on their behaviour under isotropic to fully 3D stress states. Furthermore, the novel idea of adopting multistage technique to investigate σ_2-effect, has been evaluated in the present work. In the next Chapter, the experimental methodology used for this study is explained.

3 Experimental methodology

3.1 Introduction

One of the main objectives of this work was to establish an experimental procedure to obtain mechanical properties of rocks under true triaxial stress states through compressive tests in a true triaxial stress cell (TTSC). This cell has been designed to accommodate cubic samples with dimensions of up to 300 mm edge length. Advanced geomechanical experiments have been done using this apparatus such as sand production (Younessi 2012) and hydraulic fracturing simulation (Sarmadivaleh 2012). However, this work has been the first to establish an experimental procedure to obtain true triaxial mechanical deformational properties of rocks through compressive failure tests in the TTSC.

In this work, the stress state is chosen in a way to apply the minimum and intermediate principal stresses in lateral directions, and the maximum principal stress in vertical direction. The underlying principle in these experiments is that two sets of independent lateral stresses are applied on the specimen. Thereafter, these two stresses are kept constant while the vertical stress is increased until the sample undergoes failure. The applied stresses were then changed in a series of tests to investigate dependence of rock mechanical parameters on stress conditions, here stress magnitude and anisotropy.

This technique is similar to the commonly used standard triaxial compression tests. The major difference between the true triaxial tests and the standard triaxial tests is that the latter cannot evaluate the effect of intermediate stress on the deformation behaviour of rock. Therefore in this study, a major goal was to examine the influence of changing the intermediate stress from isotropic stress conditions to anisotropic lateral stress conditions on rock strength and elastic properties.

The main target of this research was to investigate deformational behaviour of sandstones and shales under true triaxial stress conditions. Also the impact of changing saturation state on mechanical properties of shales was examined, for

which well-preserved samples were required which are often difficult to acquire. To study the effect of intermediate stress on deformational properties of sandstones, a series of synthetic sandstone specimens were manufactured. The benefits of using synthetic sandstones was that firstly, they could be reproduced and secondly, as they were isotropic, it was easier to investigate the impact of the intermediate principal stress on them apart from the complications of anisotropy as in the case of shales. Hence, these samples also assisted in establishing an accurate and efficient experimental setup and procedure. In the following sections the procedures for sample preparation and experimental setup will be described in detail.

3.2 Sample preparation

3.2.1 Synthetic sandstones

Synthetic sandstones were used in this study for different purposes, the most important of which was to determine how changing the intermediate stress could affect the mechanical properties of sandstones. Also these synthetic samples were employed to design and prepare an appropriate experimental setup and examine the test equipment and measuring/recording systems. Moreover, the properness of multistage true triaxial tests was investigated through the synthetic sandstone samples. The results from multistage tests were compared with the results obtained in single-stage tests to verify whether they give similar results. The obtained data and the conclusions found are presented and discussed in Chapter 4.

Two sets of sandstone samples were prepared: 50mm-side cubes and cylindrical cores of 76 mm length and 38 mm diameter. The preparation process, mixture ratios and settling times were relatively identical, and thus all samples are assumed to be homogenous. However, some heterogeneity in cementation between samples is expected.

The basic components of synthetic sandstones were water, sand and cement. The mechanical properties of the produced specimens depend directly on properties of the initial components, their fraction in the final mixture and the preparation and curing process.

The size of the sand grains, type of cement and water, and the ratio of initial components can significantly affect the fabricated samples (e.g. Saidi et al. 2003) and

thus these should be selected carefully depending on the purpose of the experiment. For instance in sanding analysis tests, the manufactured samples should have a specific strength range in order to be representative of the sandstone formations which are responsible for sand production. The strength in these samples is a function of the sand grain size and sand/cement and water/cement ratio (Nouri et al. 2006). However, in the present study the main purpose of manufacturing synthetic sandstones was to systematically investigate the impact of intermediate stress on rock failure properties and to establish an experimental procedure to conduct compressive true triaxial tests in the TTSC. Therefore, provided that the synthetic samples have consistent physico-mechanical properties, the absolute values of the strength and elastic properties of the final product was not critical. Accordingly, the preparation procedure for synthetic sandstones in this work is similar to the process of concrete preparation for construction purposes in civil engineering.

The composition of the synthetic sandstones comprises Portland cement, sand and water with weight ratio of 5 for sand/cement and 0.5 for water/cement. The size of the sand grains used in this study was in the range of 150-425 μm. The stages of sample preparation are presented below:

1. *Mixture preparation:*

   The volume of the required sand was roughly estimated based on the volume of the moulds and from that the weight of sand is determined. Then the required amounts of water and cement are precisely weighed according to their ratios to sand. First, sand and cement are combined for few minutes and then water is added gradually, and finally the components are mixed well for at least 10 minutes to produce an even mixture.

2. *Casting:*

   Cubical brass moulds of size 50 mm and cylindrical moulds of 38 mm diameter and length/diameter ratio of ~2 were used for casting the sandstone samples. Inner walls of the moulds were initially coated with a thin layer of oil for easier removal of samples after drying. Each mould was filled with the mixture in few stages, compressing the mixture inside it at each stage. When the mould was completely filled with mixture, the top surface was flattened using a finishing trowel. It is recommended to plough the surface of each layer before adding the next portion during casting to prevent formation of discontinuity planes (Nouri et al. 2006).

3. *Curing:*

   The samples were left in moulds for three days before being removed. During curing, no pressure was applied on the samples. The samples were then submerged in water for 21 days at ambient temperature. Afterwards they were dried in oven at 60°C. All specimens were thereafter wrapped in plastic film to minimize any alterations to their structure due to weathering during storage.

3.2.2 Shale samples

Two different types of shales have been studied in this work: Carynginia Shale and Pierre Shale. In the following sections the sample preparation procedure for both types of shale samples is explained.

Pierre Shale

Whole round shale cores were preserved in resin and subsampled plugs under mineral oil since retrieval from a quarry to avoid significant changes to their water content. The plugs were stored in the lab under identical conditions prior to testing. These steps were taken to prevent changes to the state of the sample. However, development of some microcracks is unavoidable due to core recovery, and occasionally during sample preparation (cutting and machining cubic specimens).

Specimens in the form of cubes with the dimensions of roughly 50mm×50mm×50mm were cut using a laboratory cutting machine from the larger shale blocks. A diamond-impregnated bandsaw was employed for this purpose, as it does not induce the intense vibrations common to when using a normal rock saw. The bandsaw was also used for cylindrical samples as it does not impose torsion and consequently shearing along bedding, as in the case of rotary drill bits for cylindrical samples. Thus by using the diamond bandsaw, the risk of breaking shale specimens during cutting is reduced, as these rocks are quite weak and fragile, in particular parallel to bedding planes.

Oil was used as a flushing and cooling fluid, to remove the cuttings and also to prevent desiccation of the shale specimens during cutting. The sample faces were thereafter made parallel and the edges were precisely machined to the desired dimensions by means of a grinder with a diamond disk. During grinding, oil was sprayed on the sample faces to avoid rock surface drying.

Thereafter predetermined saturation states were imposed on rock samples by placing them inside desiccators containing salts to create specific relative humidity (RH) environments. The underlying principles of this method are similar to the sorption bench technique used for obtaining water retention curves of clayey material (Laloui 2010). The RH environment is created inside a closed desiccator in which the relative humidity of the closed system is controlled by means of a saturated saline solution (Figure 3.1). Different relative humidity levels can be obtained in the system depending on the type of salt used in the saline solution (Table 3.1). The exchange of water molecules between the specimen and the solution imposes the desired saturation state. The rock samples were placed on a porous plate above the saline solution and were repeatedly weighed with a precision of 0.01 gr. When the weight evolutions became stabilized, the rock sample is considered to be in equilibrium with the applied relative humidity state (Figure 3.2). Once the specimens reached the desired levels of relative humidity they were taken out of the RH-machine for true triaxial testing. In this study Pierre Shale specimens were divided among four different desiccators with controlled humidity of 29%, 52%, 75% and 97%. The obtained water saturation degree for the four groups were 40%, 59%, 70% and 100%, respectively. The remaining pore fluid was air.

Table 3.1 Saturated salt solutions and the corresponding relative humidity percentage at 21°C (after Laloui et al. 2013).

Saturated salt solution	KOH	LiCl	$MgCl_2$	K_2CO_3	$Mg(NO_3)_2$	NaCl	KCl	K_2SO_4
Relative humidity (%)	9	11.3	33.1	43.2	54.1	75.4	84.9	97.5

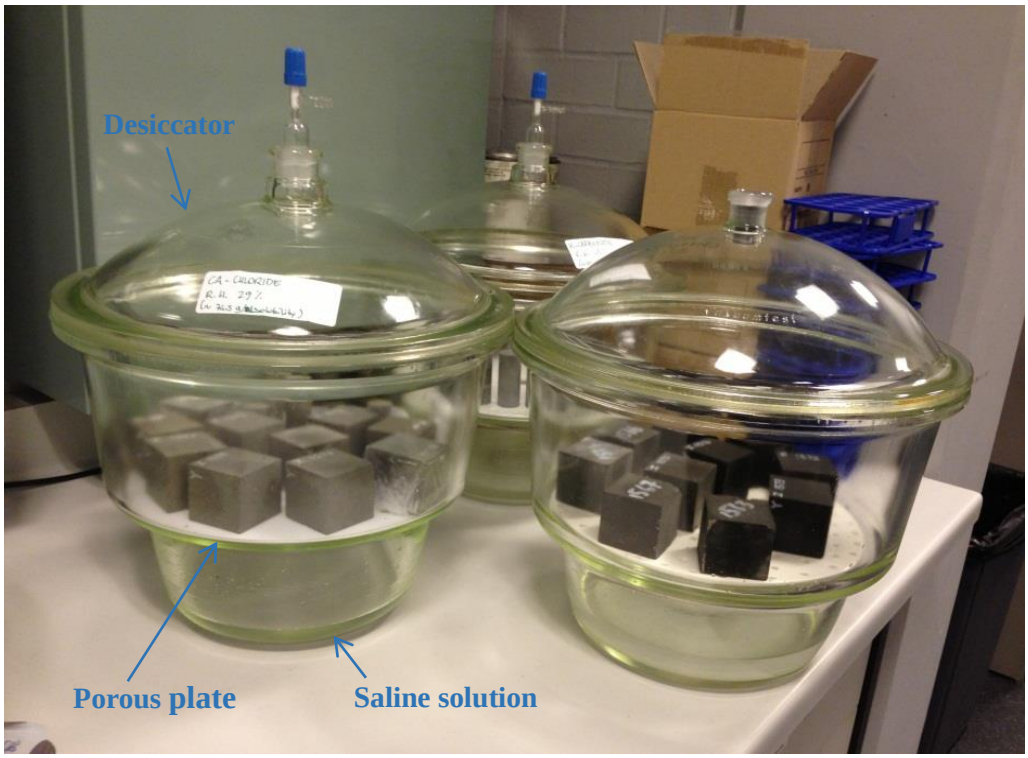

Figure 3.1 Relative humidity environments are established in glass desiccators and are used for imposing controlled partial saturation in Pierre Shale samples.

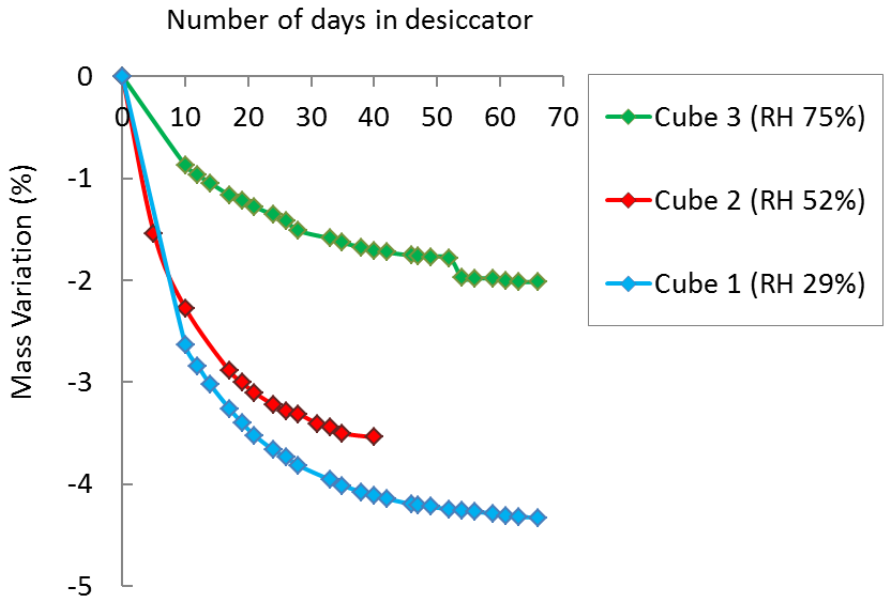

Figure 3.2 Mass variations of the cubic samples as a function of number of days in desiccators with different relative humidity (RH) environments. The specimen was considered to be in equilibrium with the applied RH level when the mass variations became quite constant.

Carynginia Shale

The Carynginia Shale samples were cut from cores extracted from a well in the North Perth Basin. The cores were not well preserved after recovery and were only covered in cling-wrap (Figure 3.3). Thus, loss of pore fluid is expected during transportation and storage. Importance of sample preservation in clay-bearing materials and influence of changing saturation on their properties has been investigated by different authors (e.g. Dewhurst et al. 2012).

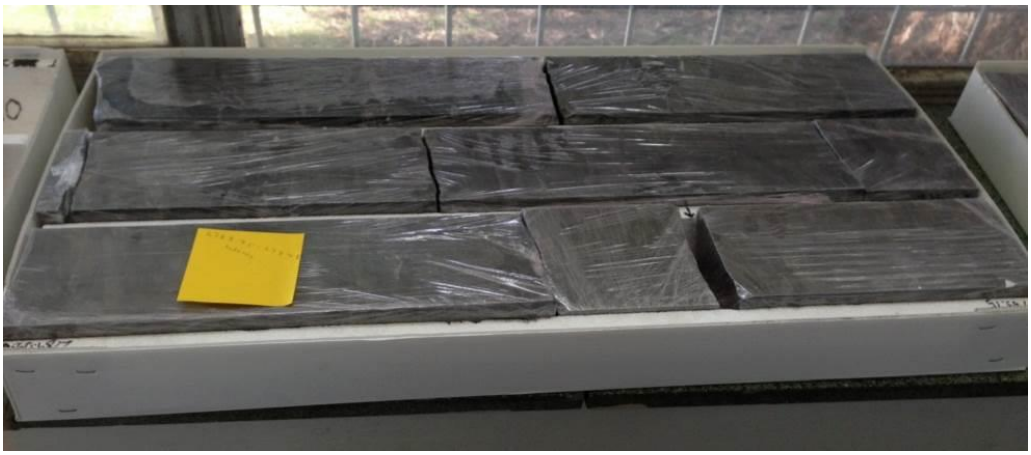

Figure 3.3 Carynginia Shale blocks were non-preserved after recovery and were only covered in cling-wrap during storage.

Experimental studies of Dewhurst et al. (2012) on cylindrical shale samples showed that, by changing saturation from fully- to partially-saturated state, Young's modulus and shear modulus significantly increased whereas the bulk modulus and Poisson's ratio decreased. They also observed a decrease in P-wave velocity and an increase in S-wave velocity by decreasing saturation. Valès et al. (2004) also found that by decreasing water saturation in shale the rock strength, elastic moduli and cohesion increased while the Poisson's ratio decreased. These findings and similar studies (e.g. Ghorbani et al. 2009) revealed that, due to presence of clay minerals and capillary effects in shales they are very sensitive to pore water. Thus, the sample preservation and core handling conditions should be carefully considered for these rocks and the parameters obtained from poorly-preserved shales only be applied for field and in-situ analysis with extreme caution.

The large Carynginia Shale cores were carefully cut and then machined into cubes of 50 mm edges. All cubes were dry-cut by normal saw, except for one (CS-02) which was cut with the diamond bandsaw under wet conditions using oil as the

cooling fluid. Cutting the specimens dry reduced the risk of opening cracks in them in particular along the bedding planes due to oil intrusion into the permeable sandstone laminations during the process (Figure 3.4). Samples were wrapped in plastic film after being machined into the size to prevent further changes in their water content during true triaxial testing.

All samples were extracted from one core and are assumed to be representative of the shale formation; however, some heterogeneity in mineral composition of specimens is expected which might induce some scattering in output results. Heterogeneity of the microstructure is also visible to the naked eye with obvious laminations and cross-beddings (Figure 3.4).

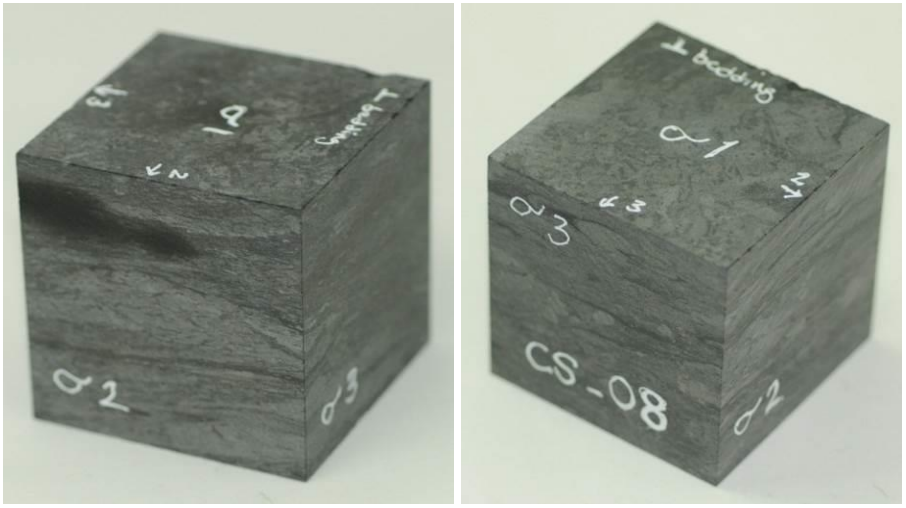

Figure 3.4 Two Carynginia shale cubes cut with normal bandsaw in wet conditions (left) and cut dry with normal saw (right). Note oil intrusion into permeable sand interlayers in the left specimen.

Shale sealing during mechanical testing

Since one of the main objectives of this study was to investigate the effect of saturation on behaviour of shales, it was very important to keep the saturation state of the shale samples unchanged during mechanical testing. To prevent desiccation of the specimen due to exposure to air during testing, the rock sample can be protected via a membrane/jacket (e.g. Valès et al. 2004). In this work, several types of jackets such as heat-shrink sleeves and plastic film were examined to find the most appropriate one, in terms of practically providing proper sealing for the cubic rock sample while introducing the least impact on the measured rock response.

Most of previous experimental studies on the influence of saturation on mechanical properties of rocks are based on testing rock cores in standard triaxial machines (e.g. Papamichos et al. 1997, Valès et al. 2004, Zhang and Rothfuchs 2004,

Dewhurst et al. 2012). Sealing such cylindrical-shape samples is easier than the samples used in this work due to their cubic shape. The usual type of jackets available for laboratory studies, such as heat-shrink and cold-shrink sleeves are normally provided in form of hollow tubes and thus are used for cylindrical samples.

In order to properly cover all six sides of a cubic rock sample, we have wrapped the cylindrical heat-shrink sleeves around the cube in two perpendicular directions. The sample is initially placed inside the sleeve, which is then heated and thus shrunk to cover four sides of the rock. Then the edges are cut, and another section of the sleeve is wrapped around the rock normal to the initial direction and the previous steps are repeated. Finally, four faces of the rock cube are jacketed with single-layer sleeves while two other faces are covered with double-layer sleeves.

In the case of the cling wrap, four sides are covered with six layers of the plastic film (nominally called “single cover”) and the other two sides are sealed with twelve layers, each (nominally named “double cover”).

To determine the impact of different sleeves on the test results, each sleeve was wrapped around an aluminium cubic sample with the same size as the rock specimens, and was subjected to stress. The aluminium block was tested separately and thus its deformation under the range of applied stresses was known. The details of these test procedures are given in sub-section 3.3.3. It was observed that while the heat-shrink sleeves cause significant non-linearity in the stress-strain curve of the aluminium cube, the cling-wrap has a minimal effect. Moreover, the latter does not involve the possibility of shale surface desiccation during the heating process as in the case of heat-shrink sleeves. Therefore, cling-wrap is considered as the sealing material in this study. Rock samples were weighed before and after each experiment to ensure that the plastic film can provide appropriate sealing of the rock samples during the mechanical test to keep their water-content unaltered. In all cases the measured weight before and after the experiment was the same. Table 3.2 presents examples of the rock sample weight measured before and after the mechanical tests for some of the specimens.

Table 3.2 The rock weight before and after mechanical testing for some of the specimens. The measurements revealed that the samples were sealed properly during the experiments and no change in their water content observed.

	Sample ID	S_w (%)	Weight-Before (gr)	Weight-After (gr)
Pierre Shale	PC-05	40	286.3	286.3
	1577	40	289.6	289.6
	1568	59	288.1	288.1
	1569	59	290.1	290.1
	1565	70	293.4	293.4
	1567	70	294.8	294.8
	PC-07	100	312.0	312.0
	PC-08	100	310.1	310.1
Carynginia Shale	CS-03	Unknown	323.4	323.4
	CS-05	Unknown	327.0	327.0
	CS-06	Unknown	326.4	326.4
	CS-08	Unknown	328.9	328.9

3.3 Testing apparatus

The experiments were conducted using a true triaxial stress cell (TTSC) in which three independent stresses were applied on cubic rock samples (Rasouli and Evans 2010). Figure 3.5 shows view of the TTSC. The lateral stresses were applied through two perpendicular pairs of hydraulic rams. For the failure tests carried out in this work, a separate hydraulic cylinder was used for applying vertical stress in the TTSC. This configuration provided good access and visibility to the sample inside the cell during the test and also allowed adequate space for the instrument cables to exit from top of the cell to the data acquisition system. Figure 3.6 displays a schematic diagram of the TTSC.

The TTSC has been designed to accommodate cubic sample of different dimensions of up to 300 mm edge length. The rock specimens tested in this study were cubes of 50 mm edge. For testing these small rock cubes in the TTSC, a plastic block made of Acetal (a polymer-type material) was used to position the specimen at the centre of the cell (Figure 3.7). Three pairs of metal shims are placed inside the holes of the plastic block around the rock sample to fill the existing gaps and transfer the load from the internal steel platens of the machine to the specimen faces. The

shims were manufactured from a heat treated aluminium alloy (alloy 2011-T4) which had enough strength to undergo the range of pressure applied in the cell with no deformation. Also, due to the lower weight of aluminium in comparison to steel, moving the shims and block assembly in and out of the cell during each test was much easier.

These spacers have rectangular cross section at contact with the rock sample and are 2 mm shorter than the rock specimen on each side to allow for sample compression. Moreover, keyways are machined on the cylindrical bodies of the spacers with metal keys installed into holes of plastic block. This special design helps to guide the spacers through the block and also once they are in position prevent them from rotation and twisting under pressure which could cause only partial stress transfer to the rock cube (see Figure 3.7).

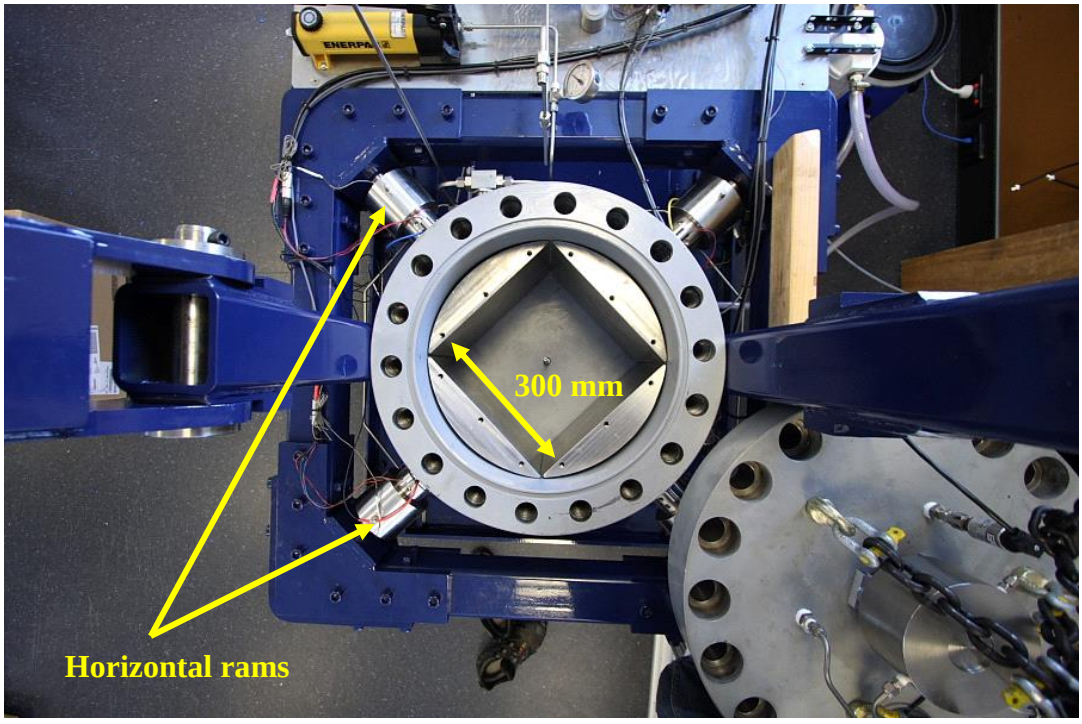

Figure 3.5 The true triaxial stress cell (TTSC) which accommodates rock cubes with dimensions less than 30 cm. The lateral stresses are applied independently through the two pairs of horizontal rams and the axial stress via a hydraulic cylinder in vertical direction.

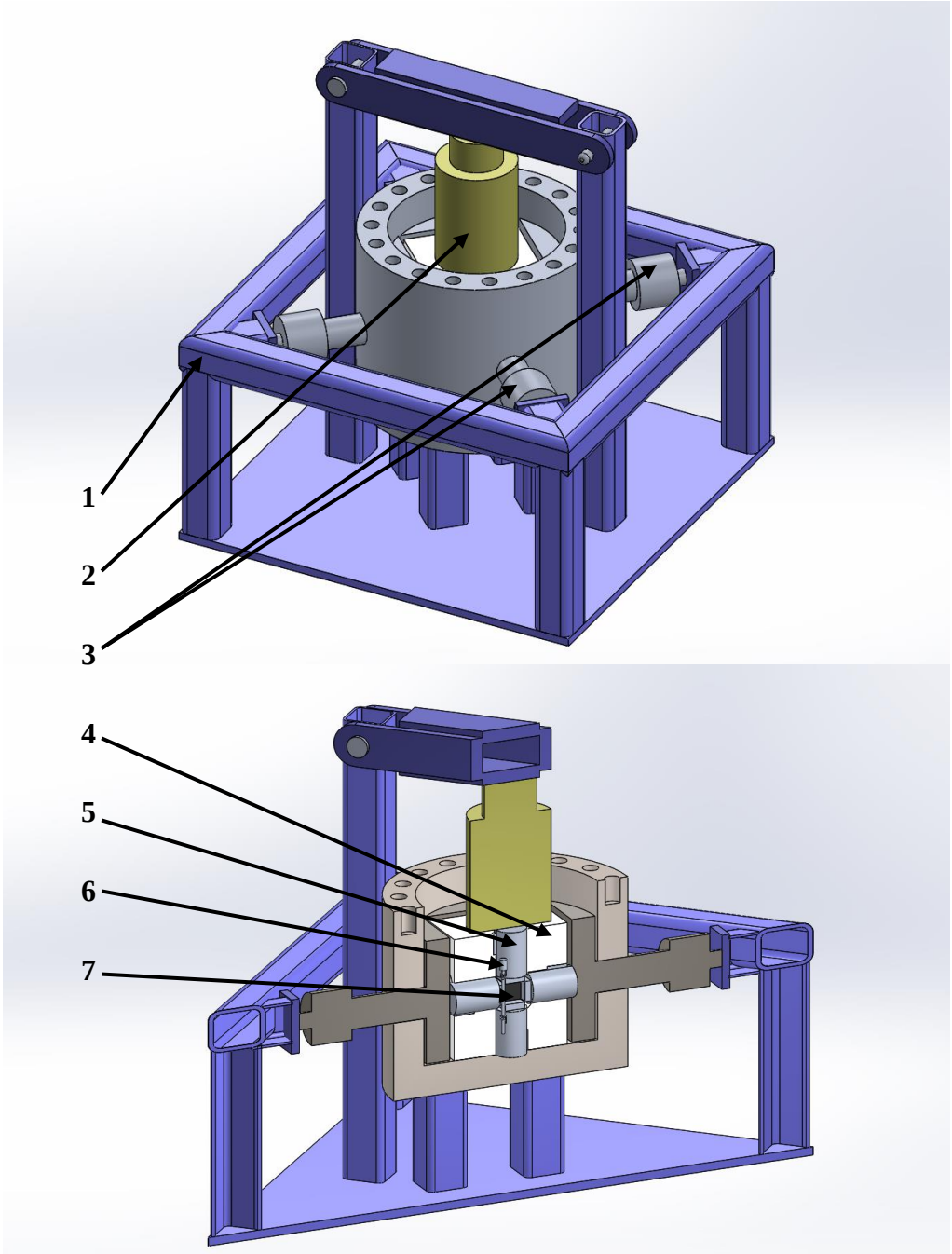

Figure 3.6 Schematic view of the TTSC: (1) fixed steel frame, (2) axial hydraulic ram, (3) horizontal hydraulic rams, (4) plastic block, (5) aluminium shims, (6) LVDT and (7) rock specimen.

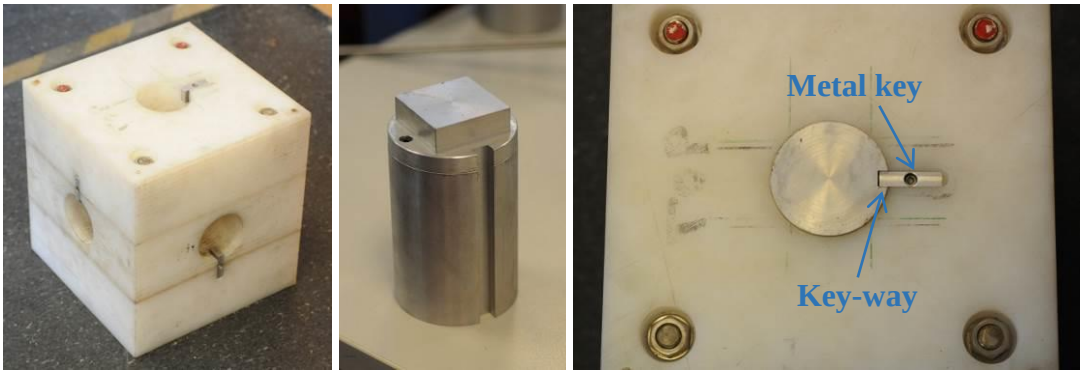

Figure 3.7 The configuration used for loading 50 mm cubes in TTSC: the plastic block for positioning sample at the centre of cell (left), the aluminium shims used for load-transfer to the sample (middle), and key and key-way design for preventing rotation of spacers around rock cube (right).

Similar to most triaxial cells (true or standard), the TTSC does not provide the possibility to observe the rock sample during the test, and such investigations are only feasible post-mortem. There are few true triaxial apparatus that allow observation of the specimen during loading. The work done by Bésuelle and Hall (2011) is an example in which the development of the strain field in rock under loading has been studied via the photographs taken of the sample through a sapphire window in the machine. In their experimental setup the intermediate stress was controlled in a way to prevent any deformation in this direction and hence created a plane strain condition. The rock specimen was observed through a hard window in this direction. Analysis of the taken photographs along with the obtained stress-strain curves revealed how axial stress peaks and stress drops were associated with the strain localization in the rock specimen. They showed the evolution of rock deformation from homogeneous deformation to a shear band and subsequently to a major fault conjugated with a set of small cracks at failure, through the images taken during the test.

3.3.1 Loading

The TTSC is not a servo-control apparatus and is only capable of loading samples under a stress-controlled mode. Therefore, the loading rate was chosen according to similar experiments reported in the literature (e.g. Ma and Haimson 2013, Naumann et al. 2007, Popp and Salzer 2007) which was thought to induce an appropriate strain-rate in the tested rock specimen.

To control the hydraulic rams independently, manual or automatic hydraulic pumps can be employed. Initially, manual pumps were examined in this work, which

were found unsuitable for the purpose of true triaxial compression testing. As the axial stress is increased on the rock sample, it would expand laterally and in response, the pressure in lateral direction will increase. However, the oil pressure behind the rams could not be adjusted instantaneously via the manual pumps. Therefore, manual pumps were not capable of keeping the lateral stresses constant at a pre-defined level during the test, and besides no certain loading rate could be applied through such pumps.

The next option was to use automatic syringe pumps which proved successful in precisely applying and maintaining stresses along three principal axes. In this study, two Teledyne ISCO 260H syringe pumps were connected to the lateral hydraulic rams and were set in constant pressure mode to apply constant horizontal stresses, while a third pump of the same type was used in pressure-gradient mode to increase the vertical stress at a constant rate. In all three pumps, the flow rate and pressure rate were adjusted in a way so that all three stresses were increased at similar stress rates on the sample. The maximum pressure that these pumps can apply is 66 MPa with an accuracy of ±0.5% of full scale. The flow rate range is 0.001-107 ml/min with an accuracy of ±0.5%. The capacity of the pumps fluid cylinder is 266 ml. The operating load limits based on the current configuration of the apparatus are ~300 KN in the axial direction and ~204 KN along the lateral rams.

3.3.2 Measuring stresses and strains

The stresses and strains were measured in three normal directions during each test. Pressure readings were done through pressure transmitters (PT) fitted along the lines of each hydraulic ram. The pressure sensors were Keller PA-33X with a working range of 70 MPa, a resolution of 0.002% FS and an accuracy of 0.1% FS (10-40°C).

Measuring and recording the rock displacement during a true triaxial compressive test is crucial to evaluate the rock strength and elastic properties. This work has been the first to measure displacement of rock along all three principal stress directions in TTSC, however due to special arrangement of the machine there have been various problems to make this feasible. Some of these issues and the approaches used to overcome them are explained below.

Initially strain gauges (SG) were employed for this purpose. Strain gauges are directly attached to the specimen surface by an adhesive and measure local displacements with reasonably high precision and resolution. At least three SGs were

glued, each on one face of the rock cube in different directions, to measure one vertical and two perpendicular lateral displacements (Figure 3.8). However, some difficulties were experienced in using SGs. The major problem was the disconnection of the wires transmitting signals from SGs to the data acquisition system under pressure. When SGs were attached on the sample surface using special glue, a pair of wires was soldered to their terminals. The other ends of the wires are connected to the data acquisition system. Afterward, the rock cube is put inside the plastic block and the metal spacers are placed around it. Hence, the SG wires could only pass through a narrow space in the keyways of the spacers to exit the cell. The seal/cover of the wires may get damaged at the contact with metal shims under pressure and consequently short circuits the system, resulting in no signal acquisition. Thus, if strain gauges were used, there was always the risk of missing deformation data during a test.

To overcome this issue, various approaches were examined, such as using very thin wires instead of normal wires and also covering the rock sample with protective sleeves so that the SGs and the wires would not get damaged at the contact with metal shims when stress level is increased. However, none of these methods could completely resolve the issue and hence there was still the risk of losing data in the middle of an experiment.

Figure 3.8 Strain gauges mounted on a sandstone specimen in three principal directions. The sample faces marked as σ_2 and σ_3 show the intermediate and minimum stress directions, respectively. σ_1 was applied in vertical direction. The strain gauges marked as S1 and S3 measured the strains along σ_1 and σ_3 principal axes. The third strain gauge (S2) was glued on the rear side of the sample and measured the strain along σ_2 axis.

Although the wire disconnection issue could probably be overcome by providing larger passages for wires in keyways of the shims, there was another potential problem in using SGs. While glue can be applied to attach the strain gauges to the surface of a dry specimen, this may not work properly on the surface of wet (fully- or partially-saturated) samples. Even if the glue adhered the SGs onto the sample, there was a significant possibility that they would peel off the sample in the middle of the experiment. Therefore, another method was sought for deformation measurements in our experiments, which was to use linear variable differential transducers (LVDT).

An LVDT is an instrument which measures linear displacement based on an induced voltage in solenoid coils inside a housing due to changes in their position with respect to each other. It receives voltage as an input signal and gives an output voltage, the magnitude of which depends on the induced voltage in the coils. After conducting some market research, the LVDTs manufactured by *Trans-Tek Incorporated* were found appropriate for the range of accuracy required in this application. Comparison between various options was done considering several parameters including: the working range, sufficient resolution and sensitivity of the measurements, compatibility of input voltage range with the existing power supply system, compatibility of output signal with existing data recording system, and proper size in order to fit inside the TTSC.

The LVDTs employed are Trans-Tek model 0351-0000 spring-loaded sensors with maximum mechanical travel of 7.87 mm, sensitivity of 165.7 mV/mm (4.2078 VDC/in), resolution of 6 μm over the total working range and maximum non-linearity of 0.216% F.S (at 24 VDC input). Since all LVDTs have been calibrated over their full working range, the non-linearity of the device does not affect the measurements.

A special fitting was designed for positioning the LVDTs on spacers around the sample in order to correctly measure deformations along three principal axes in the TTSC. Figure 3.9 shows this setup. Each LVDT was mounted on one of the shims around the sample in that direction and its tip touching an adjustment rod attached to the opposite shim. Deformation of the rock sample was obtained along three perpendicular directions by measuring the relative displacement of opposite spacers. In order to prepare the plastic block for placing LVDTs on the shims, some modifications were applied to it including drilling some new holes to host this setup.

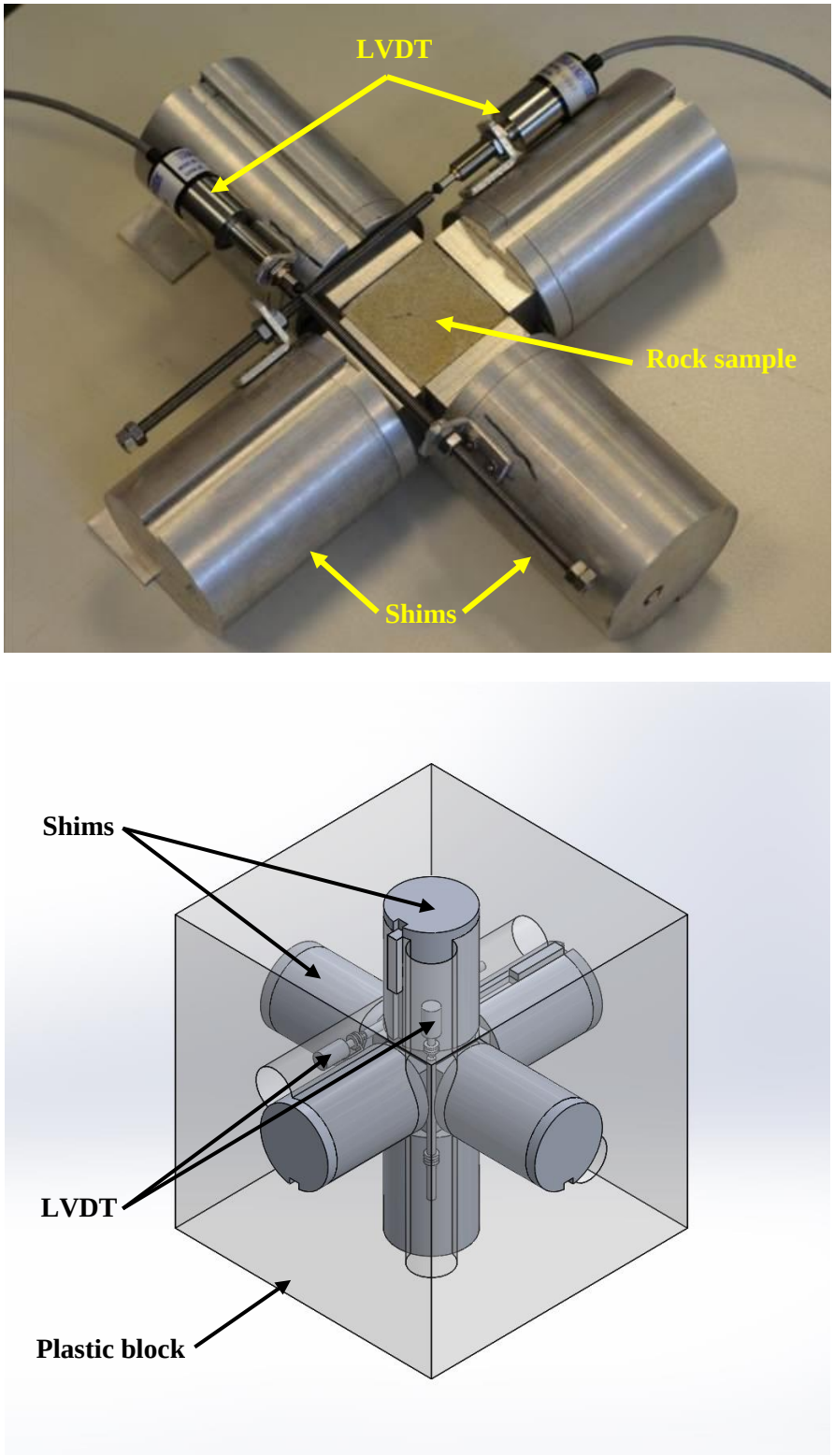

Figure 3.9 LVDTs setup around a cubic rock sample: photograph of the setup assembled on bench top (top) and schematic view of the complete assembly of the 3 pairs of spacers with the mounted LVDTs inside the plastic block (bottom). The tip of each LVDT touches a rod mounted on the opposing spacer.

As explained previously, the output of an LVDT is in form of voltage and hence to produce interpretable results, the LVDT output should be converted to displacement. This process is called "LVDT calibration", in which displacement values are assigned to the corresponding voltage readings. All LVDTs were calibrated at input voltage of 6 VDC and thus a displacement-voltage curve such as the one shown in Figure 3.10 was obtained for each LVDT.

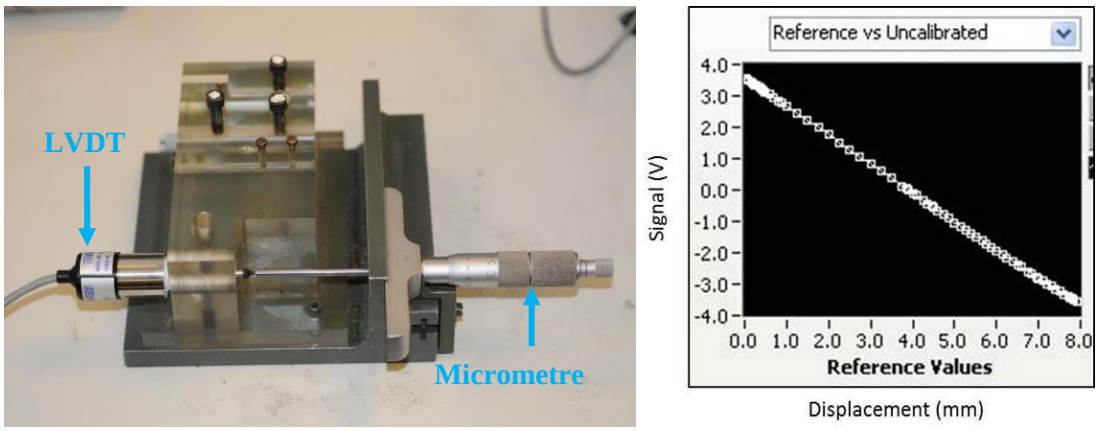

Figure 3.10 LVDT calibration device (left) and plot of displacement vs. voltage obtained as result of the calibration procedure (right). Displacement values, in mm, have been assigned to the corresponding voltage readings of the LVDT, in Volts.

3.3.3 Deformation calibration tests

Calibration tests on LVDTs have been conducted to extract the required correction parameters for applying to the true triaxial test data. As explained in section 3.3.2, LVDTs have been installed on the aluminium shims around the rock sample. It was expected that these shims would undergo compression during loading. Thus the total measured deformation in each direction would be the summation of displacements of the combined rock and spacer assembly. Net displacement of the rock sample along each direction is obtained by deducting the compression of the pair of shims and the cling wrap in that direction from the total measured deformation. For this purpose, uniaxial compressive tests were carried out on the shims themselves and also the cling-wrap assembly using a sample with known properties to plot their axial load versus axial displacement curves.

A hydraulic load cell and a rigid steel frame were employed to conduct the correction tests. To determine the effect of shims deformation on tests measurements, each two opposing shims were placed against each other in the absence of the rock

sample in between and were compressed uniaxially while the deformation was measured through the mounted LVDT. Figure 3.11 displays the calibration tests setup. The produced force-displacement curves (Figure 3.11) were then deducted from those ones obtained in testing the rock specimens in the TTSC. As shown in Figure 3.12 applying the correction curves to stress-strain data of a rock sample only resulted in a slight shift in the plotted curves.

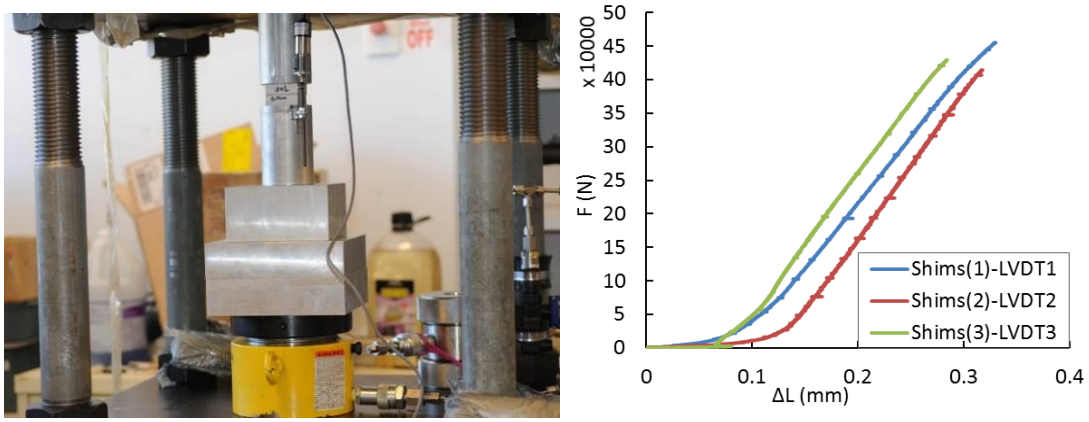

Figure 3.11 The uniaxial setup used for calibrating the effect of shims deformation on LVDT measurements (left) and force-deformation curves obtained for 3 pairs of shims in these calibration tests (right).

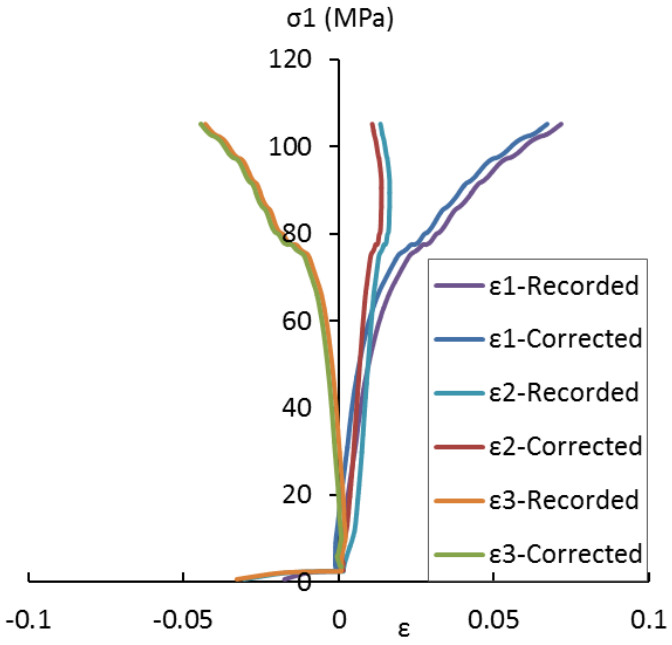

Figure 3.12 Applying the LVDT correction data on test results of a sandstone sample only caused a slight shift in the stress-strain curves.

To define the impact of sealing sleeves on the stress-strain curves of the rock, a 50×50×50 mm aluminium cube made of the same material as the shims was used. Initially, the cube was placed between two shims and was compressed uniaxially while measuring the applied pressures and displacements (Figure 3.13). Afterwards, the aluminium cube was jacketed in the sleeves and compressed over the same load range. Subtracting the force-displacement curve obtained in the unjacketed test from that of jacketed test gives the sleeve deformation under the applied pressure range which was then deducted from the rock sample stress-strain curves.

As stated in section 3.2.2, different types of sleeves were examined in this work, which included two types of heat-shrink sleeves and cling wrap. All these sleeves were tested using the above setup and the obtained stress-strain curves are displayed in Figure 3.14. Considering this plot, the heat-shrink sleeves resulted in significant deviation from linearity in force-deformation (and consequently in stress-strain) curves, in particular for the case of double-cover sleeves. However, the plastic film did not induce such non-linearity effects on the force-deformation curve and only caused a shift in the data which can be simply removed. Hence, the plastic film was far preferable for use in these tests for sealing purposes of the samples due to the minor corrections required.

Figure 3.13 Uniaxial test configuration for the 50mm aluminium cube used for correcting the effect of sealing sleeves on LVDT measurements.

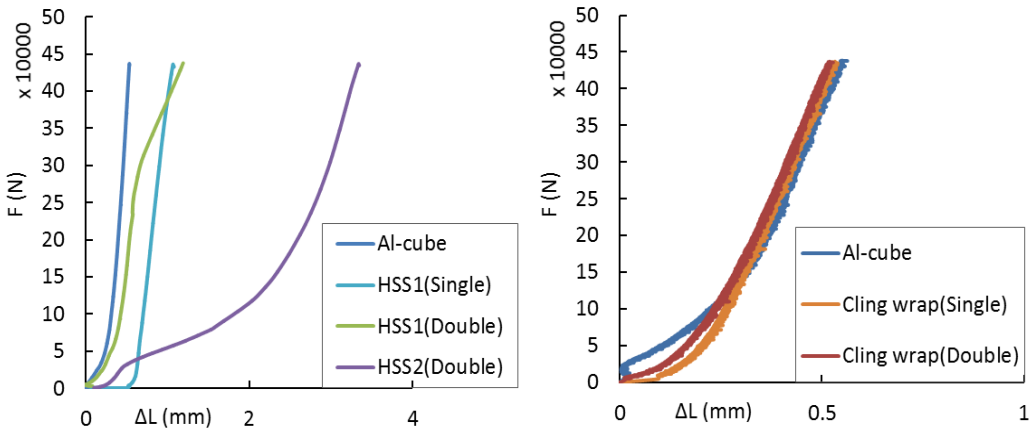

Figure 3.14 Force-deformation curves obtained for the aluminium cube and single- and double-covers of two types of heat-shrink sleeves (HSS1 and HSS2) (left) and cling-wrap (right). The heat-shrink sleeves caused significant deviation from linearity in the force-deformation curve of the aluminium cube, while the cling-wrap only caused a small shift in it.

3.3.4 Pore pressure

During the experiments conducted in this study, samples were sealed in plastic film to prevent desiccation. However, considering the low permeability of the shales, a relatively fast loading rate has been applied. Hence the water content of the specimens remained constant during the experiments and thus these tests can be classified as being done under undrained conditions. The pore pressure can change throughout an undrained test (Fjær et al. 2008). Whether the pore pressure increases or decreases during the test, depends on the dilation/contraction behaviour of the rock under loading. The total stress applied to the specimen is partly carried by the pore fluid and partly by the solid framework of the rock, known as the effective stress. The rock failure strength and deformation is associated with the effective stresses (Fjær et al. 2008). Hence, changes in pore pressure affect the measured rock properties. Basically at constant total stresses, an increase in pore pressure, decreases the effective stresses and thus causes the rock to destabilize with respect to failure, and vice versa. In a compressive test, as the rock sample is compressed under loading, the pore space is compressed and consequently the pore pressure rises until the sample fails. For brittle rocks, in which microcracks develop to form macroscopic shear fractures in the sample at failure, dilation occurs in the rock and consequently the pore pressure decreases (Horsrud et al. 1998). Figure 3.15 displays typical pore pressure response in undrained triaxial loading of a shale sample. For testing shales and low-permeability rocks the recommended testing method is the so-called Consolidated Undrained (CU) tests as depicted in Figure 3.16 (Horsrud et al. 1998, Fjær et al. 2008). In this method the rock sample is initially loaded to a predefined level of confining pressure and pore pressure. Then during the consolidation phase, drainage of the pore fluid is allowed to maintain a constant pore pressure under a constant level of confining pressure. Afterwards, axial loading is applied under undrained state until sample undergoes failure. During a CU test measurement of pore pressure is required. Figure 3.16 shows variations of stress and pore pressure in a CU test, schematically. Conducting the triaxial loading part under undrained conditions rather than drained conditions is to avoid extremely long time required in the case of drained tests, due to low permeability of shales and clay-rocks.

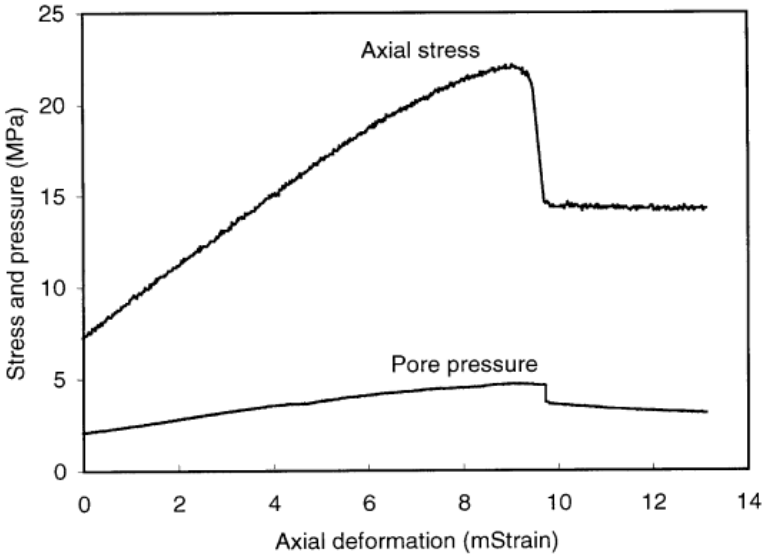

Figure 3.15 Changes of the pore pressure in undrained triaxial loading of a shale specimen under effective confining pressure of 5 MPa (Horsrud et al. 1998). As the rock contracts the pore pressure rises until dilation and failure occurs in the rock sample, after which the pore pressure drops.

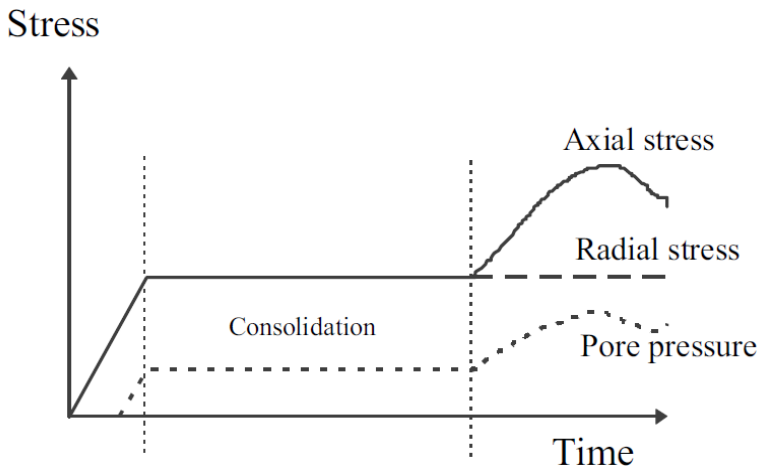

Figure 3.16 Schematic stress/pressure vs. time plot in a Consolidated-Undrained test (Horsrud et al. 1998). The rock sample is first loaded to a specific level of confining and pore pressure, then drainage of the pore fluid is allowed against a constant level in consolidation stage. Finally the axial stress is applied in undrained conditions until the sample fails. During the last stage, the pore pressure increases in the sample up to the failure point and then declines.

However, the TTSC is not equipped with pore-pressure sensors and thus the impact of pore pressure on obtained data could not be directly studied here. Nevertheless, in the case of dry synthetic sandstones and Carynginia Shale samples, due to their very low water content and saturation of the majority of the pore space with gas, the pore pressure would be effectively unchanged and hence will not influence the test results. In addition, most of the tests on Pierre Shale are done under partially-saturated conditions.

In the case of samples with high water content, or in other words close to fully-saturation state, compression of the rock due to increasing stresses during the test might result in 100% saturation conditions and consequently cause pore pressure build-up (Gräsle 2011). Since pore pressure directly depends on bulk volumetric changes, changes in pore pressure in fully saturated samples can directly indicate any changes of the rock internal structure (Yoshinaka et al. 1997). The Pierre Shale samples tested here, however, were only partially saturated with water, except for two samples which were close to 100% water saturated (PC-07 and PC-08). Therefore, it is assumed that pore pressure effects are negligible in our experimental findings apart from the two mentioned samples, for which this impact remains unknown.

3.3.5 Friction effect

In a typical arrangement of conventional compression tests, a rock is loaded between two rigid platens. The rock will have some lateral expansion related to its Poisson's ratio, which will be prevented by the platens because of friction. Thus due to the difference between the elastic properties of steel platens and rock sample, radial shearing forces are generated at their contact area (Mogi 2007). Frictional forces created at the interface of rock and steel cause inhomogeneities in the stress state and can affect the measured parameters, such as elastic properties and compressive strength (Jaeger et al. 2007).

Generally uniaxial compression tests are conducted on cylindrical samples to determine the rock unconfined compressive strength (UCS) and Young's modulus at zero confining pressure. Chau (1997) introduced a parameter λ which is the ratio of the true Young's modulus to the apparent Young's modulus (E=-σL/ΔL) to study this problem for a case in which the frictional force between the end platens and the rock is relatively high and thus no lateral expansion of the rock happens at the boundaries. For a cylindrical core with a length at least equal to its diameter, and a Poisson's ratio of less than 0.3, λ is in the range of 0.97-1.00. Greenberg and Truell (1948) did the same experiment for a prismatic rock with ν=0.33, and found a λ=0.96. Therefore, for extracting Young's modulus in engineering experiments, the frictional forces can be neglected.

Nevertheless, in most rocks these frictional forces at the rock-steel interface act inward and thus generate a clamping effect at end zones (Filon 1902). Consequently,

abrupt changes in shear stress happen near the edges at the interface, which leads to stress concentrations (Nadai 1924). Also if a fracture in the rock propagates near the end zones it may be hindered. The stress concentration tends to decrease whereas the clamping effect tends to increase the apparent strength, however, these two effects do not cancel out each other. Different approaches have been used to remove these effects, some of which are mentioned here (Jaeger et al. 2007, Mogi 2007):

- Improving sample shape in a way that the end effects do not influence the central region inside the rock sample where fracturing happens. Barnard (1964), Murrell (1965) and others have used shaped rock samples, with carefully designed shapes based on finite element analysis or photoelasticity investigations. Brace (1964) proposed a dog-bone shaped sample with reduced diameter at the middle section. If the sample has shorter diameter in the mid zone than in the ends, the stress distribution will be even at the middle part of the sample and so the true elastic modulus can be obtained using SGs in the neck part. However, such specimen would be prone to bending stresses which can be evaluated using strain gauges. The drawback of such approach is that these kinds of specimens need grinding techniques which are more difficult than preparing the typical cylindrical samples.

- Cook (1962) and other researchers suggested using metal platens with the same mechanical properties of the rock as the contact end pieces and similar diameter as the sample and having the same ν/E ratio as the sample. Therefore, the lateral expansion of the sample and the platens will be equal and shearing forces and stress concentration will be eliminated. Yet, the fractures may still intercept the ends surfaces of the specimen for typical short rock cylinders with length/diameter ratio of ~2. However, it is difficult to match the metal platen with the rock properties as most of the rocks show complex non-elastic features. So this method is not very promising.

- Labuz and Bridell (1993) investigated applying different lubricants between the platens and the sample to eliminate stress inhomogeneity in the sample. They measured radial strains in the central portion of a cylindrical core and also near the ends and observed that without applying lubricants, radial strains in the central part of the sample are 50% larger than near the end parts. They examined different types of lubricants such as graphite, molybdenum disulfide

and stearic acid on granite cores and found out that applying a mixture of stearic acid and petroleum jelly eliminated the stress inhomogeneity in the core sample. The use of lubricants at the interface is a simple method. However, vertical cracks may propagate starting from the ends of the sample due to infusion of soft lubricant into the rock. Using this technique, different compressive strengths may be obtained for different lubricants.

- Mogi (1966) proposed a design consisted of a long right cylinder connected to the metal platens via epoxy. The thickness of the epoxy fillet is gradually reduced from the rock-steel contact to the central part of the rock sample. The epoxy contains a filler of fine steel particles. The gradual decrease of epoxy thickness largely removes the stress concentration at the interface of rock and steel. To avoid the clamping effect, the length of the sample should be adequate so that the fractures propagate within the region with homogenous stress field. The use of a long sample increases the possibility of bending, which can be avoided by keeping both ends of the sample parallel, applying the axial load on a small area at the centre of the top platen and keeping the end pieces as short as possible.

The above approaches have been suggested for uniaxial and conventional triaxial tests and some of them have been adopted for true triaxial systems as well. Based on conventional triaxial and true triaxial testing of rocks, it is known that the effect of σ_2 on rock strength is generally smaller than that of σ_3, thus Mogi (1971) proposed applying σ_3 via confining fluid for accurate control and measurement, while using solid end pieces for applying σ_2 as well as σ_1. He suggested that friction at the interface of specimen and solid platens has less severe effects along σ_2 in comparison to end effects along σ_1 direction. Therefore, he used epoxy along σ_1 and lubricants (thin Teflon or rubber sheets) along σ_2 for removing friction at the interface of rock and steel end pieces. After Mogi, some true triaxial systems were constructed in different laboratories almost identical to his cell and similar techniques were applied for removing end effects (e.g. Takahashi and Koide 1989, Haimson and Chang 2000, Kwaśniewski et al. 2003).

Others have used different approaches for eliminating frictional effects based on their true triaxial system setup. Fuenkajorn et al. (2012) and Sriapai et al. (2013) used a machine in which axial pressure is applied via a hydraulic load cell and lateral

stresses are applied by means of cantilever beams. They placed Neoprene sheets between the rock surface and the platens in all directions. Tiwari and Rao (2004) employed a true triaxial system in which stresses are applied though hydraulic jacks and a pair of Teflon sheets smeared with high vacuum silicon grease were placed between the rock sample and the loading platens on all sides to remove friction.

In the present work the tops of the metal shims were covered with a thin layer of graphite powder before the tests, to act as a lubricant to minimize the friction at the interface of the rock sample and the shims. This approach is similar to the one used by Popp and Salzer (2007), as the experimental setup of their true triaxial machine is similar to the one used in this work. The rock specimens were wrapped in plastic film which prevented intrusion of the graphite into the rock sample as well as avoiding changes in the rock saturation state during the test. Although this method may not completely remove the effect of frictional shear forces, it was assumed that the friction has been reduced to a large extent and thus has left a negligible influence on stress distribution inside the rock sample and on the measured parameters.

3.4 True triaxial compressive test procedure

To define a consistent step by step experimental procedure, several true triaxial tests were conducted on synthetic sandstones. This was to detect and apply required modifications to the TTSC setup to assure precise and complete measurement of all parameters.

One of the important parameters to consider for conducting a rock mechanical test is the loading path. Many different stress paths can be applied during the course of a true triaxial test, depending on the purpose of the experiments and also the capabilities of the apparatus (see Mogi 1971, Wawersik et al. 1997, Macari and Hoyos 2001, Naumann et al. 2007, Ma and Haimson 2013). One of the most common loading paths in true triaxial tests for determining the rock strength and mechanical properties is adopted from conventional triaxial tests; i.e. isotropically increasing the three principal stresses until σ_3 and then σ_2 reach their predetermined magnitudes. From that point σ_3 and σ_2 are kept constant while σ_1 is increased monotonically (e.g. Haimson and Chang 2000). There have been also different loading paths used by different researchers based on the purposes of their studies. Ma and Haimson (2013), for example, introduced a novel loading technique for true

triaxial tests. In their experiments, the three principal stresses were initially increased isotropically up to σ_3 level, and then σ_3 was kept constant while σ_1 and σ_2 were both increased in a way to keep the deviatoric stress parameter, *N*, constant throughout each test, where:

$$N = -\sqrt{2}\,\frac{\sigma_2 - \sigma_{oct}}{\tau_{oct}} = \frac{1-2p}{\sqrt{1-p+p^2}},$$

in which σ_{oct} and τ_{oct} are the mean normal stress and octahedral shear stress, respectively, and *p* is a stress ratio defined by:

$$p = \frac{\Delta\sigma_2}{\Delta\sigma_1} = \frac{\sigma_2 - \sigma_3}{\sigma_1 - \sigma_3}.$$

In each test the ratio *p* was kept constant to maintain a constant *N*. They examined different levels of *p* (0, 1/6, 1/3, 1/2, 3/4 & 1), where *p*=0 is axisymmetric compression ($\sigma_2=\sigma_3$), *p*=1 is axisymmetric extension ($\sigma_2=\sigma_1$) and *p*=1/2 simulates pure shear conditions. Their experiments revealed that by increasing the mean stress, τ_{oct} at failure first increased, then reached a plateau and decreased by further raise in σ_{oct}. On the other hand, increasing *N*, caused an increase in σ_{oct} at failure. Increasing the mean stress also resulted in change of the failure mode from a single shear fault to conjugate shear-enhanced compaction bands then gradually shifted to pure compaction bands.

The objective of the study by Ma and Haimson (2013) was to investigate the effect of mean stress and deviatoric stress state on rock strength and failure plane angle, when the rock is subjected to a constant deviatoric stress. While in this study, the major goal is to investigate the dependence of rock strength and elastic properties on principal stress conditions (stress magnitude and anisotropy) and in particular the effect of intermediate stress on these parameters. The underlying principle was that two sets of independent lateral stresses were applied on the specimen and kept constant while the vertical stress was increased until the sample reached failure. A series of tests were then performed on multiple samples by systematically changing the stress conditions. To examine the effect of the intermediate stress, σ_2 was changed in a series of tests with constant σ_3. The tests were then repeated for increased σ_3 and different σ_2/σ_3 ratios.

In each test, all three stresses were at first increased quasi-isotropically. For all experiments we tried to keep the stress in the intended σ_1 direction slightly larger

than the intended σ_2 direction and that slightly over the intended σ_3 direction during loading. When the stresses reached the planned minimum stress level, then σ_3 was maintained at this level. Thereafter two other stresses were increased simultaneously and at equal rates up to the intermediate stress level at which σ_2 was kept constant until the end of the test and σ_1 was increased monotonically until failure point.

In this work the stress state was chosen in a way to apply the minimum and intermediate principal stresses in lateral directions, and the maximum principal stress in vertical direction. All shale samples used in this work were loaded in the TTSC such that the maximum principal stress was perpendicular to bedding planes.

3.4.1 Single-stage true triaxial tests procedure

The steps outlined below explain the procedure followed in all single-stage true triaxial tests:

1. *Sample identification:* Rock samples were photographed and their dimensions were measured along three principal stress directions (e.g. Figure 3.8) with precision of 0.01 mm. The sample dimensions were used as input into the LabVIEW code for calculation of the stresses and strains of the rock specimen.
2. *Sample sealing:* The shale specimens were wrapped in plastic film prior to testing to avoid sample desiccation during the experiment and prevent graphite powder intrusion into the specimen. Each sample was weighed before and after the experiment to ensure any alterations to its water content has been adequately prevented.
3. *Friction minimizing:* In order to reduce the friction between rock faces and the metal shims, graphite powder was used on the contact face of the shims and on the plastic film wrapped around the shale specimens.
4. *LVDT adjustment:* During true triaxial tests, the rock sample is initially compressed due to the increase in stresses in all directions. During axial loading further increase in σ_1 resulted in more compression in the axial direction and expansion in the lateral directions. Hence if the LVDT was initially in fully-extended position (i.e. the opposite adjustment rod was only touching the LVDT tip, not pushing the LVDT shaft inside the housing) when the sample expands in that direction, the LVDT tip would be no longer in contact with the adjustment rod and no displacement would be recorded. To prevent this problem, the shafts of all three LVDTs are adjusted to be about 2-3

mm into their compression range at the beginning of the test. This is done by placing the rock sample between each two facing shims on the bench-top prior to testing and regulating the position of the adjustment-rod through a pair of locking-nuts against the opposite LVDT. Consequently, when the sample is placed inside the cell, before applying any stresses each LVDT has a reading of ~2-3 mm which is called the LVDT initial value. This value is then deducted from any displacement measurements by that LVDT during the experiment to obtain the rock deformation. Therefore, by means of this method, negative displacement values could be recorded which indicates rock expansion, and this also resolved the issue of losing contact of the LVDT tip and the adjustment-rod.

5. *Sample positioning:* The sample and metal shims are placed inside the plastic block (Figure 3.5 to Figure 3.7) and a high-strength cable is wrapped around it to prevent the bottom spacer from dropping during lifting.

   The total length of a pair of lateral shims and 50 mm cubic rock sample is still less than 300 mm, thus a small gap remains between the shim and the steel rams of the cell. It is important to keep the sample holder as close as possible to the centre of the cell during the test, as the space between the corners of the 4 steel plates is very narrow. Care was taken to ensure that platens were positioned in such a way that contact between adjacent orthogonally positioned platens was avoided. Each pair of hydraulic rams is connected to a single pump. To independently control the opposing rams, four valves are installed under the pistons of these rams to regulate their movement. Once the rams have moved into position to fill the gaps between the platens and the shims, the top hydraulic load cell is placed on the top shim so axial pressure can be applied.

6. *Loading:* Before applying the designed loading-path, the sample is pre-loaded to a low stress level of ~2 MPa along the three principal stress axes. This is to ensure proper contact of the rock sample with the platens and also to initialize the hydraulic systems/pumps. Then the predetermined stress path is applied by commencing all pumps simultaneously to increase pressure with relatively the same rate in all three directions. The axial pressure has been raised in a way to impose an average strain rate in the order of 10^{-6} /sec. During loading and unloading stages it was attempted to keep the stress at the planned σ_3 direction below the planned σ_2 direction and that below the planned σ_1 direction at all

times by adjusting the rates and limits on the pumps throughout all experiments.

7. *Data monitoring/recording:* The signal sent from the LVDTs and pressure transmitters were acquired through a National Instrument DAQ9174 data acquisition system during the test, and were transferred continuously to be monitored and recorded by a LabVIEW code on a PC. The code was programmed in the system specifically for the experiments conducted in this study. In this code, the specimen size and LVDTs' initial-values are given as input parameters and the principal stresses and strains are calculated based on the sample dimension and sensors readings. Figure 3.17 demonstrates the interface of the LabVIEW code during a true triaxial test.
8. *Unloading:* When the rock undergoes failure, unloading stage is done by reversing the loading path but at a faster rate. Therefore, the unloading stress path would not impact the configuration of the fractures that formed in the specimen.

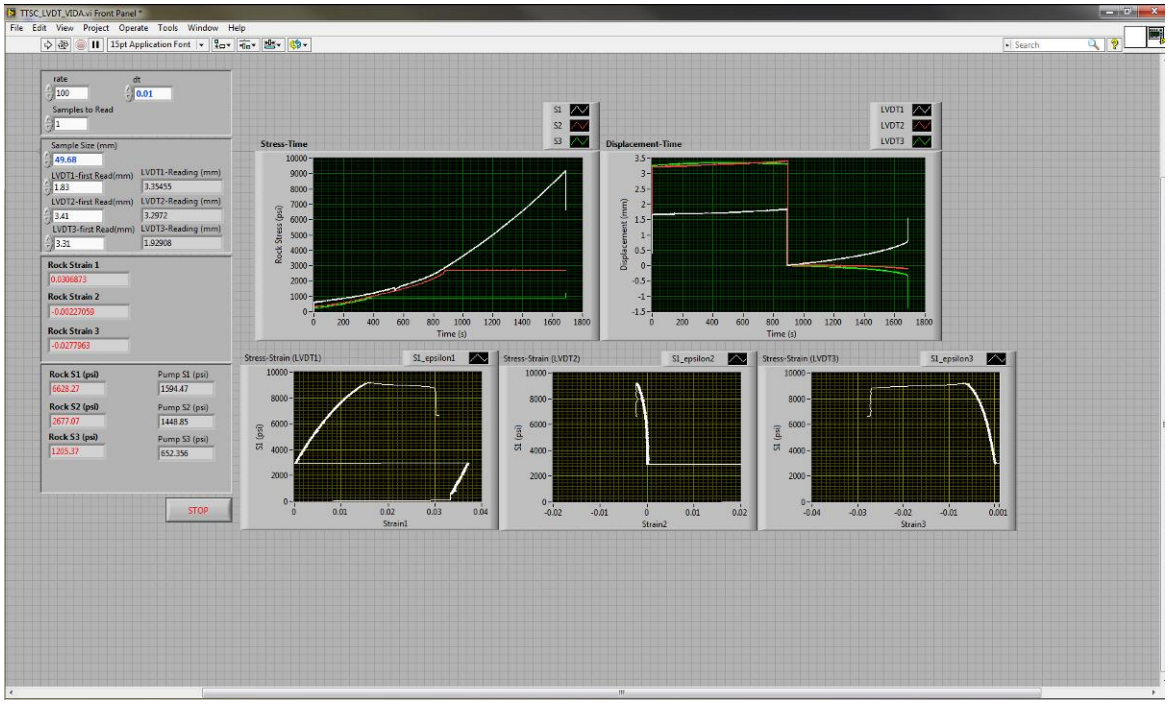

Figure 3.17 LabVIEW code interface during a true triaxial compressive test. The top two graphs show graphs of stress (left) and displacement (right) against time. The bottom three graphs show calculated axial stress-strain curves along the three principal stress axes.

3.4.2 Multistage true triaxial tests procedure

The concept and major aspects of conventional multistage triaxial tests were reviewed in Chapter 2 (section 2.6). In the present study, this technique was adopted from conventional triaxial tests to examine its properness for evaluating σ_2 effect on rock when subjected to true triaxial stress states. Conducting multistage true triaxial tests involves challenges such as early detection of the termination point during each stage and defining a stress path for loading the sample in true triaxial stress conditions. The principles of multistage true triaxial tests are discussed in Chapter 4 and the results are compared to the single-stage true triaxial measurements. Here, the experimental procedure used for performing the multistage true triaxial tests is explained.

The experimental setup of multistage true triaxial tests is the same as single-stage true triaxial tests except for the very last step (step 8). In a single-stage test, the sample is loaded to the failure point and then is unloaded. In a multistage test, the rock sample is subjected to several loading/unloading cycles (with different σ_2 levels), approaching failure without actually breaking the sample, and finally allowing the sample to go through the complete failure in the last stage.

Therefore, in step-8 of the procedure when the imminent failure point is detected, axial pressure is immediately decreased. Intermediate and maximum stresses are then increased simultaneously to the next predefined level of σ_2. Thereafter the process explained for stage-1 is repeated. In the last stage, loading in σ_1 direction continues until the sample undergoes failure and then unloading is done along all three principal axes.

3.5 Summary

In this chapter, the experimental methodology for conducting true triaxial compressive tests was explained. A new experimental setup and procedure was established to obtain rock strength and deformational properties under true triaxial stress conditions in the available apparatus. An important consideration in conducting any laboratory study is that the test procedure and experimental setup should be consistent, so the produced results from several experiments are comparable in similar conditions, and the obtained data would not be affected by different experimental conditions. In the present work, all tests were conducted in

reasonably similar conditions, including the machine setup, loading/unloading rates, measuring instruments and ambient temperature. In the next chapters the results of the true triaxial experiments will be presented and discussed.

4 Deformational properties of sandstones under true triaxial testing

4.1 Introduction

The results of true triaxial failure tests on synthetic sandstones are presented and discussed in this chapter. The aim of these experiments was to investigate mechanical behaviour of sandstones in response to the variations of applied stresses, with particular emphasis on the influence of the intermediate principal stress (σ_2) on rock deformational characteristics. Therefore, the rock specimens were subjected to three different levels of minimum stress (σ_3=2.3, 3.4 and 6.3 MPa). At any specific level of σ_3, various σ_2 values were applied on several samples, to examine the impact of the lateral stress magnitudes and anisotropy on rock failure behaviour. The procedure for conducting a true triaxial test was explained in Chapter 3. Figure 4.1 displays schematically the stress path applied during a true triaxial compressive test.

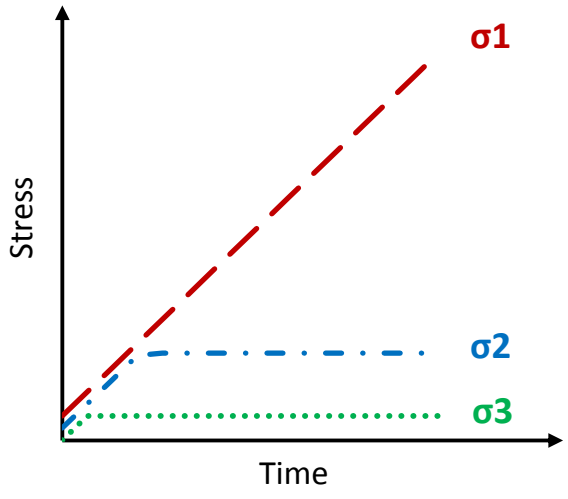

Figure 4.1 Schematic stress path used in a true triaxial test.

During the true triaxial experiments on rock samples, three principal stresses (σ_1, σ_2, σ_3) were recorded and also three principal strains (ε_1, ε_2, ε_3) were measured and recorded. From the stress-strain data, the elastic constants of the rock can be extracted, which express the linear relations of the applied stresses versus the measured strains (Fjær et al. 2008). In isotropic rocks, the mechanical behaviour under stress is independent of the direction of applied stresses. Such rocks are fully described by two independent elastic constants: Young's modulus (also in this work referred to as the elastic modulus or stiffness) and Poisson's ratio. The Young's modulus (E) is a measure of the material's stiffness and it refers to the axial strain due to axial compressive stress. The Poisson's ratio (ν) describes the lateral expansion of the rock due to the axial compressive stress, relative to the axial compaction. The synthetic sandstone samples used in this work were assumed to be isotropic rocks, as they do not seem to have any visible indication of anisotropy. Also the results of standard triaxial and permeability tests done by others on these samples demonstrated this to be a fairly reasonable assumption (Rasouli, personal communication). Therefore, elastic behaviour of these sandstones would be expressed by the two parameters E and ν.

Nevertheless, in a true triaxial test, two unequal lateral stresses were applied on the rock samples, thus two different values of Poisson's ratio could be extracted from each test: these are represented as ν_{12} and ν_{13} in this work. The first one denotes the lateral strain along σ_2 axis due to the compressive stress in σ_1 direction, and the latter refers to the lateral strain in σ_3 direction due to the same compressive stress along σ_1.

The deformational characteristics of the synthetic sandstones when subjected to true triaxial stress conditions are analysed in this chapter. This includes the rock compressive strength, elastic properties, inelastic deformation, dilatancy and failure mode. Furthermore, three multistage true triaxial tests were carried out on synthetic sandstone samples, and their results were compared against the single-stage test data. In this chapter, the obtained findings are presented and reliability of this approach is discussed in detail.

4.2 Sample Characterization

The basic mechanical properties of synthetic sandstones were estimated through some single-stage and multistage conventional triaxial tests. Cylindrical samples of

38 mm diameter and length/diameter ratio of ~2 were used to conduct triaxial compressive tests. This sample size is conventionally used for rock mechanics strength tests. The applied confining stress ranged from 2 to 10 MPa. Table 4.1 displays the applied confining pressures and corresponding peak stress, Young's modulus and Poisson's ratio. In Figure 4.2 Mohr circles obtained in single-stage and a multistage triaxial test are plotted along with the fitted Mohr-Coulomb envelopes. The average obtained values for the rock uniaxial compressive strength (UCS), cohesion and internal friction angle (ϕ) were 15.5 MPa, 4.33 MPa and 32.1 degrees, respectively.

The average dry bulk density in tested specimens was 1.88 gr/cc. The porosity and permeability of the samples were also measured using a Helium-porosimeter machine under effective confining pressures of 2.6-6.6 MPa. Average values of 26% and 380 mD were obtained for porosity and permeability of these sandstones.

Table 4.1 Stress conditions and obtained mechanical properties in conventional triaxial testing of synthetic sandstones. (σ_1-σ_3) is the effective peak differential stress and E and ν are the Young's modulus and the Poisson's ratio

Single-stage Tests	**σ_3 (MPa)**	**σ_1-σ_3 (MPa)**	***E* (GPa)**	**ν**
Test1	2.3	20.74	3.3	0.31
Test2	3.5	24.33	3.7	0.08
Test3	6.3	30.27	4.0	0.32
Test4	10	35.60	3.4	0.12
Multistage Test	**σ_3 (MPa)**	**σ_1-σ_3 (MPa)**	***E* (GPa)**	**ν**
Stage 1	2.3	21.0	6.7	0.1
Stage 2	3.5	24.1	6.1	0.28
Stage 3	6.3	27.5	10.0	0.21
Stage 4	10	43.0	8.8	0.15

4.3 Single-stage true triaxial tests results

The true triaxial experiments conducted on the sandstone samples included 16 tests under three constant levels of minimum principal stress (σ_3=2.3, 3.4 and 6.3 MPa). For each set different levels of the intermediate principal stress were applied to examine the changes in rock behaviour as a function of σ_2/σ_3 stress ratios. Table 4.2 presents the configuration of the stresses applied during the single-stage tests. In this

table σ_1 indicates the magnitude of maximum principal stress at failure and σ_1-σ_3 shows the maximum differential stress at failure. For the tests under σ_3=2.3 MPa, five levels of intermediate principal stress (σ_2=2.3, 4.6, 7.58, 9.24, 11.55 MPa) have been used to change the σ_2/σ_3 ratio from 1 to 5. For the tests under σ_3=3.4 MPa, also five levels of intermediate principal stress were examined, but at a wider range of σ_2/σ_3 ratio, from 1 to 8. Finally for the tests under σ_3=6.3 MPa, σ_2 was changed to four different levels, but within a smaller range of the σ_2/σ_3 ratio comparing to other two tests, varying from 1 to ~3.3. This was done to keep the range of applied stresses within the loading capacity of the TTSC (see Chapter 3, section 3.3.1). In testing synthetic sandstone samples, loading along σ_1 direction was done in a way to impose an average strain rate of ~6.44×10^{-6}/sec. Figure 4.3 displays a typical stress-time plot for the synthetic sandstones.

Some examples of the obtained stress-strain curves for sandstone samples are displayed in Figure 4.4 where ε_1, ε_2 and ε_3 represent the strains recorded along three principal stress directions and ε_v is the volumetric strain calculated as the summation of the principal strains. From these curves, the deformational properties of rock including its compressive strength, elastic properties and failure mode can be extracted. Each of these parameters and the impact of stress states on them will be discussed in the following sections.

From Figure 4.4, it can be inferred that depending on the applied stress conditions, the rock strength and failure mode may change. For determination of the failure mode and rock strength in this thesis, the terminology used is similar to that used by Mogi (2007). Here, the rock failure is classified as brittle if the sudden change in the slope of stress-strain curve is followed by a considerable stress drop which is due to the loss of ability to support additional loads in the rock. Consequently, the slope of the stress-strain curve in the post-failure region would be negative (downwards). The rock strength in this case was determined as the differential stress level (σ_1-σ_3) at the peak point (fracture stress). The rock failure mode is considered as ductile if no noticeable stress drop happens, and hence the slope of the stress-strain curve remains positive (upwards). The rock strength in this case was taken as the stress level at the yield point. The yield point is where a sudden change in the slope of the stress-strain curve forms a knee on the curve, which indicates transition from elastic to plastic deformation in the rock. Another case would be when the stress-strain curve reaches an apparently constant stress level and then a stress drop is observed after some

significant strain. In this case, the rock is considered to have a transitional brittle-ductile behaviour. Figure 4.5 displays the typical stress-strain curves for different failure states.

Figure 4.4 suggests that changing the applied lateral stresses not only has affected the rock true triaxial strength but also its failure mode. This matter will be discussed further in the following section.

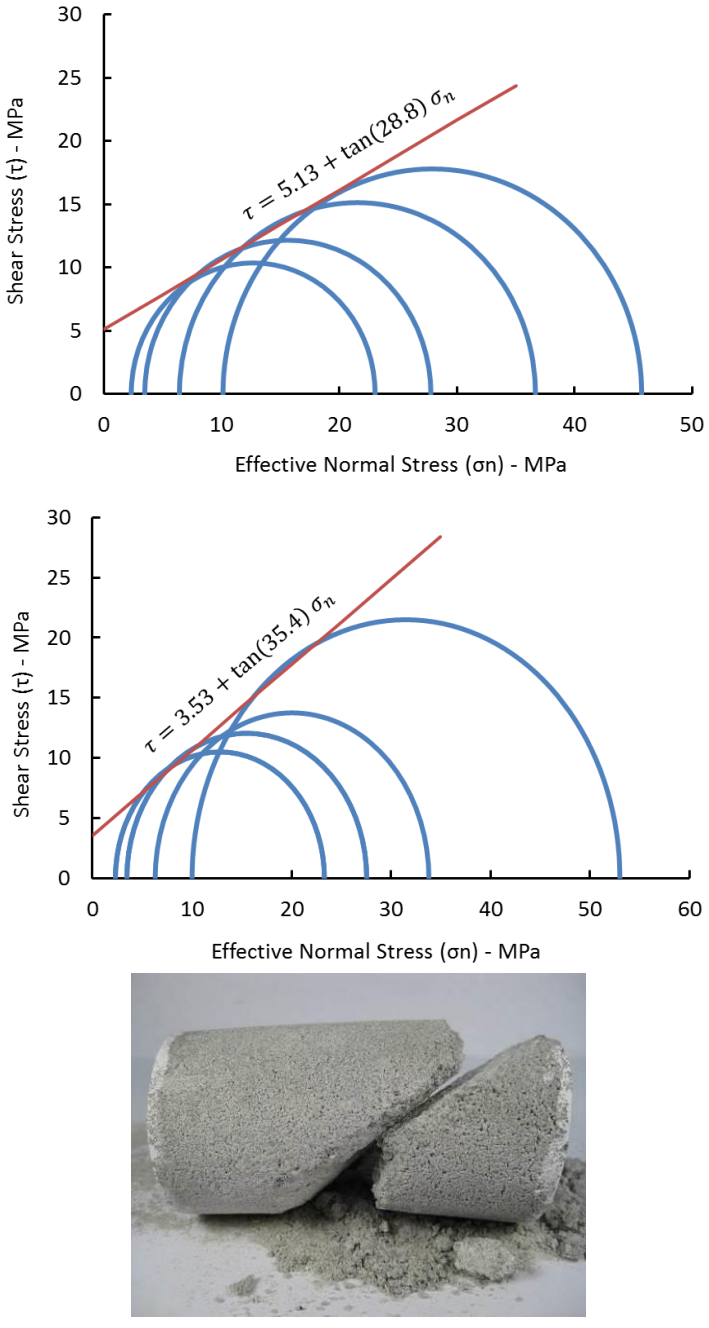

Figure 4.2 Mohr circles obtained for synthetic sandstones via a series of single-stage tests (top) and a multistage triaxial test (middle) and the typical image of the post-test core sample (bottom). The applied confining pressure levels for both single-stage tests and multistage test were 2.3, 3.5, 6.3 and 10 MPa.

Table 4.2 Stress conditions in single-stage true triaxial testing of sandstone samples. σ_1 and (σ_1-σ_3) are the axial and maximum differential stresses at failure, respectively.

Sample ID	σ_2/σ_3	σ_3 (MPa)	σ_2 (MPa)	σ_1 (MPa)	σ_1-σ_3 (MPa)
2-3	1	2.3	2.3	58	56
1-7	2		4.6	58	55
1-6	3.29		7.58	72	70
2-1	4		9.24	66	63
2-2	5		11.55	76	74
2-4	1	3.4	3.4	61	56
2-5	3.67		12.6	94	91
2-6	6		20.7	121	118
2-8	7		24.1	74	71
2-7	8		27.6	73	70
1-9	1	6.3	6.3	87	80
1-8	2		12.6	83	76
1-8’	2		12.6	78	71
1-10	2.19		13.8	119	112
1-11	3.29		20.7	148	142
1-12	3.29		20.7	147	141

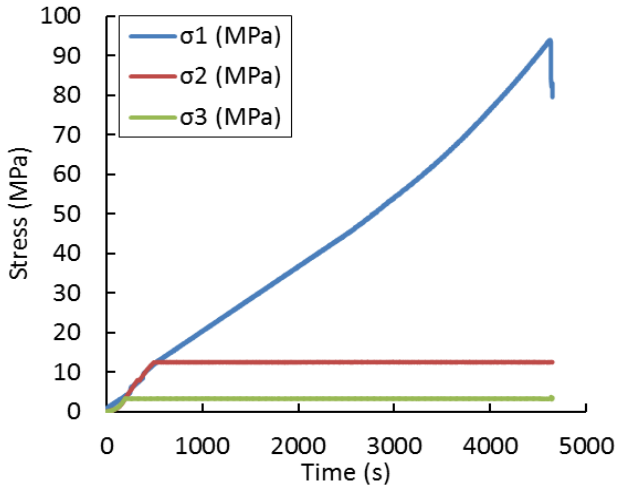

Figure 4.3 Typical loading path in true triaxial testing of synthetic sandstone samples. The three principal stresses increased quasi-hydrostatically until σ_3 and σ_2 reached the predefined levels; σ_1 was increased monotonically afterwards.

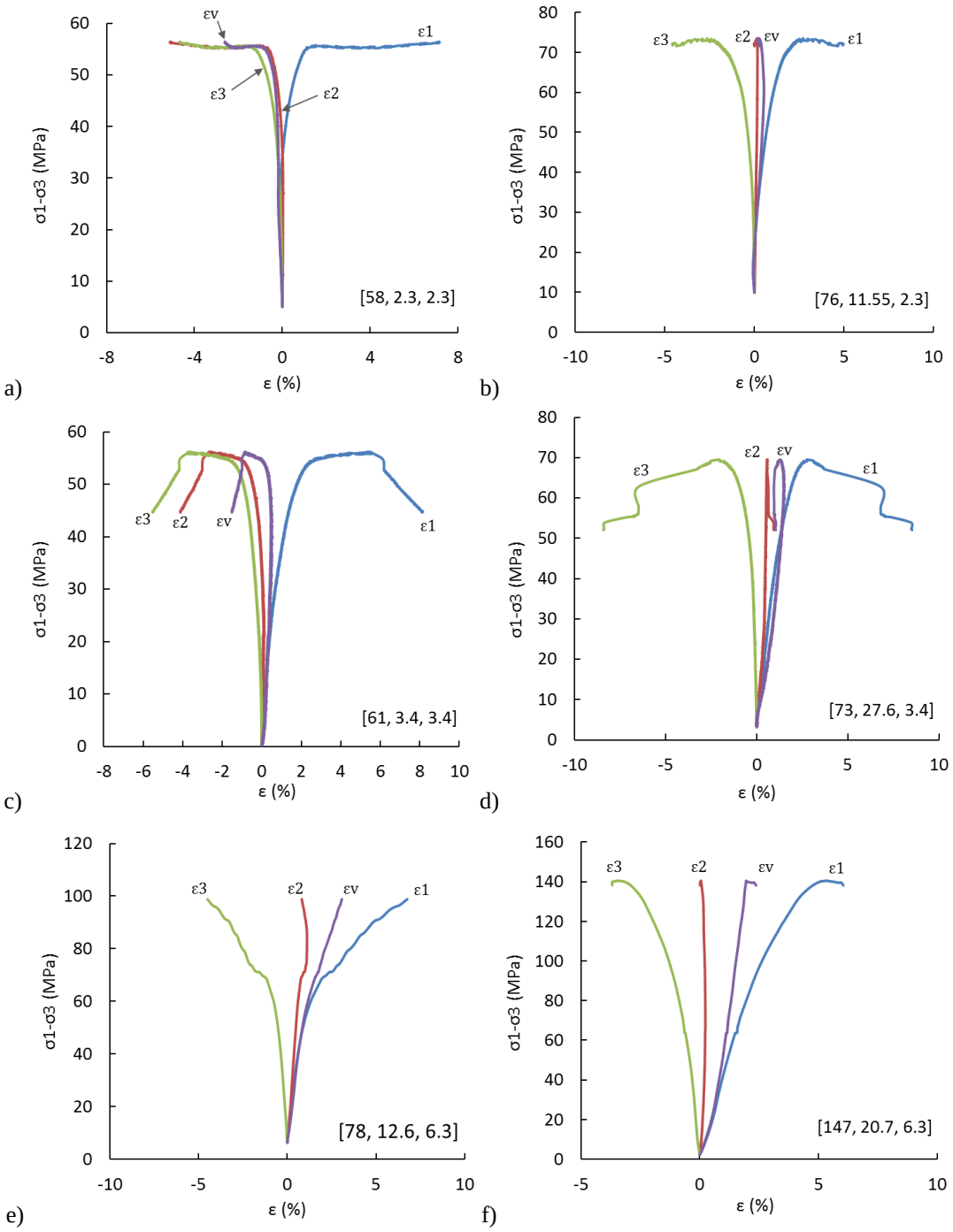

Figure 4.4 Some examples of the maximum differential stress (σ_1-σ_3) versus principal strain curves for the synthetic sandstones. ε_1, ε_2 and ε_3 are the strains along three principal stresses and ε_v is the volumetric strain. The numbers in brackets are [σ_1, σ_2, σ_3] in MPa, at failure.

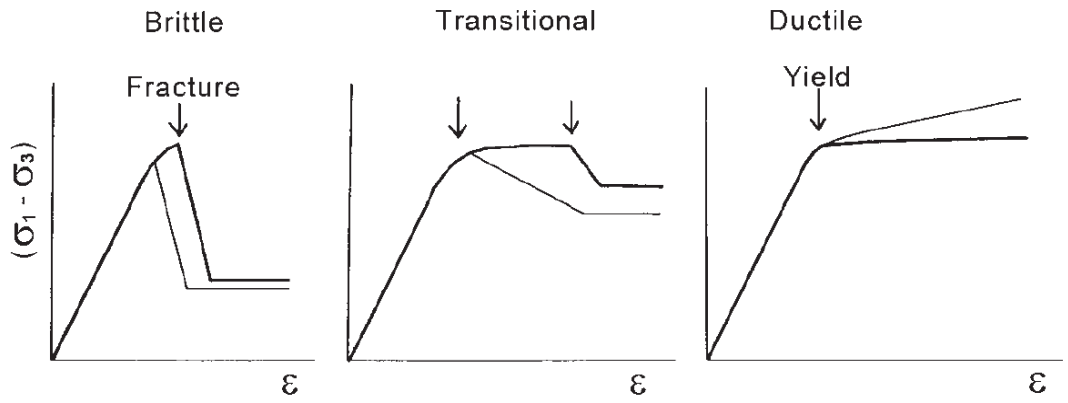

Figure 4.5 Typical stress-strain curves observed in case of the brittle, the brittle-ductile transitional and the ductile failure modes (Mogi 2007).

4.3.1 Rock strength and mode of failure

As previously mentioned, the stress-strain curves show some change in the failure regime of the synthetic sandstones (Figure 4.4). To better illustrate the changes in the failure mode of sandstone samples due to the changes in stress magnitudes, all differential stress-axial strain curves are plotted in Figure 4.6, for three different levels of σ_3 (2.3, 3.4 and 6.3 MPa).

From this figure it can be implied that under σ_3=2.3 MPa and 3.4 MPa, for most of the applied σ_2 levels, the rock failure behaviour was transitional brittle-ductile at bulk scale. For the group of samples tested at σ_3=6.3 MPa, the rock has mainly shown ductile behaviour and strain hardening under the applied σ_2 values. In general, raising the σ_3 level from 2.3 MPa to 6.3 MPa tended to increase strain hardening (strains rise upwards with greater slope) and evolve the stress-strain behaviour towards the ductile field. Previous studies on failure mode of rocks under standard triaxial and true triaxial conditions showed that increasing σ_3 can change the stress-strain behaviour from the brittle regime to a transitional brittle-ductile mode and then on to ductile failure mode (Paterson and Wong 2005, Mogi 2007).

Inspection of the post-mortem samples revealed that all samples have through-going fractures/faults, except for sample 1-7. For this sample, axial loading may have been stopped too early, perhaps before the established micro-cracks within the rock form macro-fractures (note the curve corresponding to σ_3=2.3 MPa and σ_2=4.6 MPa in Figure 4.6). Therefore, based on the observation of the macroscopic fracture planes within the samples, it can be generally inferred that the tested sandstone samples had brittle behaviour, at least in macroscopic scale, under the applied stress conditions, although some of the samples could have behaved in a ductile manner

during part of the test. The patterns of the propagated faults and fractures in the sandstone samples will be further discussed in a later section (section 4.3.5).

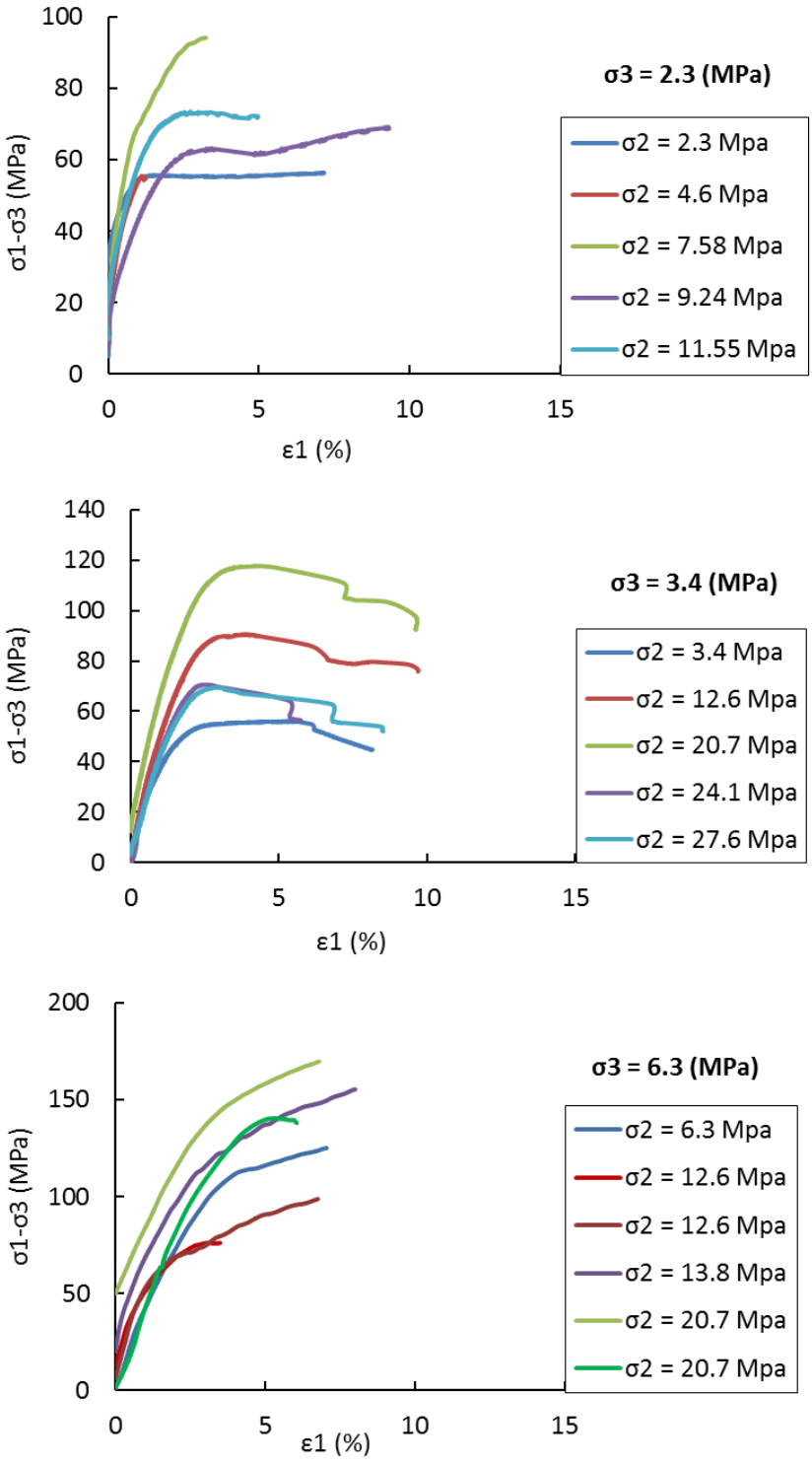

Figure 4.6 The axial strain vs. differential stress curves for all sandstone samples for tests under σ_3=2.3 MPa (top), 3.4 MPa (middle) and 6.3 MPa (bottom). The failure behaviour has been mostly transitional brittle-ductile or ductile at bulk scale but the end point has been brittle failure with through-going fractures.

To investigate the influence of the intermediate stress on strength of the tested sandstones, the maximum differential stress at failure ($\sigma_f = \sigma_1 - \sigma_3$) was plotted versus σ_2 in Figure 4.7 for three levels of σ_3. This diagram shows that in tests under σ_3=2.3 and 6.3 MPa, increasing the magnitude of σ_2 led to an overall increase in strength within the applied stress range. Studies of Crawford et al. (1995) also revealed a similar strengthening impact of increasing σ_2 on strength of two different sandstone formations. For the group of samples tested under σ_3=3.4 MPa, a wider range of σ_2/σ_3 ratios was applied. The data points corresponding to this group suggest that with increasing σ_2, the rock strength increased up to a maximum level and beyond that with further increase of σ_2, the rock strength decreased to some extent. Previous studies in the literature (e.g. Colmenares and Zoback 2002, Haimson 2006, Mogi 2007) showed that for many different brittle rocks, such as dolomite, limestone, granite, shale and sandstone under true triaxial stress states, increasing the intermediate stress at a constant σ_3, initially raised the rock strength up to a certain level, which depends on the rock characteristics and the applied stress conditions. Beyond this level, however, further increase in σ_2 caused some gradual decrease in the rock strength, although the strength value would not drop below the strength obtained in the case of triaxial stress states ($\sigma_2=\sigma_3$). Nevertheless, some other results reported in the literature indicated that for some rock types, such as hornfels and metapelite, σ_2 could have little or negligible impact on the rock strength (Chang and Haimson 2005).

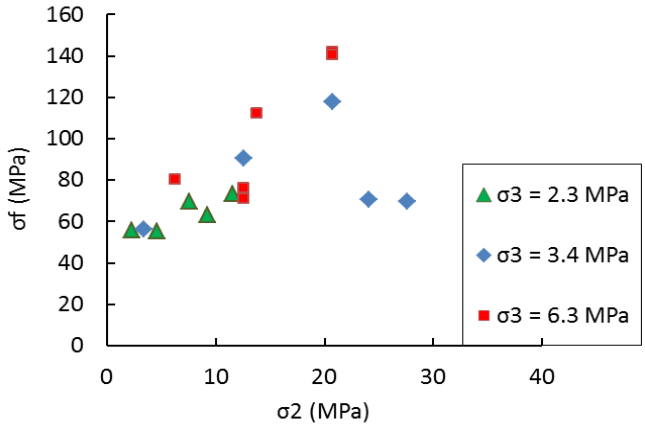

Figure 4.7 The peak stress of the synthetic sandstone specimens as a function of σ_2 for σ_3=2.3, 3.4 and 6.3 MPa. In general, increasing σ_2 induced an overall increase in the compressive strength.

Table 4.3 shows to what extent the rock strength in the synthetic sandstones has been influenced by the magnitude of σ_2. In this table, the strength values of sandstone samples under axisymmetric conditions (σ_f^C) for each level of σ_3 has been compared to the highest true triaxial strength (σ_f^T) for the same σ_3 (when $\sigma_2>\sigma_3$). The results indicated up to 32% increase in strength under σ_3=2.3 MPa, when the intermediate stress (σ_2) increased from $\sigma_2=\sigma_3$ to $\sigma_2=5\sigma_3$. For the group of samples tested under σ_3=3.4 MPa, increasing stress from $\sigma_2=\sigma_3$ to $\sigma_2=6\sigma_3$ raised the rock strength to more than twice the conventional triaxial strength. For tests under σ_3=6.3 MPa, the maximum growth observed in compressive strength was 77% when σ_2 was increased from $\sigma_2=\sigma_3$ to $\sigma_2=3.3\sigma_3$ MPa.

Figure 4.8 exhibits how raising the minimum stress level in the true triaxial tests affected sandstone strength, by plotting the variations of the peak stress as a function of the lateral stress anisotropy (σ_2/σ_3 ratio). Comparing the strength values acquired at different σ_2 and σ_3 levels but at the same σ_2/σ_3 ratio revealed that, the strength increased more than twice, from ~70 MPa to ~142 MPa, with increasing the minimum stress from 2.3 to 6.3 MPa at a stress ratio of $\sigma_2/\sigma_3\approx3.3$.

Table 4.3 Comparison between the strength obtained in conventional triaxial state (σ_f^C) and the highest true triaxial strength (σ_f^T) in the synthetic sandstone samples for three levels of the applied σ_3. The given σ_2 shows the value of the intermediate stress at which the highest true triaxial strength was acquired.

σ_3 (MPa)	**σ_f^C (MPa)**	**σ_f^T (MPa)**	**σ_2 (MPa)**	**$(\sigma_f^T - \sigma_f^C)/\sigma_f^C \times 100\%$**
2.3	56	74	11.55	32
3.4	56	118	20.7	110
6.3	80	142	20.7	77

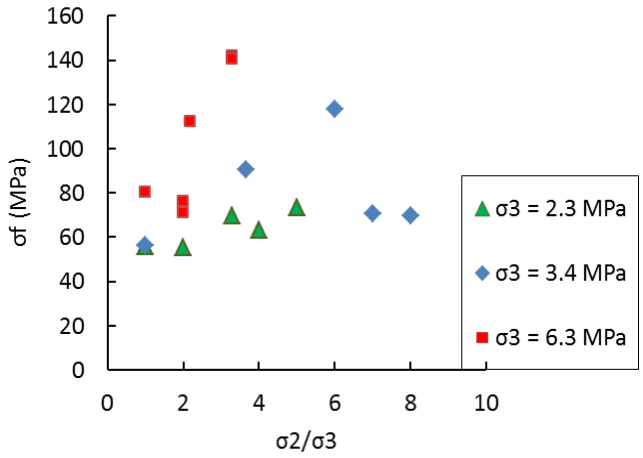

Figure 4.8 The synthetic sandstone samples strength variations versus lateral stress anisotropy (σ_2/σ_3 ratio). Increasing the minimum stress level from 2.3 MPa to 6.3 MPa in true triaxial tests increased the strength more than two times in magnitude.

4.3.2 True triaxial failure criteria

To describe the behaviour of rocks under true triaxial stress states, various 3D failure criteria have been developed (see Haimson 2006), some of which are more commonly used such as the effective strain energy criterion proposed by Wiebols and Cook (1968), Lade criterion (Lade and Duncan 1975, Ewy 1998) and Mogi (1971) criterion. Colmenares and Zoback (2002) compared different 2D and 3D failure criteria by examining them against true triaxial experimental results of different rock samples including amphibolite, dolomite, limestone, shale and sandstone. They concluded that the modified Wiebols and Cook criterion (Zhou 1994) fitted well on the test data of most rock types, especially for the rocks with high degree of σ_2-dependence, such as dolomite and limestone. According to the Wiebols and Cook model, when the intermediate stress is increased above $\sigma_2=\sigma_3$ level, the strength initially increases until it reaches a plateau and then it drops. However, the strength obtained at $\sigma_2=\sigma_1$ level would be expected to be higher than that acquired when σ_2 was set equal to the minimum stress.

The rock properties (UCS, ϕ) obtained under triaxial conditions ($\sigma_2=\sigma_3$) were used as input parameters to the modified Wiebols and Cook criterion to estimate the strength curves for the tested sandstones based on equations (2.7) to (2.14). In Figure 4.9, the test data points for synthetic sandstones are displayed along with the σ_1-σ_2 curves estimated by the modified Wiebols and Cook criterion in three different colours, one for each of the three levels of σ_3 (2.3, 3.4 and 6.3 MPa). The experimental work of Takahashi and Koide (1989) on Shirahama sandstones, showed

that the modified Wiebols and Cook criterion can well describe the impact of σ_2 on rock strength in those sandstones (see Takahashi and Koide 1989, Colmenares and Zoback 2002). However, for the sandstone samples tested in this work, the number of available data points and the applied stress range does not seem sufficient to indicate whether the experimental data fit reasonably well over the estimated failure envelopes of modified Wiebols and Cook criterion or not. Thus for examining the effectiveness of this criterion in modelling the true triaxial behaviour of these sandstones more tests under higher levels of σ_2 and σ_3 is required.

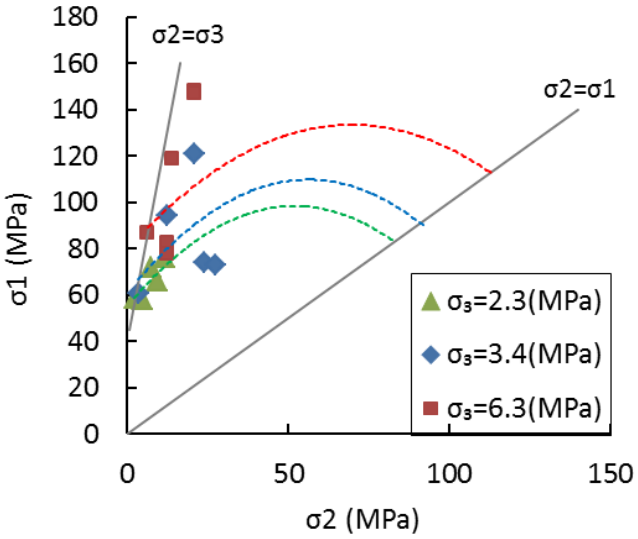

Figure 4.9 Comparison between the sandstones test data in σ_1-σ_2 diagram and the predicted trends by the modified Wiebols and Cook criterion (curves) for the three values of σ_3. Each curve has the same colour as the related group of the laboratory data points. The experimental data range was not sufficient to examine the prediction capability of this criterion for the synthetic sandstones.

Mogi (1971) proposed an empirical criterion in τ_{oct}-$\sigma_{m,2}$ domain which is probably one of the most widely used 3D criteria. This criterion is a generalized form of von Mises theory for brittle rocks and expresses octahedral shear stress (τ_{oct}) as a monotonically increasing function of $\sigma_{m,2}$ given by:

$$\tau_{oct} = \frac{1}{3}\sqrt{(\sigma_1-\sigma_2)^2+(\sigma_1-\sigma_3)^2+(\sigma_2-\sigma_3)^2}\ , \tag{4.1}$$

$$\sigma_{m,2} = \frac{1}{2}(\sigma_1+\sigma_3)\ . \tag{4.2}$$

Here, $\sigma_{m,2}$ is defined as the mean normal stress acting on the failure planes. Based on Mogi's studies, brittle rocks generally undergo failure in the form of fracturing along slip planes parallel to σ_2 direction. Thus it is rational to assume that the critical

distortional strain energy which leads to failure to be a monotonically increasing function of the mean normal stress acting on these planes rather than the octahedral normal stress (σ_{oct}=1/3 [σ_1+σ_2+σ_3]).

In Figure 4.10, the peak stresses obtained for the sandstone samples have been plotted in the octahedral space (τ_{oct}–σ_{oct}) and Mogi's proposed domain (τ_{oct}–$\sigma_{m,2}$). The test data tend to fall along a single curve in both domains. However, a considerably better fit in Mogi's proposed domain was achieved (R^2=0.98), which can express the octahedral shear stress at failure as a monotonically increasing power function of $\sigma_{m,2}$ in the form of:

$$\tau_{oct} = 0.8698\,\sigma_{m,2}^{0.9841}.$$

Although the data points lined up along a power function in Mogi's proposed space, more tests under larger magnitudes of lateral stresses and wider stress ratios are still required to determine a general failure envelope for these sandstones.

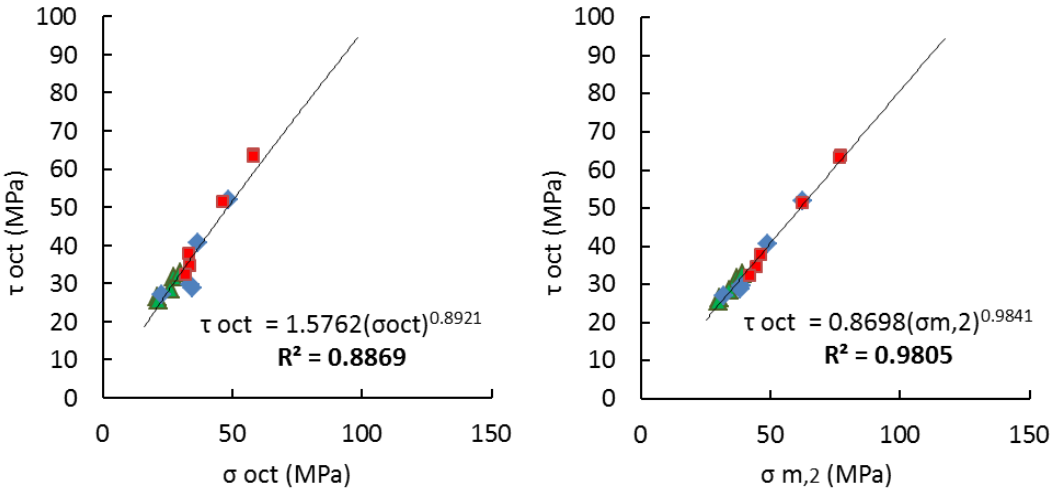

Figure 4.10 The true triaxial strength of the tested sandstones plotted in τ_{oct}–σ_{oct} domain (left) and τ_{oct}–$\sigma_{m,2}$ domain (right). The test data fitted relatively well along a power function in both domains, yet the fit in the Mogi's proposed domain is better (right plot).

4.3.3 Elastic properties

Many researchers investigated the impact of changing stress state on the elastic properties of sandstones and shales under conventional triaxial conditions (Niandou et al. 1997, Pagoulatos 2004). However, there is a lack of experimental studies in the literature focusing on the effect of lateral stress magnitudes (σ_2 and σ_3) on elastic

parameters under true triaxial stress states, in particular in sandstones and shales. Examples of the few existing studies on elastic properties of rocks subjected to true triaxial stresses include the work of Tiwari and Rao (2004) on sand-lime brick, Oku et al. (2007) on siltstone and Sriapai et al. (2013) on salt.

In the following sections, the influence of true triaxial stress states on elastic properties of the synthetic sandstone samples is investigated. For determining the Young's modulus from the axial stress-axial strain curve, several methods have been suggested in ASTM standard-D5407-95 (reapproved 2000), such as: the tangent slope at ~50% of peak strength, average slope of the linear portion of the curve (usually at ~40-60% of the peak stress) and slope of a line passing from zero stress and a fixed percentage of the maximum stress (secant modulus). The Poisson's ratio can be determined from the slope of linear part of the lateral strain versus axial strain curve. In this study *E* and ν were calculated at ~40-60% of the final strength in most cases which was found to be the linear portion of the curves.

Young's modulus

Variations of the Young's modulus in synthetic sandstones were plotted versus σ_2 values in Figure 4.11 for three levels of σ_3. These plots do not indicate a common trend of σ_2-impact on the elastic modulus. At the lowest applied minimum stress (σ_3=2.3 MPa), no clear dependency of *E* on σ_2 magnitude exists. For most true triaxial stress states ($\sigma_2>\sigma_3$) in this group, the Young's modulus value declined below the value obtained under quasi-isotropic conditions ($\sigma_2=\sigma_3$). Decreases as large as 59% were observed in Young's modulus when σ_2 was raised from $\sigma_2=\sigma_3$=2.3 MPa to $\sigma_2=4\sigma_3$=9.24 MPa. This behaviour is different to the trends observed in this sandstone at other σ_3 levels and also in the Carynginia Shale (see Chapter 5, section 5.2.2) and the Pierre Shale samples (see Chapter 5, section 5.3.2).

At σ_3=3.4 MPa and 6.3 MPa, when the intermediate stress increased, the Young's modulus showed some increase and then a gradual decrease in its value. At σ_3=3.4 MPa, the stiffness changed between 39-75% due to σ_2 variations, with the maximum growth at $\sigma_2=6\sigma_3$=20.7 MPa. For the tests under σ_3=6.3 MPa, increase in σ_2 changed the stiffness by ~3-69%, with the maximum growth at $\sigma_2=2\sigma_3$=12.6 MPa.

In order to investigate whether there was a relation between *E* values of the sandstone samples and the applied σ_3 level in the true triaxial tests, all data points were plotted against lateral stress anisotropy (σ_2/σ_3 ratio) in Figure 4.12. In

conventional triaxial tests, the Young's modulus generally increases with increasing confining pressure (see Fjær et al. 2008, Mogi 2007). However, the data in this diagram do not exhibit an expected trend of dependency on the minimum stress state in true triaxial testing. The irregular variations of *E* in these synthetic sandstones could be due to heterogeneity in cementation of the samples, as rock stiffness strongly depends on cementation at grain contacts (e.g. Saidi et al. 2003). Another possible explanation is related to the high porosity of these sandstones (ϕ~26%) and the potential for pore collapse under load. As a result of this, selection of a purely linear part on the stress-strain curves can be difficult and subjective (Paterson and Wong 2005). However, the selected range for calculation of *E* was mainly kept within 40-60% of the peak stress so that there would be a reasonable consistency between the obtained values.

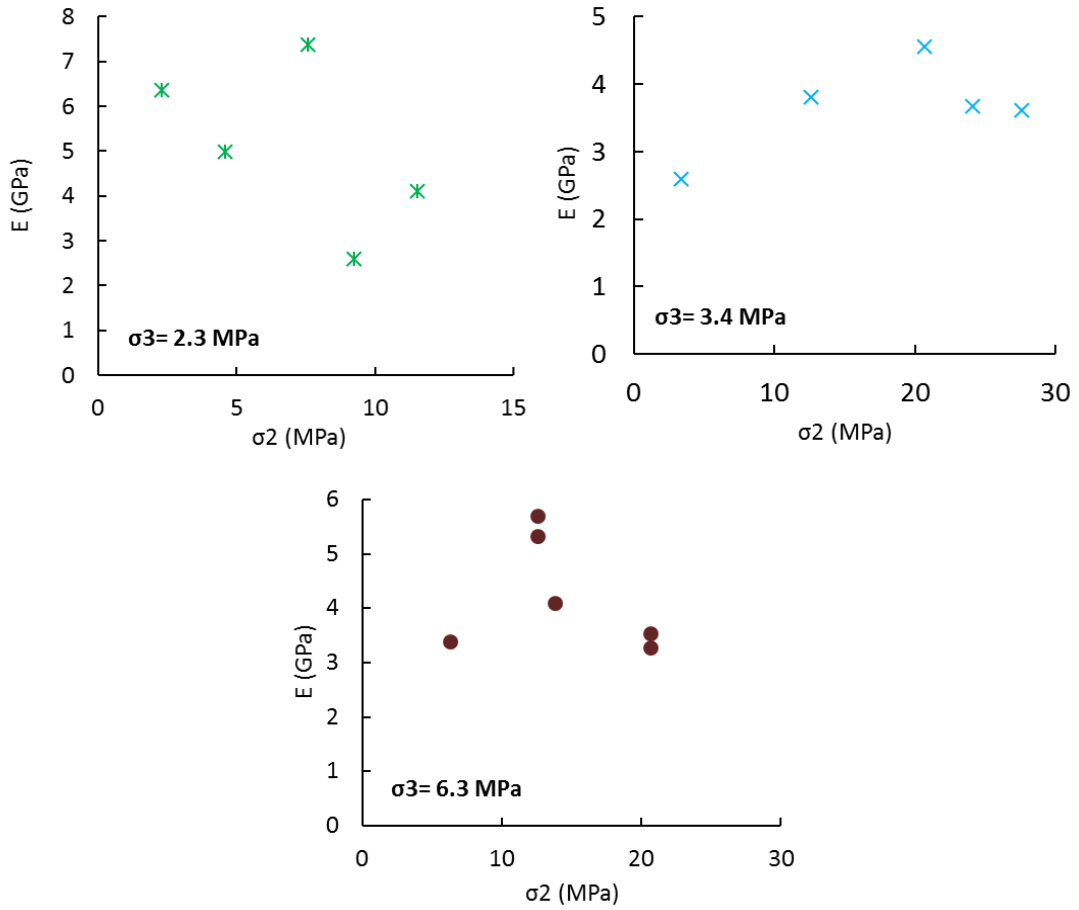

Figure 4.11 Variations of Young's modulus (*E*) in synthetic sandstones with the intermediate stress at different levels of σ_3. At σ_3=3.4 and 6.3 MPa some initial increase followed by some decrease was observed in stiffness, while at σ_3=2.3 MPa no clear dependency could be extracted.

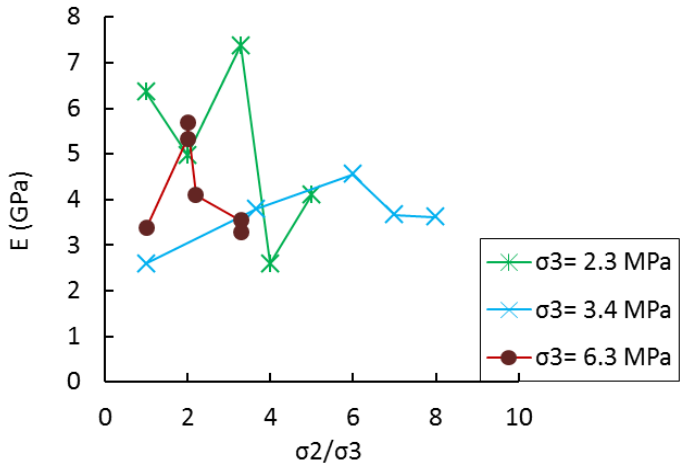

Figure 4.12 Variations of Young's modulus versus the lateral stress anisotropy (σ_2/σ_3) in sandstone samples. The Young's modulus exhibited irregular variation with the minimum stress magnitude in the synthetic sandstones.

Poisson's ratio

In true triaxial tests, the rock cube is generally subjected to two unequal perpendicular lateral stresses, resulting in two different values of Poisson's ratio for each sample. Here the Poisson's ratio along the intermediate principal axis is called ν_{12} and the one along the minimum stress axis is called ν_{13}.

Paterson and Wong (2005) explained that the stress-strain curves of rocks often show an initial non-linear part, due to closure of pre-existing cracks and/or pore collapse, which is followed by a relatively linear elastic section. The curve normally bends-over after the elastic section and eventually reaches the peak stress with increasing the applied load. In very porous rocks, the initial non-linear part might extend and the curve may simply be of convex form, inflecting from being downwards to upwards. Therefore, in such samples there may be no or a short truly linear elastic section on the curve. The stress-strain curves of the high-porosity sandstones tested in this study were mainly of this form, perhaps due to the prominent pore collapse. It was found that choosing the linear section of the curve was difficult and subjective, as slight changes in selection of the linear range led to noticeable differences in the measured values of the Poisson's ratios. The measured values in some cases exceed 0.5 (particularly ν_{13} values), which is not consistent with thermodynamics considerations for elastic materials that require the Poisson's ratios to be <0.5 for isotropic rocks (Amadei et al. 1987). Therefore, in terms of absolute values, it seems that the measurements of the Poisson's ratios in these high

porosity sandstones are not reliable. They have only been presented here as a means of comparing the impact of σ_2 and σ_3 on rock displacement. For sake of consistency, efforts were made to keep the selected linear section within 40-60% of peak.

Variations of ν_{12} and ν_{13} with the intermediate stress in sandstone samples were plotted in Figure 4.13. This diagram clearly shows that for all levels of σ_3, ν_{13} is significantly larger than ν_{12}. Such behaviour could be due to the supporting effect of the intermediate stress on rock which limits the rock deformation in this direction and causes more strain along σ_3 direction. Considering this justification, it would be sensible then, at least theoretically, to expect that by increasing the magnitude of σ_2 beyond the σ_2=σ_3 level, ν_{13} increases and ν_{12} decreases as majority of microcracks in the rock would be aligned along σ_3 axis. Besides, for the case of σ_2=σ_3, theoretically it is estimated to obtain $\nu_{12}\approx\nu_{13}$. In practice however, orientation of microcracks in rock could have a preferred direction under uniform lateral stresses resulting in unequal displacement in perpendicular directions, which might be due to presence of any heterogeneities or pre-existing microcracks in the specimen. Hence, if the difference between ν_{12} and ν_{13} is plotted versus σ_2/σ_3 ratio (Figure 4.14) it would be anticipated that the value of ν_{13}-ν_{12} increases by increasing the stress anisotropy. However, the diagrams in Figure 4.13 and Figure 4.14 does not confirm such clear simple dependency of Poisson's ratios on the intermediate stress magnitude or stress anisotropy in the tested sandstones.

The impact of raising σ_3 level in true triaxial tests on the value of Poisson's ratios is depicted in Figure 4.15. Similar to the behaviour of Young's modulus in these sandstones (Figure 4.12), no clear relation is observed in this diagram between the value of the minimum stress in true triaxial tests and the Poisson's ratios in these rocks.

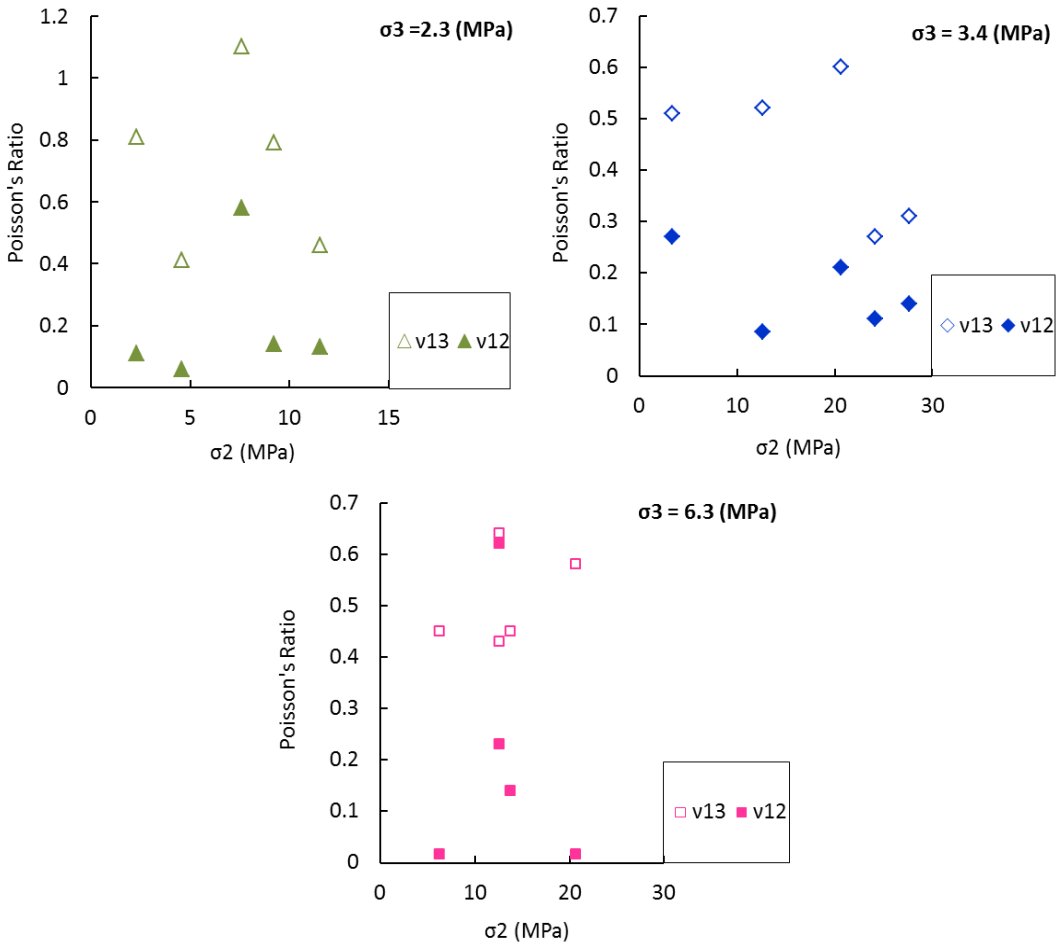

Figure 4.13 Variations of Poisson's ratio along minimum and intermediate principal directions as a function of σ_2 magnitude at σ_3=2.3 MPa, 3.4 MPa and σ_3=6.2 MPa in the sandstone samples. ν_{13} was significantly greater than ν_{12} in all groups. This confirms development of the microcracks in σ_3 direction. No clear dependency on σ_2 magnitude could be extracted for Poisson's ratios in the tested sandstones.

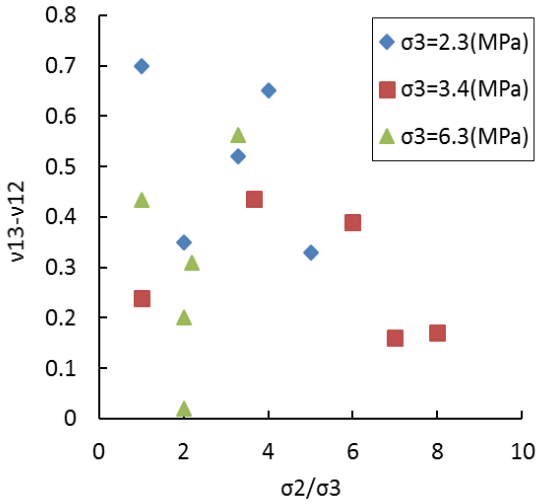

Figure 4.14 Poisson's ratio anisotropy (ν_{13}-ν_{12}) as a function of lateral stress anisotropy in sandstone samples. Some increase in ν_{13}-ν_{12} was expected by increasing the σ_2/σ_3 ratio but such dependency is not observed for these samples.

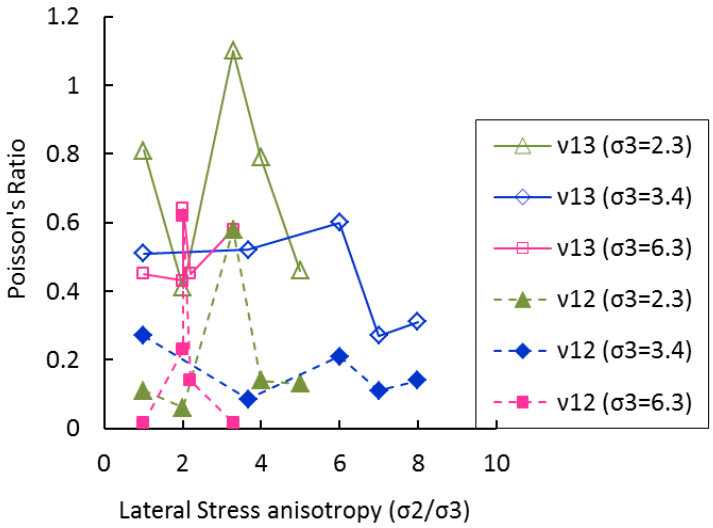

Figure 4.15 Changes in Poisson's ratios, ν_{12} and ν_{13} as a function of σ_2/σ_3 ratio in sandstone samples. The magnitude of minimum stress for each group of data points is shown in parentheses. No common relation could be extracted between σ_3 level and the value of ν_{12} and ν_{13}.

4.3.4 Inelastic deformation and dilatancy

Experimental studies of Mogi (2007) on different rock types such as trachyte, granite, marble and schist showed that by increasing σ_2 beyond σ_3, generally the strain along the axis of the intermediate principal stress (ε_2) decreases while the strain along minimum principal stress direction (ε_3) increases. This is explained by the supporting effect of the intermediate stress on the rock, which restrains rock deformation (elastic and inelastic) in this direction and consequently imposes more displacement along σ_3 direction.

Figure 4.16 presents the maximum differential stress (σ_1-σ_3) and lateral principal strains, ε_2 and ε_3, as functions of the axial strain, ε_1, in the synthetic sandstones. In this figure, the minimum principal stress is 3.4 MPa. For the typical case of a true triaxial test ($\sigma_2>\sigma_3$), the failure strength is significantly greater than the case of $\sigma_2=\sigma_3$. Under axisymmetric conditions (left plots), ε_2 is very close to ε_3, both indicate extensional strains and also large dilation of the sample in post-failure region. However, when σ_2 is larger than σ_3 (right diagrams), ε_2 is compressive (positive strain) and noticeably smaller than ε_3 in magnitude.

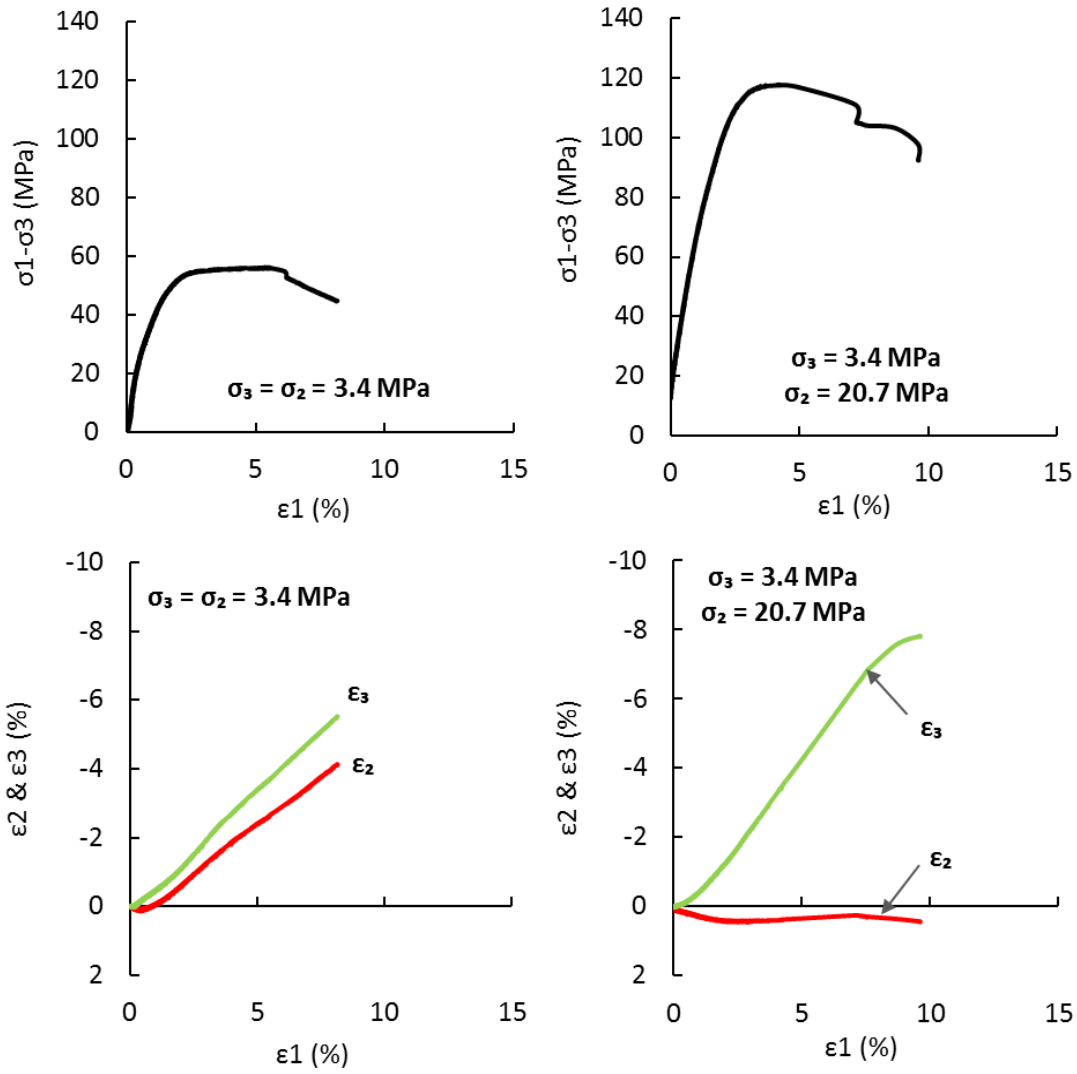

Figure 4.16 The differential stress (top) and lateral strains, ε_2 and ε_3, (bottom) as function of the axial strain, ε_1, in synthetic sandstones. Left: plots for the axisymmetric conditions ($\sigma_2=\sigma_3$); right: plots obtained under true triaxial conditions ($\sigma_2>\sigma_3$). Negative strains here show extension while positive strains show compression. The peak stress is higher for the case of $\sigma_2>\sigma_3$ (top). In the axisymmetric test, ε_2 is similar to ε_3, both showed extension while for the typical case of $\sigma_2>\sigma_3$, ε_3 is significantly larger than ε_2

Mogi's laboratory results also revealed that in a ε_1-ε_2 plot, ε_2 was non-linear for lower magnitudes of σ_2, while it was linear for larger values of σ_2. The test results also indicated that increasing the intermediate stress caused decrease in ε_2.

Variations of ε_2 against ε_1 for three levels of minimum stress are displayed in Figure 4.17 for all sandstone samples. For lower levels of the intermediate stress the curves in this diagram indicate large strains and dip upwards, towards negative ε_2 values, which mean the rock has expanded in the direction of σ_2. While by increasing σ_2, the curves became nearly linear or dip downwards, in the positive section of the

vertical axis in the plots. In other words, at larger σ_2 values, the rock showed some compression along the intermediate stress direction which was though considerably smaller than the compression along σ_1 axis. The typical stress-strain curves of the synthetic sandstone samples shown in Figure 4.4 also confirmed this behaviour. The stress-strain plots indicated that under axisymmetric conditions (σ_2=σ_3) increasing the differential stress caused elastic extension in ε_2 similar to ε_3 direction, followed by some inelastic dilation along both directions after peak stress was reached (see Figure 4.4.a and -c). Under higher levels of σ_2 (higher σ_2/σ_3 ratios), ε_2 only indicated some small compressive strains, despite ε_3 that showed relatively large extensional strains (see Figure 4.4.b, -d, -e and -f). This confirms that, as suggested by Mogi (2007), under higher magnitudes of σ_2, the rock dilatancy is mainly induced by the extension in σ_3 direction (increase in ε_3).

Dilatancy is the increase in rock sample volume due to its inelastic deformation under loading (Fjær et al. 2008). The inelastic deformation in the rock sample is basically a combination of plastic deformation and microfracturing. The plastic deformation does not result in volumetric increase of the rock sample. Thus the dilatancy is associated with the microfracturing in the brittle specimen prior to failure which includes cracks opening (Mogi 2007).

Previous laboratory studies on different rock types such as sandstone, granite, amphibolite, siltstone, marble and schist (e.g.Takahashi and Koide 1989, Haimson and Chang 2000, Oku et al. 2007, Mogi 2007) has shown that, while the minimum stress is constant, increasing the intermediate stress extends the linear elastic range of stress-strain curves. Consequently, the timing of the onset of dilatancy gradually increases, which is associated with propagation and growth of stress-induced microcracks that eventually led to through-going fault and fractures. The onset of dilatancy can be determined from the point where the volumetric strain (ε_v) versus axial strain (ε_1) curve starts deviating from linearity (see Matsushima 1960, Brace et al. 1966) or where σ_1-σ_3 versus ε_v curve deviates from linear trend (see Haimson and Chang 2000).

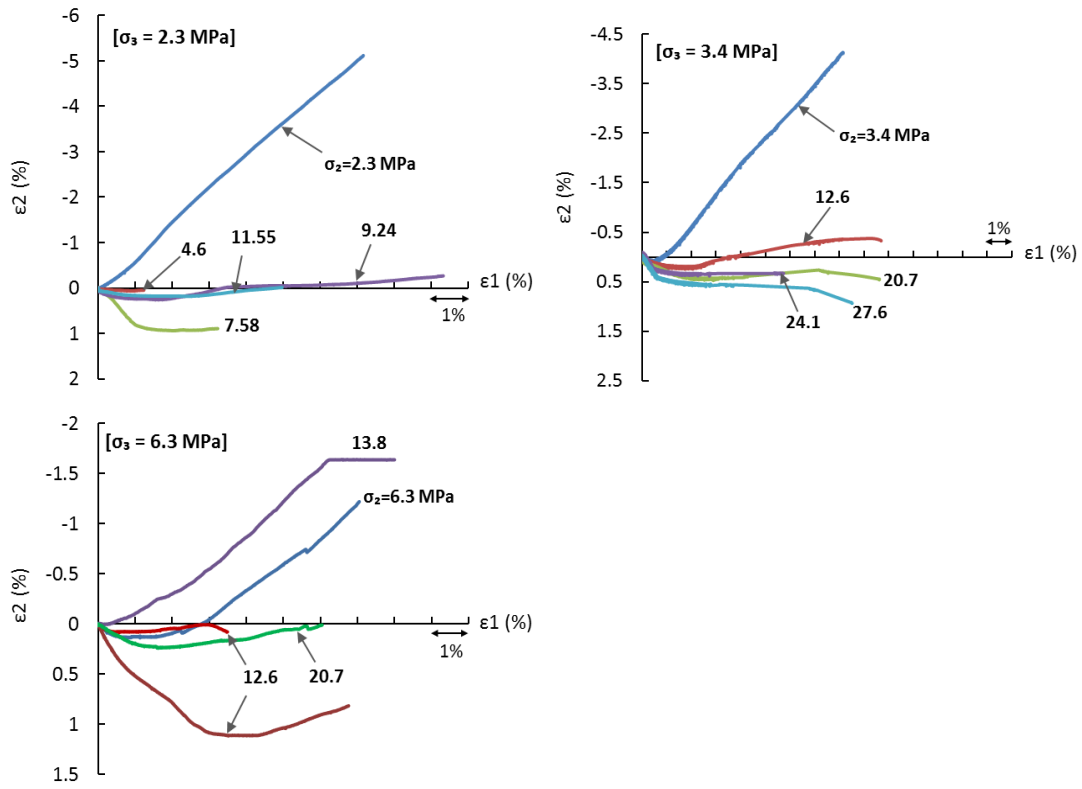

Figure 4.17 Variations of ε_2 versus ε_1, in Sandstone samples for tests under σ_3=2.3 MPa, 3.4 MPa and 6.3 MPa. The numerals on the curves show σ_2 levels, in MPa. At low σ_2 levels, ε_2 dips upwards (dilation) but at higher levels of σ_2 it becomes compressive (dips towards the positive side of the axis).

In this work, deviation of the differential stress versus volumetric strain curve from linear elastic behaviour was taken as the dilatancy onset, as shown by some examples in Figure 4.18. The obtained stress levels are displayed in Table 4.4 as percentage of the axial peak stress ($\sigma_{1\text{-peak}}$). The results showed that by raising σ_2 at a constant level of σ_3, the stress level at which rock dilation began, generally increased with respect to the peak stress. This behaviour is in good agreement with previous findings in sandstones (Takahashi and Koide 1989, Kwaśniewski et al. 2003, Ma 2014). This suggests that increasing σ_2 magnitude above the applied σ_3 inhibited the development of microfractures and consequently postponed the beginning of the brittle failure process (Lee and Haimson 2011).

It was noted that for the group of samples tested under σ_3=6.3 MPa, the volumetric stress-strain curves generally did not show a deflection towards volumetric increase (negative strains), as opposed to other groups of samples (Figure 4.19). Inspection of post-mortem samples indicated that macroscopic shear fracture planes have developed in the samples of this group. However, compaction has been

dominant in these samples, as can be seen on the stress-strain curves in Figure 4.20. Paterson and Wong (2005) explained that changes in rock volume during deformation are usually the result of two opposing mechanisms; firstly the formation and development of aligned microcracks under deviatoric loading which lead to volume increase, and secondly, pore collapse due to the combined impact of high confining pressure and deviatoric loading, which results in volume decrease. In porous rocks, significant inelastic compaction can result from either pore collapse or grain crushing (Wong et al. 1997), and tends to counterbalance the volume increase due to microcracking (dilatancy). Such an effect is often referred to as shear-enhanced compaction (Paterson and Wong 2005). The implication in case of these synthetic sandstones is that, as the samples have relatively high porosity (>25%), pore collapse and inelastic compaction under the higher lateral stresses masked the volume increase related to shear failure. Consequently, the ε_v curves mainly showed inelastic compaction prior to failure, which resulted in undetectable dilatancy onset. Ma and Haimson (2013) observed similar behaviour in volumetric strain curves of high-porosity Bentheim sandstone subjected to high true triaxial stresses. Popp and Salzer (2007) studied dilatancy in argillaceous rocks through true triaxial tests. They suggested that volumetric strain could be masked by the dominating effect of compressive strain in axial direction (normal to bedding). Thus it would be impractical to detect the dilatancy onset from the volumetric strain curves. They proposed a method based on ultrasonic wave velocities for analysis of dilatancy. The pronounced decrease in the measured P-waves and S-waves velocities during the mechanical test was used as an indication of the dilatancy onset. However, ultrasonic wave measurements were not available here for the tested samples.

4.3.5 Macroscopic fractures and cracks pattern

Figure 4.21 exhibits images of the synthetic sandstone samples after true triaxial tests. For each sample, both sides of the rock cube subjected to the intermediate stress are displayed. Through-going failure planes were observed in all specimens, except for sample 1-7. During the testing of this latter sample, axial loading was stopped too early, before macro-fractures and faults formed in the sample. Generally traces of the faults on opposing sides of each sample in Figure 4.21 are roughly symmetric and typically strike parallel to the σ_2 direction. Hence, as implied earlier

from the principal strain curves, the rock sample dilation primarily occurs along σ_3 axis under true triaxial stress conditions.

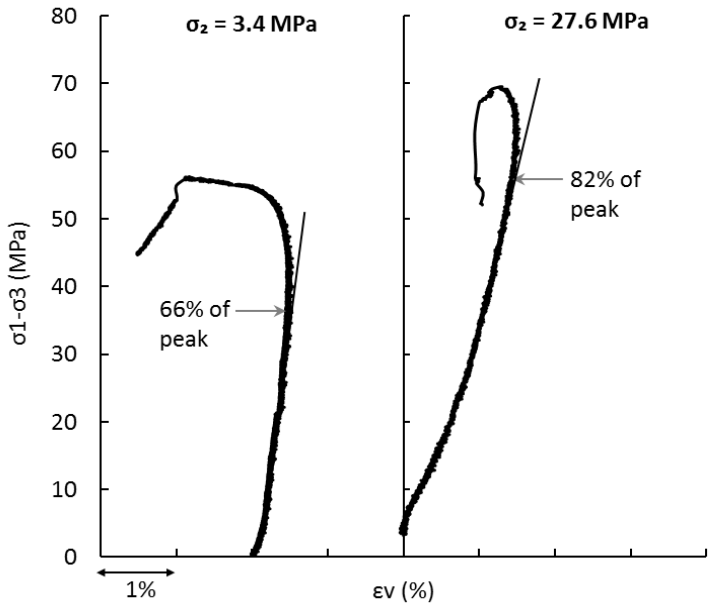

Figure 4.18 Some examples of the differential stress versus volumetric strain curves in the synthetic sandstones under σ_3=3.4 MPa and different σ_2 values. The deviation of these curves from linearity defined the onset of dilatancy.

Table 4.4 The changes in dilatancy onset with σ_2 in the sandstone samples expressed as the σ_1 level at the dilatancy beginning and the dilatancy onset stress level with respect to the peak stress ($\sigma_{1\text{-peak}}$).

σ_3 (MPa)	**σ_2 (MPa)**	**σ_1 at onset of dilatancy (MPa)**	**Dilatancy level as % of $\sigma_{1\text{-peak}}$**
2.3	2.3	31	53.1
	4.6	40.18	69.6
	7.58	47.8	66.5
	9.24	52	78.6
	11.55	63.2	83.3
3.4	3.4	39.95	65.8
	12.6	68.03	72.4
	20.7	87.52	72.3
	24.1	56.06	75.9
	27.6	59.6	81.8

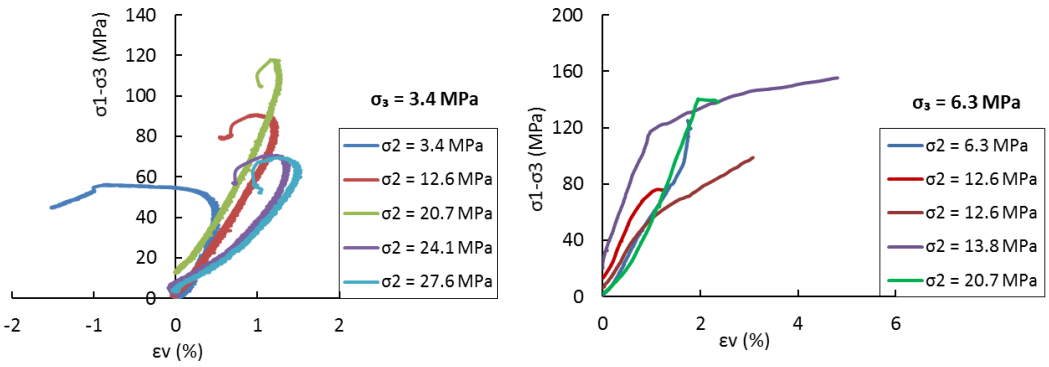

Figure 4.19 Comparison between the volumetric strain curves for two groups of sandstone samples tested under σ_3=3.4 MPa (left) and 6.3 MPa (right). In the latter group, onset of dilatancy was not detectable on the ε_v curve, as the volumetric strain has been dominated by sample compaction.

The samples tested under σ_3=2.3 MPa and various σ_2 levels showed dual sub-parallel or conjugate main faults in most cases. This behaviour identifies the upper part of the brittle range before the transitional field (Paterson and Wong 2005). The faults generally have curved and branched surfaces.

At σ_3=3.4 MPa, failure occurred along dual quasi-parallel or conjugate main faults in most samples. At the highest σ_2 levels, multiple parallel and conjugate shear fractures were propagated, which is a characteristic of transitional brittle-ductile mode (Paterson and Wong 2005). The failure plane surfaces were mostly curved and branched.

In samples tested at σ_3=6.3 MPa, mainly dual sub-parallel or conjugate (or a single) through-going faults were observed at lower σ_2 levels. For samples 1-11 and 1-12 (subjected to σ_2=20.7 MPa), a compaction band (Wong and Baud 2012) was also detected, which is a result of localization of the compaction during deformation (Paterson and Wong 2005). Observation of such compaction, which is associated with ductile pore collapse or grain crushing is an evidence of transition to ductile failure (Wong et al. 2004). This is consistent with the behaviour of the stress-strain curves in Figure 4.6, which mainly showed ductile behaviour and strain hardening for this group. Also the volumetric strain curves in Figure 4.19 confirmed the dominant compaction in these samples (shear-enhanced compaction).

The general evolution of fracture patterns due to increasing σ_3 from dual to multiple faults at σ_3=2.3 MPa and 3.4 MPa to the occurrence of compaction bands under σ_3=6.3 MPa in these sandstones is in reasonable agreement with the

observations of the stress-strain curves (Figure 4.6). These curves indicated evolution of the stress-strain behaviour from a transitional brittle-ductile behaviour towards the ductile field when the minimum principal stress increased from 2.3 MPa to 6.3 MPa. Such a transition of failure mode is in accordance with previous studies on the impact of confining pressure (or σ_3) on rock behaviour (Paterson and Wong 2005, Mogi 2007).

Previous true triaxial investigations on sandstones (Takahashi and Koide 1989, Ma 2014) showed that increasing σ_2 at a constant σ_3 may impose a transition of failure mode towards the brittle behaviour. Such an effect was not confirmed for the sandstones tested in this study. Increasing σ_2 at σ_3=3.4 MPa tended to gradually shift the failure behaviour from upper end of the brittle field towards the transitional range through increasing the number of failure planes. At σ_3=6.3 MPa, also increasing σ_2 seems to have imposed a change from transitional towards the ductile field through the occurrence of compaction bands (shear-enhanced compaction). It is possible that this behaviour is related to the high porosity of these sandstones (~26%). Hence, when σ_2 was increased over σ_3, the mean effective stress increased which promoted inelastic compaction in the samples. Ma (2014) reported a similar effect in high porosity Bentheim sandstones (~24%), which was observed from the changing shape of volumetric strain curves from dilatancy towards compaction as σ_2 increased.

In the high-porosity sandstones tested in the present work, the impact of increasing σ_2 caused an evolution of failure behaviour into the ductile field. Ma (2014) studied Coconino and Bentheim sandstones with respective porosities of 17% and 24% under true triaxial conditions. He reported that at a constant σ_3, increasing σ_2 embrittled the rock in Coconino sandstone whereas the influence of σ_2 on evolution of the failure mode was less noticeable in the higher-porosity Bentheim sandstone. The volumetric strain curves of the Bentheim sandstone also showed evolution from microcrack-induced dilatancy to inelastic compaction with raising σ_2 at some σ_3 levels, contradicting the results of the Coconino sandstone. These findings and the observations in the present work confirm the important role of porosity on the failure characteristics of sandstones (and perhaps other porous rocks). It can be inferred that the effect of porosity and stress-induced compaction in very porous sandstones may control the influence of σ_2 as to whether it embrittles the rock, similar to the trends observed in the case of more compact lower porosity rocks

such as dolomite (see Paterson and Wong 2005, Mogi 2007), or transfers the failure mode towards the ductile field, as observed in the case of the high-porosity sandstones tested in this study. However, more measurements under higher levels of both the minimum and intermediate principal stresses would be required to fully understand the evolution of failure mode in these rocks.

If the main faults can be approximated by flat planes, the fracture dip angle, defined as the angle between the slip plane and the direction of the maximum principal stress, can be measured (Mogi 2007, Haimson and Chang 2000). Experimental studies of Mogi (2007) on various rock types showed that, under true triaxial conditions, increasing σ_3 generally increased the fracture angle with respect to σ_1 axis, while increasing σ_2 decreased or did not change it. Here, however, the irregular surfaces of the major faults in the sandstone samples made it impractical to obtain the fracture angles and study its relation with the stress magnitudes.

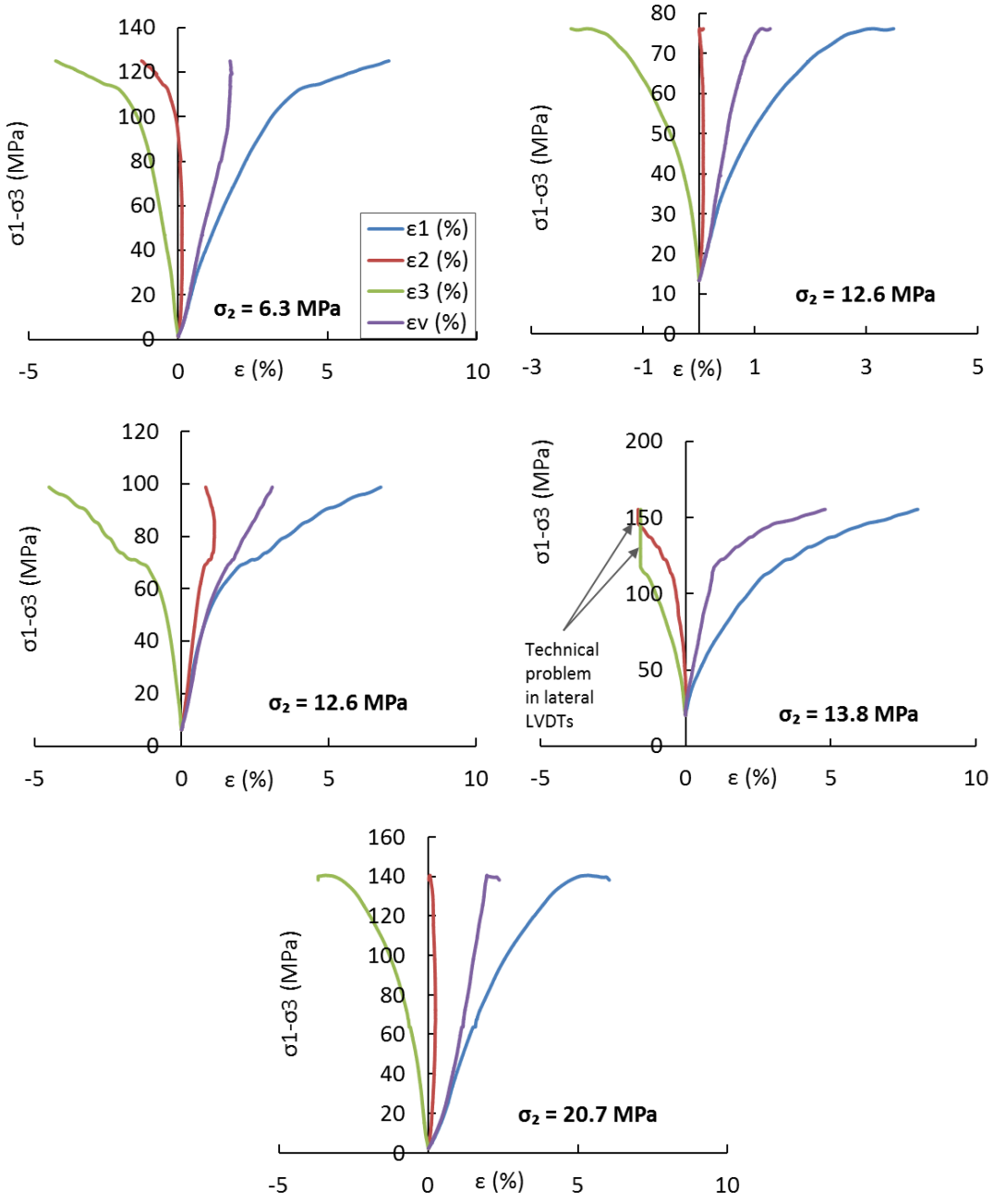

Figure 4.20 The principal and volumetric curves of the sandstone samples tested under σ_3=6.3 MPa. In this group the compressive strains are dominant and have strongly affected the volumetric strain curve. Note that the positive strains (compression) are significantly larger than the negative values (extension).

σ_3	σ_2	Sample ID	Post-failure images
2.3 MPa	$\sigma_2 = \sigma_3$	2-3	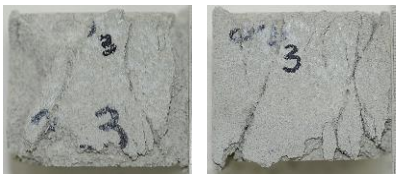
	$\sigma_2 = 2\sigma_3$	1-7	
	$\sigma_2 = 3.3\sigma_3$	1-6	
	$\sigma_2 = 4\sigma_3$	2-1	
	$\sigma_2 = 5\sigma_3$	2-2	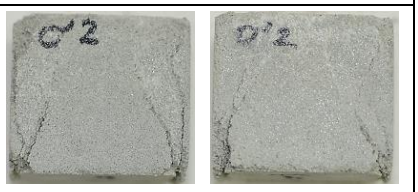

Figure 4.21 Photographs of the sandstone samples after the true triaxial tests. Here σ_1 is in the vertical direction, σ_3 in lateral direction and σ_2 perpendicular to the displayed rock side (i.e. into the page). For each sample, the two opposing sides along the σ_2 axis are displayed.

σ_3	σ_2	Sample ID	Post-failure images
3.4 MPa	$\sigma_2 = \sigma_3$	2-4	
	$\sigma_2 = 3.7\sigma_3$	2-5	
	$\sigma_2 = 6\sigma_3$	2-6	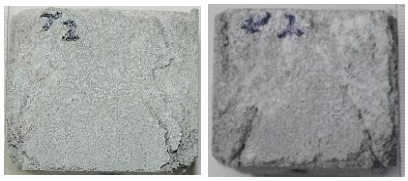
	$\sigma_2 = 7\sigma_3$	2-8	
	$\sigma_2 = 8\sigma_3$	2-7	

Figure 4.21 (Continued)

σ_3	σ_2	Sample ID	Post-failure images
6.3 MPa	$\boldsymbol{\sigma_2 = \sigma_3}$	1-9	
	$\boldsymbol{\sigma_2 = 2\sigma_3}$	1-8	
	$\boldsymbol{\sigma_2 = 2\sigma_3}$	1-8’	
	$\boldsymbol{\sigma_2 = 2.2\sigma_3}$	1-10	
	$\boldsymbol{\sigma_2 = 3.3\sigma_3}$	1-11	
	$\boldsymbol{\sigma_2 = 3.3\sigma_3}$	1-12	

Figure 4.21 (Continued)

4.4 Multistage true triaxial tests

The test results presented in above sections were obtained via single-stage true triaxial tests. In the single-stage tests constant lateral stresses were applied on a rock sample, then the sample was vertically compressed until it reached failure. Hence, the rock properties in different stress states were extracted from the measurements during a number of tests on several specimens of the same rock type. The underlying principle of multistage technique is to obtain rock characteristics under various stress states from a single specimen.

Multistage true triaxial testing was examined in this work in an attempt to obtain deformational characteristics of rocks under wider ranges of stress conditions from fewer samples, as the number of available shale samples was limited. On the other hand, the synthetic sandstone samples were reproducible, and they were assumed homogeneous. Hence to determine whether multistage true triaxial technique would be a proper approach for investigating the rock strength and deformational properties under true triaxial conditions, three multistage tests under three levels of minimum stress (2.3, 3.4 and 6.3 MPa) were conducted on the synthetic sandstones. Details of these experiments and the outcome of comparing them to the equivalent single-stage tests data are described in the following sub-sections.

4.4.1 Principal stresses during the multistage true triaxial tests

Three multistage true triaxial tests under σ_3= 2.3, 3.4 and 6.3 MPa were performed with the intermediate stress applied in a way to have σ_2/σ_3 ratios similar to the single-stage true triaxial tests. Table 4.5 displays the applied stress conditions and different stages of the three multistage tests.

In a multistage true triaxial test, initially a predefined constant pressure was applied to the rock sample equally in the three perpendicular directions. This pressure was kept constant throughout the test along the planned direction of minimum principal stress. In the planned direction of the intermediate principal stress, the pressure was raised to different levels through different stages. Within each stage, the pressure along the planned maximum principal direction was increased up to a certain stress level but loading was stopped before the rock sample failed. Determination of this termination point will be discussed below. In the last

stage, loading in the axial direction (σ_1) was continued until the sample reached failure (see Bieniawski 1968, Kim and Ko 1979).

An important aspect in conducting a multistage test is to define the termination point in each stage before the sample actually fails. Various methods have been suggested for detection of the termination point in multistage tests conducted under conventional triaxial stress conditions (see Youn and Tonon 2010). Crawford and Wylie (1987) suggested the use of the point where the volumetric strain curve returns to zero, as the stopping point. Pagoulatos (2004) proposed using the point at which the volumetric strain reached its maximum value, as the indicator of the stopping point for each stage. However, the synthetic sandstone used in this work was a relatively weak rock and the inelastic compaction of the sample has masked any noticeable dilatancy in many cases. Thus, the volumetric strain curves does not show deflection towards volumetric increase in all samples (see Figure 4.4 and Figure 4.20). Consequently, the detection techniques based on volumetric strain could not be adopted here. Youn and Tonon (2010) conducted their conventional multistage triaxial tests on cylindrical plugs of a limestone by controlling the radial strain rate and defined the stopping point based on flattening of the stress-radial strain curve. Obviously this approach was impractical here for testing cubic rock samples under true triaxial stress conditions. Therefore, in this work, a technique similar to the ISRM suggested method (Kovari et al. 1983) was used for detection of the termination point. In this method, the termination point for each stage was identified by the deviation of the axial stress-strain curve from linear trend, which corresponds to the onset of unstable fracture propagation in the sample, as described by Bieniawski (1968). This method has been commonly accepted and used by many researchers (e.g. Kim and Ko 1979, Holt and Fjær 1991, Gräsle 2011). The errors that this method is likely to induce between the picked peak strengths and the actual peak strengths are discussed in the next sub-section (section 4.4.2).

The loading path applied in the multistage true triaxial tests in this work, was adopted from the modified ISRM method suggested by Crawford and Wylie (1987) for conducting conventional triaxial multistage tests. In the proposed method, at the end of each stage, axial stress (σ_1) was reduced to the confining pressure level (σ_3); then both stresses were increased simultaneously to the next level of σ_3. Here, however, the question was whether the maximum stress should be reduced only to the σ_2 level or both σ_1 and σ_2 to be decreased down to σ_3 level, i.e. the quasi-

hydrostatic conditions. In this work, in tests with σ_3=2.3 MPa and 6.3 MPa, at the end of each stage, both σ_1 and σ_2 were decreased to σ_3 level (quasi-hydrostatic conditions), before increasing them to the next level of σ_2 (next stage). In the test where σ_3=3.4 MPa, after reaching the termination point at each stage, σ_1 was decreased down to σ_2 level and after that, both stresses were increased simultaneously to the next level of σ_2. The schematic stress paths for the three tests are displayed in Figure 4.22. Generally, the produced data from the two different loading procedures did not indicate any clear dependency of the experimental results on the applied stress paths. Hence, no conclusions could be made with regards to which stress-path would be more appropriate. However, as during a multistage true triaxial test, the minimum stress is kept constant and only the intermediate stress is changed in stages, it seems more reasonable to simply unload σ_1 down to σ_2 level and then raise these two to the next predefined level of intermediate stress.

Table 4.5 Stress conditions in multistage true triaxial testing of the sandstone samples. σ_1 and (σ_1-σ_3) are the axial and maximum differential stresses at failure, respectively.

Test	Stage No.	σ_2/σ_3	σ_3 (MPa)	σ_2 (MPa)	σ1 (MPa)	σ_1-σ_3 (MPa)
Multi.1	1	1	2.3	2.3	24	22
	2	2		4.6	42	40
	3	3.29		7.58	45	43
	4	4		9.24	54	51
	5	5		11.55	60	58
Multi.2	1	1	3.4	3.4	55	52
	2	3.67		12.6	80	76
	3	6		20.7	89	85
	4	8		27.6	93	90
Multi.3	1	1	6.3	6.3	67	61
	2	2		12.6	72	65
	3	3.29		20.7	116	110

4.4.2 Multistage true triaxial tests results

The differential stress versus principal strain curves of the multistage true triaxial tests are depicted in Figure 4.23. For the clarity of the diagrams, only ε_1 and ε_3 curves in different stages were displayed. For each stage, it was attempted to stop the

axial loading immediately after deviation from linearity was detected on the principal stress-strain curves. Strains were set to zero at the beginning of each stage. It was noticed that for all three multistage true triaxial tests, the magnitudes of the strains in the first stage are relatively larger than the strains measured in the subsequent stages, in particular in case of the axial strain (ε_1). This is likely due to compaction in these high-porosity sandstones under axisymmetric conditions.

The rock strength at each of the applied σ_2 stages was defined as the peak differential stress achieved in that step. The values of rock strength from multistage true triaxial tests have been plotted versus σ_2 in Figure 4.24 along with the peak stresses acquired in the corresponding single-stage tests on synthetic sandstone samples. These diagrams clearly show that the rock strength in multistage true triaxial tests is significantly lower than the strength magnitudes obtained under similar stress states in the single-stage tests. The true triaxial strength magnitudes from the two types of testing have been compared in Table 4.6. For tests under σ_3=2.3 MPa, the strength magnitude decreased between 19-61% below its value obtained in single-stage tests. This decrease was in the range of 8-28% and 14-24% for the tests conducted under σ_3=3.4 MPa and 6.3 MPa, respectively. Holt and Fjær (1991) compared the results of conventional triaxial single-stage and multistage tests on a relatively weak brittle sandstone. Their experimental investigations showed that the ratio of strength magnitude in multistage tests to that of single-stage tests had an average value of very close to 1.00 (~0.95). Based on their observations they concluded that the strength values obtained in both types of tests were in good agreement. It is to be noted that in this work the ratios of strength in multistage true triaxial tests to that of single-stage true triaxial tests ($\sigma_{f.m.}/\sigma_{f.s.}$) were noticeably smaller than 1, for almost all stress states (see Table 4.6). This implies that the true triaxial multistage tests conducted in this work could not represent the mechanical properties of the intact rock samples. Possible reasons for this behaviour could be improper detection of the termination point at each stage, or damage accumulation in the tested samples under cyclic true triaxial loading. These issues are discussed in further detail in the next section.

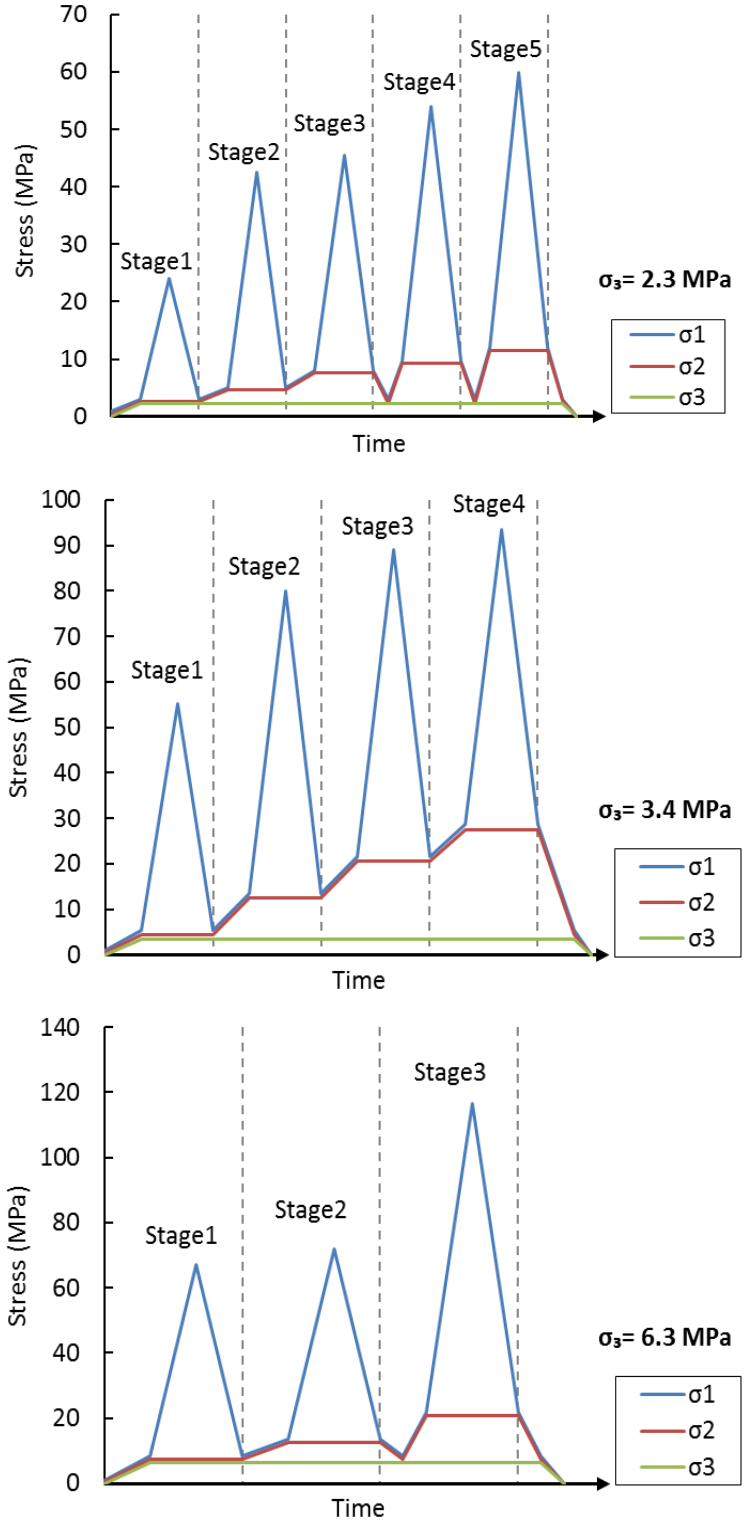

Figure 4.22 Schematic stress path in the multistage true triaxial tests on the sandstone samples. For the tests under σ_3=2.3 and 6.3 MPa, at the end of nearly all stages, σ_1 and σ_2 were decreased to quasi-symmetric stress conditions before increasing σ_2 to the next stage. While for tests under σ_3=3.4 MPa, σ_1 was only reduced to σ_2 level at the end of each stage and then both were increased to next stage.

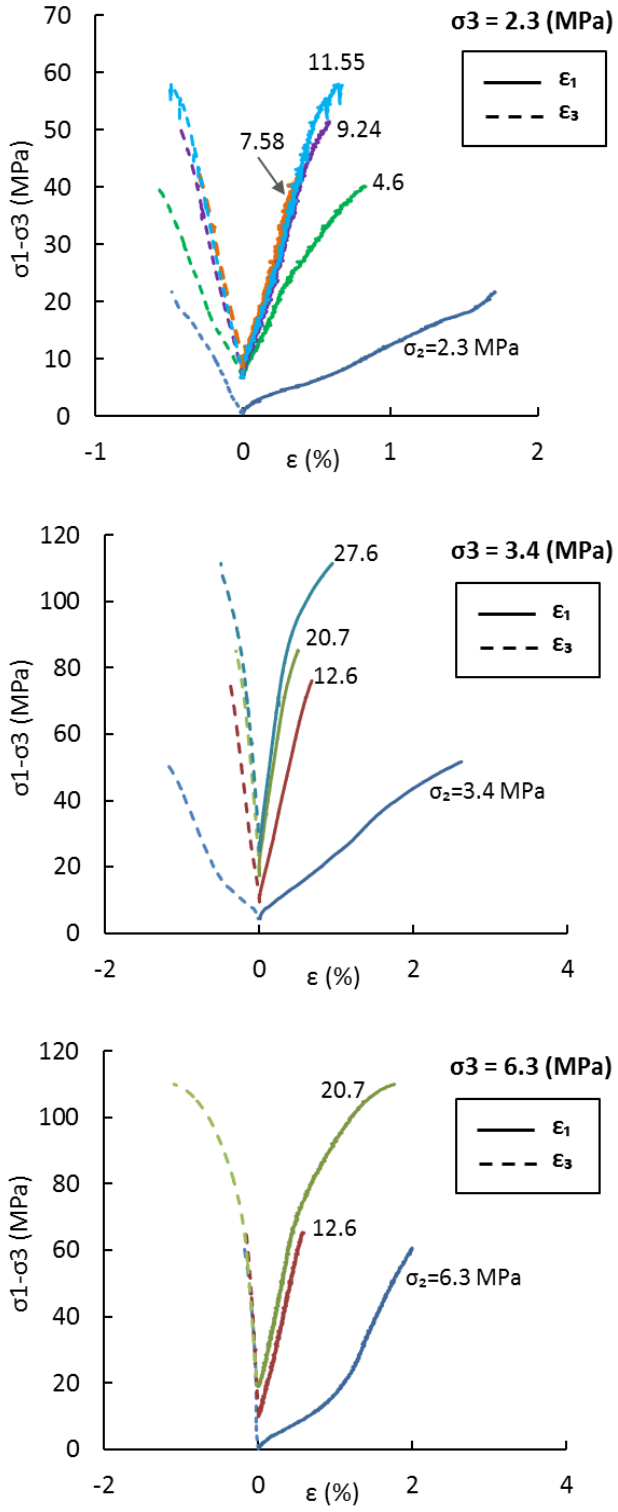

Figure 4.23 Differential stress versus principal strain curves obtained in multistage true triaxial tests. The ε_2 curves and unloading stages are not displayed here, for the clarity of plots. The values of the intermediate stress applied in each stage are displayed by numerals on the diagrams.

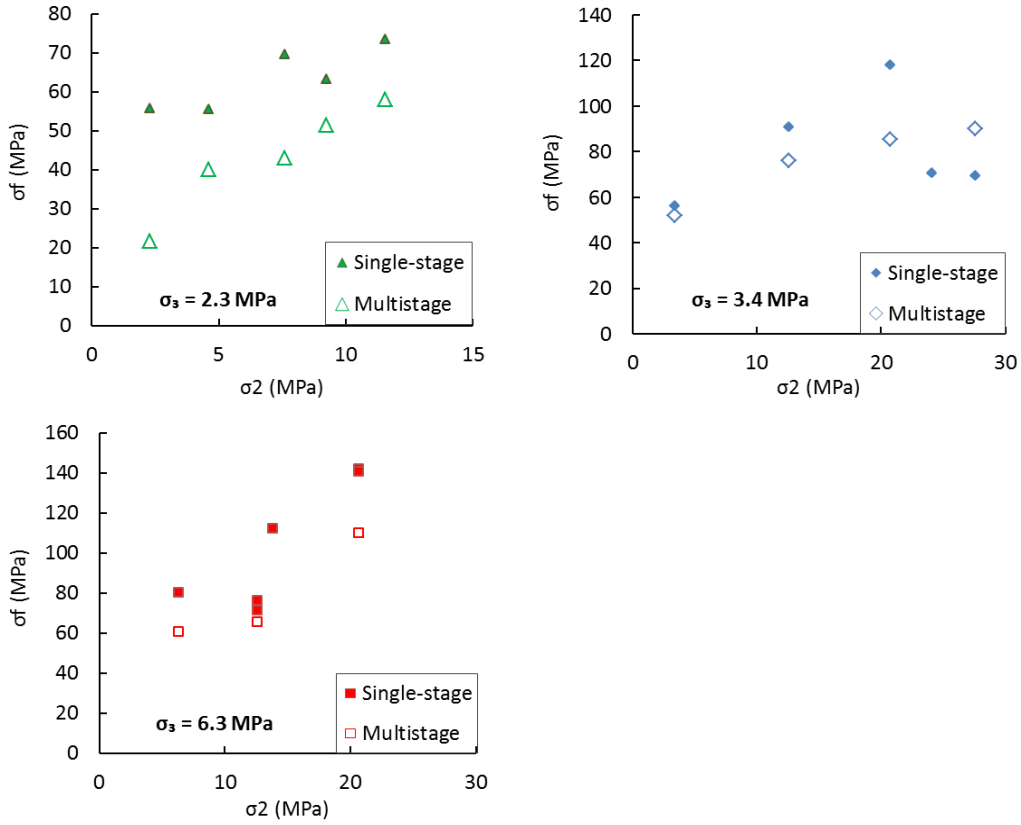

Figure 4.24 Comparison between the peak differential stress (σ_f) obtained in multistage true triaxial tests and single-stage true triaxial tests in the sandstone samples, tested at σ_3= 2.3, 3.4 and 6.3 MPa. Multistage tests generally gave lower strengths than the single tests.

To evaluate the outcome of the multistage true triaxial technique in measuring rock elastic properties, the Young's moduli measured in these tests were compared to those values measured via the single-stage true triaxial tests (Figure 4.25). However, the two groups of measurements did not show a good agreement. The values of Young's modulus extracted from multistage true triaxial tests here were noticeably larger than those measured under the same stress states in the single-stage true triaxial tests (Table 4.7). Comparing the stress-axial strain curves of the single-stage tests with the multistage true triaxial tests also confirmed that the curves became steeper from the first to the last stage of the multistage test, as shown by some examples in Figure 4.26. In other words, cyclic loading has apparently increased the rock stiffness. This indicates that true triaxial multistage tests would not be appropriate for obtaining the elastic properties of such porous sandstones. Pagoulatos (2004) compared the Young's modulus magnitude in multistage and single-stage standard triaxial tests on the Berea sandstone. He also observed that the *E* values obtained in multistage tests were larger than those measured through single-stage

tests. He explained this observation due to the closure of small cracks normal to the maximum stress axis inside the sample after the first loading cycle. Similar differences between results of single-stage and multistage tests were observed in conventional triaxial tests implemented in this work on the synthetic sandstones (Table 4.1).

Table 4.6 Comparison between the strength data obtained in multistage ($\sigma_{f.m.}$) and single-stage ($\sigma_{f.s.}$) true triaxial tests on the synthetic sandstones.

σ_3 (MPa)	σ_2 (MPa)	$\sigma_{f.s.}$ (MPa)	$\sigma_{f.m.}$ (MPa)	$[\sigma_{f.s.}-\sigma_{f.m.}]$ (MPa)	$(\sigma_{f.s.}-\sigma_{f.m.})/\sigma_{f.s.}\times 100\%$	$[\sigma_{f.m.}/\sigma_{f.s.}]$
2.3	2.3	56	22	34	61	0.39
	4.6	55	40	15	28	0.72
	7.58	70	43	26	38	0.62
	9.24	63	51	12	19	0.81
	11.55	74	58	16	21	0.79
3.4	3.4	56	52	4	8	0.92
	12.6	91	76	15	16	0.84
	20.7	118	85	33	28	0.72
	27.6	70	90	-20	-29	1.29
6.3	6.3	80	61	20	24	0.76
	12.6	76	65	11	14	0.86
	20.7	141	110	30	22	0.78

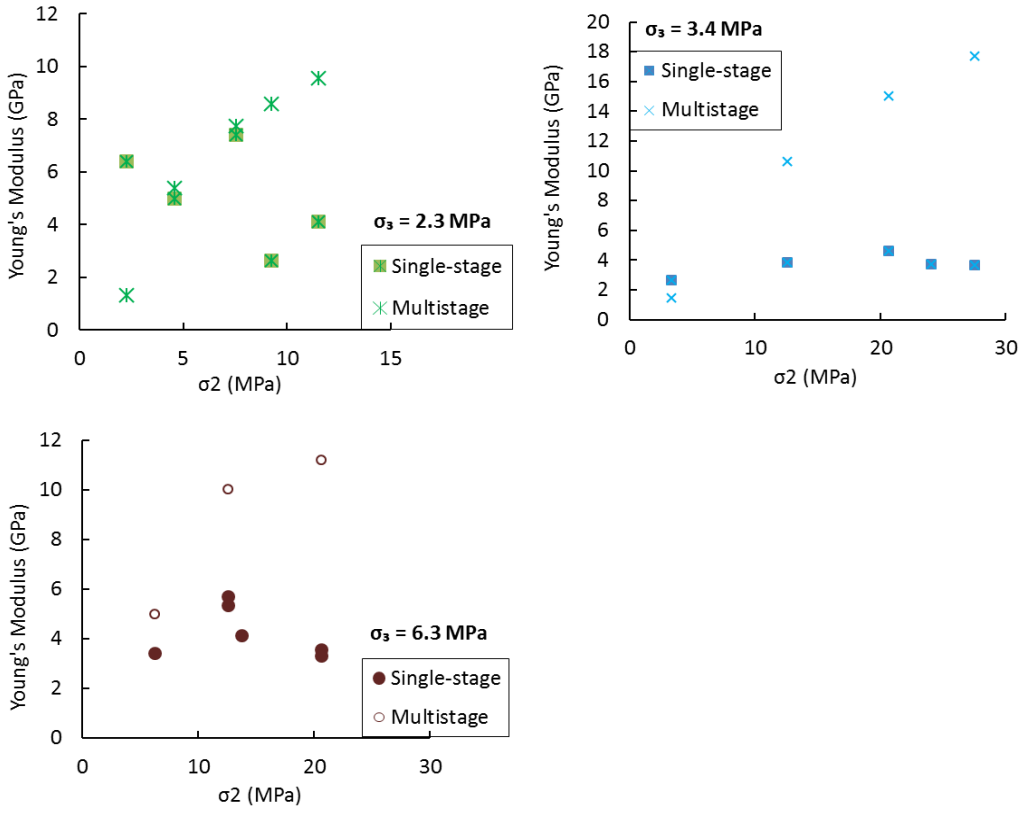

Figure 4.25 Comparison between the value of Young's modulus in multistage and single-stage true triaxial tests on the sandstone samples. *E* values in multistage tests were generally larger than the ones in single-stage tests and they showed ascending trend with σ_2 level for all three tests.

Table 4.7 Young's modulus values measured in multistage (E_M) and single-stage (E_S) true triaxial tests on the synthetic sandstones.

σ_3 (MPa)	σ_2 (MPa)	E_S (MPa)	E_M (MPa)
2.3	2.3	6.4	1.3
	4.6	5	5.4
	7.58	7.4	7.7
	9.24	2.6	8.6
	11.55	4.1	9.5
3.4	3.4	2.6	1.5
	12.6	3.8	10.6
	20.7	4.6	15
	27.6	3.6	17.7
6.3	6.3	3.4	5
	12.6	5.3	10
	20.7	3.3	11.2

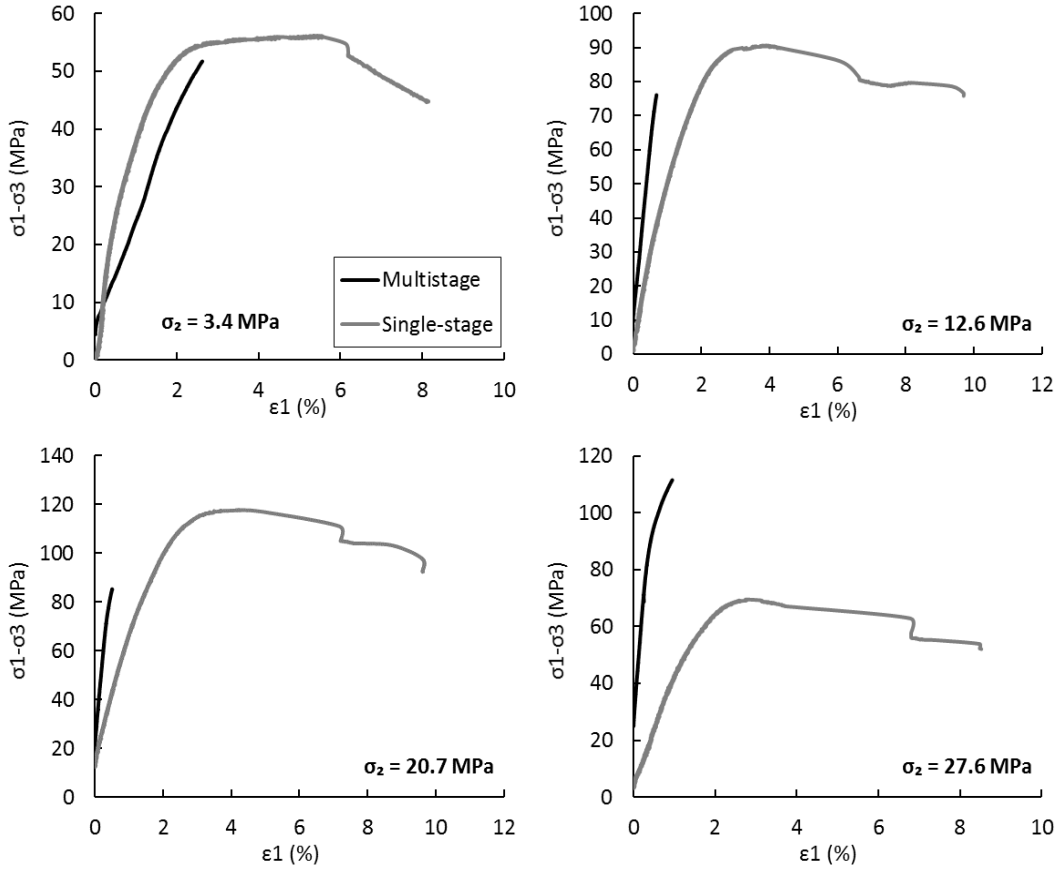

Figure 4.26 The differential stress versus axial strain curves recorded in multistage and single-stage true triaxial testing of the sandstone samples tested under σ_3=3.4 MPa. In most of the tests, the curves are noticeably steeper in the multistage tests, which justifies the higher values of Young's modulus in multistage tests in comparison to the single-stage ones.

4.4.3 Discussion

Comparing the results of the multistage true triaxial tests with the equivalent single-stage true triaxial measurements revealed that there are significant differences between the resultant rock strengths and elastic properties. Multistage tests tend to give lower rock strength values under true triaxial stress states. Potential explanations for this behaviour are:

1. Premature termination of axial loading:

   As stated earlier, the deviation of the stress-axial strain curve from linear behaviour was chosen as the indicator of termination in different steps of multistage true triaxial tests in this work. When conducting the experiments, the deviation point was picked manually based on visual inspection of the principal stress-strain curves recorded during the test. Manual detection of the deviation is strongly subjected to the experimenter's judgement and experience (see Pagoulatos 2004, Youn and Tonon 2010). Hence, it is likely here that the axial loading has been stopped prematurely during different cycles of the multistage true triaxial tests, fearing sample failure prior to performing the final stage.

   The differential stress-axial strain curves obtained in multistage and single-stage true triaxial experiments under identical stress states were compared, as shown by some examples in Figure 4.26. These plots confirm that the stress-axial strain curves of these sandstones flatten out rapidly when approaching failure. Thus, during loading stages of a multistage true triaxial test, as soon as the deviation from linear trend was observed on axial strain curve (subject to the operator's judgement), loading was terminated to prevent sample failure. This stress level is in fact the yield point of the sample and is lower than its failure strength. Therefore, such premature termination of loading can explain the underestimated strength values in the early and middle stages of a multistage true triaxial test. On the other hand, in the final stage of each multistage true triaxial test, axial loading was continued until the peak failure stress was achieved. Hence, another mechanism should be responsible for the strength differences observed in the last loading stage of these tests.

2. Excessive damage accumulation:

   Holt and Fjær (1991) argued that the results of conventional multistage triaxial tests are reliable only if cracks present in a sample during the early stages of loading were closed by increasing the confining stress level or were non-critical for the failure process during the subsequent stages. Otherwise, the rock strength would be underestimated in final stages of a conventional multistage test due to the permanent damage in the rock sample during the early stages. They suggested using acoustic measurements during multistage triaxial tests for controlling the quality of the test, as wave velocities are very sensitive to microcracks propagation in a rock sample. Rock failure in a standard triaxial test is mainly associated with propagation of microcracks primarily oriented parallel to σ_1 and bridging between these axial microcracks by wing cracks (Paterson 1978). Studies of Holt and Fjær (1991) showed that when failure was approached, P-wave velocity along σ_1 axis was constant or slightly decreased, while the radial P-wave velocity (perpendicular to σ_1 axis) showed a sudden decrease due to the opening of axially oriented cracks. Monitoring the P-wave velocity during their standard multistage triaxial tests indicated that, while at the end of each stage the velocities decreased, increasing the confining pressure to higher stress levels caused an overall increase in the wave velocities during the course of the experiment. The recovery of P-wave velocity implied that cracks opened during axial loading in each stage, were closed due to the release of axial load and an increase in confining pressure in the following stage. Hence, the rock sample is restored to a state close to its intact state after the termination of each stage in a multistage test performed under standard triaxial test conditions. Accordingly, several peak strength points can be obtained for the rock sample at different levels of confining stress without significantly damaging it. Comparison between the results of single-stage and multistage tests conducted under standard triaxial stress states on different rock types, such as shales and sandstones, indicated only slight disagreement between the strength values, if the termination level of the stages were detected before significant damage occurs in the sample (e.g. Kim and Ko 1979, Holt and Fjær 1991, Pagoulatos 2004).

   The simplified mechanism of microcrack propagation and closure in a conventional multistage triaxial test was compared to that of a multistage true triaxial test, which is depicted in Figure 4.27. Under standard triaxial test

conditions, axial stress release and increasing the magnitude of σ_3 causes closure of the microcracks opened during axial loading in the previous stage, as the confining pressure is increased in all directions around a cylindrical sample. Such axially aligned cracks are usually randomly oriented in plan view, at least until coalescence and macroscopic failure. This was confirmed by the wave velocity measurements (Holt and Fjær 1991). Under true triaxial stress conditions, as a result of increasing σ_1 during each stage, the majority of microcracks are theoretically expected to be oriented with axes parallel to the σ_1 and σ_2 directions, and opened normal to the σ_3 direction. When proceeding to the next stage, σ_3 is kept constant, while σ_2 is raised. This would favour continued opening and propagation of these pre-existing microcracks rather than closure, by inducing tensile stress at their tips aligned with the load axis (σ_2 axis) (Paterson 1978). Consequently, increasing the intermediate stress from each stage to the next stage, does not restore the specimen, but causes damage accumulation inside the rock sample. As a result, the peak strengths obtained in a multistage true triaxial test could be expected to be noticeably lower than that of the intact rock samples, as it was the case for the sandstone samples tested in this work (see Table 4.6). However, this mechanism does not explain the disagreement between the peak stress values in the first stage of the multistage true triaxial tests and the corresponding single-stage one, as during the first stage the rock sample is still representative of an intact rock.

According to the above discussion, in this study a combination of the premature termination of loading in each stage (by design), and the damage accumulated in the sample by increasing the number of stages was found to be responsible for the lower strength values measured in the multistage true triaxial tests. Manual detection of the deviation of axial strain curve may not be the ideal criterion for terminating the stages, as it is subjectively controlled by the operator's judgement. Hence, an alternative method should be sought for defining the termination points in the future works. In addition, the validity of true triaxial multistage testing should be examined in greater detail in the future by conducting tests under wider ranges of stresses and on other rock types. Measurements of acoustic wave velocities during multistage true triaxial experiments are recommended for future investigations in order to shed more light on the mechanism of microcracks propagation during such tests.

In conclusion, compared to the single-stage true triaxial tests, the multistage true triaxial tests conducted in this work gave lower absolute strength values, using the applied loading path and the employed detection method for the termination points. As such, true triaxial multistage tests are not recommended for obtaining rock mechanical properties and investigating the impact of the intermediate stress on rock strength and deformational behaviour under true triaxial stress states in weak porous sandstones.

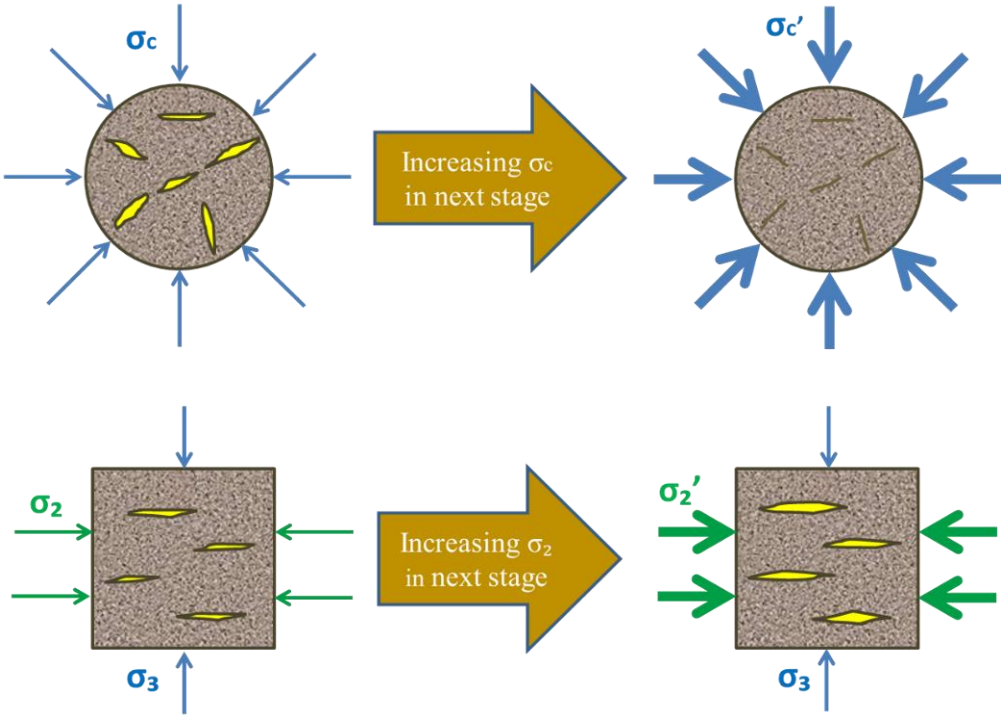

Figure 4.27 Schematic comparison between the failure mechanism in multistage tests under conventional triaxial (top) and true-triaxial stress conditions (bottom). Here, a cross-section of the cylindrical (top) and cubic (bottom) rock sample normal to σ_1 direction is depicted. Increasing the confining pressure (σ_c) from one stage to the next stage causes closure of the axially-oriented microcracks in standard triaxial tests (top row). However, at a constant σ_3, increasing σ_2 during stages of a true triaxial test (bottom row) causes propagation of the pre-existing microcracks by inducing tensile stress at their tips.

4.5 Summary

True triaxial deformation behaviour of the synthetic sandstone samples were examined by conducting experiments in a true triaxial stress cell. Cubic specimens were tested under constant levels of minimum stress and different levels of intermediate stress to cover a reasonably wide range of σ_2/σ_3 ratio. The major findings of this study were as follows:

- The laboratory measurements suggest that compressive strength of porous sandstones is affected by absolute levels of both the minimum and the intermediate principal stresses. In true triaxial tests, raising the σ_3 level increased the rock strength in a similar fashion to trends normally observed in conventional triaxial testing of rocks. Increasing the σ_2 magnitude from a conventional triaxial stress state ($\sigma_1>\sigma_2=\sigma_3$) to a true triaxial stress states ($\sigma_1>\sigma_2>\sigma_3$) caused increases in strength of up to 110% in these sandstone samples.

- The measurements fit best to a Mogi-type 3D failure criterion in τ_{oct}–$\sigma_{m,2}$ domain. Further experiments at higher minimum and intermediate stresses would be required to determine a more complete failure envelope for these sandstones.

- The Young's modulus of the sandstones indicated some increase and then a gradual decrease as a result of increasing σ_2 value, at σ_3=3.4 and 6.3 MPa. However, the variations of *E* with the intermediate stress at σ_3=2.3 MPa did not follow this trend.

- The data gathered in this work, did not reveal a simple relation between the relative values of Poisson's ratios and the magnitudes of the principal stresses.

- The evolution of the stress levels at the onset of dilatancy showed that increasing the intermediate principal stress at σ_3=2.3 MPa and 3.4 MPa extended the elastic range of the stress-strain curves and therefore postponed the brittle failure process in these sandstones. For the group of samples tested under σ_3=6.3 MPa and various σ_2 levels, the inelastic compaction of these high porosity sandstones masked any noticeable dilatancy on the volumetric strain curves.

- Evolution of deformation and fractures pattern observed in the post-test samples indicated that increase in the magnitude of minimum stress resulted in the evolution of the failure mode from the brittle field to the ductile field. Such a transition of failure mode is in accordance with previous studies on the impact of confining pressure on rock failure behaviour. The impact of increasing σ_2 on failure mode was generally in the same direction as that of σ_3, i.e. evolution towards the ductile field. While some previous true triaxial studies reported embrittling effect of σ_2 on rock, this apparently contradictory influence of σ_2 on these sandstones was likely to be related to their high initial porosity. As a result, at the higher σ_2 levels, the significant resultant increase in mean effective stress led to enhanced inelastic compaction in the specimens.

- Feasibility of multistage true triaxial tests was also investigated in this work. Young's moduli increased systematically with increasing σ_2 in multistage tests, while single-stage test results are more scattered; in addition, *E* was usually higher in the multistage tests than for single-stage tests. Furthermore, the multistage rock strength results were not consistent with the single-stage measurements. A potential explanation for this observation is that compaction in these porous specimens occurred through a number of loading-unloading cycles under true triaxial conditions which stiffened the rock through porosity reduction but reduced the strength as a result of cement breakage at grain contacts. Multistage true triaxial testing is therefore not recommended for weak porous rocks such as these sandstones and needs to be studied further in regard to other rock types.
- There may be some heterogeneity between individual samples of the synthetic sandstones which has impacted on the consistency of the results. The artificial cementation process is an inherently chaotic process and minor variations in cements at grain boundaries can significantly affect elastic and deformational properties.

In the next chapter the results of single-stage true triaxial tests on the Carynginia Shale and the Pierre Shale will be presented and their mechanical characteristics will be discussed.

5 Deformational properties of shales under true triaxial stresses and variable water saturation

5.1 Introduction

The results of true triaxial failure tests on the Carynginia Shale and the Pierre Shale specimens are presented in this Chapter. Similar to the sandstones results presented in Chapter 4, the compressive strength, elastic properties, inelastic deformation, dilatancy and failure mode of these shales are analysed and their dependence on the true triaxial stress states is discussed. Also, in this study, the impact of changing water saturation on mechanical behaviour of the Pierre Shale specimens is investigated.

The methodology of the experiments conducted on the shales was explained in Chapter 3. The principles of the laboratory data analysis and interpretation follows the techniques explained for the synthetic sandstones in Chapter 4. However, while the tested sandstones were considered to be isotropic, shales have laminations, preferred particle alignment or bedding planes and are generally classified as transversely isotopic materials. In such materials, the elastic response within the bedding planes is identical in every direction whereas it is different in the direction normal to these planes (Fjær et al. 2008). The direction parallel to bedding planes is described as the isotropic plane and line perpendicular to this plane is called the transverse isotropic (TI) axis. Transversely isotropic materials are described by five independent elastic parameters. In a coordinate system where the x-axis defines the TI axis and the y- and z-axis define the isotropic plane, the rock is described by two Young's moduli (E_x and E_y=E_z), two Poisson's ratios (ν_{xy} and ν_{yz}) and a shear modulus (G_{xy}) (Niandou et al. 1997). E_x (Young's modulus in the direction normal to isotropic plane) and E_y (Young's modulus within the isotropic plane) are extracted

from samples cut normal and parallel to bedding, i.e. tested with the maximum principal stress applied perpendicular and parallel to bedding, respectively. ν_{xy} is extracted from samples cut normal to bedding and ν_{yz} from specimens with the bedding orientation parallel to σ_1. G_{xy} indicates the angular deformation in x-y plane and can be extracted from a sample with inclined bedding orientation with respect to σ_1 axis. Niandou et al. (1997) and Valès et al. (2004) extracted the five elastic parameters of Tournemire Shale through standard triaxial tests on core plugs cut normal, parallel and in an angle between 0-90° with respect to bedding.

It should be noted however that the TI symmetry only applies where the stress field is aligned with the symmetry axis in a conventional triaxial test or in a true triaxial rig where value, at $\sigma_2=\sigma_3$. In true triaxial tests where $\sigma_2>\sigma_3$, TI symmetry will be lost and the material becomes orthorhombic. Hence, for simplicity, all the experiments in this study were conducted with σ_1 normal to bedding. Measurement of all the elastic parameters of the shales and their anisotropy was not within the scope of the study. Hence, one Young's modulus and two Poisson's ratios (ν_{12} and ν_{13}) were extracted from the true triaxial test on each sample as for the sandstones in previous chapter. ν_{12} was along the σ_2 axis, and ν_{13} was along the σ_3 direction. It is important to note that these two Poisson's ratios should not be confused with the independent elastic parameters in transversely isotropic materials explained above.

5.2 Carynginia Shale

5.2.1 Sample characterization

The petrological and physical properties of the Carynginia Shale specimens have been obtained from a sequence of plugs within a 5m depth interval extracted from a single core. The mineralogical composition of these shales was determined through X-Ray Diffraction (XRD) analysis and is summarized in Table 5.1. Table 5.2 presents the physical properties of these samples. The bulk density is the mass of the whole sample divided by its bulk volume. The effective dry grain density was calculated without pore fluid while the total dry grain density was calculated without the pore fluid and clay bound fluid. The effective porosity was determined with respect to mobile fluids and the total porosity with respect to both mobile and clay bound fluids.

Table 5.1 Mineralogical composition of the Carynginia Shale (Norwest-Energy 2011).

Mineral	**(%)**	**Mineral**	**(%)**
Total clay	**53-56**	**Total non-clay**	**44-47**
Illite/ Smectite	20-25	Quartz	22-25
Illite + Mica	17-25	K-Feldspar	4-8
Kaolinite	3	Plagioclase	4-6
Chlorite	7	Calcite	4-6
Smectite	1-2	Siderite	1
		Pyrite	4-5
		Barite	0-1
		Magnetite	0-1

Table 5.2 General physical properties of the Carynginia Shale (Norwest-Energy 2011).

Property	**Value**	
Bulk density (ρ_b)	2.618-2.619	g/cc
Total dry grain density (ρ_{grt})	2.727-2.748	g/cc
Effective dry grain density (ρ_{gre})	2.668-2.694	g/cc
Total porosity (ϕ_t)	5.98-6.75	%
Effective porosity (ϕ_e)	2.67-3.80	%
Total Organic Carbon (TOC)	2.69-3.03	wt %

The Carynginia Shale samples were not well-preserved before conducting the mechanical tests, and hence it is expected that they have lost some of their pore fluids. To determine the moisture content of the samples, the suggested method by Head (1980) and ASTM Standard D2216-10 was employed. The mass of the moist specimen (M_w) was first precisely measured. Then it was placed in an oven at 105°C. The sample mass was monitored regularly while in the oven until it became constant. The required time depends on different factors such as type and size of the sample and type of the oven. In these tests, the Carynginia Shale sample was kept in the oven for about three weeks. The sample water content was then calculated as follow (ASTM Standard D2216-10):

$$w = \frac{M_w - M_d}{M_d} \times 100 .$$

In this equation, M_w and M_d are the mass of moist specimen and oven-dried specimen, respectively. The water content of the tested samples in this work determined through this method was 1.9%. Nevertheless, the saturation and porosity

of the specimens could not be measured using the common methods. The original water saturation measured in nearby plugs after retrieval was within the range of 69-81%. However, this may have changed before conducting the mechanical experiments as the samples were not preserved after retrieval.

Some basic mechanical properties of the shale samples were measured through standard triaxial testing. Two cylindrical samples of 38 mm diameter and length/diameter ratio of ~2 were used and the load was applied normal to bedding. The applied confining pressure levels were 5, 10, 20 and 30 MPa for the first test and 3.5, 6.3, 10 and 25 MPa in the second test with zero pore pressure as the rocks were partially saturated. Figure 5.1 presents the Mohr circles obtained in multistage triaxial testing of Carynginia Shale and the fitted Mohr-Coulomb envelope, along with an image of a core sample after the test. The average uniaxial compressive strength (UCS), cohesion and internal friction angle were determined as 34.7 MPa, 7.66 MPa and 42.3 degrees, respectively.

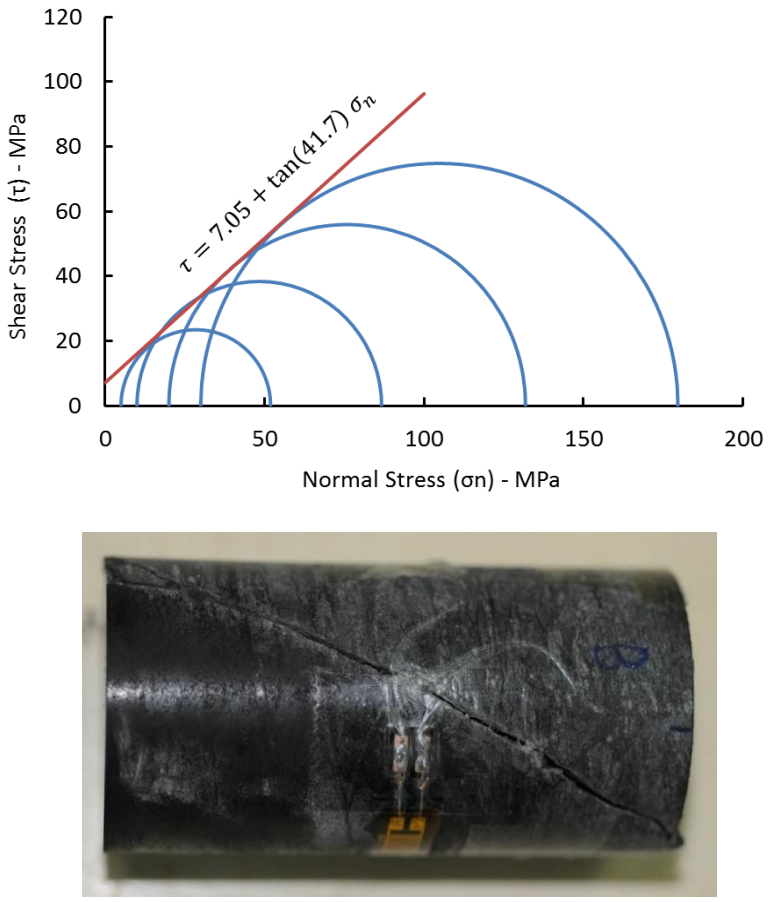

Figure 5.1 Mohr circles obtained for Carynginia Shale via a conventional multistage triaxial test and the image of the post-test core sample. The applied confining pressure levels for this test were 5, 10, 20 and 30 MPa.

5.2.2 True triaxial tests results

The experiments conducted comprise ten tests under two constant levels of minimum principal stress (σ_3=3.4 and 6.2 MPa). For each set, five different levels of intermediate principal stress (σ_2) were examined in a way to impose σ_2/σ_3 stress ratios of 1, 3, 5, 6 and 7. Table 5.3 presents the stress configurations applied to the Carynginia Shale specimens. Loading in the σ_1 direction was done with an average stress rate of 0.6 MPa/min which imposed an average strain rate of ~2.7×10^{-6}/sec.

In Figure 5.2, a typical loading path (stress versus time plot) of the Carynginia Shale specimens during a true triaxial test is shown. Figure 5.3 and Figure 5.4 present principal strain curves (ε_1, ε_2, ε_3) plotted versus maximum differential stress (σ_1-σ_3) obtained for the tested specimens. Volumetric strains (ε_v) are the summation of the strains along the three principal strain directions. All curves show a sudden stress drop at the peak point followed by strain softening (downwards slope of the curve), which indicate that the shale specimens have deformed in the brittle regime under the applied stress conditions.

Table 5.3 Stress conditions during true triaxial testing of the Carynginia Shale samples. σ_1 and (σ_1-σ_3) are the axial and maximum differential stresses at failure, respectively.

Sample ID	σ_2/σ_3	σ_3 (MPa)	σ_2 (MPa)	σ_1 (MPa)	σ_1-σ_3 (MPa)
CS-01	1	3.4	3.4	62	59
CS-02	3		10.3	78	75
CS-03	5		17.2	76	73
CS-04	6		20.7	58	55
CS-05	7		24.1	71	67
CS-06	1	6.2	6.2	80	74
CS-07	3		18.6	70	64
CS-08	5		31	86	80
CS-09	6		37.2	86	80
CS-10	7		43.4	76	70

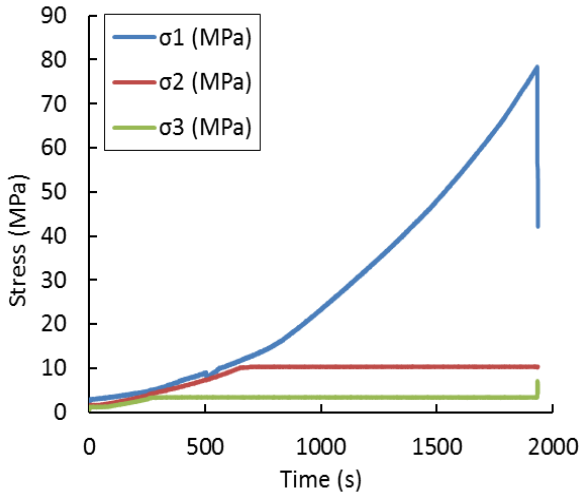

Figure 5.2 Typical loading path during true triaxial testing of the Carynginia Shale samples. The three principal stresses increased isotropically until σ_3 and σ_2 reached the predefined levels; σ_1 was increased monotonically afterwards.

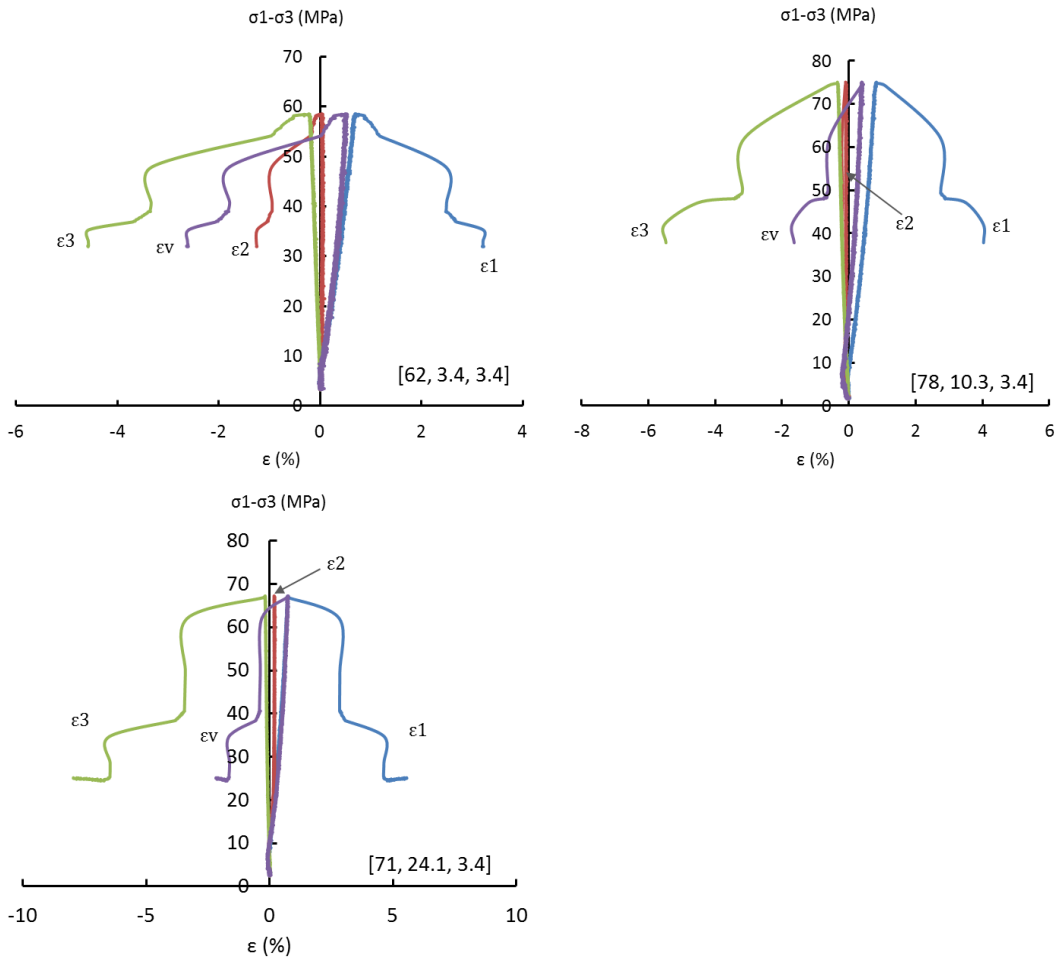

Figure 5.3 Stress-strain curves for true triaxial testing of Carynginia Shale under σ_3=3.4 MPa. Values in brackets are [σ_1, σ_2, σ_3] at failure in MPa.

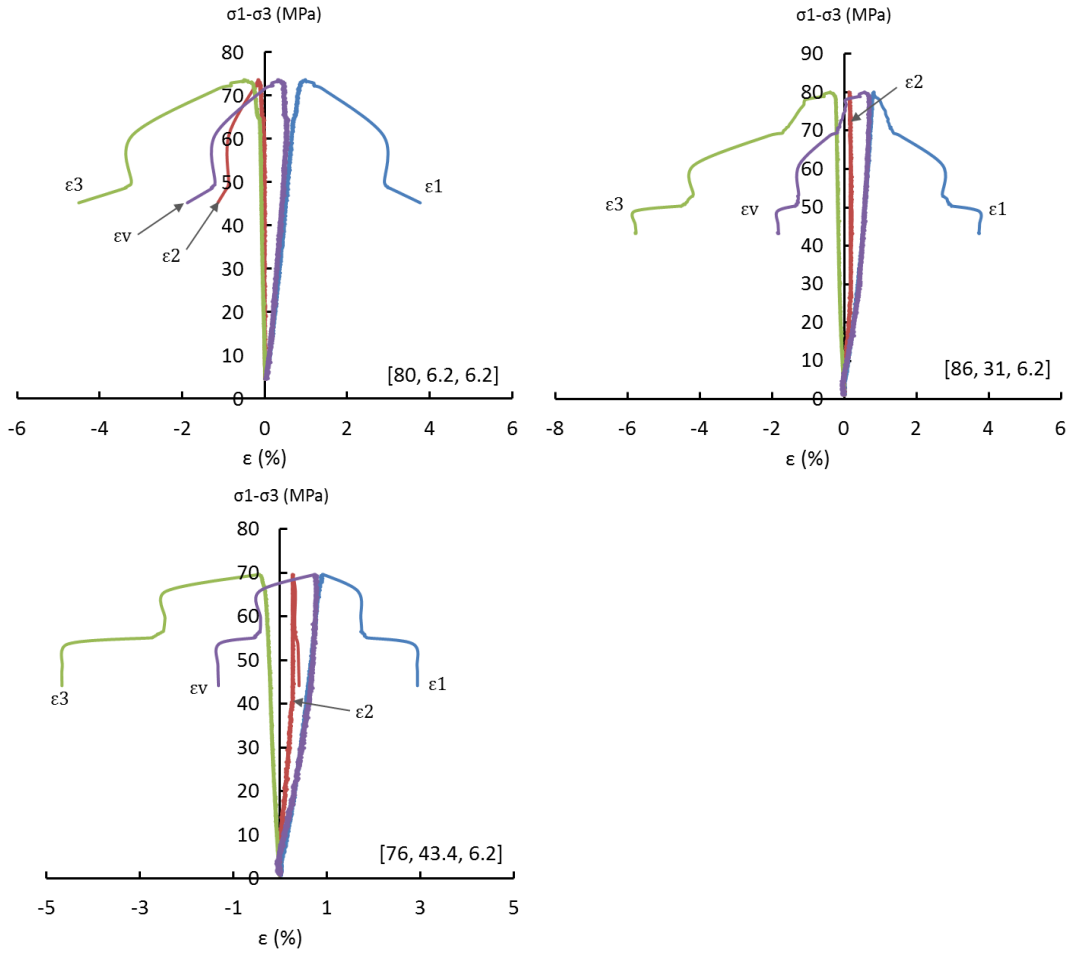

Figure 5.4 Stress-strain curves for true triaxial testing of the Carynginia Shale under σ_3=6.2 MPa. Values in brackets are [σ_1, σ_2, σ_3] at failure in MPa.

Rock strength and mode of failure

Comparing the differential stress versus axial strain curves of all the Carynginia Shale samples (Figure 5.5) indicated that, the shape of the curve is very similar in most cases. Changing σ_2 has not changed the failure mode of the tested specimens under the applied stress range and all samples have failed in the brittle mode. However, varying σ_2 has affected the peak stress level, although not completely systematically.

To determine the influence of varying σ_2 on rock compressive strength, the maximum differential stress at failure for both levels of σ_3 were plotted versus σ_2 in Figure 5.6. Studies of Takahashi and Koide (1989) on Yuubari shale, a brittle shale, showed that at a constant σ_3, increase in the magnitude of the intermediate stress beyond that of the minimum stress initially increased the failure strength until it reached a peak and then further increase in the magnitude of σ_2 slightly decreased the

strength. They also reported that the σ_2 effect on rock strength became more distinct at higher levels of σ_3. Nevertheless, the number of available Carynginia Shale specimens here was not enough to define a general trend on the influence of σ_2 on rock strength in σ_1-σ_2 diagram similar to the results reported in the literature (see Haimson 2006, Colmenares and Zoback 2002). This may also be due to variable sample saturation, which could not be controlled in these tests.

The Carynginia Shale compressive strength measured under triaxial conditions ($\sigma_2=\sigma_3$) has been compared to the highest true triaxial strength ($\sigma_2>\sigma_3$) obtained under the same σ_3 in Table 5.4. Our results indicated up to ~27% increase in strength under σ_3=3.4 MPa, when the intermediate stress increased from $\sigma_2=\sigma_3$=3.4 MPa to $\sigma_2=3\sigma_3$=10.3 MPa. For tests under σ_3=6.2 MPa, the maximum increase observed in compressive strength was ~8% when σ_2 increased from $\sigma_2=\sigma_3$=6.2 MPa to $\sigma_2=6\sigma_3$=37.2 MPa.

In Figure 5.6, the variations of compressive strength in Carynginia Shale specimens are also plotted as a function of lateral stress anisotropy (σ_2/σ_3). This plot shows how increasing the minimum and intermediate stress magnitudes while keeping σ_2/σ_3 constant, affected the shale compressive strength. Increasing both σ_3 and σ_2 magnitudes by a factor of 1.8 at different levels of stress anisotropy ratio induced ~4-45% change in strength where the maximum increase occurred at σ_2/σ_3=6.

Table 5.4 Comparison between the strength obtained in conventional triaxial tests (σ_f^C) and the highest true triaxial strength (σ_f^T) in the Carynginia Shale samples for two levels of applied σ_3. The given σ_2 shows the value of the intermediate stress at which σ_f^T was acquired.

σ_3 (MPa)	σ_f^C (MPa)	σ_f^T (MPa)	σ_2 (MPa)	$(\sigma_f^T - \sigma_f^C)/\sigma_f^C \times 100\%$
3.4	59	75	10.3	27
6.2	74	80	37.2	8

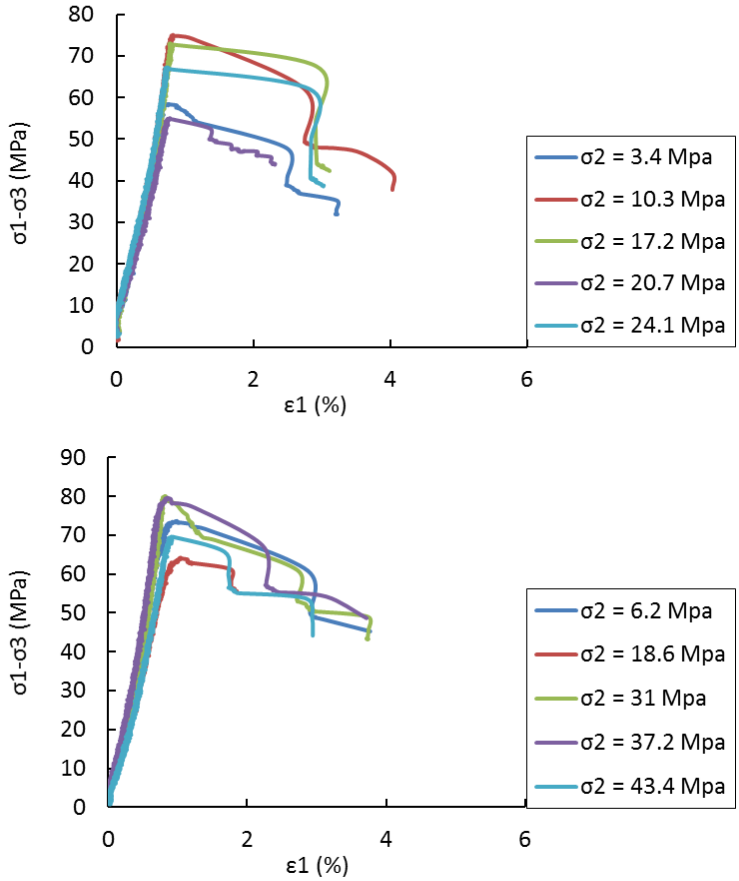

Figure 5.5 The axial strain vs. differential stress curves for all Carynginia Shale samples for tests under σ_3=3.4 MPa (top) and 6.2 MPa (bottom). The plots indicate that changing the intermediate stress has not changed the failure mode under the applied stress range. The peak stress changes but not systematically with changing σ_2.

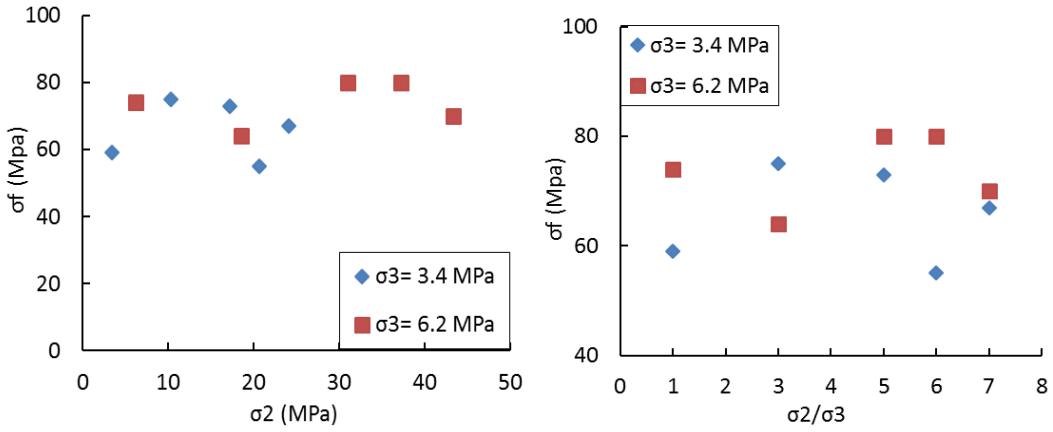

Figure 5.6 Variations of the true triaxial strength (σ_f) of Carynginia Shale samples as a function of σ_2 magnitude (left) and lateral stress anisotropy (σ_2/σ_3 ratio) (right). Increasing σ_2 value at a constant level of σ_3 caused a marginal increase in strength. Raising the σ_3 level also induced a slight increase in rock strength.

True triaxial failure criteria

Figure 5.7 presents the calculated strength curves from using the modified Wiebols and Cook criterion for Carynginia shale at σ_3=3.4 and 6.2 MPa. For calculation of these curves, equations (2.7) to (2.14) were employed. In Figure 5.7, the points represent the data obtained in true triaxial testing of these shales. The data points here show some scatter around the estimated failure curves which could be due to heterogeneity among the tested samples (see Chapter 3, section 3.2.2). Therefore, to examine how completely this criterion fits the true triaxial laboratory data of the Carynginia Shale specimens, more tests under higher levels of minimum stress would be needed.

Figure 5.8 presents the peak stresses obtained for the tested shales in octahedral stress space (τ_{oct}–σ_{oct}) and Mogi's proposed domain (τ_{oct}–$\sigma_{m,2}$). Based on the respective R-squared values of ~0.18 and ~0.75, the data fit is significantly better in the Mogi's proposed domain, which describes τ_{oct} as a function of $\sigma_{m,2}$ in the form of: $\tau_{oct} = 1.3559\,\sigma_{m,2}^{0.8427}$.

Nevertheless, in order to determine a full empirical failure criterion for these shales, further experiments under wider ranges of the minimum and intermediate stress would be required.

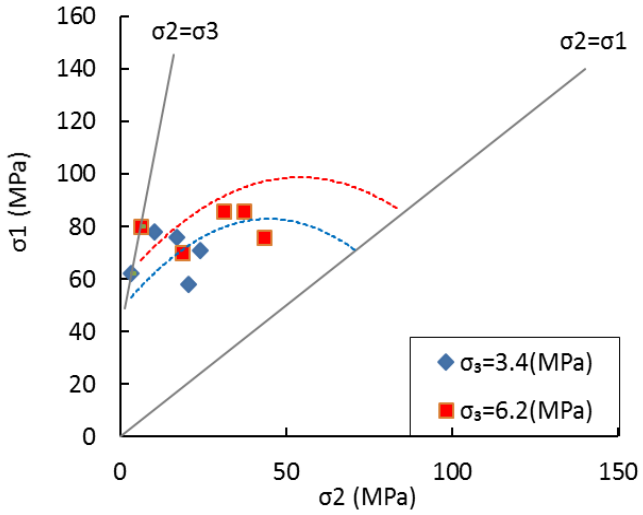

Figure 5.7 The calculated modified Wiebols and Cook failure envelopes along with the Carynginia Shale laboratory data in the σ_1-σ_2 domain. Each colour represents the data points and the related curve, obtained at a specific level of σ_3. The laboratory data show some scatter around the estimated strength curves.

Young's modulus

Variations of Young's modulus versus σ_2 magnitude and σ_2/σ_3 ratio are presented in Figure 5.9. These graphs clearly show that the rock elastic modulus is larger for tests conducted under σ_3=6.2 MPa relative to those done under σ_3=3.4 MPa. Comparing the magnitude of Young's modulus obtained at two different levels of the minimum stress but at the same σ_2/σ_3 ratio indicated a ~4-68% change in elastic modulus with the maximum growth occurring at σ_2/σ_3=6, due to increasing magnitude of σ_3.

Moreover, true triaxial test results revealed that at a specific level of minimum stress, increasing σ_2 induced a general increase in Young's modulus. A maximum rise of ~18% was observed for tests under σ_3=6.2 MPa when σ_2 increased from $\sigma_2=\sigma_3$ to $\sigma_2=6\sigma_3$. The amount of increase in Young's modulus was less pronounced for tests under σ_3=3.4 MPa and showed a maximum growth of ~1.5% when σ_2 increased to five times its initial magnitude.

Plotting variations of the elastic modulus along with the failure stress as a function of σ_2 indicated that Young's modulus response to variations of intermediate stress is very similar to that of rock strength (see Figure 5.10). Oku et al. (2007) also observed similar results in their true triaxial testing of a siltstone. Thus, when σ_2 was raised at a constant level of σ_3, the elastic moduli increased until reaching a peak level, after which the magnitudes declined. This was interpreted as a stiffening effect of the intermediate stress as a result of closing pre-existing microcracks and pores inside the sample.

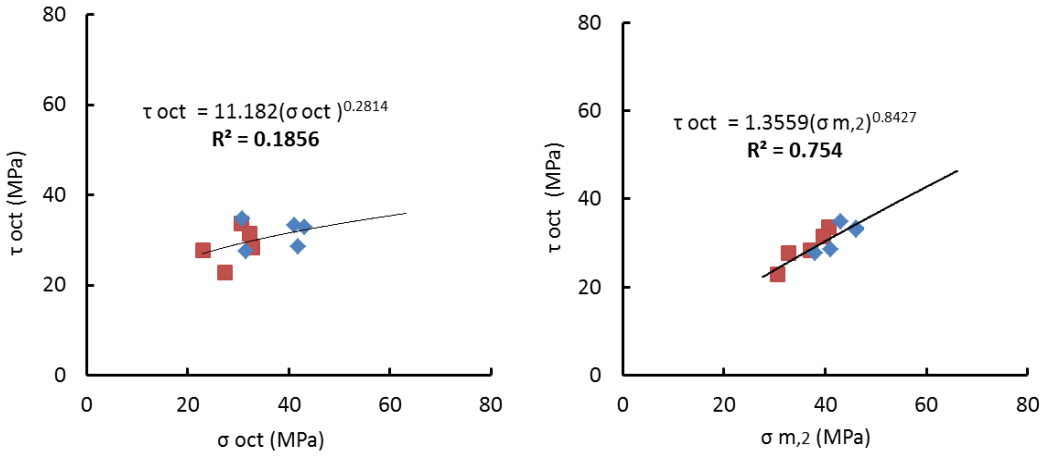

Figure 5.8 True triaxial strength data of the Carynginia Shale in octahedral stress space (left) and Mogi's proposed domain (right). Experimental data show a significantly better fit along a power function in Mogi's proposed space.

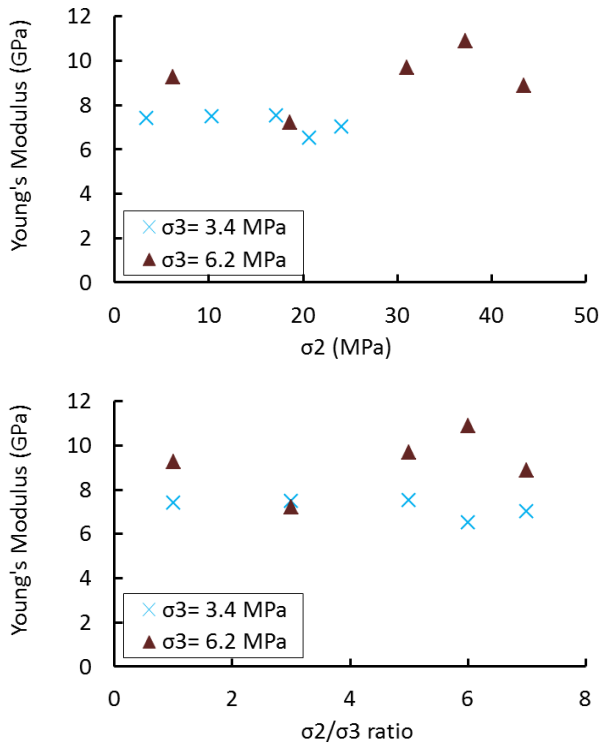

Figure 5.9 Variations of the Young's modulus in Carynginia Shale as a function of σ_2 magnitude and σ_2/σ_3 ratio. Increase in Young's modulus due to increase of σ_2 magnitude was more pronounced at higher level of minimum stress (top). Raising the minimum stress level while keeping σ_2/σ_3 ratio constant, caused 4-68% change in *E* (bottom).

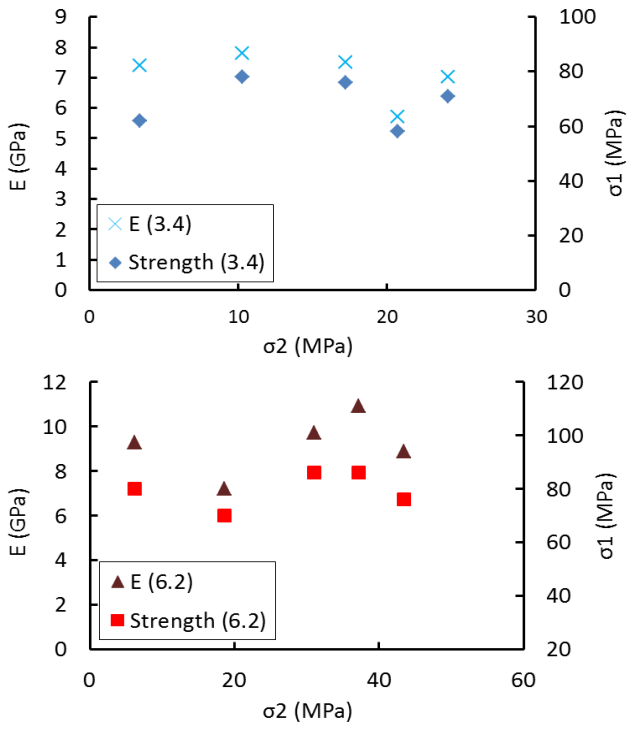

Figure 5.10 Comparison of behaviour of Young's modulus (*E*) and true triaxial strength versus σ_2 in the Carynginia Shale for σ_3=3.4 MPa and σ_3=6.2 MPa. Both rock properties show similar trends of dependency on σ_2.

Poisson's ratio

Figure 5.11 displays the Poisson's ratio along the minimum stress axis (ν_{13}) and the intermediate principal stress axis (ν_{12}) as a function of σ_2 magnitude for two levels of σ_3 (3.4 and 6.2 MPa) in the Carynginia Shale. The results of these diagrams reveal that for both levels of σ_3, ν_{13} is significantly greater than ν_{12}. Similar to the synthetic sandstones, this behaviour could be explained by the supporting effect of intermediate stress on rock. This is also confirmed by visual inspection of the Carynginia Shale samples after failure, as in all cases, fracture planes have opened perpendicular to the minimum stress axis (as will be discussed in a later section).

It is expected from a theoretical point of view that at constant σ_3, as the lateral stress anisotropy increases, the difference between ν_{13} and ν_{12} also should increase. The rationale is that increasing σ_2 magnitude would result in more microcracks aligning parallel to the σ_1-σ_2 plane. Hence, lateral expansion of the rock will reduce along the σ_2 direction but increase along the σ_3 direction. Figure 5.12 displays the Poisson's ratio anisotropy as a function of horizontal stress anisotropy. For the group of samples tested at σ_3=6.2 MPa, ν_{13}-ν_{12} increased with increasing σ_2/σ_3 ratio, as anticipated. However, for the tests under σ_3=3.4 MPa a clear trend could not be established.

Considering Figure 5.11, ν_{13} is slightly increasing with σ_2 magnitude at σ_3=6.2 MPa, but it does not show a clear dependency on σ_2 at σ_3=3.4 MPa. In case of ν_{12}, for both groups of samples, increasing σ_2 magnitude initially decreased ν_{12} and then increased it again to some extent. However, in order to draw a more general conclusion with regards to the impact of σ_2 on Poisson's ratios, more true triaxial tests would be required for these shales.

Figure 5.13 highlights the influence of the minimum stress on Poisson's ratios in true triaxial testing of the Carynginia Shale specimens. In Figure 5.13 Poisson's ratios obtained for both values of minimum stress are plotted versus stress ratio σ_2/σ_3. Raising σ_3 level in the true triaxial tests caused a general decrease in both ν_{12} and ν_{13}.

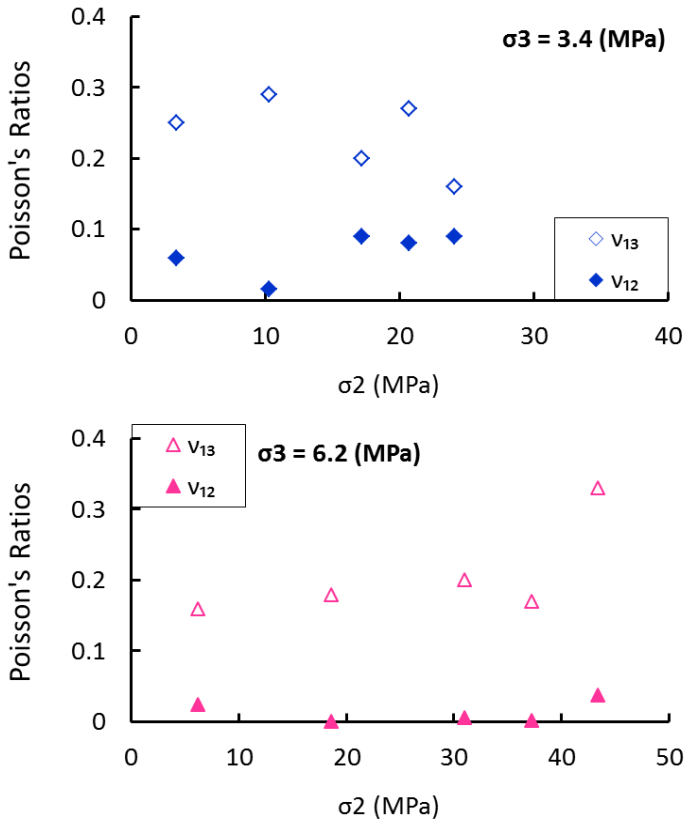

Figure 5.11 Variations of Poisson's ratio along minimum and intermediate principal directions as a function of σ_2 magnitude in the Carynginia Shale tested at σ_3=3.4 MPa and σ_3=6.2 MPa. ν_{13} was significantly greater than ν_{12} in both groups. No clear dependency on σ_2 magnitude could be extracted.

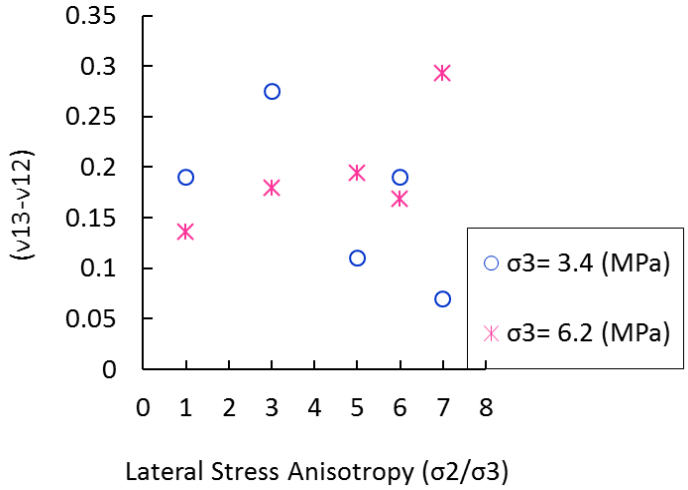

Figure 5.12 Poisson's ratio anisotropy (ν_{13}-ν_{12}) as a function of lateral stress anisotropy in the Carynginia Shale. At σ_3=6.2 MPa, the Poisson's ratio anisotropy has increased due to increasing σ_2 over σ_3, but such dependency is not observed for tests under σ_3=3.4 MPa.

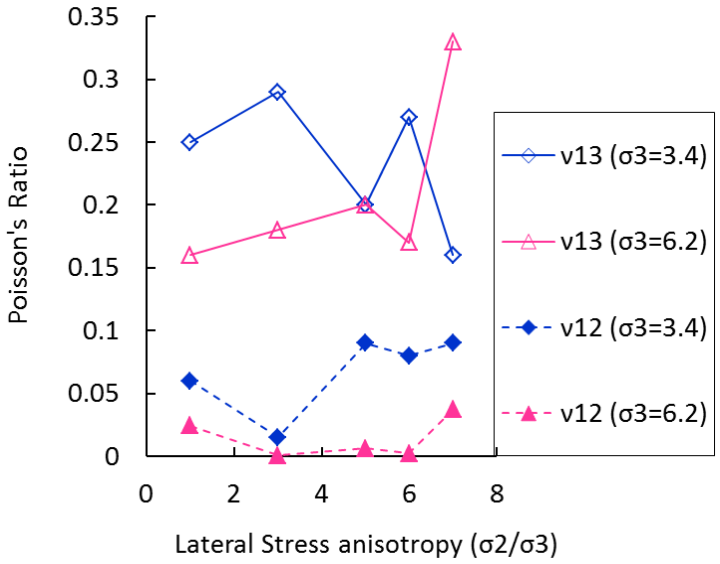

Figure 5.13 Changes in ν_{12} and ν_{13} as a function of σ_2/σ_3 ratio in the Carynginia Shale. Numbers in parentheses show the magnitude of minimum stress. Increasing σ_3 magnitude, resulted in decrease in both ν_{12} and ν_{13}.

Inelastic deformation and dilatancy

Figure 5.14 presents the maximum differential stress (σ_1-σ_3) and lateral principal strains, ε_2 and ε_3, as functions of the axial strain, ε_1, in the Carynginia Shale. In this figure, the minimum principal stress is 3.4 MPa. Where $\sigma_2>\sigma_3$, the failure strength is greater than the case of $\sigma_2=\sigma_3$. Under axisymmetric stress state (Figure 5.14, left plots), ε_3 is larger than ε_2, but both show extensional strains, in particular in the inelastic region. This reveals that under the axisymmetric stress state, after the macroscopic failure, slip along the fault plane was not constrained to be parallel to the dip of the fault, while in the case where $\sigma_2>\sigma_3$, it was significantly more constrained. Where σ_2 was higher than σ_3 (right plots), ε_2 became significantly smaller than ε_3 and does not change with increasing axial strain, which indicates rock expansion was mostly in the minimum principal stress direction.

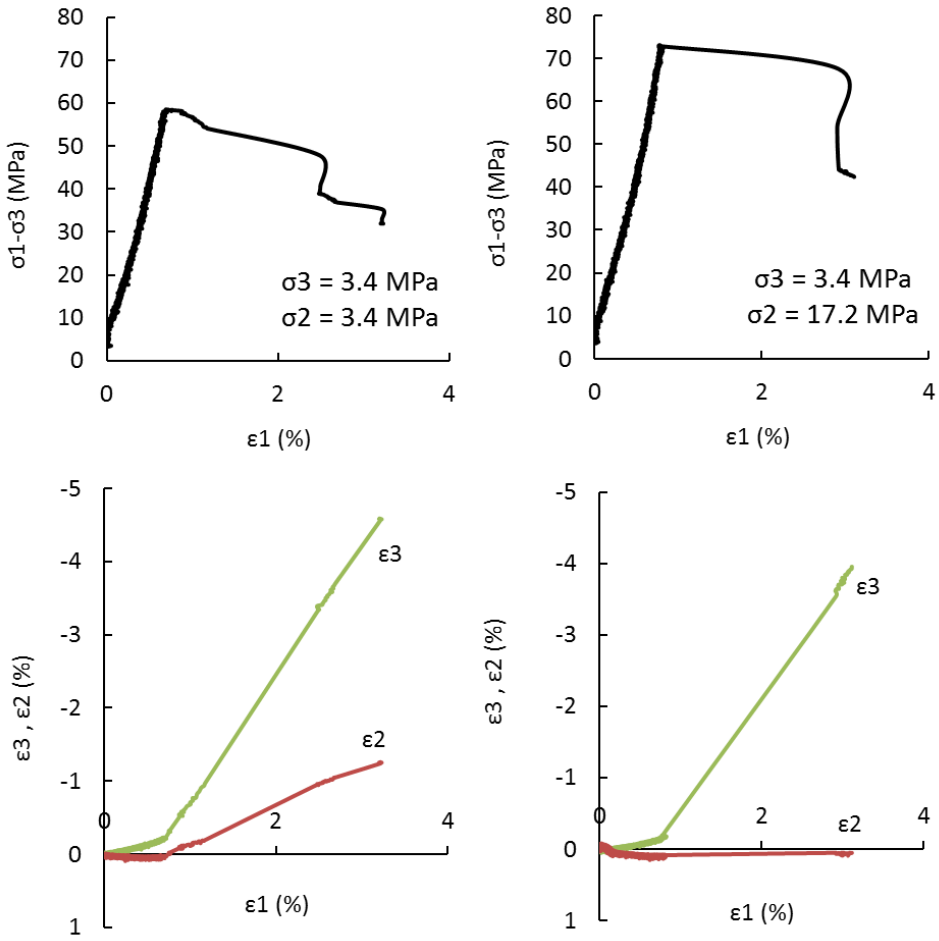

Figure 5.14 The differential stress (top) and lateral strains, ε_2 and ε_3, (bottom) as function of the axial strain, ε_1, in Carynginia Shale. Left: plots for the axisymmetric conditions ($\sigma_2=\sigma_3$); right: plots obtained under true triaxial conditions ($\sigma_2>\sigma_3$). Negative strains here show extension while positive strains show compression. The peak stress is higher for the case of $\sigma_2>\sigma_3$ (top right). In the axisymmetric test, $\varepsilon_3>\varepsilon_2$, but both show extension after failure. For typical case of $\sigma_2>\sigma_3$, ε_2 became significantly smaller than ε_3 and does not change with increasing axial strain.

Figure 5.15 displays variations of ε_2 against ε_1 for both levels of minimum stress in Carynginia Shale samples. For lower levels of the intermediate stress, ε_2 curve dips upwards and for higher levels, it becomes almost linear or dips downwards. Thus, increasing σ_2 magnitude, gradually changed ε_2 from large extensional strains (negative strain) towards considerably smaller compressive displacements (positive values). The typical stress-strain curves of Carynginia Shale presented in Figure 5.3 and Figure 5.4 also demonstrated that under higher magnitudes of σ_2 ($\sigma_2>\sigma_3$), ε_2 is nearly linear and does not change significantly with increasing the differential stress prior to failure and post-failure. Whereas ε_3 increases towards extensional strains (negative values) with the differential stress. This confirms that, under higher magnitudes of σ_2, the rock dilatancy is mainly due to the increase in ε_3 (Mogi 2007).

In the Carynginia Shale samples, the deviation of volumetric strain versus differential stress curve from linear elastic behaviour was taken as the dilatancy onset, as shown by some examples in Figure 5.16. The obtained stress levels are displayed in Table 5.5 as percentage of the axial peak stress (σ_1-peak). It was found that increasing the intermediate stress, raised the stress level at which the dilatancy starts, with respect to the peak axial stress ($\sigma_{1\text{-peak}}$). At σ_3=3.4 MPa, the dilatancy onset was increased from ~73% to ~77% of $\sigma_{1\text{-peak}}$. For the tests under σ_3=6.2 MPa, the effect of σ_2 on the dilatancy was more significant and postponed its onset from ~70% to ~94% of the peak stress level. This is similar to the sandstone behaviour noted in the previous chapter.

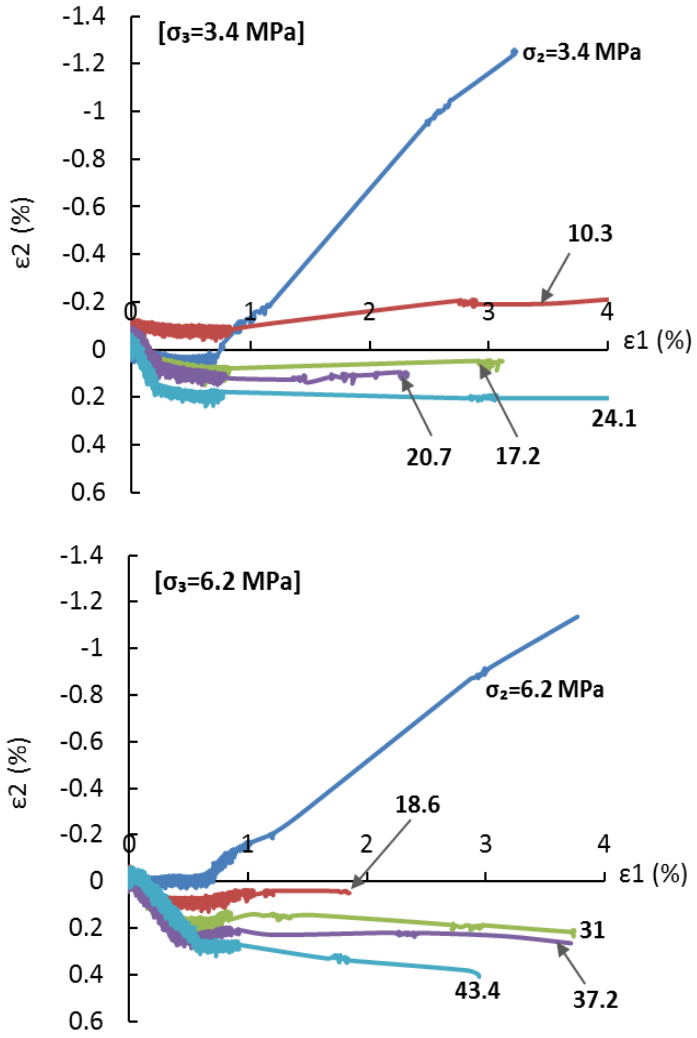

Figure 5.15 Variations of ε_2 versus ε_1, in Carynginia Shale for tests under σ_3=3.4 MPa (top) and 6.2 MPa (bottom). The numerals on the curves show σ_2 levels, in MPa. At low σ_2 levels, ε_2 dips upwards (dilation) but at higher levels of σ_2 it becomes compressive (in the positive side of the axis).

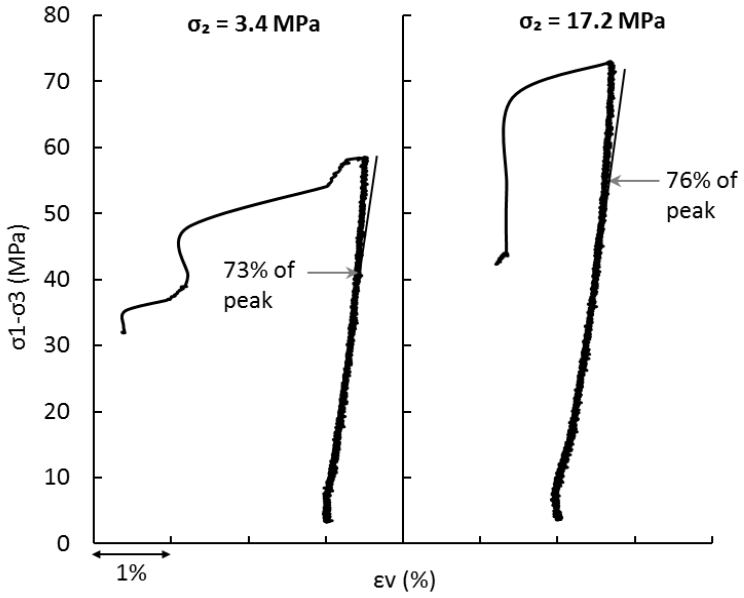

Figure 5.16 Some examples of the differential stress versus volumetric strain curves in the Carynginia Shale samples under σ_3=3.4 MPa and different values of σ_2. The deviation of these curves from linearity defined the onset of dilatancy.

Table 5.5 The changes in dilatancy onset with σ_2 in Carynginia Shale expressed as the σ_1 level at the dilatancy beginning and the dilatancy onset stress level with respect to the peak stress ($\sigma_{1\text{-peak}}$).

σ_3 (MPa)	σ_2 (MPa)	σ_1 at onset of dilatancy (MPa)	Dilatancy level as % of $\sigma_{1\text{-peak}}$
3.4	3.4	45.1	72.7
	10.3	58.3	74.7
	17.2	58.2	76.5
	20.7	44.3	76.4
	24.1	54.3	76.5
6.2	6.2	55.8	69.8
	18.6	55.4	79.1
	31	69	80.2
	37.2	76	88.4
	43.4	71.5	94.1

Macroscopic fractures and cracks patterns

Figure 5.17 displays images of the post-failure Carynginia Shale samples. For each sample, both sides of the rock cube normal to the σ_2 direction are displayed. Through-going shear fractures (faults) are observed in all specimens. The traces of the fractures on opposing faces of the specimens show relatively good symmetry, which indicates that the faults fundamentally strike parallel to σ_2 direction and dip

towards the direction of σ_3. Therefore, as inferred earlier from the principal strain curves, increasing σ_2 above σ_3 caused the rock expansion and dilatancy to occur mainly along the σ_3 direction. The fault traces on both sides of the samples exhibit curved and branched main faults with en-echelon patterns in most cases.

At σ_3=3.4 MPa, failure occurred in the form of dual conjugate clearly-defined slip planes, which are branched in most cases. This is characteristics of failure in the brittle field (Paterson and Wong 2005). At σ_3=6.3 MPa, multiple sub-parallel and/or conjugate main faults developed in the samples, which indicates that the rock entered the transitional brittle-ductile field (Paterson and Wong 2005). Thus it was revealed that increasing the minimum stress magnitude led to an evolution of the failure mode from the brittle field towards a transitional brittle-ductile mode. At each constant σ_3, increasing the σ_2 level seemingly caused formation of some small cracks or increased the number of sub-parallel fracture planes. This behaviour is also an indication of the transitional brittle-ductile region (Paterson and Wong 2005).

The observed changes of fracture patterns in the post-test samples suggests that within the range of applied stresses, the effect of increasing both minimum and intermediate stresses were similar, in that they evolved the failure mode towards the transitional behaviour. Previous true triaxial investigations on porous rocks such as sandstones (e.g. Takahashi and Koide 1989) and more compact rocks such as dolomite and marble (e.g. Mogi 2007) reported change of failure mode towards the brittle field due to increase in σ_2. However, there is a lack of true triaxial investigations in the literature which have studied the failure properties in shales. In the Carynginia Shale, similar to the sandstones tested in this study, σ_2 tends to change the rock failure mode from brittle towards the transitional field (and further into ductile regime for sandstones). In case of the sandstones, this effect was explained through the high initial porosity of the samples which led to a substantial increase in inelastic compaction in the rock. For the Carynginia Shale, however, the initial porosity is substantially lower than that of the sandstones and hence it is less likely that porosity would be responsible for the observed behaviour in Carynginia Shale in the same manner explained for the sandstones. The mechanism responsible for this behaviour in Carynginia Shale is unknown and needs more investigations through conducting more true triaxial experiments and microstructural studies.

In the tested Carynginia Shale samples, the irregular surfaces of fractures did not allow determination of the fracture angle to be taken place. Hence, no clear correlation could be developed between the shear plane angle and the magnitude of applied stresses for these shale specimens.

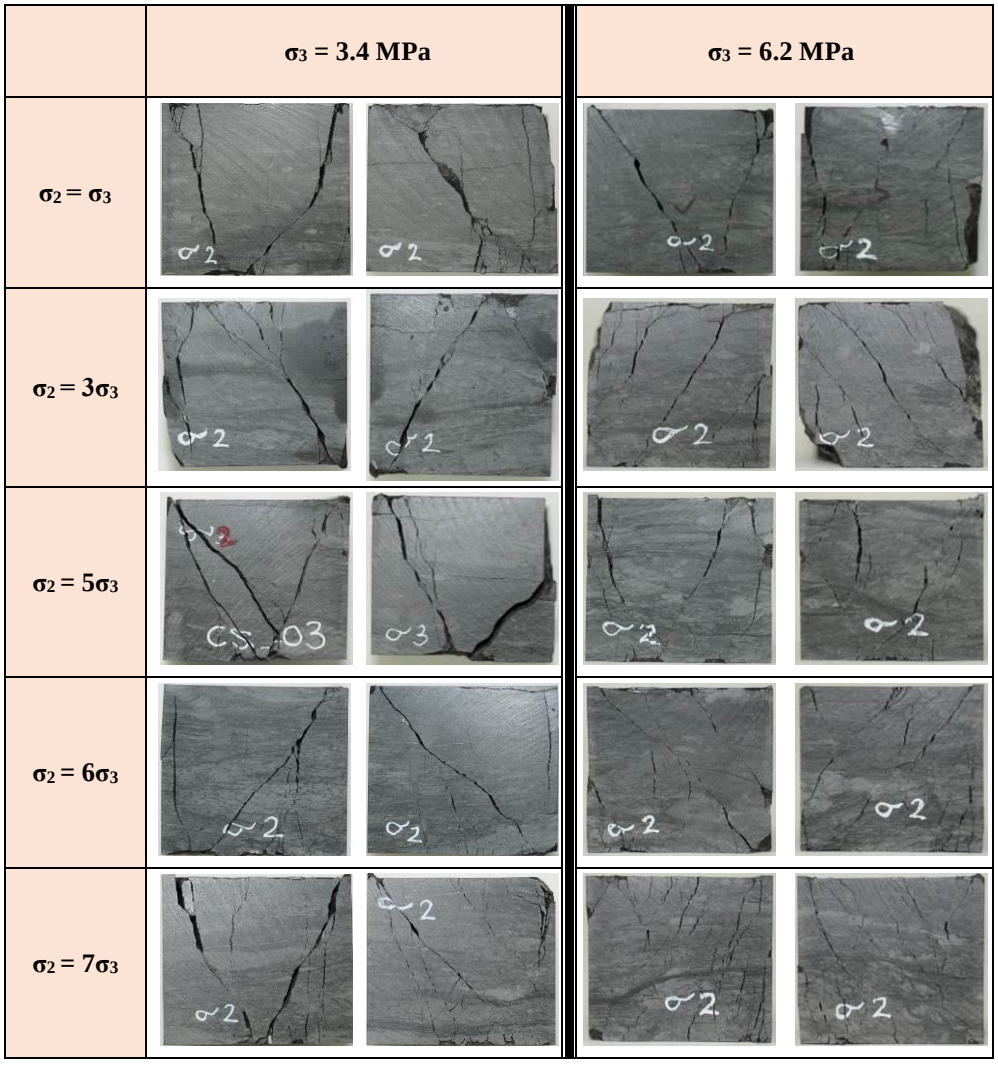

Figure 5.17 Photographs of the Carynginia Shale specimens after true triaxial tests. Here σ_1 is in vertical direction, σ_3 in lateral direction and σ_2 perpendicular to the displayed rock side (i.e. into the page). For each sample, the two opposing sides along the σ_2 axis are displayed.

5.3 Pierre Shale

5.3.1 Sample characterization

The bulk mineral composition of the Pierre Shale, determined through XRD analysis is summarized in Table 5.6. Some physical properties of the Pierre Shale samples are presented in Table 5.7. The basic mechanical parameters of the Pierre Shale specimens were extracted from several cylindrical core plugs in fully-saturated (S_w=100%) and partially-saturated (S_w=59%) conditions through standard triaxial tests. In Table 5.8, the applied effective confining pressure levels and the corresponding obtained values of the peak stress, Young's modulus and Poisson's ratio are presented. Figure 5.18 displays an example of the Mohr circles obtained from this standard triaxial testing of the Pierre Shale and the fitted Mohr-Coulomb envelope as well as a typical image of a core sample after the test. Values for the rock uniaxial compressive strength (UCS), cohesion and internal friction angle were 12.9 MPa, 4.72 MPa and 17.6 degrees in the fully-saturated state, whereas they were estimated to be 37.5 MPa, 12.74 MPa and 21.6 degrees for the partially-saturated state.

5.3.2 True triaxial tests results

A total of 24 preserved Pierre Shale specimens were available for this study, which were divided into four groups with imposed saturation states of 40%, 59%, 70% and 100%. Table 5.9 shows the samples ID numbers and applied stress conditions.

As our apparatus is not equipped with pore-pressure sensors (see section 3.3.4), only two cubes were examined at full-saturation state. The majority of specimens were tested under partial-saturation conditions: 9 samples at S_w=40%, 4 at S_w=59% and 9 at S_w=70%. In these experiments, loading in vertical direction was applied with a nominal rate of 0.6 MPa/min which induced an average strain rate of ~6.79×10^{-6}/sec. Figure 5.19 displays a typical stress-time plot when conducting true triaxial tests on Pierre Shale specimens.

Table 5.6 Bulk mineral composition of the Pierre Shale.

Mineral	**(%)**
Quartz	29
Albite	8.1
Orthoclase	3.7
Calcite	1.5
Pyrite	<1
Dolomite	2.2
Chlorite	1
Illite/ Smectite	25
Illite/ Muscovite	24
Kaolinite	4.6

Table 5.7 General physical properties of the Pierre Shale

Property	**Value**	
Bulk density	2.34-2.39	g/cc
Dry grain density	2.70	g/cc
Effective porosity	20	%
Permeability	10-20	nD
Total Organic Carbon (TOC)	0.5	wt %

Table 5.8 Stress conditions and obtained mechanical properties in conventional triaxial testing of the Pierre Shale. (σ_1-σ_3) is the effective peak differential stress and E and ν are the Young's modulus and the Poisson's ratio.

S_w	σ_3 (MPa)	σ_1-σ_3 (MPa)	E (GPa)	ν
59%	9	47.6	3	0.23
	14	53.5	2.9	0.24
	24	67.5	2.7	0.26
	34	76.2	2.7	0.27
100%	9.1	19.6	1.4	0.44
	14	25.2	1.9	0.36
	24	36.5	2.4	0.43
	34.3	41.1	2.7	0.35

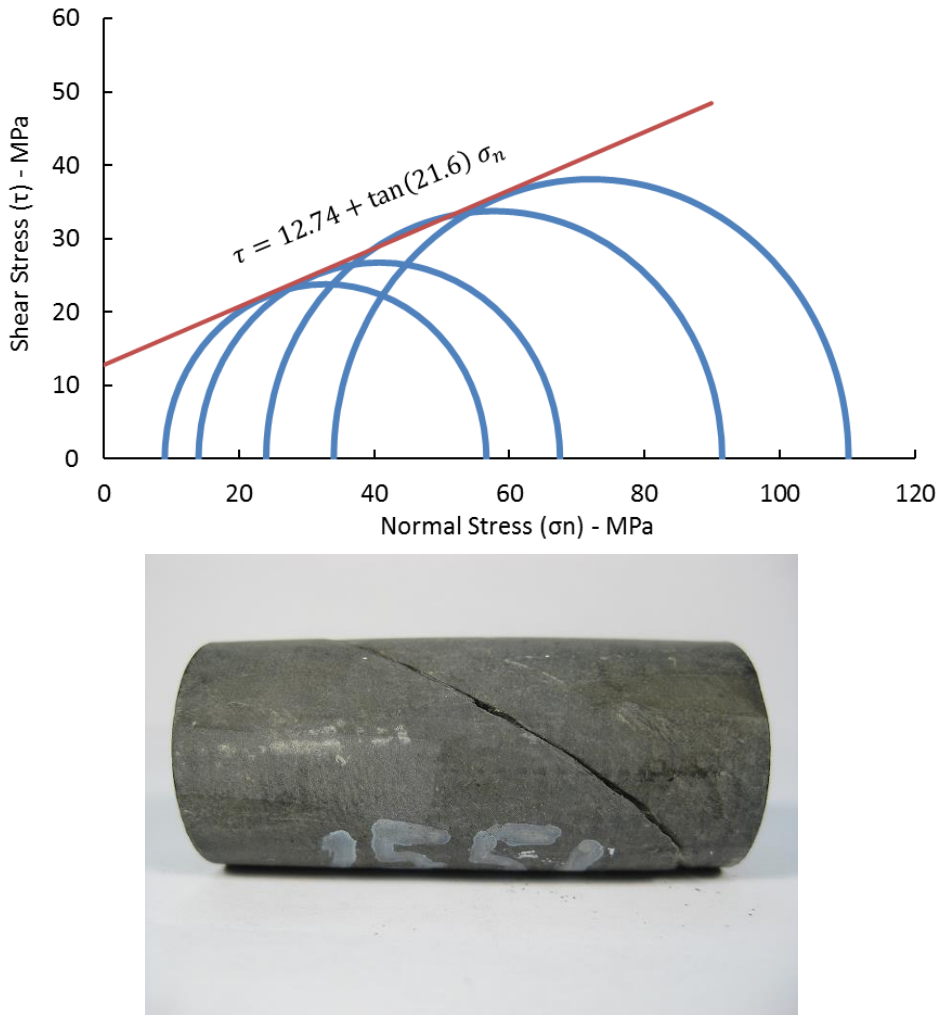

Figure 5.18 An example of the Mohr circles obtained in triaxial testing of the Pierre Shale with S_w=59% and a typical image of a post-failure sample.

The plots depicted in Figure 5.20 illustrate some examples of stress-strain curves obtained for Pierre Shale at four different saturation states. Three strains along principal axes, ε_1, ε_2 and ε_3 were recorded, while the volumetric strain (ε_v) was determined as the summation of these principal strains. In these specimens, a noticeable stress-drop at the peak stress was generally observed, followed by strain-softening. This indicates that this shale behaved mainly in brittle mode under the applied stress range.

The influence of principal stresses magnitudes and anisotropy on shale strength and elastic properties are investigated. This is followed in the next sub-section by investigating the impact of changing water saturation on rock mechanical behaviour.

Table 5.9 Relative humidity (RH), water saturation (S_w) of the Pierre Shale samples and the applied stress conditions in true triaxial experiments.

Sample ID	RH (%)	S_w (%)	σ_2/σ_3	σ_3 (MPa)	σ_2 (MPa)	σ_1 (MPa)	$\sigma_1-\sigma_3$ (MPa)
PC-01	29	40	1	3.4	3.4	37	33
PC-02			3		10.3	59	55
PC-05			5		17.2	45	42
PC-06			6		20.7	45	42
1576	29	40	1	6.2	6.2	55	49
1577			3		18.6	70	64
1578			5		31	76	70
1579			6		37.2	66	61
1580			7		43.4	58	52
PC-03	52	59	1	3.4	3.4	39	36
PC-04			3		10.3	35	32
1568			5		17.2	56	53
1569			7		24.1	57	53
1563	75	70	1	3.4	3.4	35	32
1564			3		10.3	48	44
1565			5		17.2	48	45
1566			6		20.7	39	36
1567			7		24.1	45	41
1570	75	70	1	6.2	6.2	46	40
1571			3		18.6	63	57
1572			5		31	57	51
1573			6		37.2	56	50
PC-08	97	100	1	3.4	3.4	24	20
PC-07			3		10.3	20	17

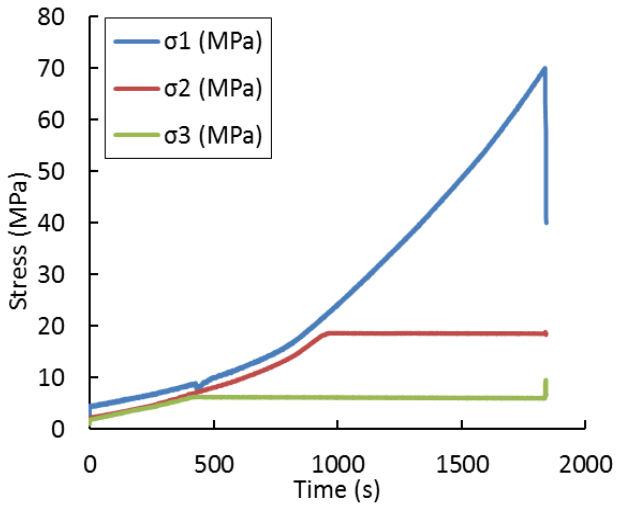

Figure 5.19 Typical loading path in true triaxial testing of the Pierre shale samples.

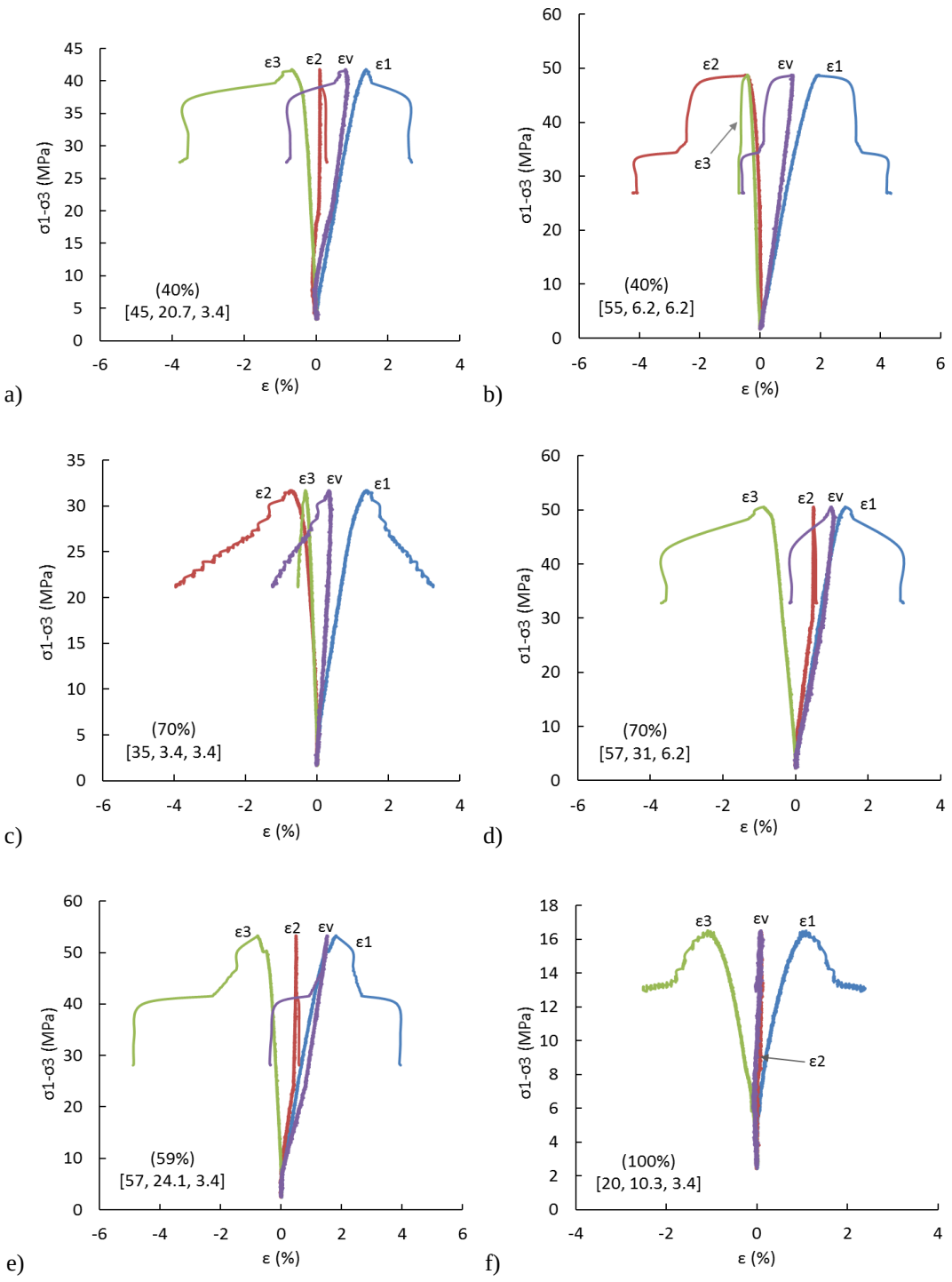

Figure 5.20 Some examples of differential stress versus principal strain curves for the Pierre shale specimens. The number in parenthesis is (S_w%) and numbers in brackets are [σ_1, σ_2, σ_3] in MPa, at failure.

Rock strength and mode of failure

Figure 5.21, Figure 5.22, Figure 5.23 and Figure 5.24 present the maximum differential stress (σ_1-σ_3) versus axial strain (ε_1) curves for all saturation states obtained under σ_3=3.4 and 6.2 MPa and different σ_2 magnitudes. The differential stress-axial strain curves suggest that the Pierre Shale specimens have mainly undergone failure in brittle manner. Although for lower water saturation levels (i.e. 40% and 59%) at low σ_2 values, the curves more indicate a transitional brittle-ductile failure mode (see Figure 5.21 and Figure 5.22). For each saturation state, changing σ_2 magnitude at a constant level of σ_3 significantly changed the fracture strength (peak stress level). Also the slope of the curves has obviously changed with σ_2 in many cases. Such noticeable change of slope was not visible on similar plots of the Carynginia Shale samples (see Figure 5.5).

In Figure 5.25 the peak differential stress at failure (σ_f) for all tests is plotted versus σ_2 magnitude. This plot shows that at a constant level of minimum stress, increasing the intermediate stress above σ_2=σ_3 has initially caused some increase in strength, after which the strength has dropped slightly with further increase of σ_2. Similar behaviour was obtained by Takahashi and Koide (1989) in their studies on Yuubari shale (Colmenares and Zoback 2002).

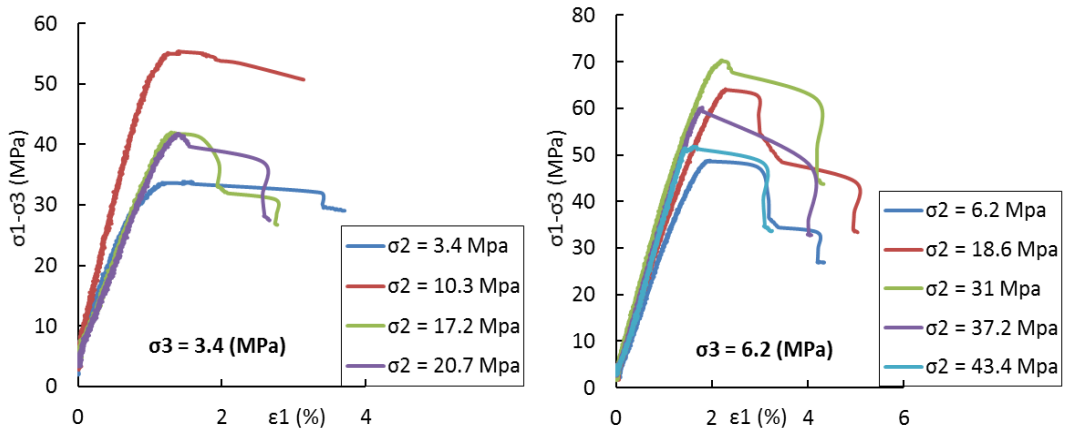

Figure 5.21 The axial strain curves plotted versus maximum differential stress for the Pierre Shale samples with S_w=40%.

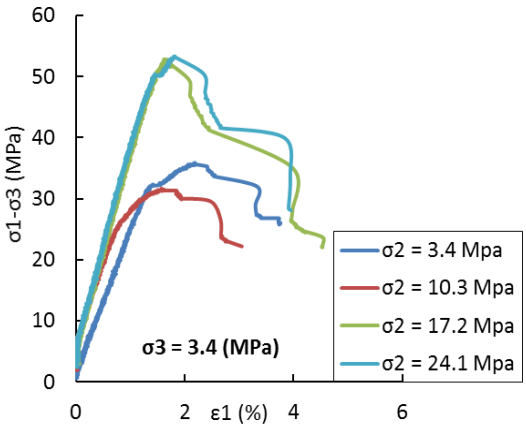

Figure 5.22 The axial strain curves plotted versus maximum differential stress for the Pierre Shale samples with S_w=59%.

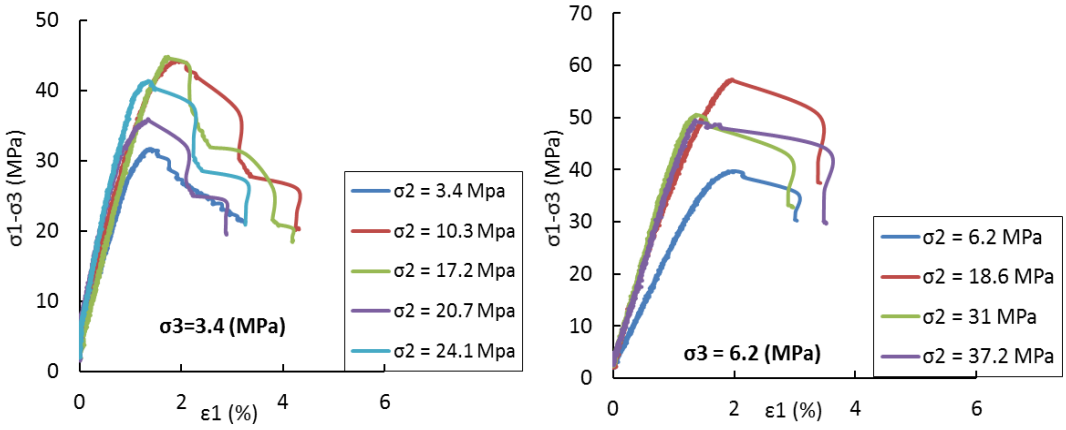

Figure 5.23 The axial strain curves plotted versus maximum differential stress for the Pierre Shale samples with S_w=70%.

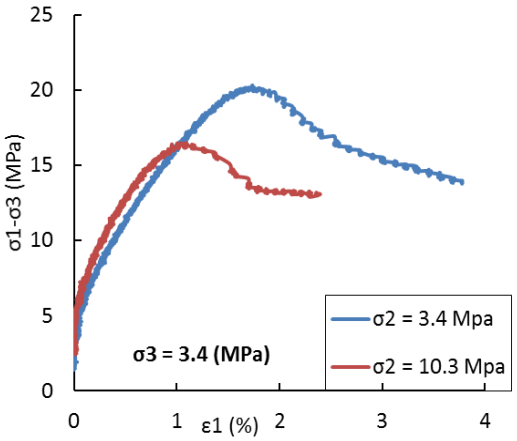

Figure 5.24 The axial strain curves plotted versus maximum differential stress for the Pierre Shale samples with S_w=100%.

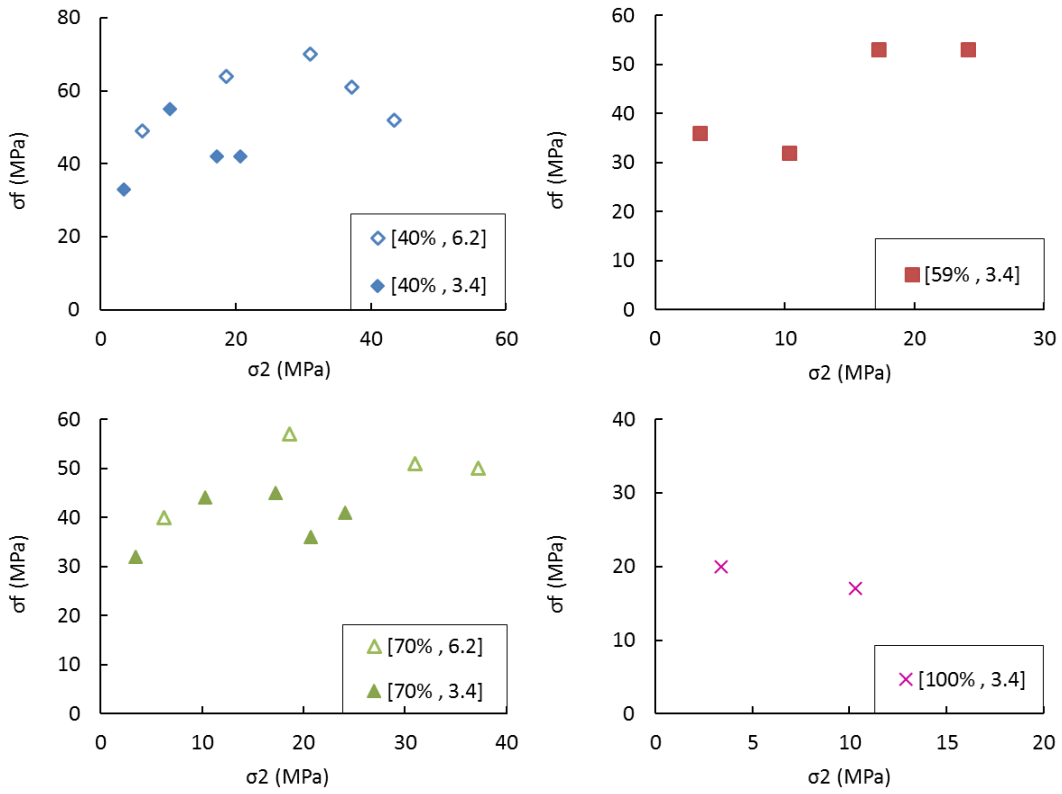

Figure 5.25 The peak differential stress ($\sigma_f=\sigma_1-\sigma_3$) versus intermediate stress (σ_2) in Pierre Shale. Numbers in brackets show [S_w(%) , σ_3(MPa)]. Increasing σ_2 in most group of samples generally increased strength up to a maximum level, and then further increase in σ_2 decreased the compressive strength in these shales.

In Table 5.10 the compressive strength of the Pierre Shale samples obtained at $\sigma_2=\sigma_3$ state has been compared to the highest true triaxial strength ($\sigma_2>\sigma_3$) achieved at the same level of σ_3. Analysis of the obtained data indicated the following results:

- At S_w=40%, increasing σ_2 to three- and five-times larger than the σ_3 level, caused up to 67% and 43% rise in the failure strength over its original value (obtained at $\sigma_2=\sigma_3$), in tests with σ_3=3.4 and 6.2 MPa, respectively.
- Increasing σ_2 from $\sigma_2=\sigma_3$ to $\sigma_2=7\sigma_3$ in tests with S_w=59% caused a maximum increase of 47% in strength.
- The samples with S_w=70% showed a maximum growth of 41% in strength under σ_3=3.4 MPa and 43% under σ_3=6.2 MPa through increasing σ_2 five- and three-folds over the σ_3 level, respectively.
- In fully-saturated conditions (S_w=100%), peak stress dropped by raising σ_2 over σ_3. In other groups of Pierre Shale samples, increasing σ_2 over σ_3 initially increased the

rock strength up to a maximum level and then further increase in magnitude of σ_2 gradually led to a reduced strength. The mechanism responsible for the different behaviour observed in samples with S_w=100% could be due to the potential changes in pore pressure under loading (see section 3.3.4). It is likely that the increase in σ_2 level implied an increase in the pore pressure which consequently reduced the effective minimum stress and hence destabilized the rock sample with respect to failure. However, due to technical limitations, measurements of pore pressure were not feasible in this study and hence the impact of pore pressure in these tests remains unknown. Another possible explanation for the observed behaviour in these samples could be related to the fact that these samples were much weaker than the partially-saturated samples, as it was evident through the measured rock UCS (12.9 MPa) (see section 5.3.1) and the obtained true triaxial peak stresses (see Table 5.9). Therefore, increasing σ_2 increased the distortional strain energy (associated with the octahedral shear stress at peak) enough to reach a critical value required for fracturing of the rock (Mogi 1971). The eventual decline in the strength due to the increase in intermediate stress magnitude in the fully-saturated samples probably happened at lower values of σ_2. However, previous studies (e.g. Mogi 2007, Haimson 2006) on different rock types have shown that rocks are generally stronger under true triaxial conditions ($\sigma_2>\sigma_3$) than under axisymmetric conditions ($\sigma_2=\sigma_3$). Hence, the slight drop observed in strength at $\sigma_2>\sigma_3$ below that at $\sigma_2=\sigma_3$, could be due to the presence of some inhomogeneities in the tested samples. Mogi (2007) also reported that inhomogeneity in a weak sandstone caused some dispersion in the measured strength data in comparison to those measured in more homogeneous rocks such as marble and dolomite. However, since there are only two data points available at this saturation state, no general trend can be established for this group of specimens.

Figure 5.26 presents the rock compressive strength as a function of σ_2/σ_3 ratio for the Pierre Shale specimens, which highlights the impact of raising the σ_3 level in the true triaxial tests. Increasing lateral stress magnitudes while keeping the stress anisotropy constant (σ_2/σ_3=c), has caused considerable growth in rock strength. Raising both σ_2 and σ_3 by a factor of 1.8 induced increase in the range of 16-67% in strength for samples at S_w=40% with the maximum growth observed at σ_2/σ_3=5. For the group with S_w=70% changing horizontal stress magnitudes caused 13-39% rise

with the highest change happening at σ_2/σ_3=6. Hence, generally the effect of raising the minimum stress magnitude has been more pronounced for samples with lower saturation.

Table 5.10 Comparison between the strength obtained in conventional triaxial tests (σ_f^C) and the highest true triaxial strength (σ_f^T) in Carynginia Shale samples for two levels of the applied σ_3. The given σ_2 shows the value of the intermediate stress at which the highest true triaxial strength was acquired.

Sw (%)	σ_3 (MPa)	σ_f^C (MPa)	σ_f^T (MPa)	σ_2 (MPa)	$(\sigma_f^T - \sigma_f^C)/\sigma_f^C \times 100\%$
40	3.4	33	55	10.3	67
	6.2	49	70	31	43
59	3.4	36	53	24.1	47
70	3.4	32	45	17.2	41
	6.2	40	57	18.6	43

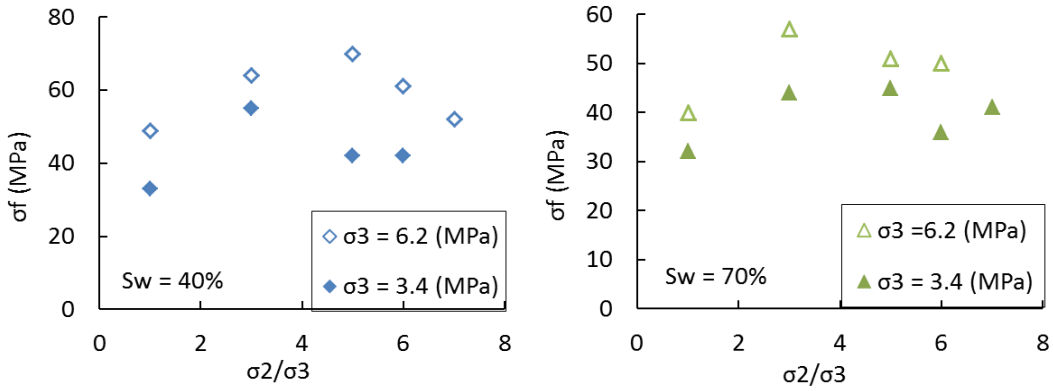

Figure 5.26 Pierre Shale peak stress ($\sigma_f = \sigma_1 - \sigma_3$) as a function of lateral stress anisotropy (σ_2/σ_3 ratio) for water saturation degrees of 40 and 70%. Increasing magnitude of both lateral stresses induced up to 67% and 39% change in rock strength for groups with S_w=40% and 70%, respectively.

True triaxial failure criterion

The calculated strength curves using the modified Wiebols and Cook criterion, equations (2.7) to (2.14), for Pierre Shale are compared to the laboratory results in σ_1-σ_2 space in Figure 5.27. This criterion fits the experimental data relatively well in this diagram for all saturation states. In comparison to the synthetic sandstones and the Carynginia Shale samples the predictive ability of the modified Wiebols and Cook criterion in modelling the true triaxial failure trends in Pierre Shale appears to

be noticeably better. The rationale could be that under similar stress states these shales had generally a lower range of peak stresses than the sandstones and Carynginia Shale (see Table 4.2, Table 5.3 and Table 5.9). Thus, over the same range of applied σ_3, similar amount of increase in the stress anisotropy ratio (σ_2/σ_3) pushed σ_2 in Pierre Shale closer to the upper limit of the typical σ_1-σ_2 diagram, which is the axisymmetric extension state ($\sigma_2=\sigma_1$). Therefore, although similar σ_2 levels were applied on the three rock groups, in Pierre Shale the obtained strength data points covered a wider range between the lower limit ($\sigma_2=\sigma_3$) and upper limit ($\sigma_2=\sigma_1$) in the σ_1-σ_2 diagram. In addition, it is possible that the controlled saturation and natural cementation also reduced scatter in results. Hence, a trend of the σ_2-impact on rock strength could be more clearly established for Pierre Shale.

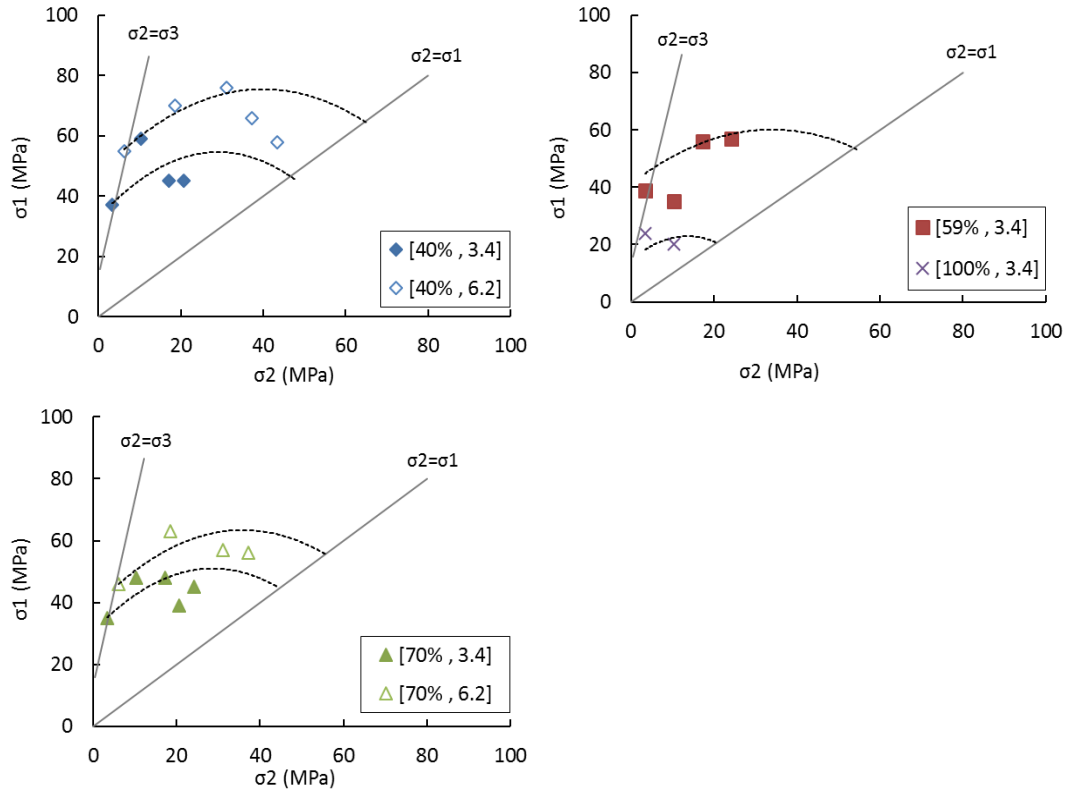

Figure 5.27 The estimated curves by the modified Wiebols & Cook criterion displayed along with the laboratory data of Pierre Shale in σ_1-σ_2 space. For the laboratory data, the saturation degree and the applied σ_3 value are identified as [S_w(%) , σ_3(MPa)]. The curves model the experimental data trends relatively well.

In Figure 5.28 the strength data have been plotted in octahedral stress space (τ_{oct}_σ_{oct}) and Mogi's proposed domain (τ_{oct}_$\sigma_{m,2}$). In both domains, the results

correlate well with power law functions but with different correlation coefficients. The respective R-squared values obtained were ~0.73 and ~0.96, which indicates that the Pierre Shale results have a considerably better fit in Mogi's proposed domain. Experimental studies of Mogi (1971) on various rock types, Haimson and Chang (2000) on granite and Oku et al. (2007) on siltstone are some examples of true triaxial laboratory results which indicated similar good fits in $\tau_{oct}\_\sigma_{m,2}$ domain. Based on the plotted data, the octahedral shear stress at failure in Pierre Shale can be expressed as a function of $\sigma_{m,2}$ in the form of:

$$\tau_{oct} = 0.629\ \sigma_{m,2}^{1.0394}.$$

It is advisable to perform more tests under larger magnitudes of σ_2 and σ_3 in the future in order to define a more general Mogi-type failure criterion for the Pierre Shale.

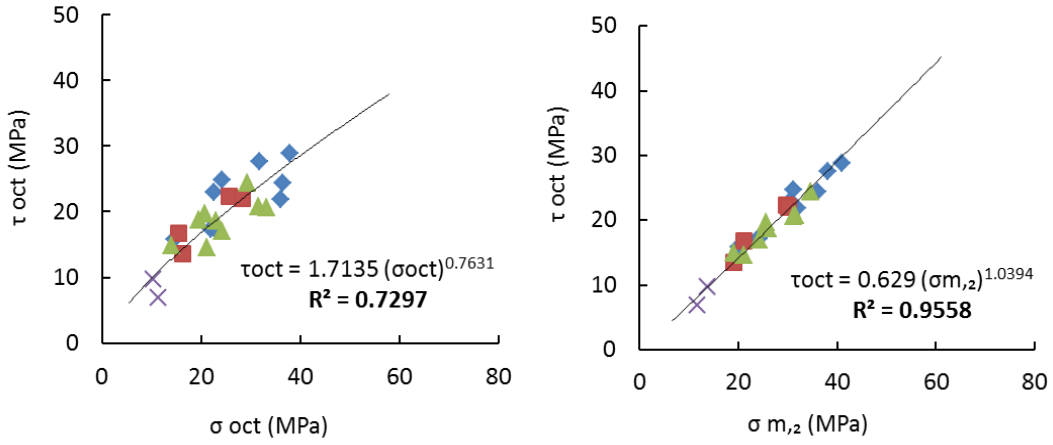

Figure 5.28 The strength data obtained for Pierre shale samples in octahedral space (left) and Mogi's proposed domain (right). The power functions fitted on the data and corresponding coefficient of determination (R^2) are displayed. The data fit in Mogi's proposed domain is significantly better.

Young's modulus

Plotting the Young's modulus (E) versus σ_2 magnitude in Figure 5.29 revealed an overall increase for all groups of samples. For samples with S_w=40%, a maximum of 48% and 24% rise was observed in stiffness as a result of increasing σ_2 to 3- and 5-times its initial level (σ_2=σ_3), at σ_3=3.4 MPa and σ_3=6.2 MPa, respectively. At S_w=59%, the maximum increase in E of 34% was obtained by changing stress state from σ_2=σ_3=3.4 MPa to σ_2=5σ_3=17.2 MPa. In specimens with S_w=70%, at both

levels of σ_3 (3.4 and 6.2 MPa) when σ_2 was increased by a factor of 5, the maximum rises in stiffness that occurred were 21% and 53%, respectively. Under fully-saturated conditions, increasing intermediate stress from $\sigma_2=\sigma_3$ to $\sigma_2=3\sigma_3$, resulted in a 22% rise in Young's modulus.

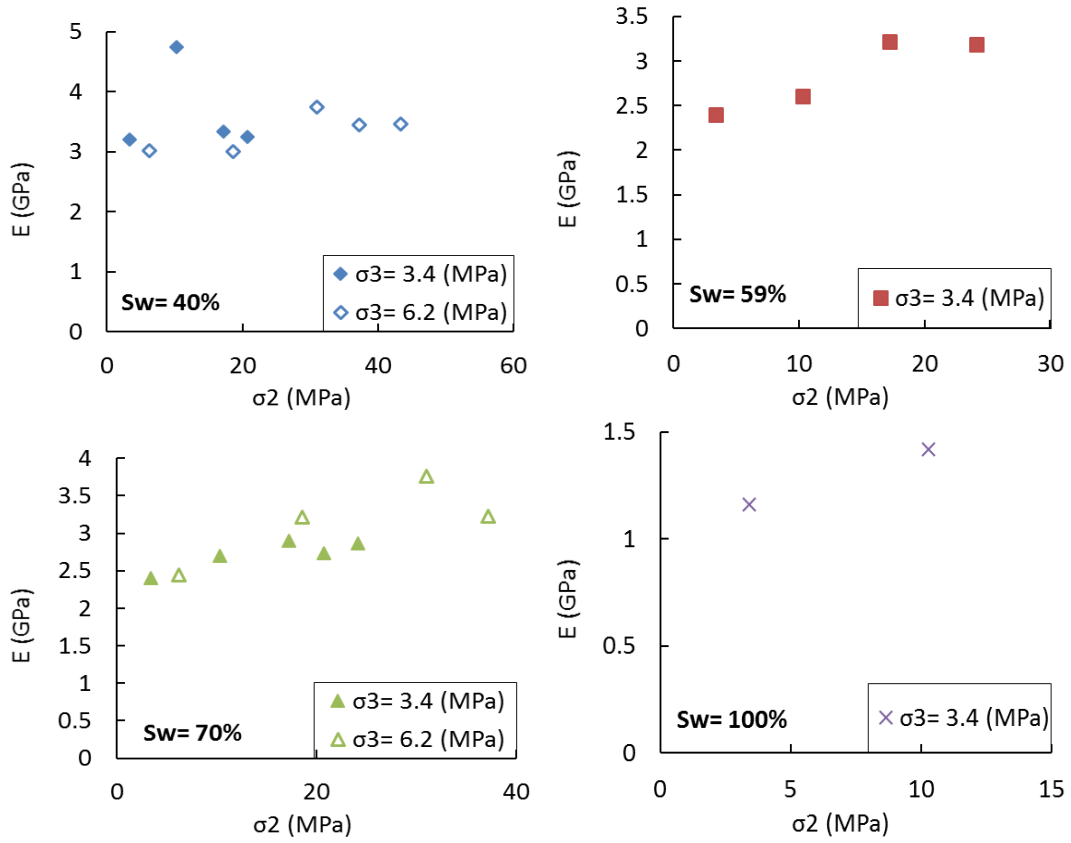

Figure 5.29 Variations of Young's modulus (E) with the intermediate stress for all saturation levels under the applied minimum stress of 3.4 MPa and 6.2 MPa.

In Figure 5.30, variations of E against σ_2 are compared to variations of peak stress versus σ_2, which reveals very similar trends. The same behaviour was observed in the Carynginia Shale samples (Figure 5.10). Hence, increasing the intermediate stress at a constant level of minimum stress in the Pierre Shale, increased the stiffness up to a peak point, after which further increase in σ_2 gradually decreased the stiffness.

In Figure 5.31 the Young's modulus obtained for samples with S_w= 40% and 70% has been plotted as a function of lateral stress anisotropy (σ_2/σ_3 ratio). For the group with S_w=70%, increasing the σ_3 level has induced a 2-30% rise in stiffness with the highest change at σ_2/σ_3=5. However, for the specimens with S_w= 40%, raising the minimum stress level caused 6% and 37% decrease at σ_2/σ_3=1 and 3, and 12% and

6% increase for the case of σ_2/σ_3=5 and 6, respectively. The large decrease of ~37% in stiffness while increasing the minimum stress level is unexpected, which could be due to the heterogeneity between different specimens especially in case of sample PC-02 (related to data point at σ_3=3.4 and σ_2/σ_3=3). The Young's modulus and strength obtained for this sample (PC-02) are considerably higher than other samples in this group, while its Poisson's ratio is much lower (see Figure 5.32). Generally Figure 5.29, Figure 5.30 and Figure 5.31 suggest that the impact of σ_2 on shale stiffness could be as significant as that of the least principal stress, a result that is overlooked in conventional triaxial tests.

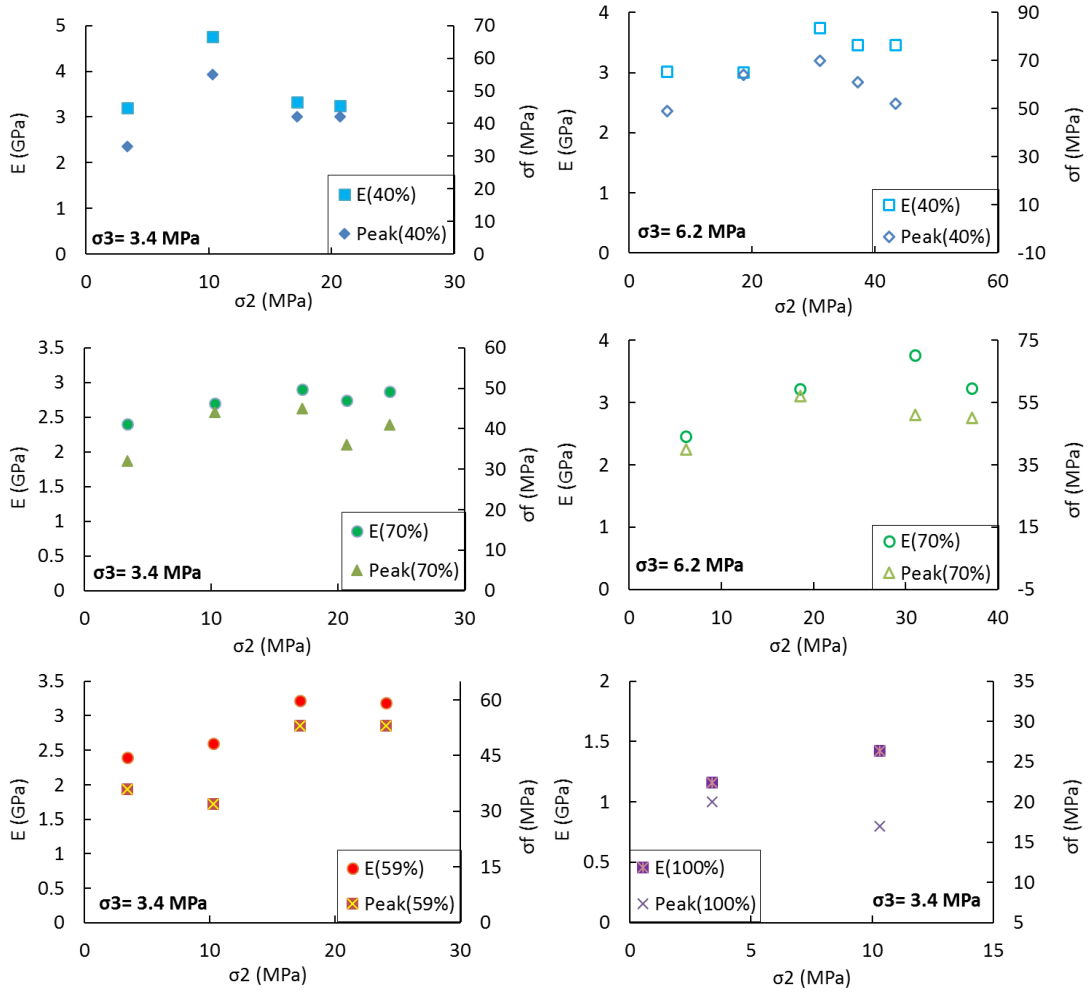

Figure 5.30 Comparing the variation of Young's modulus (E) and peak stress (σ_f) versus σ_2 in the Pierre-shale samples. The numbers in parentheses show the saturation degree for each plot.

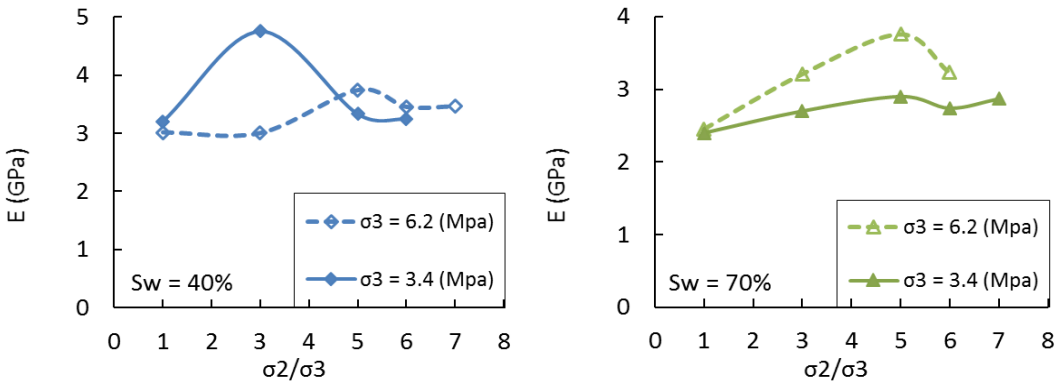

Figure 5.31 Young's modulus (E) as a function of σ_2/σ_3 ratio for the Pierre Shale samples with saturation of 40% and 70%. Increasing σ_3 level enhanced the stiffness at S_w=70%. At S_w=40% some unexpected decrease in E occurred at σ_2/σ_3=1 and 3, while raising both lateral stresses magnitudes.

Poisson's ratio

In Figure 5.32 and Figure 5.33 both Poisson's ratios in Pierre Shale, ν_{12} and ν_{13}, were plotted against the intermediate stress for tests with σ_3=3.4 and 6.2 MPa, respectively. The magnitudes of Poisson's ratios displayed in these figures are in some cases larger than 0.5. It should be noted that due to thermodynamic constraints which require the strain energy of an elastic material to be always positive, the value of Poisson's ratio in isotropic rocks cannot be larger than 0.5. However, in anisotropic and transversely isotropic rocks, the thermodynamic constraints are less restrictive, which broadens the domain of possible variations of Poisson's ratio in such materials (Amadei et al. 1987, Amadei 1996). For transversely isotropic rocks such as shales, Poisson's ratios larger than 0.5 have been reported in the past (see Amadei et al. 1987).

In Figure 5.32 and Figure 5.33 it is noted that similar to Carynginia Shale and the synthetic sandstones at almost all tests ν_{12} is substantially smaller than ν_{13}. This is explained by the constraining effect of σ_2 on the rock which restrains rock deformation (elastic and inelastic) in this direction and consequently imposes more displacement along σ_3 direction.

Generally when increasing the intermediate stress some decrease in ν_{12} and increase in ν_{13} might be expected which is once more justified by the restraining impact of σ_2. However, such behaviour is not confirmed for all samples in Figure 5.32 and Figure 5.33. For ν_{13} in most cases a noticeable increase is detected by raising σ_2; except for the samples in the group S_w=40% and 59% tested under σ_3=3.4

MPa. In case of ν_{12}, it seems that increasing σ_2 magnitude initially decreased ν_{12} value and then increased it again to some extent for almost all group of samples. A similar trend was observed in Carynginia Shale. However, due to the insufficient experimental data points for the tested rocks and lack of relevant evidence in the literature, no general conclusions can be drawn here with respect to the impact of σ_2 on changing the magnitude of Poisson's ratio.

To showcase the difference between Poisson's ratios in two perpendicular directions, the value of (ν_{13}-ν_{12}) for each test has been plotted in Figure 5.34 against different σ_2/σ_3 ratios. Generally it is anticipated that as the lateral stress anisotropy increases, the difference between ν_{12} and ν_{13} rises, as the restraining effect of σ_2 would become more pronounced. Figure 5.34 shows that the Poisson's ratio anisotropy (ν_{13}-ν_{12}) increases with lateral stress anisotropy for all groups of samples except for the ones with S_w=59% and S_w=40% tested at σ_3=3.4 MPa.

The influence of increasing σ_3 level on Poisson's ratio could be only investigated for samples with partial saturation degrees of 40% and 70%, which have been tested under two levels of σ_3 (3.4 and 6.2 MPa). Figure 5.35 displays ν_{12} and ν_{13} versus σ_2/σ_3 ratio for samples with S_w=40% and Figure 5.36 presents those plots for samples with S_w=70%. Despite the Carynginia Shale samples that indicated overall decrease in ν_{12} and ν_{13} with increasing σ_3 value, these shales do not show a clear dependency of Poisson's ratios on the minimum stress level in the true triaxial tests. Therefore, generally no common trend of dependency of Poisson's ratios on true triaxial stress states could be established for these samples.

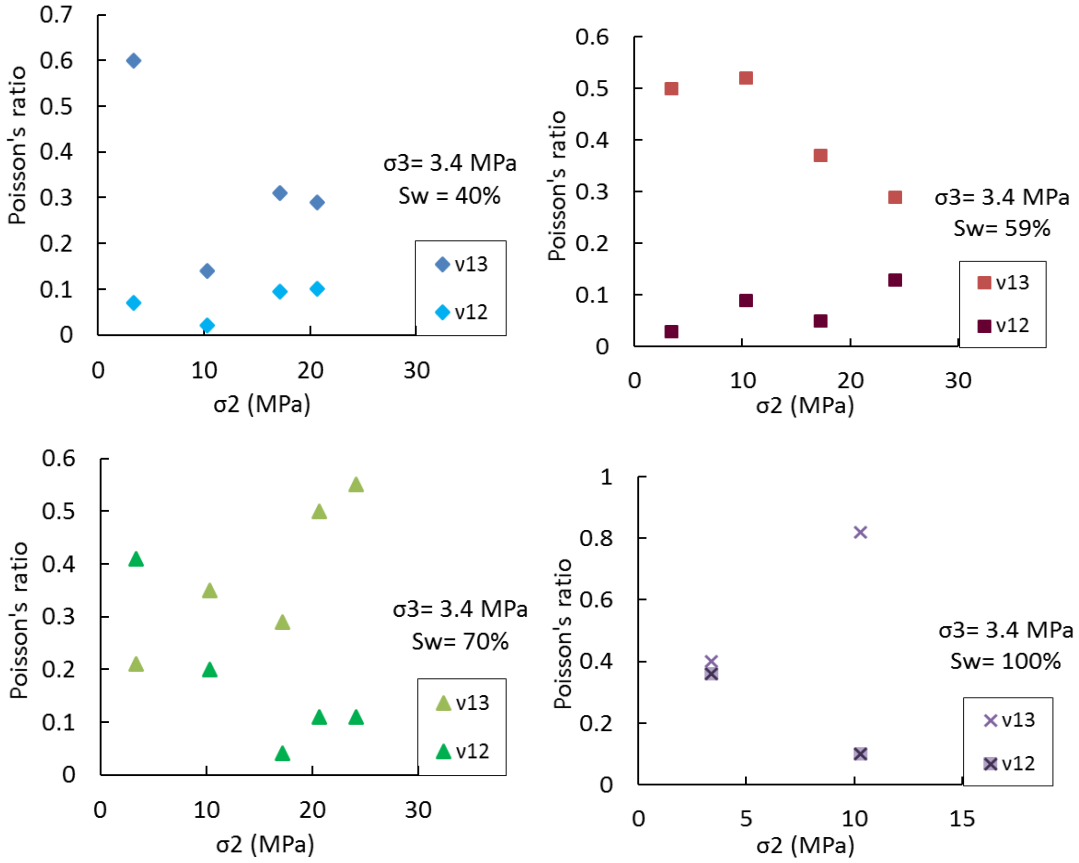

Figure 5.32 Variations of ν_{12} and ν_{13} versus the intermediate stress for all saturation levels at σ_3= 3.4 MPa in Pierre Shale. ν_{13} is substantially greater than ν_{12}, however no simple common dependency of Poisson's ratios on σ_2 could be extracted.

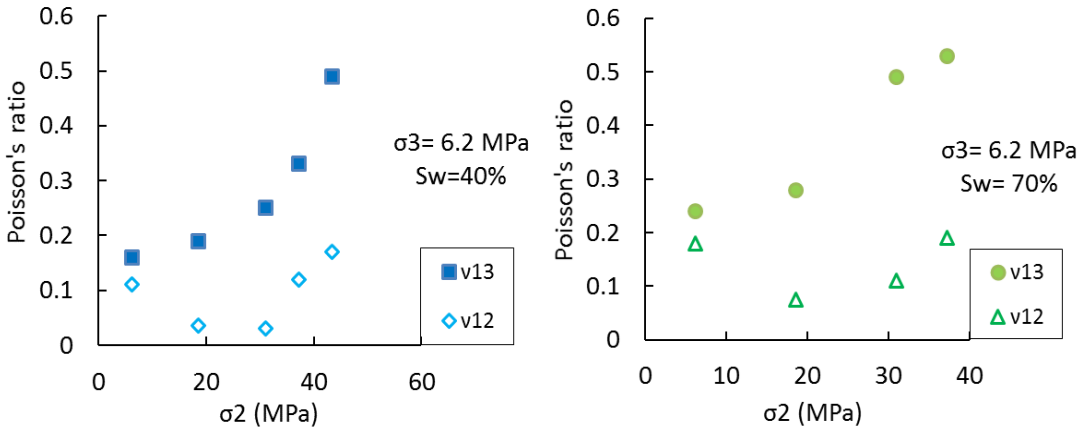

Figure 5.33 Variations of ν_{12} and ν_{13} versus intermediate stress for partial saturation levels of 40% and 70% at σ_3= 6.2 MPa in Pierre Shale. ν_{13} is significantly greater than ν_{12} in all samples. Increasing σ_2 induced an overall increase in ν_{13}, however no clear dependency of ν_{12} on σ_2 could be extracted.

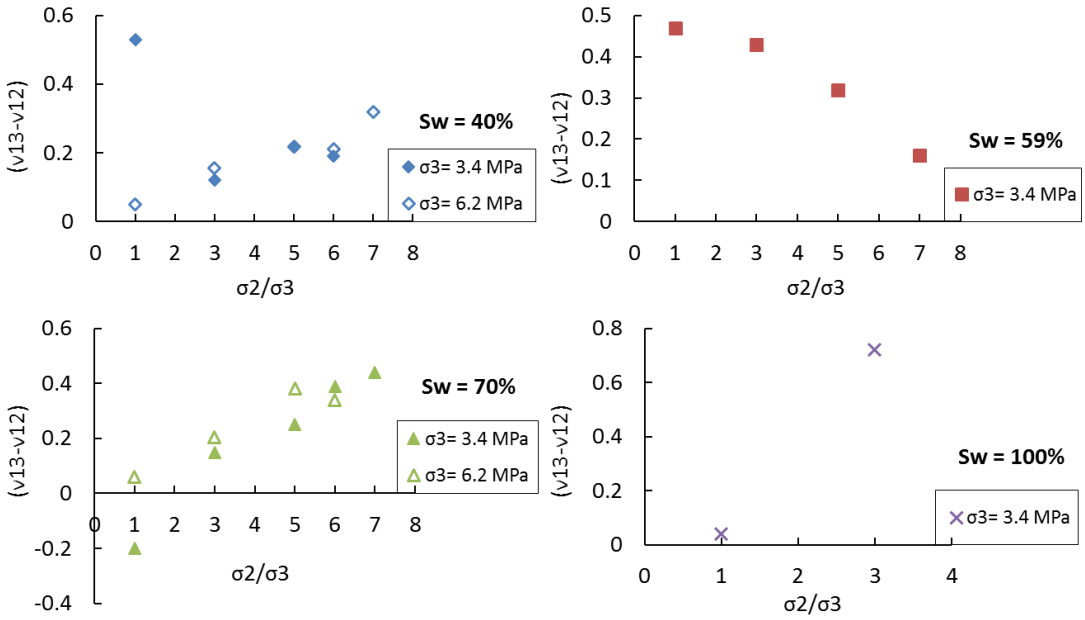

Figure 5.34 The Poisson's ratio anisotropy (ν_{12}-ν_{13}) as a function of σ_2/σ_3 ratio in the Pierre shale samples.

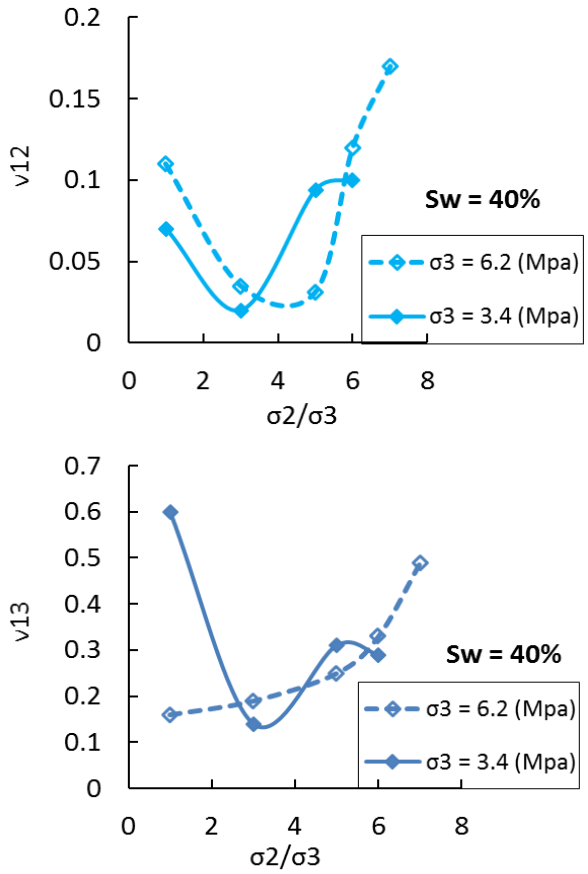

Figure 5.35 Variation of ν_{12} and ν_{13} with σ_2/σ_3 ratio at S_w= 40%. No common trend of dependency on the minimum stress level could be extracted for these samples.

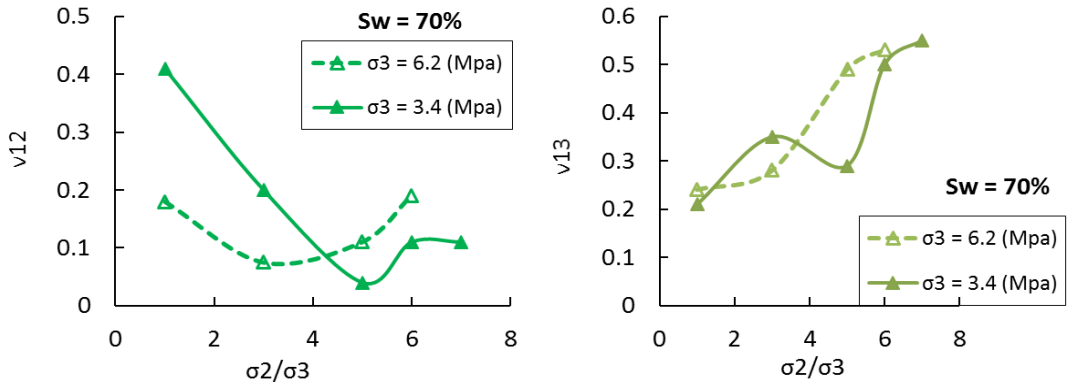

Figure 5.36 Variations of ν_{12} and ν_{13} as a function σ_2/σ_3 ration at S_w=70%. No common trend of dependency on the minimum stress level could be extracted for these samples.

Inelastic deformation and dilatancy

The maximum differential stress (σ_1-σ_3) and lateral principal strains, ε_2 and ε_3, are plotted as functions of the axial strain, ε_1, in Figure 5.37 for Pierre Shale. The applied minimum stress in this case was 3.4 MPa and the sample saturation was 70%. Comparing the two cases of axisymmetric (left plots) and typical true triaxial conditions (right plots) reveals that, when $\sigma_2>\sigma_3$, the rock strength (peak stress) is greater than when $\sigma_2=\sigma_3$. Under equal lateral stresses, ε_2 is larger than ε_3, in particular in the inelastic region, but both dip towards negative strains and show extensional strains. On the other hand, when σ_2 is raised above σ_3 (Figure 5.37, right plots), ε_2 becomes noticeably smaller than ε_3 and curves towards positive strains. This shows that the rock has slightly compressed along σ_2 axis in particular in the inelastic post-fracture part, while it has significantly dilated along σ_3 direction.

Figure 5.38 and Figure 5.39 depict changes of ε_2 against ε_1 for both levels of minimum stress and various levels of σ_2 for Pierre Shale samples. The magnitudes of the applied intermediate stresses are shown on the plots. Under axisymmetric conditions ($\sigma_2=\sigma_3$), the ε_1-ε_2 curve dips upwards, and deformation along σ_2 axis is generally dilational prior to failure and post-failure. When σ_2 is increased over σ_3, the curves in ε_1-ε_2 domain become nearly linear or dip downwards towards positive strains. Thus the displacement along σ_2 direction became compressive as the σ_2 level increased.

The typical stress-strain curves of Pierre Shale in Figure 5.20 also confirmed this trend. At lower levels of σ_2 (lower σ_2/σ_3 ratios), increasing the maximum principal stress caused elastic and inelastic extension in ε_3 direction and similarly in ε_2

direction (see for example Figure 5.20.b and -c). Under higher levels of σ_2, ε_2 curve indicated only small elastic strain during the differential loading. Then within inelastic region and after the peak stress was reached, ε_2 shows slight compression despite ε_3 which indicates significant dilation of the rock sample along σ_3 direction (see for instance Figure 5.20.a, -d and -e). This confirms that, when increasing the magnitude of σ_2, the rock dilatancy would be mainly induced by the extension along σ_3 direction.

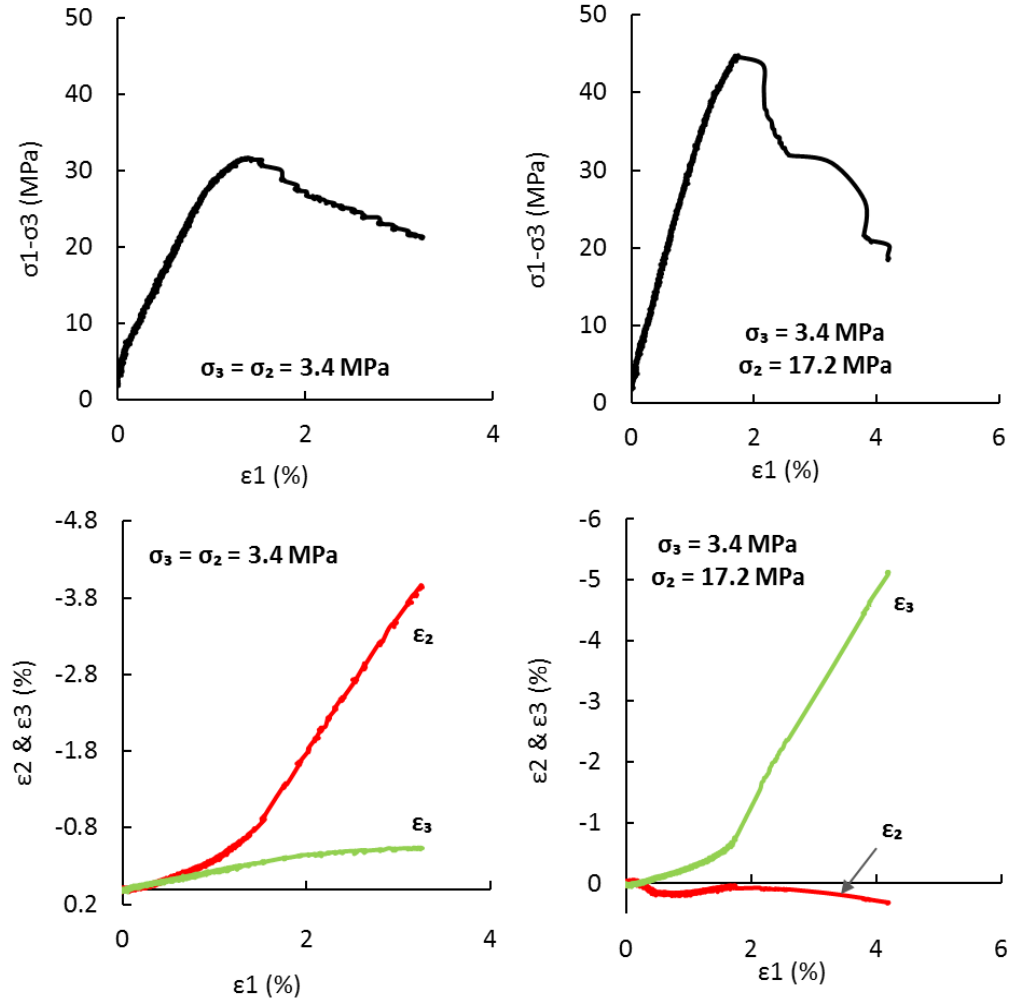

Figure 5.37 The differential stress (top) and lateral strains, ε_2 and ε_3, (bottom) as function of the axial strain, ε_1, in Pierre Shale with 70% water saturation. Left: plots for the axisymmetric conditions ($\sigma_2=\sigma_3$); right: plots obtained under true triaxial conditions ($\sigma_2>\sigma_3$). Negative strains here show extension while positive strains show compression. The peak stress is higher for the case of $\sigma_2>\sigma_3$ (top). In the axisymmetric test, ε_2 is similar to ε_3, both showed extension after the failure. For typical case of $\sigma_2>\sigma_3$, ε_3 is significantly larger than ε_2.

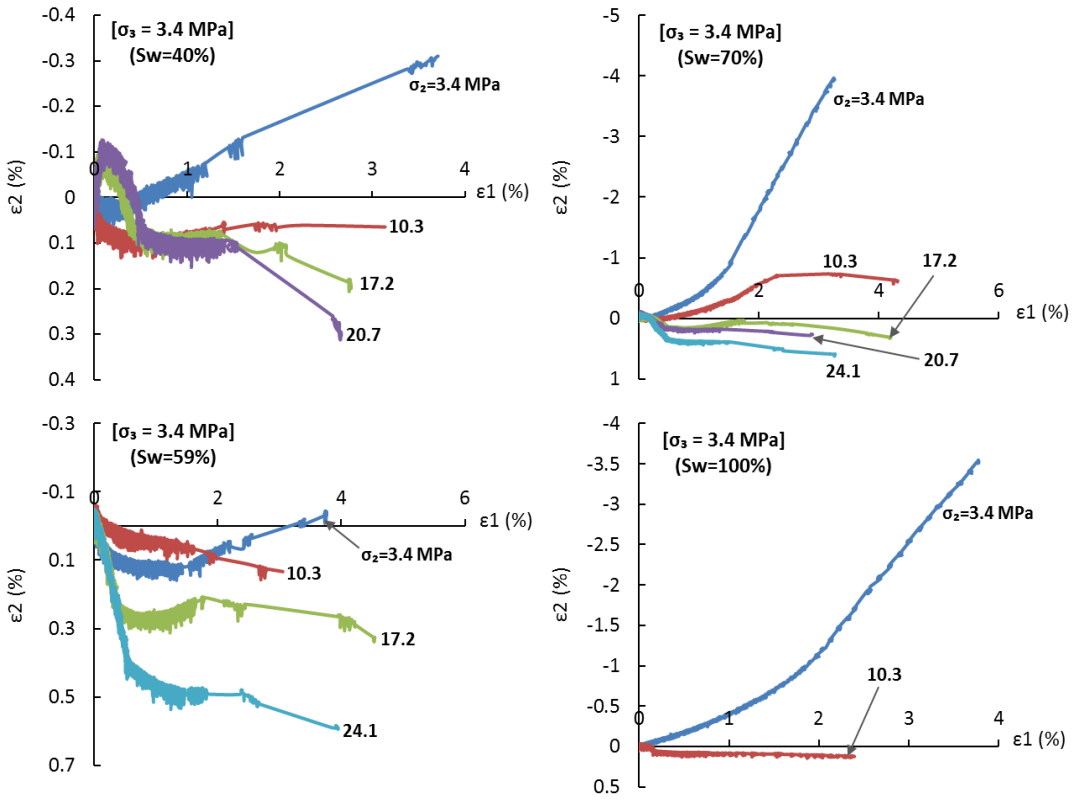

Figure 5.38 Variations of ε_2 versus ε_1, in Pierre Shale for tests under σ_3=3.4 MPa and different saturation states. The numerals on the curves show σ_2 levels. Generally by increasing σ_2 magnitude, ε_2 gradually changes from expansion (negative axis) towards compression (positive axis).

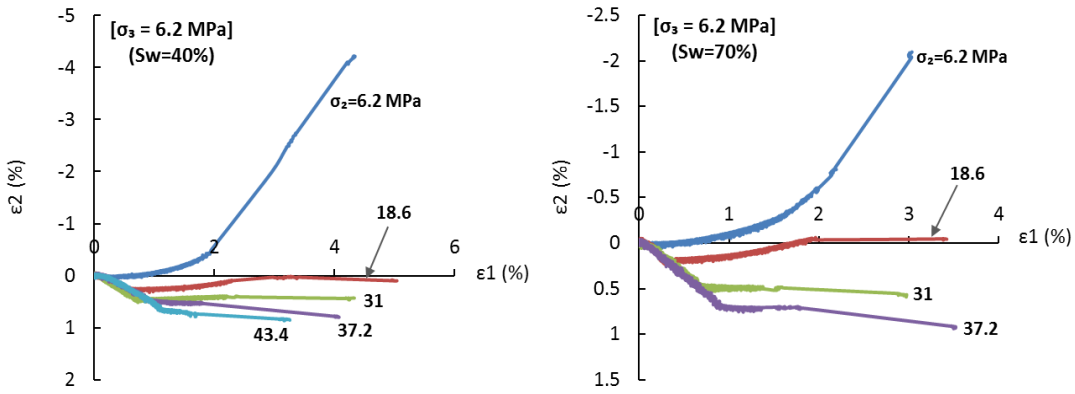

Figure 5.39 Variations of ε_2 versus ε_1, in Pierre Shale for tests under σ_3=6.2 MPa and different saturation states. The numerals on the curves show σ_2 levels. Generally by increasing σ_2 magnitude, ε_2 gradually changes from expansion (negative axis) towards compression (positive axis).

The obtained stress levels at the onset of dilatancy for Pierre Shale specimens are displayed in Table 5.11 as percentage of the axial peak stress ($\sigma_{1\text{-peak}}$). Dilatancy onset was determined as the stress level at which the volumetric strain curve started deviating from linear trend, as shown by some examples in Figure 5.40. The data

displayed in Table 5.11 clearly demonstrate that increasing the magnitude of intermediate stress at a constant level of σ_3 raised the stress level at which the dilatancy starts with respect to the peak axial stress. This means that by increasing σ_2, the linear elastic region was extended while the beginning of the brittle failure process was delayed.

Table 5.11 The changes in dilatancy onset with σ_2 in the Pierre Shale expressed as the σ_1 level at the dilatancy beginning and the dilatancy onset stress level with respect to the peak stress ($\sigma_{1\text{-peak}}$).

S_w (%)	**σ_3 (MPa)**	**σ_2 (MPa)**	**σ_1 at onset of dilatancy (MPa)**	**Dilatancy level as % of $\sigma_{1\text{-peak}}$**
40	3.4	3.4	31	83.8
		10.3	51.9	88
		17.2	41	91.1
		20.7	41.1	91.3
40	6.2	6.2	45	81.8
		18.6	57.6	82.3
		31	70.3	92.5
		37.2	63.5	96.2
		43.4	57.4	99
59	3.4	3.4	31.9	81.8
		10.3	29.5	84.3
		17.2	48.6	86.8
		24.1	54.9	96.3
70	3.4	3.4	27.2	77.7
		10.3	40.9	85.2
		17.2	43	89.6
		20.7	36.3	93.1
		24.1	43.9	97.6
70	6.2	6.2	36.4	79.1
		18.6	58.7	93.2
		31	54.8	96.1
		37.2	54.9	98
100	3.4	3.4	20.7	86.3
		10.3	18.3	91.5

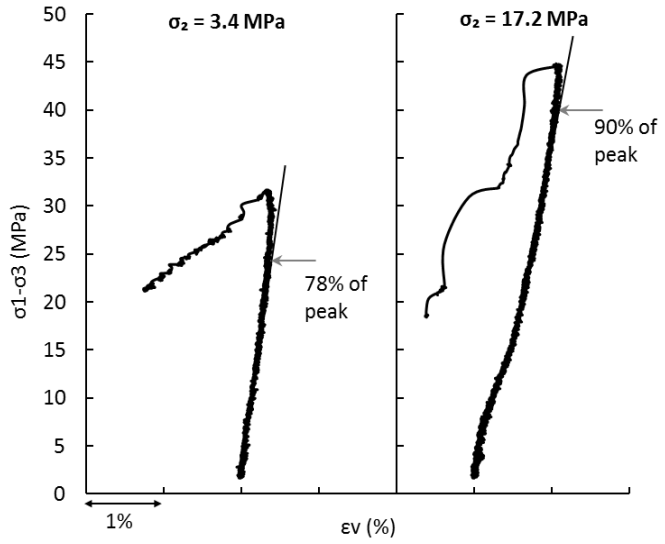

Figure 5.40 Some examples of the differential stress versus volumetric strain curves in the Pierre Shale samples with S_w=70%, tested under σ_3=3.4 MPa and different values of σ_2. The deviation of these curves from linearity defined the onset of dilatancy.

Macroscopic fractures and cracks patterns

Figure 5.41 shows post-failure images of the Pierre Shale samples. For each sample, both sides of the rock cube normal to the σ_2 direction are displayed. All specimens show fault and fracture traces on planes normal to σ_2 direction, which means they strike along the σ_2 axis and dip towards the σ_3 direction under true triaxial conditions. Therefore, as inferred earlier from the principal strain curves, increasing σ_2 above σ_3 caused the rock dilation to occur mainly along the direction of σ_3. The observed main faults in these samples are generally curved and branched and have some small asperities. Hence the fracture angles could not be determined.

At S_w=40%, under both levels of minimum stress (3.4 and 6.2 MPa), in most cases a zone of intense deformation comprising small en-echelon sub-parallel fractures is observed that dips towards the σ_3 direction. The traces of the fractures are oriented oblique or normal to the main shear zone boundary faults. These deformation zones are likely to be Riedel shears that have developed as a result of stress rotation through the shear zone during progressive deformation (Logan et al. 1992). Development of a zone of shear deformation instead of a single clearly defined shear fracture is a characteristic of the transitional brittle-ductile failure (Paterson and Wong 2005). The shear zones narrowed as the magnitude of σ_2

increased and also some slip planes appeared in the specimens. This indicates that increasing σ_2 tended to gradually push the failure mode towards the brittle side of the transitional field.

At S_w=59%, under axisymmetric stress conditions ($\sigma_2=\sigma_3$), the specimen shows multiple sub-parallel fractures and again several small minor cracks in en-echelon patterns were observed. Under true triaxial conditions ($\sigma_2>\sigma_3$), the specimens often display a deformation zone composed of sub-parallel fractures with their axes normal or oblique to the overall direction of the developed shear zone. Such behaviour is indicative of the brittle-ductile transitional regime. Increasing the intermediate stress has narrowed the shear zone and led to occurrence of multiple parallel or conjugate slip planes. This indicates that increasing σ_2 again tended to move the rock failure mode towards the brittle field.

For the specimens with S_w=70%, under axisymmetric conditions ($\sigma_2=\sigma_3$), a wide shear zone comprising parallel and sub-parallel small fractures is observed. Increasing stress anisotropy caused the shear zone to narrow. Also a single, sub-parallel or conjugate dual or multiple slip planes appeared. Again this shows the effect of raising σ_2 in pushing the failure mode towards the brittle field. The faults surfaces are generally curved and/or branched and en-echelon patterns are observed in many cases.

For the fully-saturated samples, under axisymmetric stress conditions ($\sigma_2=\sigma_3$), a shear zone of parallel and sub-parallel small fractures is identified. Under true triaxial stress state ($\sigma_2>\sigma_3$), the shear zone nearly disappeared and a substantially symmetrical sharply defined single fault was detected. Such evolution implies that the shale failure behaviour was shifted towards the brittle field through increasing σ_2 magnitude, similar to the behaviour observed at other levels of water saturation.

Increasing the magnitude of σ_2 at a constant σ_3 in Pierre Shale tended to gradually evolve the failure behaviour from transitional towards brittle mode. Such effect is in agreement with some of the previous true triaxial investigations on some other rock types (e.g. Takahashi and Koide 1989, Mogi 2007).

S_w (%)	Stress State	**σ_3 = 3.4 MPa**	**σ_3 = 6.2 MPa**
40%	**$\sigma_2 = \sigma_3$**	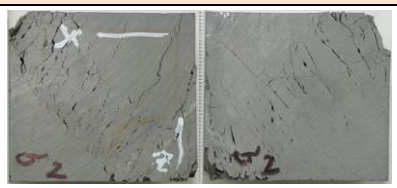	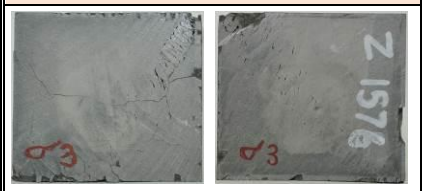
	$\sigma_2 = 3\sigma_3$	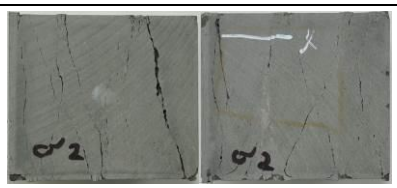	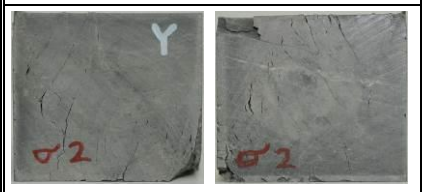
	$\sigma_2 = 5\sigma_3$	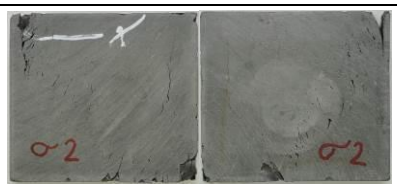	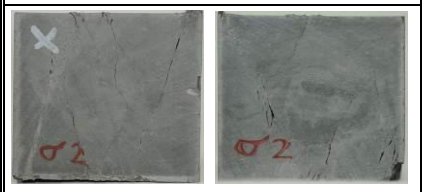
	$\sigma_2 = 6\sigma_3$		
	$\sigma_2 = 7\sigma_3$		

Figure 5.41 Photographs of the Pierre shale specimens after true triaxial test. Here σ_1 is in vertical direction, σ_3 in lateral direction and σ_2 perpendicular to the displayed rock side. For each sample, the two opposing sides are displayed.

S_w (%)	Stress State	σ_3 = 3.4 MPa
59%	$\sigma_2 = \sigma_3$	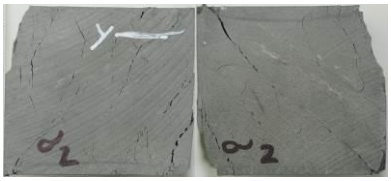
	$\sigma_2 = 3\sigma_3$	
	$\sigma_2 = 5\sigma_3$	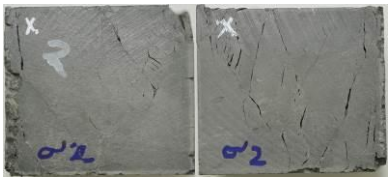
	$\sigma_2 = 7\sigma_3$	

Figure 5.41 (Continued)

S_w (%)	Stress State	σ_3 = 3.4 MPa	σ_3 = 6.2 MPa
70%	$\sigma_2 = \sigma_3$		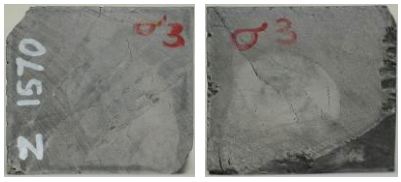
	$\sigma_2 = 3\sigma_3$	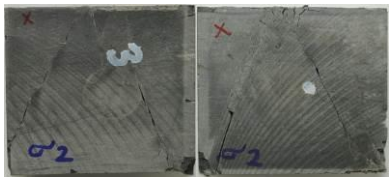	
	$\sigma_2 = 5\sigma_3$		
	$\sigma_2 = 6\sigma_3$	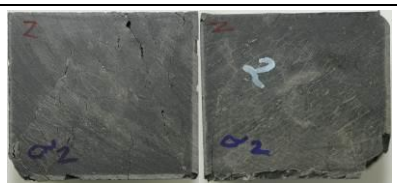	
	$\sigma_2 = 7\sigma_3$	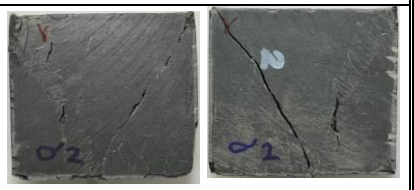	

Figure 5.41 (Continued)

S_w (%)	Stress State	σ_3 = 3.4 MPa
100%	$\sigma_2 = \sigma_3$	
	$\sigma_2 = 3\sigma_3$	

Figure 5.41 (Continued)

5.3.3 Saturation impact

The influence of changing water saturation (S_w) on deformational behaviour of the Pierre Shale specimens under true triaxial stress states was also examined in this work. To investigate this relation, the experimental data obtained from partially- to fully-saturated samples subjected to identical stress conditions were compared. The obtained failure stresses (strength), Young's modulus and two Poisson's ratios have been plotted versus water saturation degree in Figure 5.42 to Figure 5.45.

Figure 5.42 displays the true triaxial strength of the Pierre Shale samples against water saturation degree. Each diagram in this figure presents the data obtained from samples with different saturation states but under the same stress conditions. Generally, at all stress states reducing the water content below the full saturation conditions caused an increase in the peak stress to some extent. This is explained through the capillary suction forces that are created in shales due to the partial water saturation state. The surface tension at the contact of water and air in neighbouring pores causes a frictional force which acts as cohesion and pulls grains together. On the other hand, at high water saturations, the capillary bonds between the grains are destroyed and the apparent cohesion is decreased (Papamichos et al. 1997).

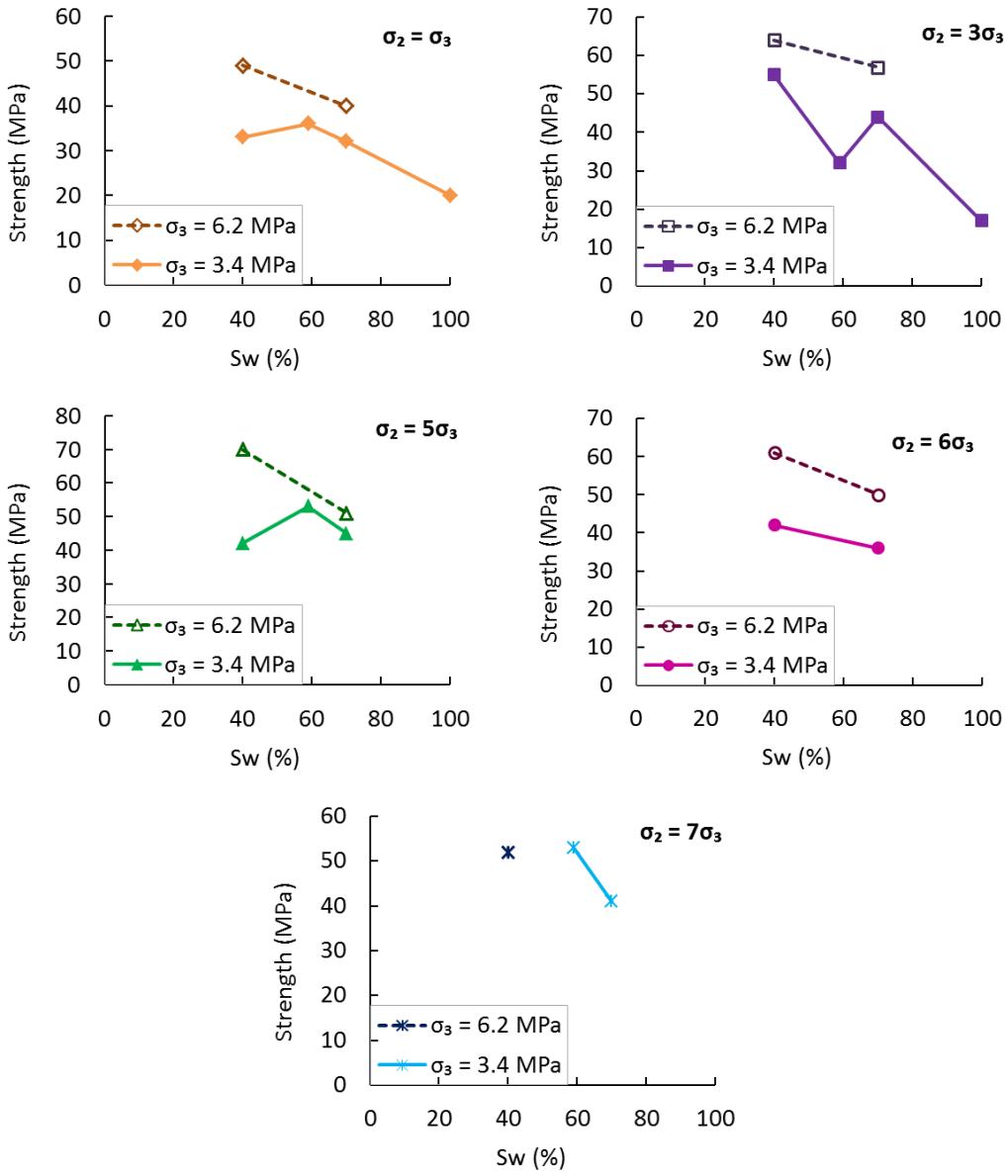

Figure 5.42 The Pierre Shale true triaxial compressive strength as a function of water saturation. Each plot displays data obtained from rocks with various S_w (%) but at same σ_2/σ_3 ratio. Increasing the water saturation generally decreased the compressive strength.

Table 5.12 shows the largest growth occurred in rock strength due to desiccation. Based on the obtained data here, decreasing the water saturation caused up to 38 MPa growth in the compressive strength of these shales. This corresponds to ~223% raise in rock strength due to decreasing the water saturation of the shales by 60%. The results also indicated up to ~37% increase in the failure strength of these shales when reducing the saturation by 30%, at σ_3=6.2 MPa.

In Figure 5.43, the static Young's modulus values were plotted against the water saturation degree for both levels of the minimum stress. Each colour in these

diagrams represents a group of tests with the same stress conditions (σ_2/σ_3 ratio) but different water saturation levels. At σ_3=3.4 MPa, decrease in water saturation from 100% to 40% caused up to ~3 times increase in rock stiffness. Increase in stiffness by reduction in water saturation is probably related to the intergranular cohesion generated by capillary forces at partial water saturation states, which has an impact as if cementation at grain contacts in the rock was increased (Papamichos et al. 1997). At σ_3=6.2 MPa, for some stress states (σ_2/σ_3=1 and 6), the stiffness increased with saturation reduction while for other stress conditions (σ_2/σ_3=3 and 5), stiffness decreased or remained constant. Young's modulus generally increases with decreasing saturation for tests under σ_3=6.2 MPa but not for all tests. Nevertheless it should be noted that the measurements obtained in the latter case were not sufficient to establish general trends, as only samples with two saturations (40% and 70%) were available to be tested under the minimum stress level of 6.2 MPa.

Figure 5.44 and Figure 5.45 display the changes of Poisson's ratio ν_{12} and ν_{13} versus water saturation. At σ_3=6.2 MPa, decreasing the saturation from 70% to 40% caused reduction in both ν_{12} and ν_{13} for all σ_2/σ_3 ratios. However, from the data obtained under σ_3=3.4 MPa no obvious trend of dependency on water saturation can be established.

Table 5.12 Largest growths in true triaxial strength (σ_f) of the Pierre Shale samples due to the reduction in their water saturation level. Here the comparison was done between the strength values obtained from different samples tested under similar stress states.

σ_3 (MPa)	σ_2/σ_3	Maximum rise in σ_f (MPa)	Maximum rise in σ_f (%)	S_w drop (%)
3.4	1	16	80	41
	3	38	223.5	60
	5	8	17.8	11
	6	6	16.7	30
	7	12	29.3	11
6.2	1	9	22.5	30
	3	7	12.3	30
	5	19	37.3	30
	6	11	22	30

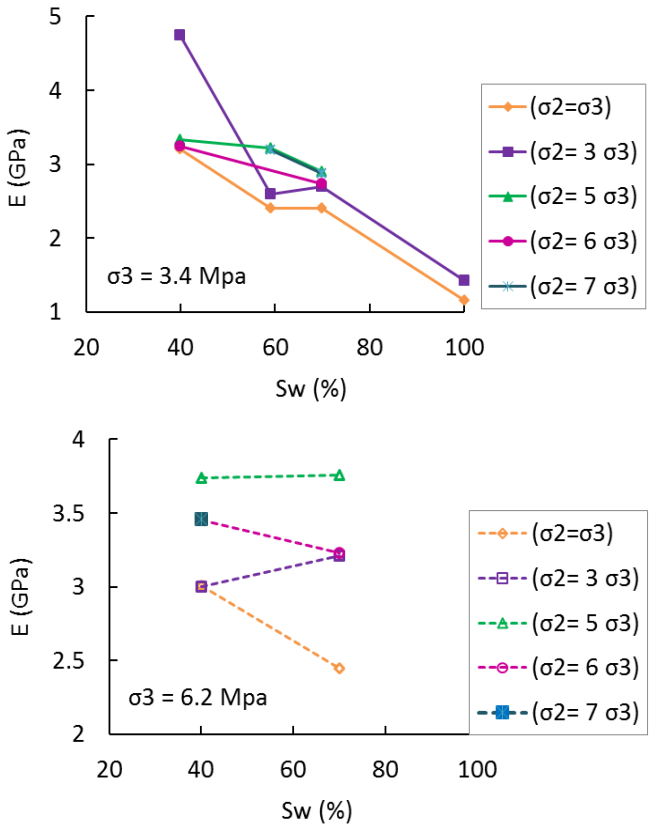

Figure 5.43 Pierre shale Young's modulus as a function of water saturation.

Our findings generally support the observations made by Valès et al. (2004) under conventional triaxial stress conditions on Tournemire shales. Their experimental work revealed an increase in the compressive strength and Young's modulus and a decrease in the Poisson's ratio as a result of reducing water saturation in shales. Also studies of Dewhurst et al. (2012) indicated an increase in the elastic modulus and a significant decrease in the Poisson's ratio of Officer-Basin shales due to a decrease in water saturation under conventional triaxial stress states.

In order to highlight the effect of water saturation degree on dilatant behaviour of the Pierre Shale, the axial stress levels at the onset of dilatancy, previously presented in Table 5.11 were restructured here in Table 5.13. Comparing the dilatancy-onsets for samples with different saturation states tested at identical stress conditions revealed that in most cases, higher water saturations decreased the stress level at the beginning of dilatancy. This can be explained through capillary and suction effects which are induced as shales lost water during drying (e.g. Laloui et al. 2010), which consequently expedited the beginning of the brittle failure process of the rock. Valès et al. (2004) observed marked decrease in the stress level at the onset of dilatancy

due to increasing water saturation in Tournemire Shale samples loaded normal to bedding. They explained that in the presence of water, increase of volume occurs through microfracturing and sliding of the clay grains or layers.

It was attempted here to examine the relation between the fracture patterns in the post-failure Pierre Shale samples with the water saturation level. Inspecting the rock sample images in Figure 5.41 showed that in the majority of specimens at different saturation levels, failure occurred in the form of a shear zone composed of parallel and sub-parallel small fractures which was accompanied by some slip planes at higher σ_2 levels. Therefore, no general conclusion could be made here with respect to the influence of the water saturation state on fractures patterns in the Pierre Shale samples.

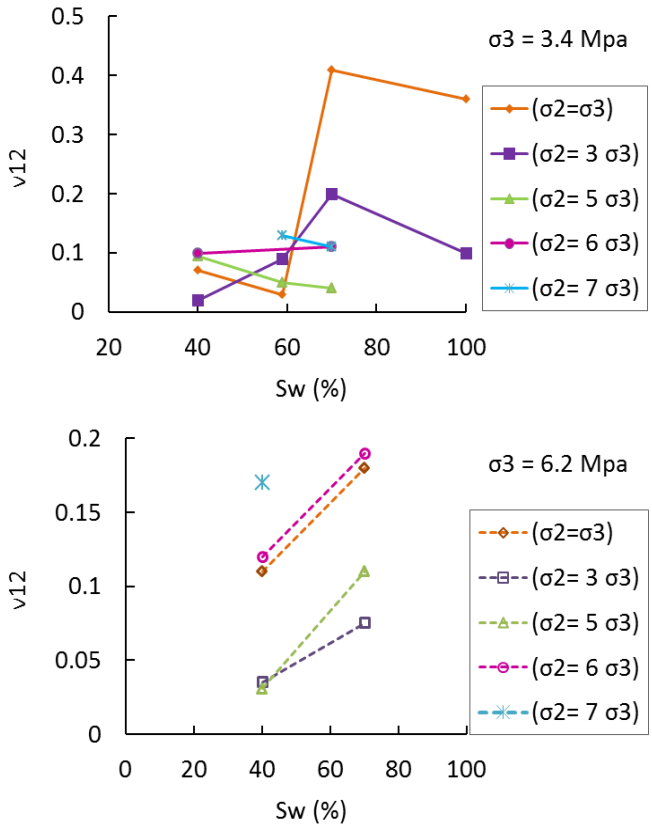

Figure 5.44 Variations of Poisson's ratio ν_{12} along saturation degree in the Pierre Shale samples.

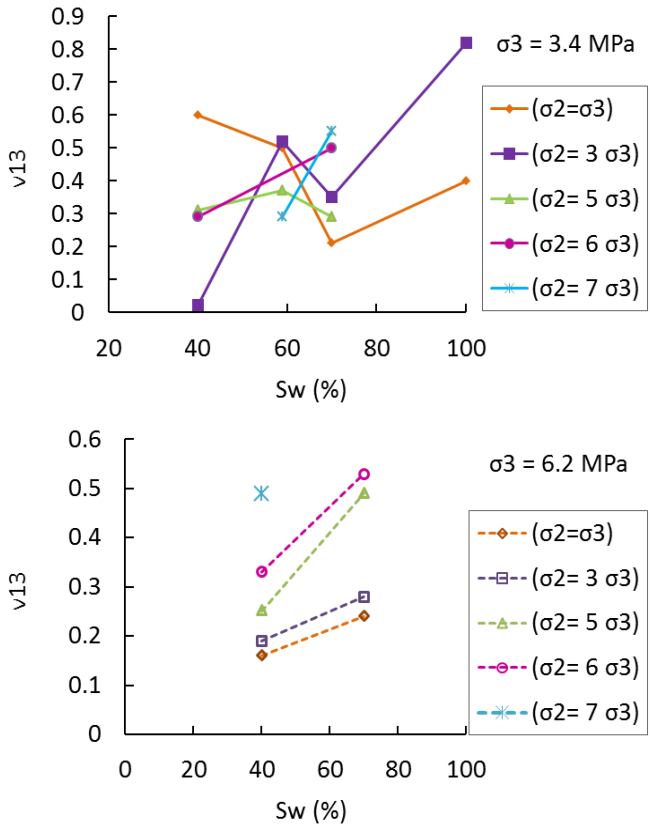

Figure 5.45 Variations of Poisson's ratio ν_{13} along saturation degree in the Pierre Shale samples.

Table 5.13 Comparing the axial stress level at the onset of dilatancy (σ_D) for the Pierre Shale samples with different S_w tested at identical stress conditions.

S_w (%)	σ_3 (MPa)	σ_2 (MPa)	σ_D (MPa)	S_w (%)	σ_3 (MPa)	σ_2 (MPa)	σ_D (MPa)
40	3.4	3.4	31	40	6.2	6.2	45
59	3.4	3.4	31.9	59	6.2	6.2	-
70	3.4	3.4	27.2	70	6.2	6.2	36.4
100	3.4	3.4	20.7	100	6.2	6.2	-
40	3.4	10.3	51.9	40	6.2	18.6	57.6
59	3.4	10.3	29.5	59	6.2	18.6	-
70	3.4	10.3	40.9	70	6.2	18.6	58.7
100	3.4	10.3	18.3	100	6.2	18.6	-
40	3.4	17.2	41	40	6.2	31	70.3
59	3.4	17.2	48.6	59	6.2	31	-
70	3.4	17.2	43	70	6.2	31	54.8
100	3.4	17.2	-	100	6.2	31	-
40	3.4	20.7	41.1	40	6.2	37.2	63.5
59	3.4	20.7	-	59	6.2	37.2	-
70	3.4	20.7	36.3	70	6.2	37.2	54.9
100	3.4	20.7	-	100	6.2	37.2	-
40	3.4	24.1	-	40	6.2	43.4	57.4
59	3.4	24.1	54.9	59	6.2	43.4	-
70	3.4	24.1	43.9	70	6.2	43.4	-
100	3.4	24.1	-	100	6.2	43.4	-

5.4 Summary

In this chapter the influence of the lateral stress magnitude and anisotropy on behaviour of the Carynginia Shale and Pierre Shale was investigated, with particular emphasis on the impact of the intermediate principal stress and water saturation. The major findings of this study were as follows:

- The laboratory data gathered here revealed that increasing σ_2 from a conventional triaxial stress state ($\sigma_1>\sigma_2=\sigma_3$) to true triaxial stress states ($\sigma_1>\sigma_2>\sigma_3$) resulted in up to 27% and 67% increase in strength of Carynginia Shale and Pierre Shale respectively. The strengthening effect of the intermediate stress observed here was in a good agreement with previous findings on shales and some other rocks. This is an effect which is overlooked in conventional triaxial tests.

- The peak stresses obtained for the two shales fitted well on a single curve in Mogi's proposed domain (τ_{oct}–$\sigma_{m,2}$). Further experiments under wider ranges of stresses can assist to establish a more complete failure envelope for each of the two shales.

- The rock elastic modulus showed noticeable increases with increased σ_2 in both shales. The behaviour of rock stiffness and true triaxial strength as a function of σ_2 magnitude, were found to be correlated in these shales. This is in agreement with the good correlation normally found in conventional tests between the rock strength (UCS) and Young's modulus (e.g. Horsrud et al. 1998).

- No clear relationship was found between the Poisson's ratios and the applied stress states in testing the Carynginia Shale and Pierre Shale specimens.

- Studies on dilatancy revealed that increasing σ_2 increased the stress level at the onset of dilatancy. This indicated that increasing the intermediate stress postponed the propagation of microcracks in the shale samples.

- Studies on the fractures pattern indicated that in Carynginia Shale, increasing σ_3 resulted in changes in the failure mode from dual conjugate to multiple sub-parallel and conjugate faults. This revealed that increasing σ_3 tends to change the failure behaviour from brittle to transitional mode, in a similar fashion as normally observed in conventional triaxial tests. Increasing σ_2 at a constant σ_3 also shifted the behaviour more towards the transitional region through development of arrays of cracks and shear zones of intense deformation.

- In the Pierre Shale, most of the post-test specimens showed shear zones of intense closely spaced en-echelon fractures which is characteristic of the transitional brittle-ductile behaviour. The shear zones generally narrowed as the magnitude of σ_2 was increased and also some slip planes appeared in the specimens. This indicates that increasing σ_2 tended to gradually evolve the failure mode towards the brittle side of the transitional field. Such effect is in agreement with previous true triaxial investigations on some other porous rocks (e.g. Takahashi and Koide 1989).
- In the Pierre Shale, the impact of changing water saturation on mechanical characteristics was also investigated. Our results indicated an increase in the true triaxial strength and elastic modulus and decrease in the Poisson's ratios due to reduction of water saturation. This is associated with the capillary suction phenomena which has a cohesion-controlling influence. Decreasing water saturation increases capillary suction which leads to increase in apparent cohesion of the material (Schmitt et al. 1994). The suction effect is often compared to the effect of confining pressure on material (Fjær et al. 2008), which is in agreement with the observed increase in strength and stiffness due to decreasing saturation. Capillary suction is related to the pore size distribution of a porous material and is higher the smaller the pore sizes are.

In the next chapter the deformational properties of the sandstone samples and the two shale specimens under true triaxial stress states as presented in the preceding and this Chapter will be compared and some mechanisms responsible for the observed behaviours are discussed.

6 Experimental results: Comparison and discussion

6.1 Introduction

In this Chapter, the deformational behaviour of the three tested rock types under true triaxial stress conditions are compared and discussed. The synthetic sandstone samples manufactured and used in this work were assumed to be isotropic rocks, whereas shales are generally classified as transverse-isotropic materials due to the presence of bedding planes, laminations or preferred particle orientation. While comparison of these two different rock types (i.e. isotropic versus TI) may appear unreasonable in the first instance, the discussions presented in this Chapter present some valuable information in terms of the effect of intermediate stress on mechanical behaviour of these rocks. Mogi and his colleagues studied various rock types, including homogenous, inhomogeneous, isotropic and anisotropic rock specimens, under true triaxial stress states (see Mogi 1959, 1979, 2007; Xu et al. 1980; Kwaśniewski and Mogi 1990, 1996, 2000). These studies mainly investigated the influence of the intermediate stress on rock strength, deformational properties and failure. Mogi (2007) presented the laboratory results of a series of true triaxial tests done by Kwaśniewski and Mogi (1990, 1996, 2000) on a schist in which the direction of the applied principal stresses was changed with respect to foliation in the sample. He compared the stress-strain curves and the impact of intermediate stress on rock strength in these samples. The results showed that changing the σ_1 and σ_2 axes with respect to the foliation (weak planes) direction, markedly affected the extent of the influence of σ_2 on rock strength and failure characteristics. The findings suggested that when the maximum principal stress was applied perpendicular to the direction of beddings/foliations, the anisotropic rock behaved close to an isotropic rock under true triaxial stress conditions, because the anisotropy did not tend to have

a large effect on the rock failure behaviour. However, inclined bedding planes with respect to σ_1 and σ_2 directions largely influenced the rock mechanical response.

In case of testing inhomogeneous rocks, experimental studies of Mogi (2007) showed that some considerations and corrections should be applied to reduce the dispersion of the obtained data. Hence, the impact of σ_2 on behaviour of these rocks could be detected clearly and precisely, similar to the trends obtained in case of homogenous rocks. The method includes dividing the samples into different groups based on their standard mechanical properties. Then each group would be examined individually and hence the influence of σ_2 on rock behaviour could be investigated more accurately within each set.

Both types of the shale samples in this work were tested in a way to apply the maximum principal stress perpendicular to beddings. Therefore, the results obtained for the shale samples are expected to be unaffected by the structural anisotropy related to the bedding planes. With regards to rock sample homogeneity, the sandstone and the Pierre Shale specimens were assumed to be homogeneous at macroscopic scale. In the Carynginia Shale, some inhomogeneity in the samples was visible to the naked eye. However, the amount of heterogeneity has not caused significant scattering in the laboratory data obtained in the Carynginia Shale samples. Thus for the purpose of comparing the mechanical response under true triaxial stress conditions, generally it would be sensible to assume all the three rocks to be relatively isotropic and homogeneous, unaffected by any significant heterogeneity and anisotropy related to bedding. In the following sections the deformational behaviour of these three rock groups under similar stress conditions will be compared.

6.2 Stress-strain behaviour

Comparing the stress-strain curves obtained under similar stress states for the sandstones, the Carynginia Shale and Pierre Shales in Figure 4.4, Figure 5.3, Figure 5.4 and Figure 5.20 shows that the magnitudes of strains, and in particular the axial strain (ε_1), are markedly larger in the sandstones in comparison to both shales. This is related to the high initial porosity of the sandstone samples, which resulted in pore collapse and overall sample compaction under compressional loading. The differential stress-axial strain curves of these rocks obtained at the minimum stress of

3.4 and ~6.2 MPa, under similar σ_2 values were re-plotted in Figure 6.1 and Figure 6.2. For easier comparison, identical limits and scales were used for the horizontal and vertical axes of all the diagrams.

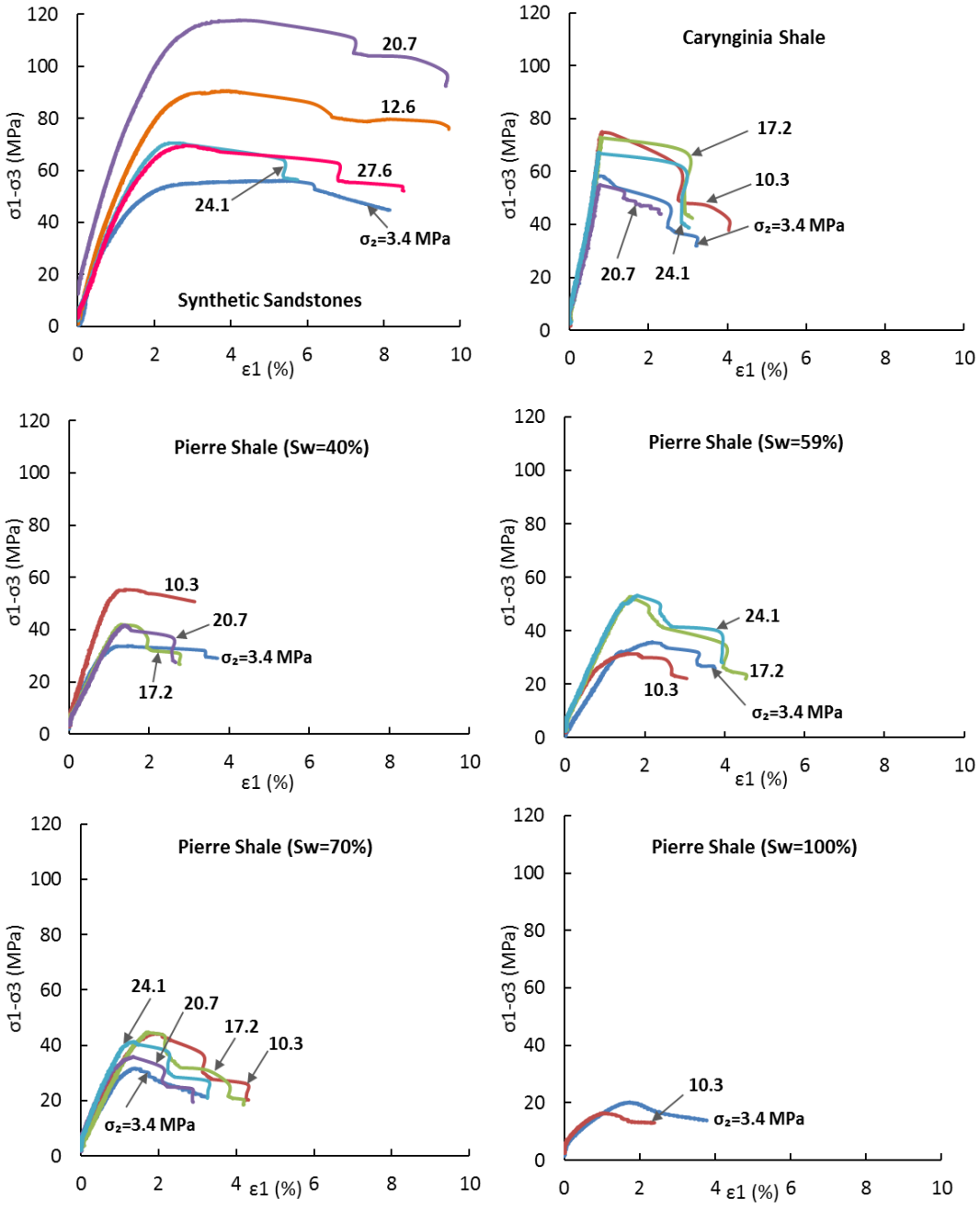

Figure 6.1 The differential stress versus axial strain curves for the synthetic sandstones, the Carynginia Shale and the Pierre Shale with different S_w (%), tested under σ_3=3.4 MPa. The numbers on the curves show value of the applied σ_2, in MPa.

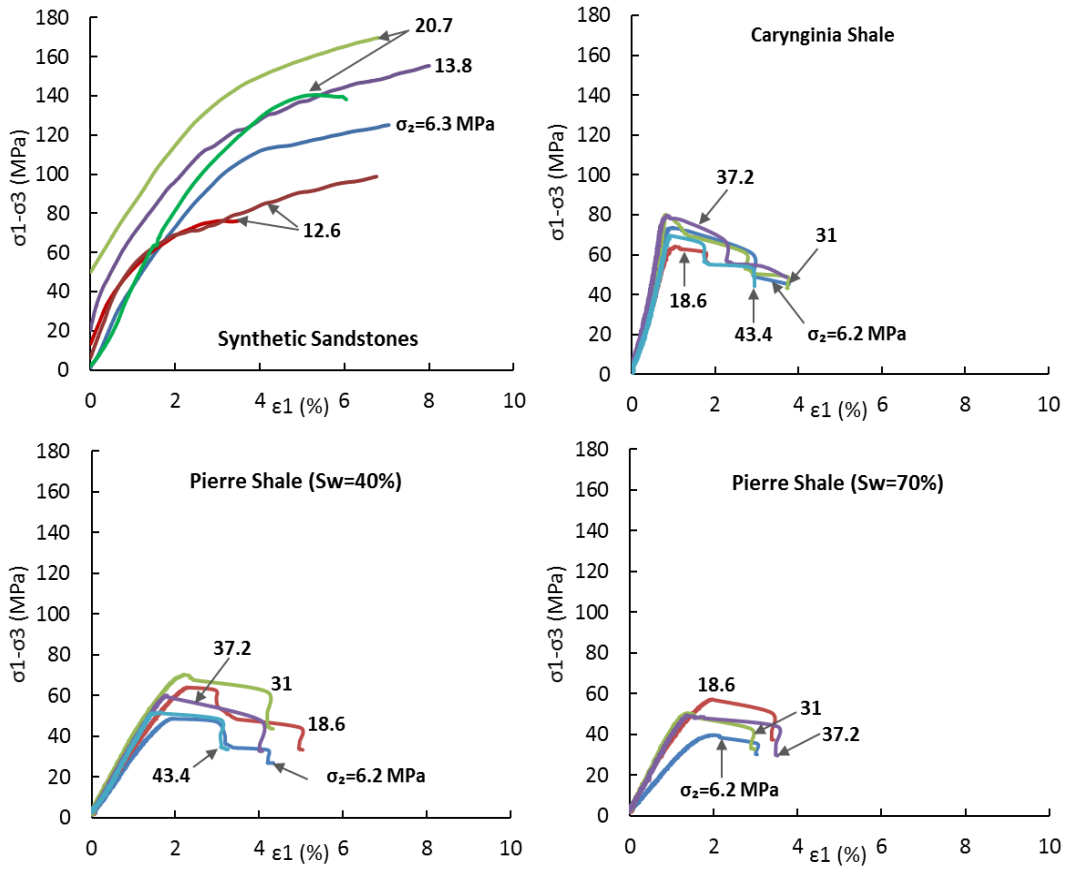

Figure 6.2 The differential stress versus axial strain curves for the synthetic sandstones, the Carynginia Shale and the Pierre Shale with different S_w (%), tested under $\sigma_3 \approx 6.2$ MPa. The numbers on the curves show value of the applied σ_2, in MPa.

At σ_3=3.4 MPa, the stress-strain curves of the Carynginia Shale and the Pierre Shales with higher saturation levels, exhibited brittle failure followed by strain softening. On the other hand the sandstone samples and the Pierre Shale specimens with the lower saturation degree (S_w=40% and 59%) at lower σ_2 values, mainly displayed a transitional failure mode. At $\sigma_3 \approx 6.2$ MPa, the sandstone samples mainly indicated strain hardening after failure, while both shales showed strain softening. In other words, under these stress conditions, the sandstones failed in a ductile regime, while both shales generally had a brittle failure mode. This tendency of the stress-strain behaviour towards strain hardening and ductility in these sandstones is a result of increasing σ_3. Previous studies on failure mode of rocks under standard triaxial and true triaxial conditions showed that increasing σ_3 can change the stress-strain behaviour from the brittle regime to a transitional brittle-ductile mode and finally to a ductile failure mode (Paterson and Wong 2005, Mogi 2007). The possible reason that under similar stress states such a transition was not observed in the two shales is

because the transition pressure from brittle to ductile field in a rock, depends on many parameters such as porosity, grain size, presence of clay minerals and nature of cementation (Paterson and Wong 2005, Wong et al. 1997). Thus it is likely that as the sandstones had significantly higher initial porosity (26%) and larger grain size in comparison to shales (ϕ~3.2% and 20% in Carynginia Shale and Pierre Shale respectively), the transition of stress-strain behaviour towards the ductile regime occurred at lower σ_3 levels for sandstones. The evolution of the deformation patterns in the sandstones also confirmed this transition through occurrence of enhanced inelastic compaction in the rock due to the increase in the magnitude of lateral stresses (see Chapter 4, section 4.3.5). From Figure 6.1 and Figure 6.2, it is evident that generally the sandstones had higher failure strength than the two shales. In terms of the stress drop at failure, the Carynginia Shale specimens showed the most distinct peak stresses.

6.3 Stress-dependency of mechanical properties

Table 6.1 presents the range of strength and stiffness values obtained for the synthetic sandstones, the Carynginia Shale and the Pierre Shale samples under similar stress states. The dependency of the compressive strength, Young's modulus and dilatancy onset in the studied rocks on true triaxial stress states and in particular on σ_2, are compared in the following sections. Since the Poisson's ratios did not indicate a clear dependency on the stress state in true triaxial testing of the three groups of samples, this parameter is not discussed here.

Table 6.1 The range of obtained values for rock strength (σ_f) and elastic modulus (E) of the synthetic sandstones, the Carynginia Shale and the Pierre Shale under similar stress conditions.

Rock Type	Sw (%)	σ_3 (MPa)	σ_2/σ_3 ratio	σf (MPa)	*E* (GPa)
Synthetic sandstones	NA	3.4	1-7	56 – 118	2.6 – 4.56
Carynginia Shale	NA	3.4	1-7	55 – 75	6.5 – 7.5
Pierre Shale	40	3.4	1-6	33 – 55	3.2 – 4.75
	59		1-7	32 – 53	2.4 – 3.2
	70		1-7	32 – 45	2.4 – 2.87
	100		1.3	17 – 20	1.1 – 1.4
Synthetic Sandstones	NA	6.3	1-3.3	71 – 142	3.3 – 5.7
Carynginia Shale	NA	6.2	1-7	64 – 80	7.2 – 10.9
Pierre Shale	40	6.2	1-7	49 – 70	3 – 3.7
	70		1-6	40 – 57	2.45 – 3.76

6.3.1 True triaxial compressive strength

Figure 6.3 displays variations of the true triaxial strength in the sandstones and the two shales as a function of σ_2, for two levels of the minimum stress. For both levels of σ_3, the synthetic sandstone samples showed higher strength than the shales, as it was also obvious from Figure 6.1 and Figure 6.2. This is perhaps related to the mineral composition of these rocks, as shales are mainly composed of clay minerals while the main constituents of the sandstone was more rigid minerals such as quartz. Between the two shales, the Carynginia Shale samples had higher compressive strength than the Pierre Shale specimens, under similar stress conditions. The lower strength of Pierre Shale can be related to its higher initial porosity and greater degree of water saturation, which would result in lower capillary suctions and a decrease in apparent cohesion (as explained in Chapter 5).

Comparing the magnitude of strength obtained under axisymmetric conditions ($\sigma_2=\sigma_3$) to the highest true triaxial strength ($\sigma_2>\sigma_3$) indicated 110% and 77% increase in strength of the sandstones by increasing σ_2 at σ_3=3.4 and 6.3 MPa, respectively (see Table 4.3). In the Pierre Shale samples, the maximum growth of strength at σ_3=3.4 MPa was 67% (see Table 5.10). At σ_3=6.2 MPa, the Pierre Shale specimens showed up to 43% increase in strength value by increasing σ_2 level. The Carynginia Shale samples indicated the least changes in strength with the variations of intermediate stress. In these samples, maximum of 27% and 8% growth in strength was observed due to the increase in σ_2 level, at σ_3= 3.4 and 6.2 MPa, respectively (see Table 5.4).

This revealed that the strength of the synthetic sandstones was markedly sensitive to σ_2 changes. The growth in compressive strength under similar stress states was less pronounced in the shales. The mechanism responsible for this observation is believed to be associated with rock initial porosity. Previous studies have shown that good correlations exist between strength and porosity in shales (Horsrud 2001, Dewhurst et al. 2010) and sandstones (e.g. Vernik et al. 1993, Chang et al. 2006, Dunn et al. 1973). Dewhurst et al. (2010) showed that shale strength is relatively insensitive to porosities larger than ~15%. However, for porosities below ~15%, the rock strength rapidly increases with reduction in porosity. In sandstones, strength is also inversely correlated with porosity (Palchik 1999). In mechanical tests, increases in confining stress, result in some initial compaction in porous rocks (Paterson and

Wong 2005). Such compaction would be more significant in higher porosity materials, and increases in lateral stresses consequently can lead to more pronounced strength increases. In this study, the initial porosity of the tested sandstones (~26%) was higher than that of Pierre Shale (~20%) and both higher than the porosity in Carynginia Shale (<4%). Consequently, the strength in the sandstones was more sensitive to stress variations whereas in the Carynginia Shale, it was the least prone to change.

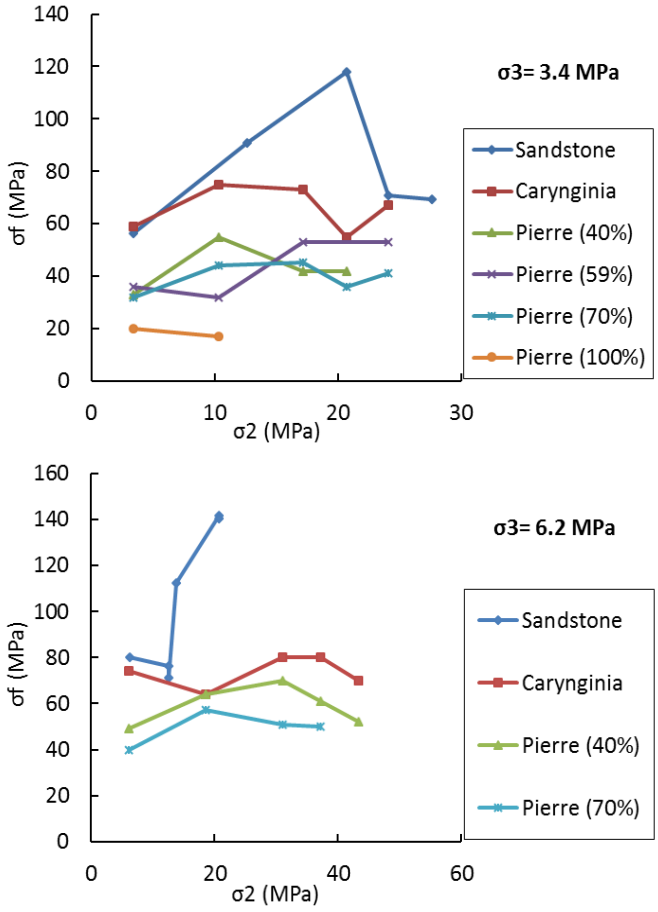

Figure 6.3 Variations of the failure strength (σ_f) with σ_2 value, in the sandstones and the two shales, at σ_3=3.4 and 6.2 MPa. For the Pierre Shale specimens, the saturation level is shown by the numbers in parentheses. The sandstone samples has the highest and the Pierre Shale has the lowest strength under the applied stress conditions.

6.3.2 Elastic modulus

Variations of Young's modulus with σ_2 are plotted in Figure 6.4 for the sandstones and the two shales. From this diagram it is obvious that the Carynginia Shale is significantly stiffer than the sandstones and the Pierre Shale under both levels of the

minimum stress. It is likely that as the inherent porosity in Carynginia Shale was lower, its Young's modulus was higher (e.g. Horsrud et al. 1998). Also it should be kept in mind that these samples were not well-preserved, which have probably caused drying of their clay minerals. Such desiccation can result in high capillary suctions in materials with small pore throats and as such can significantly increase effective stress and reduce porosity. This would result in increased peak strength and Young's modulus (stiffness). The sandstone samples also had higher stiffness than the Pierre Shales, except for some lower water saturation Pierre Shale specimens (S_w=40%) tested at σ_3= 3.4 MPa. This is perhaps associated with the presence of water in Pierre Shale which cause increases in stiffness and strength as water saturation reduces (see Valès et al. 2004).

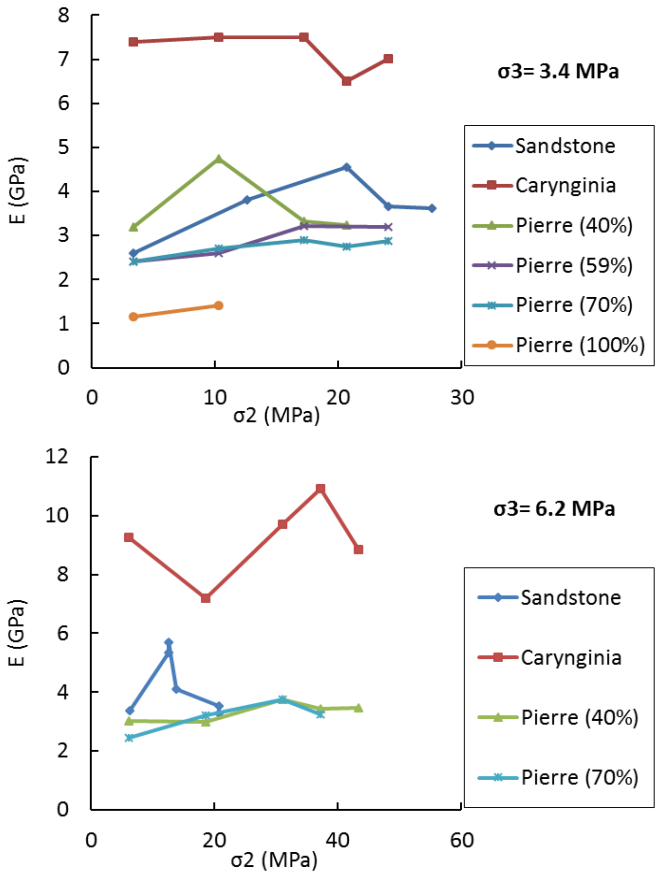

Figure 6.4 Variations in the elastic modulus (E) with σ_2 value, in the sandstones and the two shales, at σ_3=3.4 and 6.2 MPa. For the Pierre Shale specimens, the saturation level is shown by the numbers in parentheses. The Carynginia Shale samples were noticeably stiffer than the other two rocks. Stiffness of the sandstones was also generally higher than the Pierre Shale specimens.

Plotting variations of the Young's modulus and the true triaxial strength as a function of σ_2 in Carynginia Shale (Figure 5.10) and Pierre Shale (Figure 5.30) indicated that Young's modulus response to variations of the intermediate stress is very similar to that of the rock strength. The same diagram was plotted for sandstone samples in Figure 6.5. However, in case of the synthetic sandstones, only the group of samples tested under σ_3=3.4 MPa show similar trend of dependency on σ_2 for elastic modulus and strength. The inconsistent behaviour of the Young's modulus in sandstone specimens could be due to the heterogeneity in samples cementation, as slight variations of cementation at grain contacts could introduce a significant impact on elastic properties (see Saidi et al. 2003).

In the sandstone samples, increasing stress anisotropy from 1 (σ_2=σ_3) to higher levels resulted in up to 75% and 69% increase in the Young's modulus at σ_3=3.4 MPa and 6.3 MPa, respectively. In the Pierre Shale samples, the maximum growth of *E* at σ_3=3.4 MPa due to increase in σ_2 level was 48%. At σ_3=6.2 MPa, the maximum raise in the magnitude of *E* was 53% in these specimens. The percentage of increase in Young's modulus due to σ_2 changes was less pronounced in the Carynginia Shale. Maximum growths in *E* obtained at σ_3=3.4 MPa and 6.2 MPa were 1.5% and 18% respectively. Therefore, changes in the rock stiffness as a function of the intermediate stress, was more significant in the sandstones than in the shales. Among the two shales, the elastic modulus of the Pierre Shale samples was more sensitive to σ_2 variations than that of the Carynginia Shale. Some potential explanations for such behaviour are discussed below.

Generally both strength and *E* in sandstones were found to be more prone to change as a function of σ_2 in comparison to the shales. Among the two shales, the strength and stiffness in the Pierre Shale showed more pronounced variations with σ_2, compared to the Carynginia Shale. Previous uniaxial and standard triaxial studies in the literature on shales (e.g. Lashkaripour and Dusseault 1993, Horsrud et al. 1998) and sandstones (e.g. Bradford et al. 1998, Palchik 1999) found good correlations between rock strength (UCS) and Young's modulus. In this study, it was also observed that variations in Young's modulus with applied stresses was in good agreement with the variations in strength (see Figure 5.10, Figure 5.30 and Figure 6.5), for each of the three tested rocks (except for the sandstones subjected to σ_3=2.3 and 6.3 MPa, probably as a result of variations in artificial cementation at grain

contacts). Therefore, the initial porosity which was believed to be responsible for strength behaviour in these rocks (section 6.3.1), can probably explain the Young's moduli measurements, as well. The stiffening impact of increasing σ_2 can be interpreted as a result of closure of pores or pre-existing microcrack in the rock (Oku et al. 2007). The higher initial porosity of sandstones resulted in more compaction in these samples as the intermediate stress increased, which caused their stiffness and strength to be more stress-sensitive. Among the shales, the Pierre Shale had higher inherent porosity than the Carynginia Shale that perhaps led to the observed more pronounced increase in its strength and Young's modulus by increasing σ_2.

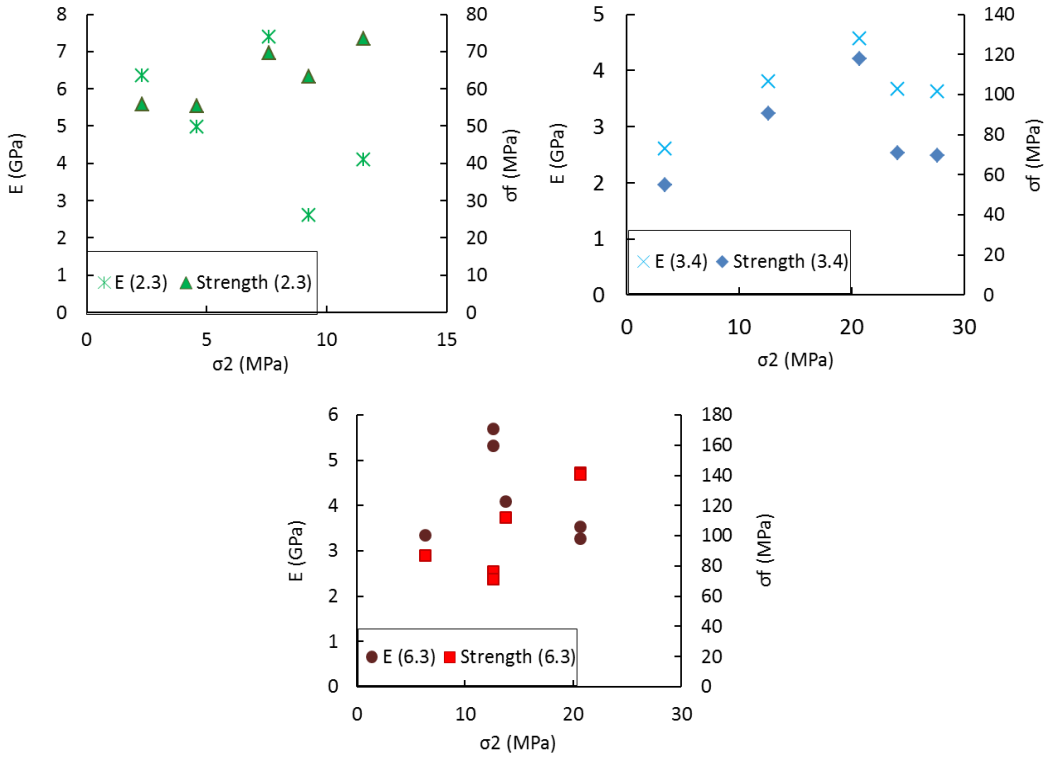

Figure 6.5 Comparing the variation of Young's modulus (E) and peak stress (σ_f) versus σ_2 in the synthetic sandstone samples. The value of the minimum stress for each group is shown in parentheses, in MPa. Only at σ_3=3.4 MPa the two parameters show similar trends of dependency on σ_2.

6.3.3 Dilatancy

The axial stress levels at the onset of dilatancy in the synthetic sandstones, the Carynginia Shale and the Pierre Shale were extracted in Table 4.4, Table 5.5 and Table 5.11, respectively. The dilatancy onset stress level as a percent of the peak stress was plotted against σ_2 value in Figure 6.6, for the three rock groups. For the

sandstone samples, the dilatancy could not be investigated in the samples tested at σ_3=6.3 MPa, due to inelastic compaction masking dilatancy at this stress state. The plots clearly show that by raising the σ_2 magnitude, the dilatancy onset as a ratio of the peak stress, increased similarly in all rock sets. Therefore, as was confirmed by previous studies for different rock types (e.g. Takahashi and Koide 1989, Haimson and Chang 2000, Oku et al. 2007, Mogi 2007), increasing the intermediate stress level above that of the minimum stress postponed the formation and growth of microcracks in the tested sandstones and shales in this work.

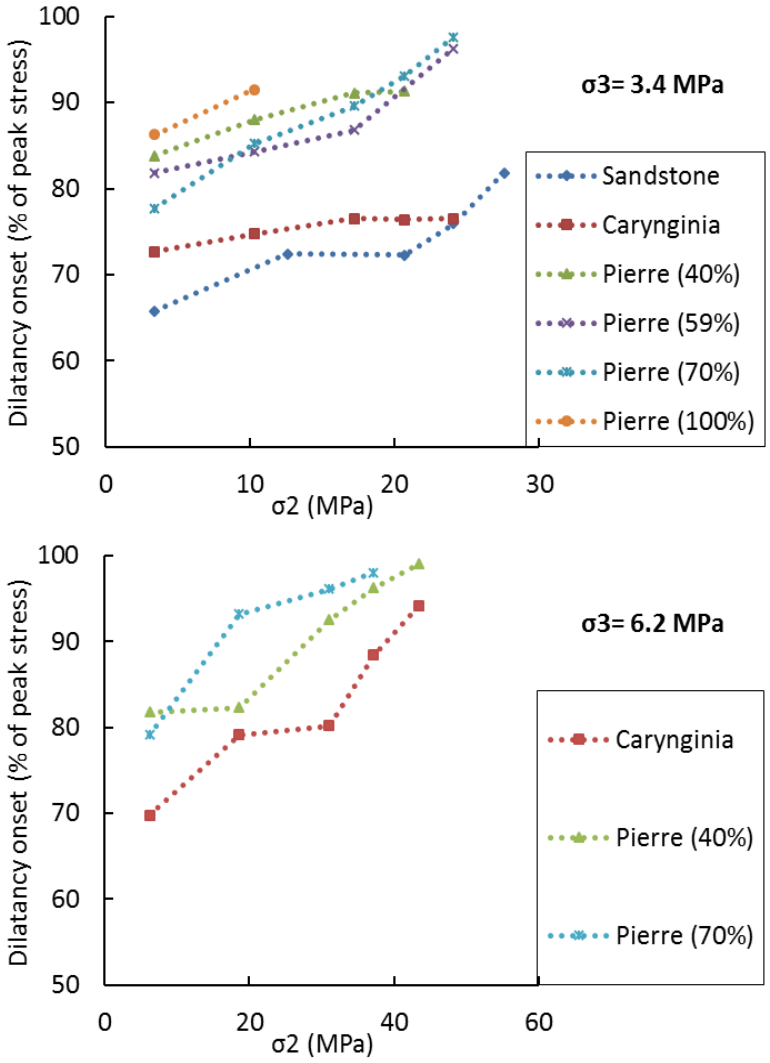

Figure 6.6 Variations of the dilatancy onset stress level as percentage of the peak stress against σ_2 value in the sandstones and the two shales. For the Pierre Shale specimens, the saturation level is shown by the numbers in parentheses. In all rock groups the dilatancy onset was postponed by increasing the σ_2 level.

In order to investigate the impact of σ_3 on rock dilatancy in true triaxial tests, the dilatancy data obtained at axisymmetric stress conditions ($\sigma_3=\sigma_2$) corresponding to two different levels of σ_3 are presented in Table 6.2. The axial stress level (σ_1) at the beginning of dilatancy and the dilatancy onset stress level as percentage of the peak stress ($\sigma_{1\text{-peak}}$), were compared for the three groups of rocks. The measurements indicate that increasing σ_3 resulted in an increase in the σ_1 level at the onset of dilatancy for all the samples. It has also caused a general increase in the dilatancy onset with respect to the peak stress. This indicates that increasing the minimum stress level retarded the onset of dilatancy in the tested rocks. It is well known from earlier studies (e.g. Paterson and Wong 2005) that increasing confining pressure in standard triaxial tests increases the absolute stress level at the onset of dilatancy and extends the elastic behaviour range. This effect has been found to be closely connected to the porosity in that reduction in porosity in porous rocks increases rock strength and extends the elastic range of rock behaviour (e.g. Matsushima 1960). Kwaśniewski et al. (2003) observed a similar impact of σ_3 on dilatant behaviour of a medium-grained sandstone tested under true triaxial stress conditions.

Table 6.2 The changes in dilatancy onset with σ_3 in the sandstone and shale samples expressed as the σ_1 level at the dilatancy beginning and the dilatancy onset stress level with respect to the peak stress ($\sigma_{1\text{-peak}}$). Measurements were done under axisymmetric conditions ($\sigma_3=\sigma_2$).

Rock	**S_w (%)**	**$\sigma_3 = \sigma_2$ (MPa)**	**$\sigma_{1\text{-peak}}$ (MPa)**	**σ_1 at onset of dilatancy (MPa)**	**Dilatancy level as % of $\sigma_{1\text{-peak}}$**
Sandstone	NA	2.3	58	31	53.1
		3.4	61	39.95	65.8
Carynginia Shale	NA	3.4	62	45.1	72.7
		6.2	80	55.8	69.8
Pierre Shale	40%	3.4	37	31	83.8
		6.2	55	45	81.8
	70%	3.4	35	27.2	77.7
		6.2	46	36.4	79.1

6.3.4 Fractures patterns and failure mode

Inspection of the post-test samples, revealed the presence of fault traces and failure planes on the rock faces in σ_2 direction which dipped towards the σ_3 direction for all the sandstone and shale specimens (see Figure 4.21, Figure 5.17 and Figure 5.41). This observation is consistent with earlier true triaxial studies on different rocks (see

Haimson 2006, Mogi 2007). In this section, the fracture patterns observed in the sandstone and the two shales are compared and the influence of stresses on evolution of failure behaviour is discussed.

Microscopical investigations in the literature (e.g. Dunn et al 1973) have shown that the micromechanical process of brittle failure, i.e. initiation and propagation of stress-induced microcracks which lead to macroscopic fractures in porous rocks such as sandstones are different from that of more compact rocks (see Paterson and Wong 2005). In porous sandstones, shear bands can form by coalescence of clusters of damage related to Hertzian fractures at grain contacts (Menéndez et al. 1996), whereas in more compact rocks, this process may involve transgranular cracking and microfracturing both within the matrix and within the grains (Paterson and Wong 2005). However, such micromechanical investigations were out of the scope of this study and recommended to be conducted in future. Here, failure patterns have been only discussed from the macroscopical point of view.

In the sandstones, at σ_3=3.4 MPa, fractures pattern evolved from dual to multiple parallel or conjugate shear fractures, which showed a change from the brittle to the transitional regime with increasing σ_2 (Paterson and Wong 2005). At σ_3=6.3 MPa, mainly dual sub-parallel or conjugate faults were observed accompanied by compaction bands at higher σ_2 levels, which indicated an evolution of the failure mode towards ductile field.

In Carynginia Shale, failure mainly occurred in the form of dual conjugate shear planes at σ_3=3.4 MPa, which evolved to quasi-parallel or conjugate multiple faults at σ_3=6.2 MPa. Increasing σ_2 tended to cause formation of small cracks and increased the number of fracture planes, which shows evolution of the failure mode from the brittle regime towards more transitional behaviour.

In Pierre Shale, under σ_3=3.4 MPa at different saturation states, failure mainly took the form of a shear zone of intense small fractures which is characteristic of the transitional brittle-ductile behaviour. The shear zones were generally narrowed as the magnitude of σ_2 increased and also some slip planes appeared in the specimens. This indicates that increasing σ_2 tended to gradually evolve the failure mode towards the brittle side of the transitional field. At σ_3=6.2 MPa, failure behaviour was substantially similar to that under σ_3=3.4 MPa, however the stress-strain curves in Figure 6.1 and Figure 6.2 show slightly smaller strains prior to macroscopic failure

for the tests at σ_3=3.4 MPa. This implies a gradual change in the failure behaviour towards the ductile field with increasing σ_3.

It was noted that the shear failure planes developed in Carynginia Shale samples were generally more sharply defined than the ones propagated in the sandstones or Pierre Shale. This can be related to the lower initial porosity of the Carynginia Shale and its more brittle nature. These characteristics could be also inferred from the stress-strain curves in Figure 6.1 and Figure 6.2. The curves show that the amount of strain that this shale has undergone prior to macroscopic fracture (peak stress) was generally smaller than that of the sandstones and of Pierre Shale. This may imply that the extent of microcracking and inelastic deformation was lower prior to failure which led to the faulting of the samples in the post-peak part to be more brittle and violent (Kwaśniewski et al. 2003, Paterson and Wong 2005).

It was further found that, in accordance with previous studies (e.g. Paterson and Wong 2005), an increase in σ_3 in these rocks generally tended to cause a gradual transition from brittle towards a transitional and more ductile behaviour. However, increasing σ_2 had different impacts on the behaviour of the three rock types. In the Carynginia Shale and the sandstones, increase in σ_2 tended to change the failure mode from brittle towards the transitional and ductile regime, while in Pierre Shale the effect was in the opposite direction, i.e. evolution towards the brittle side. In the sandstones, the mechanism responsible for the observed effect can be related to their high initial porosity. Hence, increase in σ_2 could favour a reduction in pore space and lead to inelastic compaction of the specimen, which was shown by the appearance of localized compaction bands at higher σ_2 levels. In Carynginia Shale, however, the initial porosity was much lower than that of the sandstones and hence this mechanism cannot explain the effect of σ_2 on failure evolution in these shales. There is a lack of evidence in the literature on the dependence of failure properties on the intermediate stress in shales. Hence, the mechanism responsible for this behaviour in Carynginia Shale is unknown and would require more investigation.

In the Pierre Shale, increasing σ_2 tended to gradually push the failure mode towards the brittle field. This behaviour is supported by earlier findings of true triaxial investigations on some other porous rocks (e.g. Takahashi and Koide 1989, Ma 2014). This effect is due to the tendency of increasing σ_2 to restrict the microcracking process (Kwaśniewski et al. 2003). The higher intermediate stresses

retard deformation parallel to the σ_2 axis and result in propagation of microcracks that lead to macroscopic fractures along the σ_3 direction (see Mogi 2007).

For all three rock groups, the main faults had irregular surfaces with small asperities and were generally curved and branched. Consequently, investigations on the angle of the failure planes were impractical.

6.4 Summary

The deformational mechanical properties of the synthetic sandstones, the Carynginia Shale and the Pierre Shale samples, when subjected to similar true triaxial stress conditions, were compared in this Chapter. Following is a summary of the findings of this study:

- The sandstone samples tested in this work showed noticeably higher strengths in comparison to the shales. This is likely the result of being composed of rigid minerals such as quartz while the major constituents of these shales are clay minerals which typically are weaker. Between the two shales, the Carynginia Shale samples had higher strength than the Pierre Shale specimens. The lower strength of Pierre Shale can be related to its higher initial porosity and higher degree of water saturation.

- The Carynginia Shale samples were the most brittle specimens among the three rock groups. This is probably related to their initial porosity being lower than the sandstones and the Pierre Shale and also drying out of its constituent clay minerals as these shales were not well-preserved.

- Generally, the strength and Young's modulus of the sandstones was found to be more sensitive to stress variations, in comparison to the two shales. This is likely to be related to the sandstones having the highest porosity of the tested rocks. This resulted in more compaction in the rock due to the increase in σ_2 and hence the mean stress. Consequently, due to increasing σ_2, a larger increase in sandstone strength and stiffness occurred.

- Among the two shale groups, the strength and stiffness of the Carynginia Shale were less prone to change with σ_2. This is because it was significantly stiffer than the Pierre Shale and again due to its lower initial porosity. In Pierre Shale, the higher porosity led to more compaction through increasing σ_2, which resulted in

more pronounced increase in the strength and Young's modulus, in comparison to Carynginia Shale.

- Increasing the intermediate stress raised the stress level at the onset of dilatancy for all rock groups. This indicates that the supporting effect of σ_2 on rock postponed propagation of microcracks and the initiation of the failure process.
- Investigations on the post-test specimens indicated different fracture patterns and failure modes under similar stress conditions. Increasing σ_3 generally shifted the rock failure behaviour towards the ductile field in these rocks. In the sandstones and Carynginia Shale, increasing σ_2 tended to evolve the rock failure mode in a similar fashion to increasing σ_3. The mechanism responsible for such an effect was probably initial high porosity in sandstones which resulted in inelastic compaction under higher stresses. However, the mechanism in Carynginia Shale is unclear. In Pierre Shale, increasing σ_2 led to the evolution of failure mode to more brittle behaviour.
- It was found that the differences in the mechanical response of the tested shales and sandstone to similar true triaxial stress conditions could be associated with some of their intrinsic physical properties, such as porosity, grain size, composition and saturation state. Initial higher porosity in sandstones made their failure properties more sensitive to variations of applied stresses. In Carynginia Shale, however, the lowest porosity among the three rocks resulted in its properties to be less prone to changes with increasing stresses. The lower stiffness and strength measured in Pierre Shale in comparison to two other rocks, is associated with not only the initial porosity, but also with the presence of water (through capillary effects). However, more detailed investigations would be required to better understand the relation between the mechanical responses of these rocks with their physical characteristics.

In the next Chapter the most important conclusions of the experimental studies carried out in this work will be reviewed and some future research directions will be suggested.

7 Conclusions and recommendations

The primary objective of this thesis was to investigate the dependence of failure characteristics and mechanical behaviour of sandstones and shales on principal stress magnitudes, under 3D stress conditions. To reach this goal, a laboratory procedure was established and several sandstone and shale samples were subjected to isotropic to anisotropic 3D stress states in a true triaxial stress cell. A suite of well-preserved shale specimens was also used for the purpose of evaluating the influence of varying degrees of water saturation on the mechanical response of shales. In addition, a multistage true triaxial testing technique was evaluated in this thesis for determining the effect of intermediate stress on rock mechanical behaviour. The reliability of this method was examined by comparing the results of such tests on synthetic sandstones with the results of single-stage true triaxial tests. The following sections summarize the most important findings and conclusions of the present study. At the end, some future research directions are recommended.

7.1 True triaxial failure strength

- **Impact of σ_2 and σ_3 on compressive strength:** The laboratory measurements suggest that compressive strength of porous sandstones and shales is affected by absolute levels of both minimum and intermediate principal stresses. In true triaxial tests, raising the σ_3 level increased the measured rock strength in a similar fashion to trends normally observed in conventional triaxial testing of rocks. The amount of respective increase in the strength of sandstones, Carynginia Shale and Pierre Shale were up to 104%, 45% and 67%. Increasing the σ_2 magnitude from a conventional triaxial stress state ($\sigma_1>\sigma_2=\sigma_3$) to a true triaxial stress state ($\sigma_1>\sigma_2>\sigma_3$) also markedly affected the measured rock strength, which was in accordance with earlier true triaxial studies on different rock types. It was found that increasing σ_2 at a constant σ_3, led to a maximum of 110%, 27% and 67% growth in the measured strength value for the sandstones, the Carynginia Shale and the Pierre Shale, respectively. The

strengthening effect of σ_2 in these rocks revealed the drawback of conventional triaxial tests where this influence is overlooked.

- **Extent of stress-dependency of strength:** The measurements revealed that the strength of the synthetic sandstones was more sensitive to changes in the applied stresses compared to the tested shales. Among the two shales, the strength in the Pierre Shale samples was more prone to change with increased stresses than the strength of Carynginia Shale. The extent of stress-dependency of strength was found to be closely associated with initial porosity. This is due to the compaction that occurs in the rock under stress, which is larger in rocks with higher porosities. The tested sandstones had the highest initial porosity (26%) among the three rock groups, and therefore their strength was more prone to change with variations of σ_2 and σ_3. The Carynginia Shale had the lowest porosity (<4%) and the lowest sensitivity to the applied stresses.
- **True triaxial failure criterion:** For the sandstones, Carynginia Shale and Pierre Shale, the obtained failure stress measurements fit best to a Mogi-type 3D failure criterion in τ_{oct}–$\sigma_{m,2}$ domain, which was represented by a power law function. Further experiments at higher minimum and intermediate stresses would be required to determine a more complete failure envelope for these rocks.

7.2 Elastic properties

- **Young's modulus:** It was found that the measured Young's modulus in the studied sandstones and shales was a function of the intermediate principal stress. Increasing stress anisotropy from 1 ($\sigma_2=\sigma_3$) to higher levels ($\sigma_2>\sigma_3$) at a given σ_3, resulted in a maximum of 75%, 53% and 18% increase in stiffness of the sandstones, Pierre Shale and Carynginia Shale respectively. It was further revealed that variations of stiffness against σ_2 was similar to that of rock strength. However, some synthetic sandstones tested under σ_3=2.3 MPa and 6.3 MPa did not show the similarity in dependency on σ_2 for elastic modulus and strength, which could be due to the heterogeneity in cementation at grain contacts. The obtained general similarity in the response of Young's modulus and strength to σ_2 is in a good agreement with findings of very few true triaxial

studies on stiffness of some other rock types. However, no true triaxial investigations have been performed on this relation in sandstones and shales in the past.

- **Extent of stress-dependency of rock stiffness:** It was evident that changes in the rock stiffness as a function of the intermediate stress, was more significant in the sandstones than in the tested shales. Among the two shales, the elastic modulus of Pierre Shale was more sensitive to σ_2 variations than that of the Carynginia Shale. As known well from earlier uniaxial and conventional triaxial studies and also found here under true triaxial stress states, the variations of strength and stiffness in sandstones and shales are in good agreement. Thus it was inferred that initial porosity is a major controlling parameter in defining the degree of stress-dependency of rock stiffness in a similar manner to that of the rock strength. The higher initial porosity of the sandstones resulted in more compaction in these samples by increasing the intermediate stress level, which caused their stiffness to be more stress-sensitive. Among the shales, the Pierre Shale had higher inherent porosity than the Carynginia Shale which led to more pronounced increase in their Young's modulus by increasing σ_2.

- **Poisson's ratio:** As two unequal lateral stresses were applied on rock samples in the true triaxial tests, two different values of Poisson's ratio were extracted for each sample: ν_{12} along the intermediate principal stress axis and ν_{13} along the minimum principal stress axis. The measurements of the Poisson's ratios in the high porosity synthetic sandstones showed values higher than 0.5 in some cases and hence in terms of absolute values, these measurements were not reliable. Thus any conclusions with regards to the Poisson's ratios are based on relative variations not absolute values. It was found that ν_{13} was significantly larger than ν_{12} in all samples. It signifies that the intermediate stress restrained the rock deformation in σ_2 direction and consequently imposed more strain along σ_3 direction. With regards to the impact of changing σ_2 and σ_3 on the Poisson's ratios in sandstones and shales, no general conclusion could be drawn in this study due to the insufficient experimental data points and lack of relevant evidence in the literature.

7.3 Inelastic deformation and dilatancy

- **Inelastic deformation:** In all three rock groups, increasing the intermediate principal stress magnitude beyond the axisymmetric stress level, gradually changed deformation along the σ_2 axis from larger extensional strains towards considerably smaller compressive displacements. This confirmed that increasing σ_2 above σ_3 arrested the development of microcracks in σ_2 direction and imposed rock dilation along the direction of minimum stress. Such effect of lateral stress anisotropy on rock deformation has been also documented by earlier true triaxial studies on different rock types.

- **Dilatancy onset:** It was found that in all the rock sets, increasing the magnitude of σ_2 at a specific level of σ_3, raised the onset of dilatancy relative to the peak stress. This signifies the strengthening effect of the intermediate stress on rock which postponed the development of microcracks and hence retarded the onset of the brittle failure process in rock, as also suggested by previous true triaxial investigations on sandstones. However, studies on the evolution of dilatancy onset with σ_2 have been rare for shales. It was found that for the sandstone samples tested under σ_3=6.3 MPa, inelastic compaction of these high porosity sandstones masked any noticeable dilatancy on the volumetric strain curves. By comparing the dilatancy onset levels obtained under axisymmetric conditions (σ_2=σ_3) in the sandstones and shales, it was evident that increasing σ_3 under true triaxial conditions increased the absolute stress level at the onset of dilatancy and hence delayed the dilatancy in the tested rocks. This is in accord with earlier findings on the influence of confining pressure on dilatancy in conventional triaxial tests, which is closely connected to the increase in rock strength due to the reduction in porosity for porous specimens as a result of increasing σ_3.

7.4 Fractures patterns and failure mode

- **Fractures pattern in sandstones:** In the sandstone samples, failure generally took the form of dual main faults at the lowest σ_3 level, which evolved to dual to multiple quasi-parallel and conjugate faults at σ_3=3.4 MPa. This behaviour identifies the upper part of the brittle range and a shift towards the transitional

brittle-ductile field due to increase in σ_3. At σ_3=6.3 MPa, some localized compaction bands appeared along with the shear fractures at the highest σ_2 levels. This was also observed from the stress-strain curves by ductile behaviour and strain hardening due to the dominant inelastic compaction.

- **Fractures pattern in Carynginia Shale:** In Carynginia Shale specimens, failure mainly occurred in the form of dual conjugate shear planes at σ_3=3.4 MPa, which evolved to quasi-parallel or conjugate multiple faults at σ_3=6.2 MPa. Therefore, failure occurred in a brittle manner and then gradually evolved to the transitional brittle-ductile field. Increasing σ_2 tended to cause a shift towards a transitional failure mode through the formation of small cracks and an increase in the number of fractures. The shear fractures in Carynginia Shale samples were noted to be more sharply defined than the ones propagated in the sandstones and Pierre Shale. This was likely to be the result of lower initial porosity and more brittle intrinsic properties of this shale. This was also implied by the smaller strains prior to macroscopic failure and the more distinct stress drop at the peak from the stress-strain curves.

- **Fractures pattern in Pierre Shale:** In majority of the Pierre Shale samples tested under σ_3=3.4 MPa, failure took the form of a shear zone of intense small sub-parallel fractures which is a characteristic of the transitional brittle-ductile behaviour. The shear zone generally narrowed as the magnitude of σ_2 increased and also some slip planes appeared in the specimens, which indicates a tendency towards the brittle side of the transitional field. At σ_3=6.2 MPa, the failure behaviour was substantially similar to that under σ_3=3.4 MPa, however the stress-strain curves showed slightly smaller strains prior to the macroscopic failure in the latter. This implies a gradual change in the failure behaviour towards a ductile field as σ_3 increases.

- **Stress-dependency of failure mode:** It was found that increases in σ_3 generally tended to cause a gradual evolution from brittle towards transitional and more ductile behaviour in these rocks, which was in accordance with the impact of σ_3 in previous conventional triaxial and true triaxial tests. Whereas, increasing σ_2 at a constant σ_3 had different impacts on the behaviour of the three rock types. In the sandstones and Carynginia Shale, increasing σ_2 tended

to change the rock failure mode in similar fashion to increasing σ_3, i.e. towards the ductile field. The mechanism responsible for such an effect was probably the high initial porosity in the sandstones, which resulted in inelastic compaction under higher stresses. It was inferred that the effect of porosity and stress-induced compaction in very porous sandstones may control the influence of σ_2 as to whether it embrittles the rock or pushes the failure mode in the opposite direction (towards a ductile mode). Hence, these observations confirmed the important role of porosity on failure characteristics of porous rocks such as sandstones. However, the mechanism for the observed failure evolution in Carynginia Shale is unclear and requires further investigation through more true triaxial experiments. In Pierre Shale, increasing σ_2 led to an evolution in the failure mode to more brittle behaviour, which is consistent with previous findings on some other porous rocks and is explained through the tendency of increasing σ_2 to restrict the microcracking process in rock.

- **Failure-plane angle:** Images of the failed specimens of the sandstone and the two shales indicated that the faults and fractures traces on the sample faces normal to the applied σ_2 direction were roughly symmetrical and they typically strike along the σ_2 axis under true triaxial stress conditions. For all three rock groups, the main faults generally had curved and branched surfaces and showed some small asperities. Consequently, investigations on the angle of failure plane were impractical in this study.

7.5 Saturation impact in Pierre Shale

- **Effect on strength:** The laboratory measurements revealed that reduction in water saturation in Pierre Shale markedly influenced the true triaxial compressive strength. The results of this study support the earlier findings on the effect of water saturation on strength of shales under uniaxial and conventional triaxial conditions. It was evident that decreasing water saturation resulted in an overall increase in the measured peak stresses, probably through increasing capillary suction. Decreases in water content from fully-saturated to partially-saturated states, caused up to 38 MPa growth in the strength of these shales, which is equivalent to a significant ~223% increase in the magnitude of strength.

- **Effect on stiffness:** It was found that decreasing the water saturation generally increased the Young's modulus in Pierre Shale subjected to true triaxial stress conditions. Laboratory measurements of the static Young's modulus resulted in a 3-fold increase in stiffness of Pierre Shale due to reduction in water saturation from 100% to 40%. Such an effect of desiccation on shales stiffness has been previously documented by other researchers, although only under uniaxial and conventional triaxial stress conditions. This behaviour has been explained through the intergranular cohesion and increased effective stress generated by capillary forces in the rock under partial saturation states.
- **Effect on Poisson's ratios:** Our measurements indicated that both Poisson's ratios obtained under true triaxial stress states (ν_{12} and ν_{13}) are affected by the water saturation degree in Pierre Shale. In tests under σ_3=6.2 MPa, decreasing the saturation caused reduction in both ν_{12} and ν_{13}. However, for tests under σ_3=3.4 MPa such a simple relationship could not be established. The results are generally consistent with the earlier findings on the impact of water saturation on static and dynamic Poisson's ratio under conventional triaxial stress states.
- **Effect on dilatancy:** It was found that at lower water saturations, the stress level at the onset of dilatancy was generally higher. This is perhaps due to the strengthening effect of the induced suction forces as shales lose water during drying, which consequently impeded the beginning of the failure process in the rock. Such an impact is in good agreement with the findings of conventional triaxial investigations in shales.

7.6 Multistage true triaxial tests

- The reliability of multistage true triaxial technique in evaluating the σ_2 impact on rock mechanical properties of synthetic sandstones was investigated in this study. Comparing the results of the multistage true triaxial tests on the synthetic sandstones with the equivalent single-stage measurements revealed that there are significant differences between the resultant rock strengths and elastic properties.
- Young's moduli increased systematically with increasing σ_2 in multistage true triaxial tests, while single-stage true triaxial test results are more scattered; in

addition, *E* was usually higher in absolute magnitude in the multistage tests than for single stage tests. Furthermore, the multistage rock strength results were not consistent with the single-stage measurements and generally gave lower measured values. A potential explanation for this observation is that compaction in these porous specimens occurred through a number of loading-unloading cycles under true triaxial conditions which stiffened the rock through porosity reduction but reduced the strength as a result of cement breakage at grain contacts.

- Multistage true triaxial tests, based on the applied loading path and the employed detection method for the termination points (which was subjective), were found to be inappropriate for obtaining rock mechanical properties in the synthetic sandstone samples. Thus this approach is not recommended for investigating the impact of σ_2 on strength and deformational behaviour of weak porous rocks such as these sandstones and needs to be studied further in regard to other rock types.

7.7 Recommendations for future work

In this section some potential research directions for further investigations are suggested:

- The current study showed the influence of σ_2, as well as σ_3, on mechanical response of the sandstones and shales. The number of obtained data points for each rock type was, however, insufficient to achieve general correlations between their strength, deformational properties and failure characteristics with the principal stresses. The reason was firstly due to the limited available specimens, which allowed applying only 2-3 different levels of minimum stress for each rock type; secondly, at each level of σ_3, the range of applied σ_2 values were not wide enough. Future true triaxial experiments can be performed on these sandstones and Carynginia Shale and Pierre Shale under higher levels of both σ_2 and σ_3, to draw more general conclusions with regards to the dependency of different rock parameters such as strength, Young's modulus, Poisson's ratios and failure mode on principal stresses. Also, if a more complete suite of strength measurements are gathered a general 3D failure envelope can be established for each of the rocks under study.

- In the present study, investigations of the failure mode and fracture patterns in the specimens were conducted based on macroscopic visual observations. Microstructural studies can provide valuable information about the failure process and deformational characteristics of rocks. The samples used in this study have not been preserved in epoxy after the mechanical tests and hence would not be good candidates for microstructural studies of failure. It is recommended that for potential future true triaxial tests on the sandstones and shales used in this work, micromechanical investigations would be performed to provide a better understanding of the failure process, characteristics of the induced deformation, failure mode, microstructural damage, for example.

- The true triaxial tests conducted in this work were performed under stress-controlled conditions due to the technical limitations of the experimental setup. Based on such experiments, the behaviour of the rock up to the peak point, where macroscopic failure occurs, can be investigated. However, after the rock is fractured, the rate of deformation would be fast and cannot be controlled and thus such tests does not provide the possibility of investigations on post-peak behaviour of the rock. It is recommended that true triaxial tests under strain-controlled conditions be performed on these sandstones and shales to study their post-failure response, such as residual strength and evolution of rock inelastic deformation along the principal directions after the macroscopic failure took place. Acoustic emission (AE) measurements can also be employed during true triaxial tests for monitoring the process of crack nucleation, growth, propagation and coalescence.

- In the present study, graphite powder was used at the interface of rock samples and the metal shims to reduce the frictional end effects. It is recommended that direct shear tests would be performed with and without the graphite on the samples to precisely measure the frictional forces and also to compare the efficiency of this approach in removing frictional effects in comparison to other techniques such as the use of Teflon sheets and stearic acid.

- The tests on the Pierre Shale and Carynginia Shale were conducted with the maximum principal stress axis normal to the bedding direction. True triaxial tests can be performed on these rocks with various σ_1 and also σ_2 orientations with respect to the bedding direction (e.g. both σ_1 and σ_2 parallel to bedding;

σ_1 parallel and σ_2 normal to bedding; both σ_1 and σ_2 in an angle to bedding). Thus the anisotropy of strength and failure properties of the rocks could be investigated.

- This study has been perhaps the first to investigate the influence of water saturation on mechanical properties of shales under true triaxial stress states, and was conducted using a limited number of available preserved Pierre Shale specimens. It is advisable to conduct more true triaxial tests on the Pierre Shale samples with various saturation degrees from to ~0% to ~100%, at wider ranges of lateral stresses to illuminate the correlation of the failure properties of the shale with water saturation level. For the saturation levels close to full-saturation, pore pressure should be measured during the tests to obtain effective stresses.

- Comparing the results of multistage true triaxial tests on the synthetic sandstones with the equivalent single-stage tests revealed that such technique is probably inappropriate in case of these weak porous sandstones. The validity of true triaxial multistage testing in evaluating the variations of failure properties of rock with σ_2, should be examined in greater detail in the future through conducting tests under wider ranges of stresses and on other rock types (perhaps less porous and more compact). It was further found that manual detection of deviation of stress-strain curves was not an ideal criterion for terminating the stages, due to the subjectivity of the method. Hence, an alternative method should be sought for defining the termination points in future work. Measurements of acoustic wave velocities during multistage true triaxial experiments are also recommended for future investigations in order to shed more light on the timing and mechanism of microcrack propagation during such tests. Moreover, detailed theoretical analysis could be performed to model the formation and development of stress-induced microcracks under cyclic loading in the σ_2 direction, during a multistage true triaxial test.

References

Amadei, B. 1996. Importance of anisotropy when estimating and measuring in situ stresses in rock. Paper read at International journal of rock mechanics and mining sciences & geomechanics abstracts.

Amadei, B., W.Z. Savage, and H.S. Swolfs. 1987. Gravitational stresses in anisotropic rock masses. Paper read at International Journal of Rock Mechanics and Mining Sciences & Geomechanics Abstracts.

Amann, Florian, Peter Kaiser, and Edward Button. 2012. "Experimental Study of Brittle Behavior of Clay Shale in Rapid Triaxial Compression." *Rock Mechanics and Rock Engineering* no. 45 (1):21-33. doi: 10.1007/s00603-011-0195-9.

Barnard, P. R. 1964. "Researches into the complete stress-strain curve for concrete." *Mag. Concr. Res.* no. 16:203–10.

Bésuelle, P., and S. A. Hall. 2011. "Characterization of the Strain Localization in a Porous Rock in Plane Strain Condition Using a New True-Triaxial Apparatus." In *Advances in Bifurcation and Degradation in Geomaterials*, edited by Stéphane Bonelli, Cristian Dascalu and François Nicot, 345-352. Netherlands: Springer Netherlands.

Bieniawski, ZT. 1968. Propagation of brittle fracture in rock. Paper read at The 10th US Symposium on Rock Mechanics (USRMS).

Blatt, H., R.J. Tracy, and B. Owens. 2006. *Petrology: igneous, sedimentary, and metamorphic*: Macmillan.

Blumling, T., H.J. Alheid, C. Plaindoux, M. Fukaya, and J.C. Mayor. 2002. "Geomechanical investigations at the underground rock laboratory Mont Terri." In *Hydromechanical and thermohydromechanical behaviour of deep argilaceous rock:Theory & experiments*, edited by N. Hoteit, K. Su, M. Tijani and J. F. Shao. Swets & Zeitlinger.

Böker, R. 1915. "Die Mechanik der bleibenden Formänderung in kristallinisch aufgebauten Körpern." *Verhandl. Deut. Ingr. Mitt. Forsch.* no. 175:1-51.

Boyer, C., J. Kieschnick, R. Suarez-Rivera, R. Lewis, and G. Walter. 2006. "Producing gas from its source." *Oilfield Review* no. 18 (3):36-49.

Brace, W. F. 1964. "Brittle fracture of rocks." In *State of Stress in the Earth's Crust*, edited by W.R Judd, 111–174. New York: Elsevier.

Brace, W.F., B.W. Paulding, and C.H. Scholz. 1966. "Dilatancy in the fracture of crystalline rocks." *Journal of Geophysical Research* no. 71 (16):3939-3953.

Brace, WF, and DL Kohlstedt. 1980. "Limits on lithospheric stress imposed by laboratory experiments." *Journal of Geophysical Research: Solid Earth (1978–2012)* no. 85 (B11):6248-6252.

Bradford, I.D.R., J. Fuller, P.J. Thompson, and T.R. Walsgrove. 1998. Benefits of assessing the solids production risk in a North Sea reservoir using elastoplastic modelling. In *SPE/ISRM Eurock '98 held in Trondheim*. Norway.

Bresler, B., and K.S. Pister. 1957. "Failure of plain concrete under combined stresses." *Transactions of the American Society of Civil Engineers* no. 122 (1):1049-1059.

Chang, C., and B. Haimson. 2000. "True triaxial strength and deformability of the German Continental Deep Drilling Program (KTB) deep hole amphibolite." *Journal of Geophysical Research* no. 105 (B8):18,999-19,014.

Chang, C., and B. Haimson. 2005. "Non-dilatant deformation and failure mechanism in two Long Valley Caldera rocks under true triaxial compression." *International Journal of Rock Mechanics and Mining Sciences* no. 42 (3):402-414.

Chang, C., M.D. Zoback, and A. Khaksar. 2006. "Empirical relations between rock strength and physical properties in sedimentary rocks." *Journal of Petroleum Science and Engineering* no. 51 (3):223-237.

Chau, K. T. . 1997. "Young's modulus interpreted from compression tests with end friction." *J. Eng. Mech.* no. 123:1-7.

Colmenares, LB, and MD Zoback. 2002. "A statistical evaluation of intact rock failure criteria constrained by polyaxial test data for five different rocks." *International Journal of Rock Mechanics and Mining Sciences* no. 39 (6):695-729.

Cook, N . G.W. (1962). . 1962. *A Study of Failure in the Rock Surrounding Underground Excavations*. Ph.D. thesis, University of Witwatersrand, Johannesburg.

Corkum, A. G., and C. D. Martin. 2007. "The mechanical behaviour of weak mudstone (Opalinus Clay) at low stresses." *International Journal of Rock Mechanics and Mining Sciences* no. 44 (2):196-209. doi: 10.1016/j.ijrmms.2006.06.004.

Crawford, A.M., and D.A. Wylie. 1987. A modified multiple failure state triaxial testing method. Paper read at The 28th U.S. Symposium on Rock Mechanics (USRMS), June 29 - July 1, 1987, at Tucsan, AZ.

Crawford, BR, BGD Smart, IG Main, and F Liakopoulou-Morris. 1995. Strength characteristics and shear acoustic anisotropy of rock core subjected to true triaxial compression. Paper read at International Journal of Rock Mechanics and Mining Sciences & Geomechanics Abstracts.

Delle Piane, C., DN Dewhurst, AF Siggins, and MD Raven. 2011. "Stress induced anisotropy in brine saturated shale." *Geophysical Journal International* no. 184 (2):897-906.

Dewhurst, D.N., B. Maney, B. Clennell, C. Delle Piane, C. Madonna, E.H. Saenger, and N. Tisato. 2012. Impact of Saturation Change on Shale Properties. In *3rd EAGE Shale Workshop - Shale Physics and Shale Chemistry*. Barcelona, Spain: EAGE.

Dewhurst, D.N., V. Minaeian, C. Delle Piane, M. Josh, L. Esteban, J. Sarout, and B. Clennell. 2013. Geomechanics and Petrophysics of Partial Saturation in Shales. Paper read at Houston Geological Society Conference on Micro to Macro Geomechanics For Unconventional Resources, at Houston, Texas.

Dewhurst, D.N., J. Sarout, C. Delle Piane, A.F. Siggins, M.D. Raven, and U. Kuila. 2010. Prediction of shale mechanical properties from global and local empirical correlations. Paper read at 2010 SEG Annual Meeting.

Dewhurst, D.N., A.F. Siggins, J. Sarout, M.D. Raven, and H.M. Nordgård-Bolås. 2011. "Geomechanical and ultrasonic characterization of a Norwegian Sea shale." *Geophysics* no. 76 (3):WA101-WA111.

Drucker, D.C., and W. Prager. 1952. "Soil mechanics and plastic analysis or limit design." *Quart. Appl. Math.* no. 10:157–165.

Dunn, D.E., L.J. LaFountain, and R.E. Jackson. 1973. "Porosity dependence and mechanism of brittle fracture in sandstones." *Journal of Geophysical Research* no. 78 (14):2403-2417.

Ewy, Russell. 1998. Wellbore stability predictions using a modified Lade criterion. Paper read at Proceedings of Eurock 98: SPE/ISRM Rock Mechanics in Petroleum Engineering.

Filon, L.N.G. 1902. "On the elastic equilibrium of circular cylinders under certain practical systems of load." *Philosophical Transactions of the Royal Society of London. Series A, Containing Papers of a Mathematical or Physical Character* no. 198:147-233.

Fjær, E., R.M. Holt, A.M. Raaen, R. Risnes, and P. Horsrud. 2008. *Petroleum related rock mechanics*. 2 ed: Elsevier Science.

Freudenthal, A. 1951. The inelastic behavior and failure of concrete. Paper read at Proceedings, First US National Congress of Applied Mechanics.

Fuenkajorn, Kittitep, Tanapol Sriapai, and Pichit Samsri. 2012. "Effects of loading rate on strength and deformability of Maha Sarakham salt." *Engineering Geology* no. 135–136 (0):10-23.

Gautam, Rajeeb. 2005. *Anisotropy in deformations and hydraulic properties of Colorado shale*. NR04595, University of Calgary (Canada), Canada.

Ghorbani, A, M Zamora, and P Cosenza. 2009. "Effects of desiccation on the elastic wave velocities of clay-rocks." *International Journal of Rock Mechanics and Mining Sciences* no. 46 (8):1267-1272. doi: 10.1016/j.ijrmms.2009.01.009.

Gräsle, W. 2011. "Multistep triaxial strength tests: Investigating strength parameters and pore pressure effects on Opalinus Clay." *Physics and Chemistry of the Earth, Parts A/B/C*.

Greenberg, H. J. , and R. Truell. 1948. "On a problem in plane strain." *Q. Appl. Math.* no. 6:53-62.

Haimson, B. 2006. "True triaxial stresses and the brittle fracture of rock." *Pure and Applied Geophysics* no. 163:1101-1130.

Haimson, B., and C. Chang. 2000. "A new true triaxial cell for testing mechanical properties of rock, and its use to determine rock strength and deformability of Westerly granite." *International Journal of Rock Mechanics and Mining Sciences* no. 37 (1–2):285-296. doi: 10.1016/s1365-1609(99)00106-9.

Haimson, B.C. 1978. The hydrofracturing stress measuring method and recent field results. Paper read at International Journal of Rock Mechanics and Mining Sciences & Geomechanics Abstracts.

Handin, J., HC Heard, and JN Magouirk. 1967. "Effects of the intermediate principal stress on the failure of limestone, dolomite, and glass at different temperatures and strain rates." *Journal of Geophysical Research* no. 72 (2):611-640.

Head, K.H. 1980. *Manual of Soil Laboratory Testing, Volume 1: Soil Classification and Compaction Tests*. Vol. 1: Pentech Press.

Holt, A.M., and E.M. Fjær. 1991. Validity of Multiple Failure State Triaxial Tests In Sandstones. Paper read at Proc. VII Int. Congress on Rock Mechanics, at Aachen.

Horsrud, P. 2001. "Estimating mechanical properties of shale from empirical correlations." *SPE Drilling & Completion* no. 16 (2):68-73.

Horsrud, P., E.F. Sønstebø, and R. Bøe. 1998. "Mechanical and petrophysical properties of North Sea shales." *International Journal of Rock Mechanics and Mining Sciences* no. 35 (8):1009-1020.

Ingraham, M.D. 2012. *Investigation of Localization and Failure Behavior of Castlegate Sandstone Using True Triaxial Testing*, Clarkson University.

Ingraham, M.D., K.A. Issen, and D.J. Holcomb. 2013. "Response of Castlegate sandstone to true triaxial states of stress." *Journal of Geophysical Research: Solid Earth* no. 118 (2):536-552.

Jaeger, J. C. , N. G.W. Cook, and R. W. Zimmerman. 2007. *Fundamentals of Rock Mechanics*. 4th ed: Blackwell Publishing.

Kim, M. M., and H. Y. Ko. 1979. "Multistage triaxial testing of rocks." *Geotechnical testing journal* no. 2 (2):98-105.

Kovari, K, and A Tisa. 1975. "Multiple failure state and strain controlled triaxial tests." *Rock mechanics* no. 7 (1):17-33.

Kovari, K., A. Tisa, HH Einstein, and JA Franklin. 1983. "Suggested methods for determining the strength of rock materials in triaxial compression: revised version." *International Journal of Rock Mechanics and Mining Sciences* no. 20 (6):283-290.

Kwaśniewski, M, and K Mogi. 1990. Effect of the intermediate principal stress on the failure of a foliated anisotropic rock. Paper read at Proceeding of International Conference of Mechanics of Jointed and Faulted Rock, at rotterdam, Balkema.

Kwaśniewski, M., M. Takahashi, and X. Li. 2003. Volume changes in sandstone under true triaxial compression conditions. Paper read at In ISRM 2003 – Technology Roadmap for Rock Mechanics; Proc. 10th Int. Congr. Rock Mech., 8–12 September, at Sandton.

Kwaśniewski, M.A., and K. Mogi. 1996. "Faulting of a foliated rock in a general triaxial field of compressive stresses." In *Tectonophysics of Mining Areas*, edited by A. Idziak, 209–232. Uniwersytet Śląski.

Kwaśniewski, M.A., and K. Mogi. 2000. Faulting in an anisotropic, schistose rock under general triaxial compression. Paper read at Pacific Rocks 2000, Proceedings of the 4th North American Rock Mechanics Symposium, 31 July-3 August, at Seattle, Washington.

Labuz, J . F., and J . M. Bridell. 1993. "Reducing frictional constraint in compression testing through lubrication." *Int. J. Rock Mech.* no. 30:451–55.

Lade, P.V., and J.M. Duncan. 1975. "Cubical triaxial tests on cohesionless soil." *Journal of the Soil Mechanics and foundations Division* no. 99 (10):793-812.

Laloui, L., S. Salager, M. Nuth, and P. Marschall. 2010. Anisotropic Mechanical Response of a Shale. Paper read at EAGE Shale Workshop 2010.

Laloui, L., S. Salager, and M. Rizzi. 2013. "Retention behaviour of natural clayey materials at different temperatures." *Acta Geotechnica* no. 8 (5):537-546.

Laloui, Lyesse. 2010. *Mechanics of unsaturated geomaterials*: ISTE.

Lashkaripour, G.R., and M.B. Dusseault. 1993. "A statistical study on shale properties: Relationships among principal shale properties." In *Probabilistic Methods in Geotechnical Eng.*, edited by Li and Lo. The Netherlands.

Lee, Hikweon, and Bezalel C. Haimson. 2011. "True triaxial strength, deformability, and brittle failure of granodiorite from the San Andreas Fault Observatory at Depth." *International Journal of Rock Mechanics and Mining Sciences* no. 48 (7):1199-1207.

Lin, W., and F.E. Heuze. 1987. Comparison of in situ dynamic moduli and laboratory moduli of Mesaverde rocks. Paper read at International Journal of Rock Mechanics and Mining Sciences & Geomechanics Abstracts.

Logan, J.M., C.A. Dengo, N.G. Higgs, and Z.Z. Wang. 1992. "Fabrics of experimental fault zones." In *Fault Mechanics and Transport Properties of Rocks*, edited by B. Evans and T-f. Wong, 33-67. London: Academic Press.

Ma, X., and B. Haimson. 2013. Failure characteristics of a quartz-rich, high-porosity sandstone subjected to true triaxial testing. In *47th US Rock Mechanics/Geomechanics Symposium*. San Francisco, CA, USA.

Ma, Xiaodong. 2014. *Failure Characteristics of Compactive, Porous Sandstones Subjected to True Triaxial Stresses*, THE UNIVERSITY OF WISCONSIN-MADISON.

Macari, E. J., and L.R.Jr. Hoyos. 2001. "Mechanical behavior of an unsaturated soil under multi-axial stress states." *Geotechnical testing journal* no. 24 (1):14-22.

Matsushima, S. 1960. "On the deformation and fracture of granite under high confining pressure." *Bulletins-Disaster Prevention Research Institute, Kyoto University* no. 36:11-20.

McGarr, Arthur, and N.C. Gay. 1978. "State of stress in the earth's crust." *Annual Review of Earth and Planetary Sciences* no. 6:405-36.

Menéndez, B., W. Zhu, and T-F. Wong. 1996. "Micromechanics of brittle faulting and cataclastic flow in Berea sandstone." *Journal of structural geology* no. 18 (1):1-16.

Mese, A. 1995. *Effects of fluid saturation and stress state on the mechanical and chemical properties of shale*. 9617307, The University of Texas at Austin, United States -- Texas.

Michelis, P. 1985. "A true triaxial cell for low and high pressure experiments." *International Journal of Rock Mechanics and Mining Sciences & Geomechanics Abstracts* no. 22 (3):183-188. doi: 10.1016/0148-9062(85)93233-4.

Mogi, K. 2007. *Experimental rock mechanics*: Taylor and Francis Group.

Mogi, K. 1959. "Experimental Study of Deformation and Fracture of Marble (1). On the Fluctuation of Compression Strength of Marble and the Relation to the Rate of Stress Application." *Bull. Earthq. Res. Inst.* no. 37:155-170.

Mogi, K. 1966. "Some precise measurements of fracture strength of rocks under uniform compressive stress." *Felsmechanik und Ingenieurgeologie* no. 4 (1):41-55.

Mogi, K. 1971. "Fracture and flow of rocks under high triaxial compression." *Journal of Geophysical Research* no. 76 (5):1255-1269.

Mogi, K. 1979. Flow and fracture of rocks under general triaxial compression. Paper read at Proc. 4th Congress of the ISRM, at Balkema, Rotterdam.

Murrell, S . A. . 1965. "The effect of triaxial stress systems on the strength of rocks at atmospheric temperatures." *Geophys. J. Roy. Astron. Soc.* no. 10:231–81.

Murrell, S.A.F. 1963. "A criterion for brittle fracture of rocks and concrete under triaxial stress and the effect of pore pressure on the criterion." *International Journal of Rock Mechanics and Mining Sciences and Geomechanics Abstracts* no. 31 (6):643-659.

Nadai, A. 1924. "Über die Gleitund Verzweigungsflächen einiger Gleichgewichtszustände." *Z. Physik* no. 30:106.

Nádai, A. 1950. *Theory of Flow and Fracture of Solids, v. 1*. New York: New York: McGraw-Hill.

Naumann, M., U. Hunsche, and O. Schulze. 2007. "Experimental investigations on anisotropy in dilatancy, failure and creep of Opalinus Clay." *Physics and Chemistry of the Earth, Parts A/B/C* no. 32 (8):889-895.

Niandou, H., J. F. Shao, J. P. Henry, and D. Fourmaintraux. 1997. "Laboratory investigation of the mechanical behaviour of Tournemire shale." *International Journal of Rock Mechanics and Mining Sciences* no. 34 (1):3-16. doi: 10.1016/s1365-1609(97)80029-9.

Norwest-Energy. 2011. Integrated tight rock analysis shale gas Australia Arrowsmith-2 well. TerraTek.

Nouri, A., H. Vaziri, H. Belhaj, and M. Islam. 2006. "Sand-production prediction: a new set of criteria for modeling based on large-scale transient experiments and numerical investigation." *SPE Journal* no. 11 (2):227-237.

Oku, Haruyuki, Bezalel Haimson, and Sheng-Rong Song. 2007. "True triaxial strength and deformability of the siltstone overlying the Chelungpu fault (Chi-Chi earthquake), Taiwan." *Geophysical research letters* no. 34 (L09306). doi: 10.1029/2007GL029601.

Pagoulatos, Aristotelis. 2004. *Evaluation of multistage triaxial testing on Berea sandstone*, University of Oklahoma.

Palchik, V. 1999. "Influence of porosity and elastic modulus on uniaxial compressive strength in soft brittle porous sandstones." *Rock Mechanics and Rock Engineering* no. 32 (4):303-309.

Papamichos, E., M. Brignoli, and FJ Santarelli. 1997. "An experimental and theoretical study of a partially saturated collapsible rock." *Mechanics of Cohesive-frictional Materials* no. 2 (3):251-278.

Paterson, M. S. 1978. *Experimental rock deformation-the brittle field*: Springer Verlag.

Paterson, M.S., and T-f. Wong. 2005. *Experimental rock deformation-the brittle field*: Springer Verlag.

Popp, T., and K. Salzer. 2007. "Anisotropy of seismic and mechanical properties of Opalinus clay during triaxial deformation in a multi-anvil apparatus." *Physics and Chemistry of the Earth, Parts A/B/C* no. 32 (8):879-888.

Popp, Till, Klaus Salzer, and Wolfgang Minkley. 2008. "Influence of bedding planes to EDZ-evolution and the coupled HM properties of Opalinus Clay." *Physics and Chemistry of the Earth, Parts A/B/C* no. 33, Supplement 1 (0):S374-S387. doi: 10.1016/j.pce.2008.10.018.

Ramos da Silva, Mikaël, Christian Schroeder, and Jean-Claude Verbrugge. 2008. "Unsaturated rock mechanics applied to a low-porosity shale." *Engineering Geology* no. 97 (1–2):42-52. doi: 10.1016/j.enggeo.2007.12.003.

Rao, K.S., and R.P. Tiwari. 2002. "Physical simulation of jointed model materials under biaxial and true triaxial stress states." *Research Report*:30.

Rasouli, V., and J.B. Evans. 2010. "A True Triaxial Stress Cell (TTSC) to simulate deep downhole drilling conditions." *APPEA journal* no. 50:61-70.

Saidi, F., Y. Bernabé, and T. Reuschlé. 2003. "The mechanical behaviour of synthetic, poorly consolidated granular rock under uniaxial compression." *Tectonophysics* no. 370 (1):105-120.

Sarmadivaleh, M. 2012. *Experimental and numerical study of interaction of a pre-existing natural interface and an induced hydraulic fracture*. PhD thesis, Department of Petroleum Engineering, Curtin University.

Schmitt, L., T. Forsans, and F. J. Santarelli. 1994. "Shale testing and capillary phenomena." *International Journal of Rock Mechanics and Mining Sciences & Geomechanics Abstracts* no. 31 (5):411-427. doi: 10.1016/0148-9062(94)90145-7.

Smart, B. G. D. 1995. "A true triaxial cell for testing cylindrical rock specimens." *International Journal of Rock Mechanics and Mining Sciences & Geomechanics Abstracts* no. 32 (3):269-275. doi: 10.1016/0148-9062(94)00042-2.

Sriapai, Tanapol, Chaowarin Walsri, and Kittitep Fuenkajorn. 2013. "True-triaxial compressive strength of Maha Sarakham salt." *International Journal of Rock Mechanics and Mining Sciences* no. 61 (0):256-265.

Takahashi, M., and H. Koide. 1989. Effect of the intermediate principal stress on strength and deformation behavior of sedimentary rocks at the depth shallower than 2000 m. In *ISRM International Symposium*. Pau, France.

Tiwari, R. P., and K. S. Rao. 2004. "Physical modeling of a rock mass under a true triaxial stress state." *International Journal of Rock Mechanics and Mining Sciences* no. 41 (3):433.

Tsang, C. F., J. D. Barnichon, J. Birkholzer, X. L. Li, H. H. Liu, and X. Sillen. 2012. "Coupled thermo-hydro-mechanical processes in the near field of a high-level radioactive waste repository in clay formations." *International Journal of Rock Mechanics and Mining Sciences* no. 49 (0):31-44. doi: 10.1016/j.ijrmms.2011.09.015.

Tshibangu, J.P. 1997. The effect of a polyaxial confining state on the behaviour of two limestones. Paper read at Proceedings Environmental and safety concerns in underground construction, 29 June-2 July, at New York.

Tucker, E. 2001. *Sedimentary Petrology: An Introduction to the Origin of Sedimentary Rocks*: Wiley.

Valès, F., D. Nguyen Minh, H. Gharbi, and A. Rejeb. 2004. "Experimental study of the influence of the degree of saturation on physical and mechanical properties in Tournemire shale (France)." *Applied Clay Science* no. 26 (1–4):197-207. doi: 10.1016/j.clay.2003.12.032.

Vernik, L., M. Bruno, and C. Bovberg. 1993. Empirical relations between compressive strength and porosity of siliciclastic rocks. Paper read at International journal of rock mechanics and mining sciences & geomechanics abstracts.

Vernik, L., and M. D. Zoback. 1992. "Estimation of maximum horizontal principal stress magnitude from stress-induced well bore breakouts in the Cajon Pass Scientific Research borehole." *Journal of Geophysical Research: Solid Earth (1978–2012)* no. 97 (B4):5109-5119.

von Karman, T. 1911. "Festigkeitsversuche unter all seitigem Druck." *Z. Verein Deut. Ingr.* no. 55:1749-1759.

Wawersik, W. R., L. W. Carlson, D. J. Holcomb, and R. J. Williams. 1997. "New method for true-triaxial rock testing." *International Journal of Rock Mechanics and Mining Sciences* no. 34 (3–4):330.e1-330.e14.

Wawersik, Wolfgang R, John W Rudnicki, Patricia Dove, Jerry Harris, John M Logan, Laura Pyrak-Nolte, Franklin M Orr Jr, Peter J Ortoleva, Frank Richter, and Norman R Warpinski. 2001. "Terrestrial sequestration of CO2: An assessment of research needs." *Advances in Geophysics* no. 43:97-I77.

Wiebols, G. A., and N. G. W. Cook. 1968. "An energy criterion for the strength of rock in polyaxial compression." *International Journal of Rock Mechanics and Mining Sciences & Geomechanics Abstracts* no. 5 (6):529-549.

Wong, T-F., C. David, and B. Menéndez. 2004. "Mechanical compaction." In *Mechanics of fluid-sturated rocks*, edited by Y. Guéguen and M. Boutéca, 55-114. Amsterdam: Elsevier Academic Press.

Wong, T-f., C. David, and W. Zhu. 1997. "The transition from brittle faulting to cataclastic flow in porous sandstones: Mechanical deformation." *Journal of Geophysical Research: Solid Earth (1978–2012)* no. 102 (B2):3009-3025.

Wong, Teng-fong, and Patrick Baud. 2012. "The brittle-ductile transition in porous rock: A review." *Journal of Structural Geology* no. 44 (0):25-53.

Xu, D.J., W. Liu, H. Mochizuki, and K. Mogi. 1980. Mechanical behavior of soft sandstone under true triaxial compression. In *1980 Meeting Seismol. Soc. Japan*. Japan.

Yoshinaka, R., T.V. Tran, and M. Osada. 1997. "Pore pressure changes and strength mobilization of soft rocks in consolidated-undrained cyclic loading triaxial tests." *International Journal of Rock Mechanics and Mining Sciences* no. 34 (5):715-726.

You, M. 2009. "True-triaxial strength criteria for rock." *International Journal of Rock Mechanics and Mining Sciences* no. 46 (1):115-127.

Youn, Heejung, and Fulvio Tonon. 2010. "Multi-stage triaxial test on brittle rock." *International Journal of Rock Mechanics and Mining Sciences* no. 47 (4):678-684. doi: 10.1016/j.ijrmms.2009.12.017.

Younessi, A. 2012. *Sand production simulation under true-triaxial stress conditions*. PhD thesis, Department of Petroleum Engineering, Curtin University.

Young, R.P., M.H.B. Nasseri, and L. Lombos. 2012. "Imaging the Effect of the Intermediate Principal Stress on Strength, Deformation and Transport Properties of Rocks Using Seismic Methods." In *True triaxial testing of rocks*, edited by M.A. Kwasniewski, X. Li and M. Takahashi, 167-179. Beijing.

Young, RP, MHB Nasseri, and L Lombos. 2011. "Imaging the Effect of the Intermediate Principal Stress on Strength, Deformation and Transport Properties of Rocks Using Seismic Methods." In *True Triaxial Testing of Rocks*, edited by M. Kwasniewski, X. Li and M. Takahashi. Beijing: CRC Press.

Zhang, C., and T. Rothfuchs. 2004. "Experimental study of the hydro-mechanical behaviour of the Callovo-Oxfordian argillite." *Applied Clay Science* no. 26 (1–4):325-336. doi: 10.1016/j.clay.2003.12.025.

Zhou, S. 1994. "A program to model the initial shape and extent of borehole breakout." *Computers & Geosciences* no. 20 (7–8):1143-1160.